technische universität
dortmund

mpi
dortmund

Stem Cell-Based Phenotypic Screening and Characterization of Novel BMP Mimetics

Dissertation

Zur Erlangung des akademischen Grades

Doktor der Naturwissenschaften

(Dr. rer. nat.)

Fakultät für Chemie und Chemische Biologie

der Technischen Universität Dortmund

vorgelegt von

Fabian Weßeler

geboren am 26.02.1992 in Kempen

Dortmund 2021

Die vorliegende Arbeit wurde im Zeitraum von Juli 2017 bis November 2021 unter der Anleitung von Prof. Dr. Dennis Schade und Prof. Dr. Dr. h.c. Herbert Waldmann an der Fakultät für Chemie und Chemische Biologie der Technischen Universität Dortmund und dem Max-Planck-Institut für Molekulare Physiologie in Dortmund angefertigt.

1. Gutachter: Prof. Dr. Dr. h.c. Herbert Waldmann
2. Gutachter: Prof Dr. Dennis Schade

The most beautiful thing we can experience is the mysterious.

Das Schönste, was wir erleben können, ist das Geheimnisvolle.

Albert Einstein

Results presented in this thesis contributed to the following publication:

Fabian Wesseler, Daniel Riege, Mahesh Puthanveedu, Jonas Halver, Eva Müller, Jessica Bertrand, Andrey P. Antonchick, Sonja Sievers, Herbert Waldmann, Dennis Schade, “Probing embryonic development enables the discovery of unique small molecule bone morphogenetic protein potentiators”, *Submitted* 2021

In preparation:

Fabian Wesseler, Stefan Lohmann, Daniel Riege, Aileen Roth, Christian Pichlo, Sabrina Weber, Sonja Sievers, Sepand Rastegar, Jessica Bertrand, Ulrich Baumann, Uwe Knippschild, Herbert Waldmann, Dennis Schade, “Triazolo[1,5-*c*]quinazolines Expand The Druggable Space of Bone Morphogenetic Protein Amplifiers By Combined Targeting of CK1δ/ε and PI3Kγ Isoforms”

ACKNOWLEDGEMENTS

The past years have strongly formed me as a person and also as a scientist. Having found great interest in scientific work and research through my undergraduate studies, I wanted to take the opportunity to work on a project myself and thus follow the desire to explore and discover. I was particularly interested in the field of chemical biology, which investigates and integrates fundamental questions at the molecular level in a biological context.

For the opportunity to work on such an interesting project in the course of a PhD, I would therefore like to thank in particular Prof. Dr. Dr. h.c. Herbert Waldmann and Prof. Dr. Dennis Schade. I would like to thank Prof. Waldmann for the opportunity to gain insight into the diverse projects, to be able to carry out my work at the Max Planck Institute in Dortmund and for his highly appreciated support.

I would also like to express my sincere gratitude to Prof. Dr. Dennis Schade for his assistance and for the numerous discussions and inspiring ideas related to the results and progress achieved within this thesis. Furthermore, I am truly grateful to Dennis Schade for his constructive advice and experience on both a scientific and personal level over the now many years of collaboration. I also have to thank him for my enthusiasm for work and research with stem cells.

My special thanks go to Dr. Sonja Sievers, the group leader of the COMAS screening facility, who provided very helpful guidance and support for the screening procedures. I am grateful to her for valuable discussions, for her help in all technical aspects and for always having an open ear.

I would like to thank Dr. Jonas Halver for the excellent introduction to his work with stem cells and his support with project-related questions before and during my project.

I would like to thank my colleagues from AG Schade, Stefan Lohmann for synthesizing small molecules and Daniel Riege for performing biological experiments that support the mechanistic studies in the projects. Both have an important part in the projects and I thank them for the productive exchange.

Moreover, I would like to thank Dr. Andrey Antonchick and Mahesh Puthanveedu who contributed to the chromenone project and provided me with newly synthesized derivatives. I would also like to thank Dr. Slava Ziegler for her support in terms of scientific discussions and helpful suggestions on biological hypotheses.

I would also express my gratitude to Eva Müller, Mandy Koennecke and Prof. Dr. Jessica Bertrand from the University Hospital Magdeburg who established the mineralization assay to

test the identified compounds that completed the osteogenic function validation of the small molecules. In addition, I thank Dr. Sepand Rastegar and Sabrina Weber from the Karlsruhe Institute of Technology who supported our studies with *in vivo* zebrafish experiments. Special thanks is given to our collaborators in the CK1 project, Aileen Roth and Prof. Dr. Knippschild from the University Hospital Ulm, for performing biochemical CK1 selectivity and kinetic studies and providing plasmids, Dr. Christian Pichlo and Prof. Dr. Baumann for generating a crystal structure and preparing binding pose figures.

I am grateful to the whole COMAS team for technical and experimental support, in particular Christiane Pfaff and Carina Birke for assistance with screening and the compound management team for compound handling and quality control. For technical support, I would like to thank Dr. Michael Schulz for his help with FACS analysis and Dr. Sven Müller for his guidance in operating the confocal microscope.

A big thank goes also to Tanja Schuh, who helped with ideas and experimental support in the context of her bachelor thesis. I am also grateful to Bernd Rathmer, who taught me during my student training how to work precisely in cell biology as well as how to handle stem cells and continued to support me with valuable advice.

For the pleasant and friendly working atmosphere I would like to thank all members of the Department of Chemical Biology, COMAS and AG Schade. Namely, in addition to the people already mentioned, I would like to thank Carina Birke, Dr. Matthias Bischoff, Dr. Carmen Carrillo Garcia, Jana Flegel, Dr. Gernot Hahne, Dr. Philipp Lampe, Dr. Axel Pahl, Christiane Pfaff, Dr. Elena Reckzeh for experimental support, scientific discussions, insightful comments, and social company. I also appreciated the welcoming atmosphere at the institute and the people and colleagues I met through the scientific exchange with the Students' Chapter Dortmund of the International Chemical Biology Society (ICBS), the scientific and social events of the institute and the MPI football team.

Last but not least, I would like to thank my friends and family from the deepest of my heart, without whom I would not have been able to complete this journey and who have supported me in both good and difficult times and have always motivated me.

TABLE OF CONTENTS

I ABSTRACT

The identification of selective small molecule cytokine mimetics and signaling activators holds great promise for numerous applications in biomedicine as they overcome the typical drawbacks of physiological peptide- or protein-based ligands. Yet, the development of such modalities remains a challenging task in drug discovery. In this thesis, a phenotypic, target-agnostic, high-throughput screening assay is presented that probes Bone Morphogenetic Protein (BMP) signaling during mesodermal patterning of murine embryonic stem cells. This approach represents a novelty in BMP activator identification by harnessing embryonic development *in vitro*, hence potentially expanding the druggable space of BMP signaling activators. During mesoderm specification, BMP signaling can be temporally discriminated from Transforming Growth Factor-β (TGFβ)-driven stages of cardiac differentiation. This selective and authentic orchestration of BMP signaling cues can be recapitulated for the discovery of genuine BMP activator- or potentiator chemotypes. Here, a robust hit validation workflow has been devised, including the orthogonal assessment of BMP activation during osteoblastogenesis as well as BMP-dependent reporter assays. Proof-of-concept is demonstrated from screening of nearly 7,000 chemically diverse compounds, yielding 2,3-disubstituted 4*H*-chromen-4-ones as a new potent BMP activating chemical modality.

Chromenone 1 enhanced osteogenic differentiation and mineralization *in vitro*. Structure-activity relationship (SAR) studies with 29 different Chromenones revealed pharmacophoric features relevant to BMP activity and provided a valuable toolkit of active and structurally closely related inactive derivatives. Interestingly, mechanistic studies suggested that Chromenone 1 enhances canonical nuclear BMP-Smad signaling outputs through an unparalleled, kinase-independent, negative TGFβ-Smad feedback loop. This is in sharp contrast to the reported BMP sensitizer PD407824, revealing novel BMP potentiator biology as desired from a conceptionally new morphogenic and phenotypic drug discovery approach.

An additional screening of 1,408 known bioactive compounds eventually furnished the triazolo[1,5-*c*]quinazoline CGS-15943 as a novel and unique BMP activating chemotype that exhibited highest selectivity among all profiled and characterized BMP modulators in the present work. Its capacity to amplify BMP signaling during embryogenesis could be further substantiated *in vivo* during zebrafish development (i.e., ventralization phenotypes). Target

deconvolution studies unraveled novel targets of CGS-15943 with a pronounced potency for CK1δ- and -ε-isoforms. Mechanistically, CGS-15943 amplifies osteogenic BMP signaling outputs through a dual targeting of CK1δ/ε and PI3Kγ (p110γ) isoforms by enhancing BMP signaling independent of a TGFβ-feedback.

Together, the presented work underscores proof-of-concept for a novel phenotypic drug discovery strategy to identify unique BMP signaling modulators. Two new chemotypes ultimately expanded the druggable space of osteogenic BMP activators and sensitizers that may serve as valuable tools for various applications in (stem) cell biology and regenerative medicine. Notably, this work might spur future translation to even more complex 3D-gastruloid and organoid systems.

II ZUSAMMENFASSUNG

Die Identifizierung selektiver niedermolekularer Zytokin-Mimetika und Signalweg-Aktivatoren verspricht zahlreiche Anwendungen in der Biomedizin, da sie die typischen Nachteile physiologischer Liganden auf Peptid- oder Proteinbasis überwinden. Dennoch bleibt die Entwicklung solcher chemischen Substanzen eine anspruchsvolle Aufgabe in der Arzneimittelforschung. In dieser Arbeit wird ein phänotypischer, targetagnostischer Hochdurchsatz-Screening-Assay vorgestellt, der die Signalübertragung von BMP (*Bone Morphogenetic Protein*) während der mesodermalen Strukturierung von embryonalen Mäuse-Stammzellen untersucht. Dieser Ansatz stellt ein Novum in der Identifizierung von BMP-Aktivatoren dar, indem die *in vitro*-Embryonalentwicklung ausgenutzt und so der chemische Raum existierender BMP-Signalaktivatoren potenziell erweitert wird. Während der Mesoderm-Spezifikation konnte der BMP-Signalweg zeitlich von den *Transforming Growth Factor*-β (TGFβ)-getriebenen Stadien der kardiopoietischen Differenzierung unterschieden werden. Diese selektive und authentische Orchestrierung von BMP wurde erfolgreich für die Entdeckung neuartiger BMP-Aktivator- oder -Potentiator-Chemotypen rekapituliert. Es konnte ein robuster Arbeitsablauf zur Hit-Validierung entwickelt werden, der die orthogonale Validierung der BMP-Aktivierung während der Osteoblastogenese sowie BMP-abhängige Reporter-Assays umfasst. Über das Screening einer Bibliothek von fast 7.000 chemisch diversen Verbindungen wurde die Machbarkeit des neuen Ansatzes bestätigt, da 2,3-disubstituierte 4*H*-Chromen-4-one als neue potente BMP-aktivierende Substanzen gefunden wurden.

Das identifizierte Chromenon 1 verbesserte die osteogene *in vitro*-Differenzierung und -Mineralisierung. Studien zur Struktur-Aktivitäts-Beziehung mit 29 verschiedenen Chromenonen lieferten Hinweise auf für die BMP-Aktivität relevante pharmakophore Strukturmerkmale, sodass ein wertvolles Set aus strukturell eng verwandten aktiven und inaktiven Derivaten generiert werden konnte. Mechanistische Studien deuteten auf einen neuartigen BMP-aktivierenden Mechanismus von Chromenon 1 hin, der die kanonischen nukleären BMP-Effekte über einen Kinase-unabhängigen, negativen TGFβ-Smad-Feedback verstärkt. Dieser Mechanismus unterscheidet sich zum beschriebenen BMP-Sensibilisator PD407824 und offenbart neuartige Möglichkeiten den BMP-Signalweg zu verstärken und

unterstreicht den Mehrwert des konzeptionell neuen phänotypischen Screening-Ansatzes für die Arzneistoffentwicklung.

Ein zusätzliches Screening von 1.408 bekannten bioaktiven Verbindungen ergab schließlich das Triazol[1,5-*c*]chinazolin CGS-15943 als neuen und einzigartigen BMP-aktivierenden Chemotyp, der unter allen profilierten und charakterisierten BMP-Modulatoren in der vorliegenden Arbeit die höchste Selektivität aufwies. Seine Fähigkeit, die BMP-Signalübertragung während der Embryogenese zu verstärken, konnte *in vivo* während der Zebrafischentwicklung, d.h. über Phänotypen der Ventralisierung, weiter bestätigt werden. Mittels verschiedener Strategien wurden neue Targets von CGS-15943 identifiziert und eine ausgeprägte Potenz für CK1δ- und -ε-Isoformen aufgedeckt. Mechanistisch verstärkt CGS-15943 die osteogenen BMP-Signale durch eine duale Inhibition der CK1δ/ε- und PI3Kγ (p110γ)-Isoformen in TGFβ-unabhängiger Weise.

Zusammengenommen bekräftigt die vorgestellte Arbeit die Machbarkeit des einer neuartigen phänotypischen Strategie zur Identifizierung einzigartiger BMP-Signalwegmodulatoren. So haben zwei neue Chemotypen den chemischen und pharmakologischen Raum bekannter osteogener BMP-Aktivatoren und –Sensibilisatoren erweitert. Diese Substanzen werden als wertvolle Werkzeuge für verschiedenste Anwendungen in der (Stamm-)Zellbiologie und regenerativen Medizin genutzt werden können. Vor allem könnte diese Arbeit zukünftig auf noch komplexere 3D-Gastruloid- und Organoid-Systeme übertragen werden.

1 INTRODUCTION

1.1 Stem Cells and Regenerative Medicine

Embryonic stem cells (ESC) are pluripotent cells that can proliferate indefinitely *in vitro* and differentiate into almost any mature cell in the human body.[1] They arise from the blastocyst of a multicellular embryo and form the three embryonic germ layers, the ectoderm, endoderm, and mesoderm, which determine subsequent differentiation into specific cell lineages.[2] Their potential to provide access to any specialized cell has made stem cell technologies among the hottest research topics in medicine.[3] More recently, stem cell-based research has become important in the context of regenerative medicine, an emerging interdisciplinary field of research and clinical application, particularly to enable targeted differentiation and reprogramming into specialized cells and tissues, and thus repair and regeneration of damaged tissues and whole organs.[4] Relevant examples in which regenerative medicine has played a significant role in the past decade include cardiovascular and osteopenic diseases, both representing a major challenge for our healthcare systems, especially in view of the demographic change and our aging society. Cardiovascular diseases (CVD) are the leading cause of death for about 18.6 million deaths worldwide in 2019 and 1.8 million in the EU in 2017, accounting for more than one-third of all cases.[5,6] Over the past 25 years hospitalization rates increased steadily with hypertension as the major risk factor for CVD-linked mortality, that in total costs the EU economy about €210 billion per year.[7] The majority of deaths is caused by coronary heart disease (CHD) including chronic ischemic heart disease, acute myocardial infarction, and heart failure. When acute circulatory disturbance occurs as a result of arterial occlusion, irreversible damage to the myocardial tissue occurs and life-threatening numbers of myocardial cells die.[8] The ischemically damaged heart constricts due to scar tissue formation, where cardiac fibroblasts differentiate to myofibroblasts and heart failure may result.[9] To counteract the failing heart, hypertrophy of cardiomyocytes occurs, which in combination leads to organ damage and subsequent death.[10] Because pharmaceuticals are administered only to treat symptomatic disease, the loss of heart muscle is almost irreversible. In severe cases heart transplantation represents the only therapeutic option.[11]

In addition to CVD, about one in four people aged 85 is diagnosed with hip osteoarthritis, while one in two has an arthritic knee.[12] Injuries to bone tissue or joints caused by accidents or

overstressed joints are additional unpredictable factors. In the U.S. alone, the cost of treatments exceeds $80 billion per year, and the chances of success of such treatments with tissue grafts or connective tissue are limited.[13] Administration of bone-inducing growth factors across various therapeutic applications in treating skeletal trauma and disorders raised in clinics.[14] Such applications are based on cell therapies addressing mesenchymal stem cells or osteogenic progenitors *in vivo* or for bone graft generation.[15] Due to the tremendous demand to develop more efficient and safer therapies, novel pharmaceuticals are of great interest that may have enormous potential treating skeletal trauma and diseases.

Over the past two decades, the field of stem cell biology has advanced greatly, and new approaches have been described for the discovery of drug-like small molecules that could potentially lead to strategies for tissue regeneration. In terms of regenerative medicine, the discovery of the efficient and reproducible generation of induced pluripotent stem cells (iPSCs), which physiologically mimic embryonic stem cells, was groundbreaking.[16] Yamanaka and colleagues showed for the first time that adult somatic cells such as fibroblasts can be reprogrammed into pluripotent cells capable of generating all three embryonic germ layers by transducing the four transcription factors Oct4, Sox2, Klf4, and c-Myc.[16,17] Different transcription factors have been reported soon after, such as Lin28 or Nanog, expanding the understanding and potential of somatic nuclear transplantation.[18,19] Interestingly, iPS generation has been successful even in the absence of Oct4 overexpression, resulting in reduced off-target gene activation leading to an enhanced developmental potential.[20] The revolutionary discovery by Yamanaka and colleagues enables ethically unproblematic use of human pluripotent stem cells and the potential targeted growth of tissues or whole organs from patient-derived cells. Hence, the finding was awarded the Nobel Prize in medicine in 2012 for its great therapeutic potential and fundamental cellular insights, exactly 50 years after John B. Gurdon described the potential of adult somatic cells to develop into an entire organism.[21,22] This patient-oriented application of stem cells enables personalized medicine. Just a couple of years after this, in 2009 the world's first clinical trial of a hESC-based therapy for treating spinal cord injury was initiated with great attention, indicating the huge expectation and hope for revolutionary regenerative therapies in clinics.[23] A decade later, the first clinical application of autologous hiPSCs was approved, and furthermore, hiPSC-derived mesenchymal cells will likely be the first successful human clinical application for the treatment of graft-versus-host disease.[24] In addition, hiPSCs are being used extensively to create artificial tissues, such as

3D-engineered heart tissue.[25] A breakthrough was reported in the summer of 2021, in which Heartseed and Novo Nordisk announced a global collaboration and the start of a clinical trial using hiPSC-derived cardiomyocytes for the treatment of heart failure, under the name HS-001.[26]

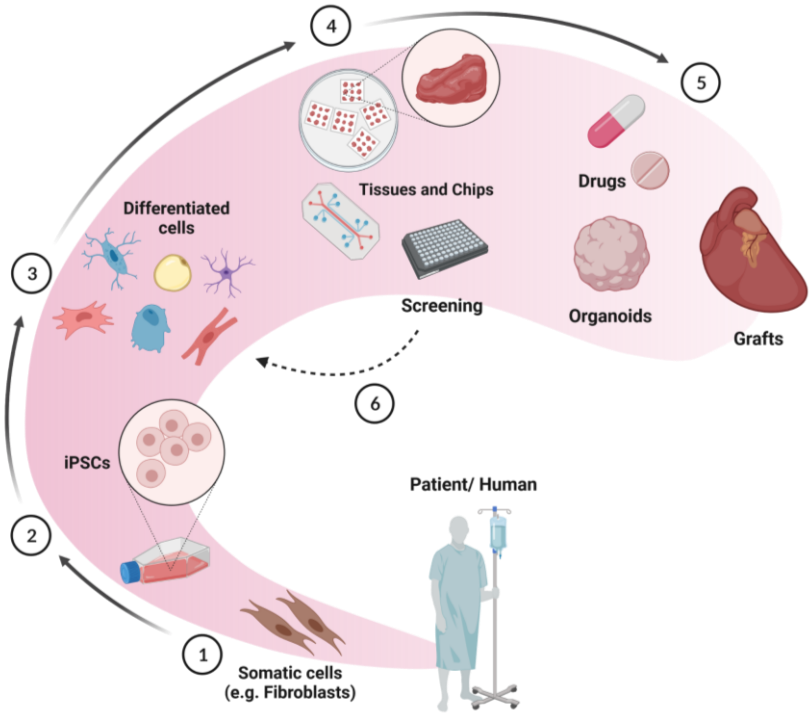

Figure 1: Therapeutic application of human induced pluripotent stem cells. Isolated somatic cells from a patient (1) are reprogrammed into iPSCs (2) and subsequently used for differentiation to the desired cell lineage (3). Differentiated cells mimic the pathological potential of a patient, which can be utilized for screening for novel therapeutics by screening approaches of cells, multicellular tissues, and body/organ-on-a-chip systems (4). Further, cells can be grown to more complex system such as organoids or ultimately to mature organs/grafts for transplantation (5), while, in addition, screening of disease-relevant markers can enable personalized treatment. Conversely, newly identified substances can be used to optimize reprogramming and differentiation processes, leading to safer methods (6).

A major goal in replacement therapies is the control of stem cell induction to direct cellular differentiation, e.g., iPSC differentiation and transdifferentiation or transition from tissue-derived cells *in vitro* or *in vivo*.[27] One approach could be to use tissue-specific multipotent adult stem cells such as hematopoietic or mesenchymal stem cells from bone marrow for co-transplantation or cardiac progenitor cells for cardiomyocyte induction.[28,29] Adult stem cells can be targeted by modulating the environment, thus inducing the "stem cell niche" promoting active differentiation and migration of stem cells in the tissue.[27] Another alternative might be to target proliferation of somatic cells in healthy tissues to induce cell cycle and regeneration *in vivo*, as has been shown for the limited proliferative capacity of cardiomyocytes, for which

various cell cycle factors and the Hippo signaling pathway have been identified as suitable targets.[30,31] Moreover, direct reprogramming of somatic fibroblasts to cardiomyocyte-like cells by treatment with a specific drug cocktail in a full chemical approach has been successfully demonstrated, indicating an attractive alternative to hiPSC differentiation.[32]

Human stem cells capable of differentiating into cardiomyocytes have been isolated from various human tissues, but the pool of adult and multipotent cells is limited in its differentiation potential.[33] Somatic cell-derived induced PSCs can overcome these problems and are more cost-effective.[34] However, for clinical application of iPSC lines, various challenges must be tackled. For instance, patient-derived iPSCs vary in natural variability, purity and yield and extensive safety testing regarding genetic mutations must be considered.[35] Moreover, reprogramming can induce genomic and epigenetic changes in cells, so early genetic control mechanisms of hiPSCs are crucial, even if the epigenomic profile remains very similar.[36] As a negative side effect of the great intrinsic proliferating potential, tumorigenicity risk is a critical issue, particularly for transformed undifferentiated pluripotent cells of transplanted iPSC-derived tissue. In addition, cell mutation occurs, since iPSCs have been subjected to reprogramming stress and culture adaption, and the transcription factors used for reprogramming are known oncogenes.[37] To reduce tumorigenic potential, a fail-safe system has been developed in which a caspase9 vector induces apoptosis of degenerated cells, demonstrating that this system may be suitable to avoid adverse effects after transplantation.[38] Another important factor is the immune recognition of the transplanted cells, causing an immune response and subsequent rejection, even though the cells are autologous. Changes in antigen expression due to genetic or epigenetic changes of iPSC derivatives may contribute to a T-cell dependent response, indicating the importance of a robust screening test system of reprogrammed embryonic cells.[39] Given the broad clinical application of iPSC cells, in the long term, allogeneic therapies from already reprogrammed cell banks are the more cost-effective and less time-consuming alternative.[40] Nevertheless, autologous iPSC transplants are generally considered a safer strategy than allogeneic transplants, which require long-term treatment with immunosuppressants. However, current clinical applications of grafts, e.g., retinal pigment epithelial cells for rescue of retinal degeneration and functional regeneration, seem to be very promising in terms of safety aspects, followed by recent consecutive studies addressing different aspects of iPSC grafts.[41,42] To increase safety and yield of iPSC-derived tissues and grafts, fully optimized protocols for differentiation and

application are highly desired and the early application of good manufacturing practice is becoming increasingly important.

1.2 Phenotypic Drug Discovery

Phenotypic screening approaches are used to access novel bio-active agents, including small molecule modalities as potential pharmaceuticals. In the context of forward chemical genetics, the influence of a compound in complex living systems is examined in its entirety in phenotypic cell-based screenings.[43] In contrast to hypothesis-driven, targeted drug discovery (TDD), the observation of phenotypic changes in a physiologically relevant model system contributes to the discovery of relevant mechanisms.[44] It can be assumed that small molecules have multiple binding partners (are promiscuous), therefore also affecting different targets including different phenotypes *in vivo*. For this reason, it is important that disease-relevant assays elicit specific phenotypes. Phenotypic drug discovery (PDD) holds great potential for successful translation to *in vivo* models and thus to clinical trials. Certain knowledge on disease pathophysiology is important for successful implementation of a phenotypic drug discovery approach. Meaningful readouts are key to identify high-quality hits, while generic readouts such as viability or apoptosis are less likely to be useful for the identification of novel targets or mode of actions.[45] Subsequently, target deconvolution presents the next critical step in understanding the mechanism and safety issues for new pharmaceuticals, which is the most elaborate and time-consuming step in PDD. Here, the identification of targets is becoming more promising thanks to recent advances in proteomics- and genomics-based technologies.[46] To validate target engagement and to rationalize biological significance of the target in the cellular context, a variety of methods are available.

Because of the paradigm shift in stem cell biology in terms of cellular reprogramming and its enormous potential for a broad range of clinical applications, as described earlier in Chapter 1, the use of stem cells in phenotypic screening has increased, particularly to identify novel small molecules that modulate differentiation, reprogramming, and self-renewal. The collaboration of PDD with stem cell-based systems could lead to a rapid translation of model systems to *in vivo* applications, hence to preclinical trials and ultimately to personalized medicine, as illustrated in Figure 2.[47] In addition, the introduction of hiPSCs derived from

isolated cells of patients may contribute to homogenous disease-relevant cultured cells that can be used in phenotypic screening campaigns.

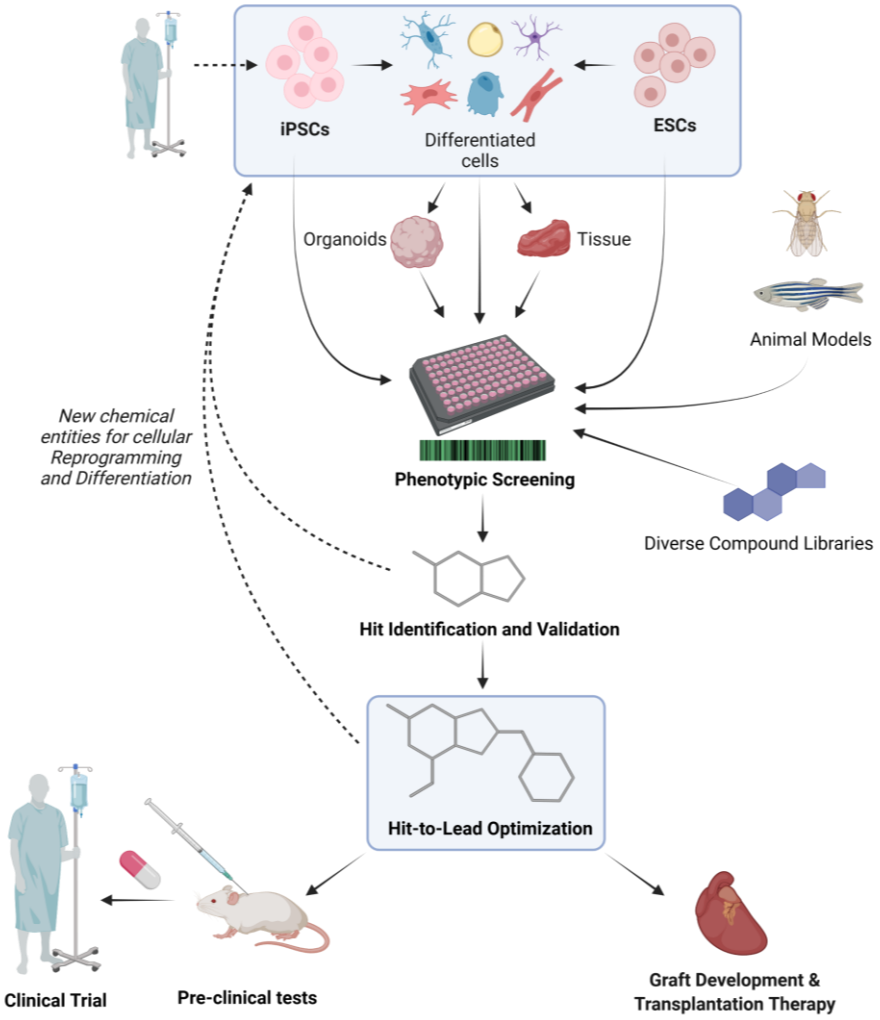

Figure 2: Schematic workflow of stem cell-based Phenotypic Drug Discovery (PDD). A certain morphological change and disease signature can be monitored from a high-throughput screen using different model systems, such as stem cells, stem cell-derived specialized cells, tissue-derived primary cells, 3D organoids or animal models systems. Integrating novel chemical biology techniques to expand the chemical space could lead to the identification of true chemical hits that are subsequently validated and optimized towards early lead compounds for experimental *in vivo* pharmacology. Identified compounds could expand the chemical space for stem cell reprogramming and differentiation. Lead compounds will eventually be used for the development of engineered tissues (graft) or undergo classic preclinical testing as a potential drug candidates. The figure was created with BioRender.com and modified from Vandana et al., 2021.[48]

Generated hiPSCs can also contribute to phenotypic screening of multicellular structures, such as organoids or “organs-on-chips” with high physiological relevance.[49] An interesting feature of organoids derived from human samples is the recapitulation of genetic mutations and pathological morphology, thus allowing *in vitro* drug screening of tumor-organoids and personalized treatment.[50] One of the major limitations of hiPSCs is their lack of robust cultivation and reproducible, efficient differentiation, which hinders broad screening in such

systems. A recently introduced 3D-culture screening procedure for efficient generation of differentiated cells could be the basis for more efficient differentiation protocols, where culture conditions, signal inputs, doses, etc. were tested against each other.[51] Besides organoid screening of therapeutics for toxicity, metabolism and efficacy, recent advances in microfluidic platforms, like “organ-on-a-chip”, are attractive and cost-efficient alternatives for preclinical and pharmacokinetic studies.[52] Combinations of such systems can recapitulate whole-body models (body-on-a-chip systems), and the use of hiPSC-derived cells has also been successfully demonstrated in proof-of-concept studies.[53] For instance, hiPSC-derived cardiomyocytes were successfully cultured with primary hepatocytes from the liver in a multi-organ system and various functional readouts for the determination of the contractility and electrical conductivity of the cardiomyocytes, as well as the investigation of metabolites of the drugs used, facilitate new and detailed preclinical investigations.[54] Recently, a library of organoids generated from hPSCs was already used in SARS-CoV-2 pathophysiology studies to investigate respiratory failure of organs in response to viral infection and in which efficacies of anti-viral drugs can be evaluated.[55] In contrast to stem cell-based PDD, whole-animal screenings have shown to be suitable systems for drug discovery in physiological context and *in vivo* administration, however, due to recent breakthroughs and advances in stem cell-technologies and disease modeling, animal models become less attractive.[48]

An important factor in screening procedures is the early identification of substances that interfere with readout or undesirable mechanisms that cause a comparable biological phenotype of interest. Such compounds have been known as Pan Assay Interference Compounds (PAINS) for several years.[56] They occur as frequent hitters in compound libraries and are generally substances that, for example, consist of certain chemical properties such as protein-reactive or fluorescent structures, which are usually not target-associated and can therefore interfere with biological mechanisms or assay readouts. Every substance library faces these interfering compounds, which is why, in addition to a valid and well-designed screening process, the quality and chemical diversity of the substances also plays a crucial role, especially since the identification of such substances after phenotypic screening can waste significant time and resources. A very comprehensive recent review summarized experiences and problems of this phenomenon and optimized future pipelines to reduce the impact of so-called nuisance compounds.[57] It is especially critical for phenotypic assay, to distinguish between technological and non-technological-related artefacts, like cytotoxicity and

autofluorescence. In cellular context, target and pathway-associated unspecific effects can occur, e.g., metabolic, membrane or cell cycle perturbations.[57] A prominent bioactive drug class that has been shown not to hit the intended target but to cause an off-target effect within a putative mode of action are the cationic amphiphilic agents (CADs). These have recently gained significance in antiviral research and usually induce phospholipidosis, i.e., an accumulation of phospholipids in the lysosome, which is a known mechanism for inhibiting virus production.[58] Therefore, chemical modalities or genetic perturbants causing certain phenotypes should be considered with caution, especially because new mechanisms and targets are increasingly being identified even for known therapeutics.[59] Further, it is essential to establish a valid pipeline for the identification of nuisance compounds at an early stage and, ideally, to test possible interference compound classes during assay development. An approach that is gaining increasing importance and insight into the bioactivity and classification of biological compound classes is the morphological fingerprinting of compounds.[60] Here, a complex image analysis of morphological changes is used to generate a biological fingerprint of substances, thus allowing correlations between bioactivity and chemical structure in an unbiased manner at an early drug discovery stage.[61] With regards to image-based profiling, machine learning strategies could improve understanding of the relationship between drug and phenotype and lead to accelerated drug discovery.

Altogether, the interplay of novel chemical biology technologies with stem cell-based phenotypic screens offers tremendous potential for drug discovery by expanding the chemical space for specific mechanisms of action and targets in a disease-relevant context.

1.3 BMP signaling pathway

1.3.1 Overview of the BMP signaling transduction

Bone Morphogenetic Proteins (BMPs) are cytokines that belong to the TGFβ-superfamily including at least 20 ligand members causing an array of physiological responses.[62] The BMP signaling pathway is highly conserved among multi-cellular organisms and at least 1.2 billion years old.[14] It is especially important in embryogenic and skeletal development, cell fate decision, cell differentiation and tissue homeostasis.[63] The potential of BMPs was first described in 1965, by the induction of ectopic bone formation and repair of bone tissue.[64,65]

Among the ligands of TGFβ-superfamily, BMPs are exclusive in their bone-inducing potential, but in addition they have distinct and overlapping functions depending on the tissue and receptor expression levels. In 1998, BMPs were described to be required for murine embryonic stem cell self-renewal and stem cell maintenance and for osteoblastic differentiation of mesenchymal stem cells.[66] While BMP signaling is required for stem cell proliferation, it is also essential for early mesoderm and trophoblast differentiation.[67] Specific BMPs (BMP-2/-4/-7) are able to induce cardiac myogenesis, firstly described for chicken embryos, in which mesoderm tissue differentiated towards cardiomyocytes upon contact to cardiogenic BMPs.[68]

BMP growth factors vary in their structural homology and can be classified into four different subgroups, including BMP2/4, BMP5/6/7/8, BMP9/10 und BMP12/13/14 group.[69] One of the cysteines of BMPs form a covalent disulfide bond with another BMP, resulting in a homo- or heterodimer, capable of activating receptor complexes. In comparison to homodimers, BMP hetero-dimers typically have an enhanced affinity towards specific receptors and vary in their function, like BMP-2/7 and BMP-4/7.[69] Generally, BMPs are translated to the secretory pathway after cleavage of the proprotein, whereas uncleaved BMPs like BMP-2, BMP-4 or GDF5 contain a bipartite nuclear localization signal, that can lead to translocation to the nucleus.[70] This can also result from alternative start codon translation of the specific BMPs, ultimately resulting in cell cycle inhibition and accumulation of cells in G0 phase.[71] It is suggested that nuclear BMP-4 accumulation results in cell death, yet the function is unknown. Some BMPs have exclusive physiological functions, such as BMP-1, a metalloproteinase, which acts as a propeptidase for type I collagen, or BMP-3 (Osteogenin), that was also shown to suppress osteoblast differentiation by blocking BMP receptor signaling.[69] The closely related Growth Differentiation Factors (GDFs) differ in function during development and the regulation of specific processes. For instance, BMP-9, or GDF-2, is involved in iron metabolism and homeostasis by increasing levels of the peptide hepcidin1, or GDF-3, also known as Vg-related gene 2 (Vgr-2), which is specifically expressed in pluripotent embryonic cells as regulators for balancing BMP and TGFβ signaling.[72,73] It is able to inhibit BMP proteins and potentiate Nodal signaling in pre-gastrulated mouse embryos, crucial for anterior-posterior axis patterning. Some GDFs are also found as direct binders to BMPs, such as GDF6 (BMP-13), which can inactivate Noggin and form hetero-dimers with BMP-2.

Depending on the ligand type and dimerization, the binding affinity towards BMP receptors varies. There are two types of BMP receptors in mammals, that are specifically bound by

BMPs: the type I receptors, consistent of four receptors (ALK1/2/3/6) and the type II receptors.[74] Three different type II receptors exist, the BMP specific BMPR2 and two activin type II receptors (ActR-IIA, ActR-IIB), which transduce signaling from BMPs, Activins and Myostatin. Both types share an intracellular serine-threonine kinase domain, while type II receptors are constitutively active, and phosphorylate and activate the glycine-serine rich domain (GS) of type I receptors.[74] Among the four BMP-dependent BMP type I receptors, ALK3 and ALK6 share high structural similarity and function, whereas ALK1 is closely related to ALK2. The abundance of ALK1 is limited to endothelial cells and some other specific cells, whereby the expression of ALK2 and ALK3 is widespread in different cell types, indicating a high dependency on the cellular context and tissue of receptor expression levels.[74] In addition, BMP signaling response depends on the specific binding affinity of BMPs to their receptors, in particular to type I receptors. For instance, BMP-2 and BMP-4 bind exclusively to ALK3 and ALK6, directing the recruitment to BMPR2 and ActRIIA, whereas BMP-6 and BMP-9 bind to ALK2 and weakly to ALK6.[75,76]

In principle, BMPs bind to type I BMP receptors (ALK1/2/3/6), inducing the formation of a heterotetrameric complex with two type II BMP serine/threonine receptor kinases.[75] Upon binding of homo- or heterodimerized BMP ligands on the transmembrane domain the canonical BMP signaling pathway is activated, as depicted in Figure 3. In close proximity, the constitutively active type II receptor trans-phosphorylates BMP type I receptors, which in turn activate regulatory SMAD1/5/8/9.[74] Phosphorylated SMAD1/5/8/9 then forms a complex with the co-SMAD protein SMAD4, which translocates to the nucleus, leading to the modulation of BMP target genes, such as the induction of the *Inhibitor of DNA binding* (*ID*) gene family.[77]

In general, three different types of SMAD proteins exist and are defined as regulatory, common mediator and inhibitory SMADs. Specifically, R-SMADs consist of a *N*-terminal MH1 and a *C*-terminal MH2 domain, linked by a proline-rich region and that form an autoinhibitory structure between the two domains.[78] Phosphorylation and activation occurs at an SSXS-motif at the MH2-domain, leading to trimeric complex formation with SMAD4.[62] In addition to receptor recognition, the MH2 domain mediates oligomerization and transcription factor formation, whereas the MH1 domain interacts with DNA and transcription factors. A lysine-rich nuclear localization signal (NLS) is located in the MH1 domain and conserved in all R-SMADs, that is exposed upon phosphorylation and leads to nuclear translocation.[78] The inhibitory SMADs

are limited to SMAD6 and SMAD7, that lack the MH1 domain, and mainly regulate and mediate R-SMAD degradation, which is explained in more detail in chapter 1.3.2.

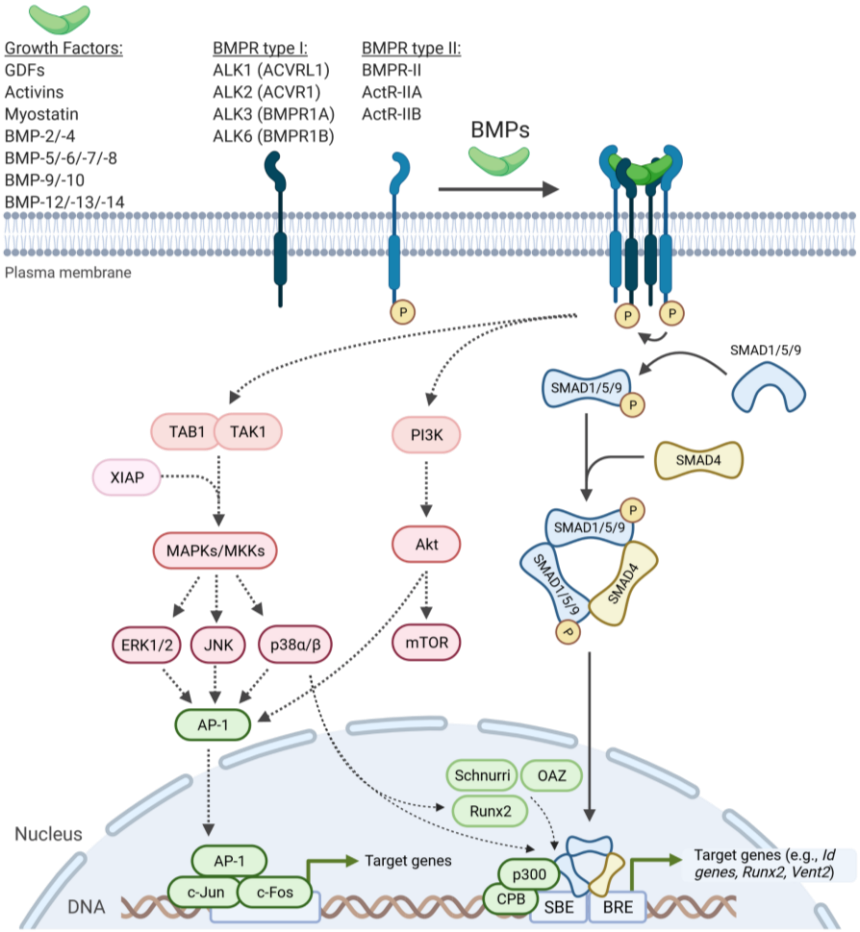

Figure 3: Schematic representation of the BMP signaling pathway. Upon binding of BMP ligand homo- or heterodimers or other growth factors, canonical BMP signaling is mediated by SMAD1/5/9 activation and nucleic translocation. Non-canonical signaling is transduced via PI3K or TAB1/TAK1-mediated MAPK signaling, which regulates specific target gene expression and SMAD signaling.

After translocation to the nucleus, SMAD complexes recruit a wide range of transcriptional co-activators and DNA-binding proteins. The co-activators CBP and p300 are essential for DNA-binding of the SMAD transcriptional complex by DNA acetylation, thus enhancing transcriptional potential of the target gene region. Recruitment of specific transcriptional co-factors also regulates the promoter that is activated.[79] The BMP-specific binding response element (BRE) consists of a GC-rich sequence, typically the Bre7 (T)GGCGCC motif, transcribed in the promoter region for different target genes like *Bambi*, *hepcidin*, *Smad7* or *Vent2*.[80,81] Other GC-rich sequences, such as the GCCGnCGC motif was found in the promoter region of SMAD6, indicating the direct activation of a negative feedback loop.[82] The Smad-binding element (SBE), selective for TGFβ-target genes, consists of a GTCT and AGAC

sequence, that are recognized by SMAD3 and -4, and which were found in the *Id1* promoter region in combination with a GC-rich box sequence.[83] The CAGAC box is encoded multiple times and the promoter contains a palindromic GC sequence to enhance SMAD-binding and responsiveness to SMAD1/4.[84] The BMP-specific transcription of *Id* genes results in negative regulation of basic helix-loop-helix proteins (bHLH), thus inhibiting the transcription of bHLH target genes and preventing cell differentiation.[83] Despite the transcriptional activation of I-SMADs, SMAD9 transcription is induced by BMP signaling, but has been shown to form suppressive complexes with SMAD1, giving it an exclusive mode of action beyond R-SMADs.[85] Complex formation with specific transcription factors defines and regulates target gene expression and biological response. For instance, runt-related transcription factor2 (Runx2), also known as core-binding factor subunit alpha-1 (CBFα-1), functions as a master regulator of osteoblastogenesis.[86] Recruitment of Runx2 by BMP-SMADs promotes gene expression of osteogenic factors and proteins. Another transcription factor, the so-called Schnurri (Shn), has various modes and mechanisms in BMP signaling, depending on organism and tissue. In fly *Drosophila* embryos, BMP signaling is suppressed by the expression repressor Brinker, whose gene expression is inhibited by the DNA binding protein Schnurri.[87] When BMP signaling occurs, Schnurri recruits Mad and Medea (i.e., SMAD1 and SMAD4 orthologs in Drosophila) and binds to the SBE and BRE elements at the promoter site to repress *Brinker* gene activation, and thus acting as a general “on switch” for BMP target gene expression.[87] One of the first identified transcription partner of SMADs, OAZ, the OE/EBF-associated zinc-finger protein, is involved in gene expression of *Vent1* and *Vent2*, that induces cell fate change and dorsoventral patterning by inducing ventralization and inhibiting dorsal inducer Goosecoid (Gsc) in *Xenopus* mesoderm.[88] For transcriptional activation, SMAD1 and OAZ induce gene expression, that has been shown to be enhanced by Vent2 in a positive feedback loop.[89] Interestingly, the *Vent* gene is not encoded in mouse or rat genomes, but in the human genome.[90] Moreover, OAZ co-factor complexation with SMAD1/4 activates BMP signaling and represses SMAD6 transcription in a cell context-specific manner as it is not expressed in all cells, including the C2C12 cell line.[88]

Beside canonical signaling, BMP signaling can be mediated through Smad-independent, i.e. non-canonical pathways, such as the mitogen-activated protein kinase (MAPK), c-Jun amino-terminal kinase (JNK), phosphoinositol-3 kinase (PI3K) and Akt signaling pathways, that can also act cooperatively with the canonical pathway and are important for different cellular

responses (see Figure 3).[91] The MAPK pathway is induced by association of TGF-β-activated kinase 1 (TAK1), Tak binding protein 1 (TAB1) and X-chromosome-linked inhibitor of apoptosis protein (XIAP) with BMP type I receptors upon ligand binding. TAK1 shares high similarity to the MAP kinase Raf-1 and acts upstream of MAPK signaling, activating and recruiting its binding partners to from an adapter complex with enhanced activity for subsequent phosphorylation of p38 and JNK.[91] In addition, the BMP-activated MAP kinase can phosphorylate SMADs, including inhibitory SMADs, and regulates R-SMAD activity and subcellular distribution, suggesting a universal BMP-dependent modulation.[92] Early studies on the TAK1 interacting protein XIAP found that the expression of ventral mesodermal genes in *Xenopus* embryos was dependent on BMP-2- and BMP-4-induced p38 activation by TAB1-TAK1, indicating the importance of non-canonical pathways in early embryonic patterning.[93,94] In contrast to these findings, BMP-4 was found to inhibit MAPK signaling in the ectoderm via TAK1 and p38, suggesting a biphasic nature of BMP activation.[95] Furthermore, in *Xenopus* and murine hybridoma cells, BMP-2-induced TAK1 overactivation leads to cell apoptosis and is in fine balance with ventral mesoderm formation, that is partially controlled by co-activation of the antagonistic SMAD6.[93,96] Beside TAK1-mediated signaling, MAPK-dependent Ras and extracellular signal-regulated kinase (ERK) induction via BMP-2/-4 occur within minutes in response to ligand binding in various cell types, whereas ERK can also be activated by SMAD signaling.[97] SMAD-independent signaling also depends on BMP specificity, for instance in chondrogenesis, GDF5 (BMP-14) has been shown to induce p38 and ERK phosphorylation, but not JNK.[98] In case of BMP-2, in mouse osteoblastic MC3T3 cells, p38 phosphorylation and nuclear accumulation is essential for BMP-2 induced activation of SMAD5 and the synergistic induction of the osteogenic driver *Dlx3*.[99] In summary, the activated kinases translocate to the nucleus to activate transcriptional co-factors such as AP-1 (with SMAD4), the Jun family and c-Fos, that induce target gene expression.[97] Additionally, it has been shown, that ERK and p38 are essential for BMP-2-induced expression of various bone matrix proteins and thus mediating osteoblastic differentiation.[97] Furthermore, BMPs can induce the PI3K and Akt signaling pathways in a SMAD-dependent and -independent manner.[91] Upon activation, PI3Ks phosphorylate and activate Akt in the cell membrane, which results in further downstream events, such as phosphatidylinositol and mTOR activation.[100] Moreover, PI3K activation has been shown to support and promote SMAD-dependent differentiation to osteogenic lineages. In one study, negative PI3K and Akt kinase regulation were shown to

inhibit BMP-2-induced BMP transcription and Alp induction, while PI3K activation was necessary for SMAD5 dependent transcription.[101] However in the same year, the inhibition of PI3K and p38 MAPK signaling in C2C12 has been shown to enhance BMP-2-induced SMAD signaling.[102] In the latter case the mode of action depends on additional myogenic inhibition caused by PI3K blockage, leading to osteogenic potentiation, again suggesting the importance of canonical and non-canonical BMP signaling in different cell types.

1.3.2 Regulatory mechanisms of BMP signaling

BMP signal transduction is regulated at many different levels and is tightly controlled by binding and activation enhancement or competition of ligands, receptors, or intracellular signal transducers.[62] The great interactome of the BMP pathway indicates the fine dosing of BMP activity, controlling embryogenesis and different cell-type specific differentiations. For morphogenic gradient regulation in embryogenic development, extracellular antagonists like Noggin or Chordin are secreted, that inhibit BMP ligands by direct binding, thus preventing receptor binding and signaling.[103] These antagonists are homodimers like BMP ligands and classified in different families, depending on their cysteine knot motifs, such as the Chordin/Noggin or DAN/Cerberus family. One of the most important inhibitors and regulator in embryogenesis is Noggin, which binds specifically to BMP-2, -4, -5, -6, -7, -13 and BMP-14, by wriggling around the epitopes for binding to both receptor types.[104] Typically, Noggin expression is induced upon BMP activation, thus functions as a negative feedback regulator and stabilizing the sensitive cellular or tissue response to BMP. Noggin expression strongly depends on the tissue and is essential for BMP gradient-dependent dorsal-ventral patterning and germ layer formation in the early embryogenesis at the Spemann organizer.[104,105] The antagonists differ in their expression depending on the tissue like Gremlin, which is expressed in osteoblasts and in the limb bud and inhibits BMP-2/-4 and BMP-7 with high affinity.[106] In contrast, Cerberus (CER1) is only expressed in embryonic development in the anterior endoderm and able to inhibit BMP, Nodal and Wnt signaling.[107] Its secretion is essential for head and heart formation in vertebrates, depending on BMP or Nodal inhibition.[108] An even more diverse antagonist, Coco, induces neural formation by inhibiting BMP, Wnt and TGFβ ligands, but is only expressed in pre-gastrula embryos.[103] These findings underline the tissue dependency and secretion of BMP antagonists for embryonic patterning and differentiation. In

addition to antagonists, extracellular activators can potentiate BMP signaling. For instance, sulfated polysaccharides like heparins or dextran sulfate enhance BMP-2, -4 and -7 activity of both homo- and heterodimers by enhancing their stability and suppressing accumulation of BMPs into the cell layer.[109] In some species, BMP-1 homologs were identified, for example Tolloid and Xolloid, that cleave extracellular Chordin, hence releasing “trapped” BMPs and activating BMP signaling.[110]

BMP signaling induction through receptor activation is also regulated by co-receptors, such as Betaglycan, a TGFβ-receptor (TGFβ-RIII) that enhances binding of BMPs to type I BMP receptors (see Figure 4). It was shown to be essential for epithelial-to-mesenchymal (EMT) transition in the developing heart.[111]

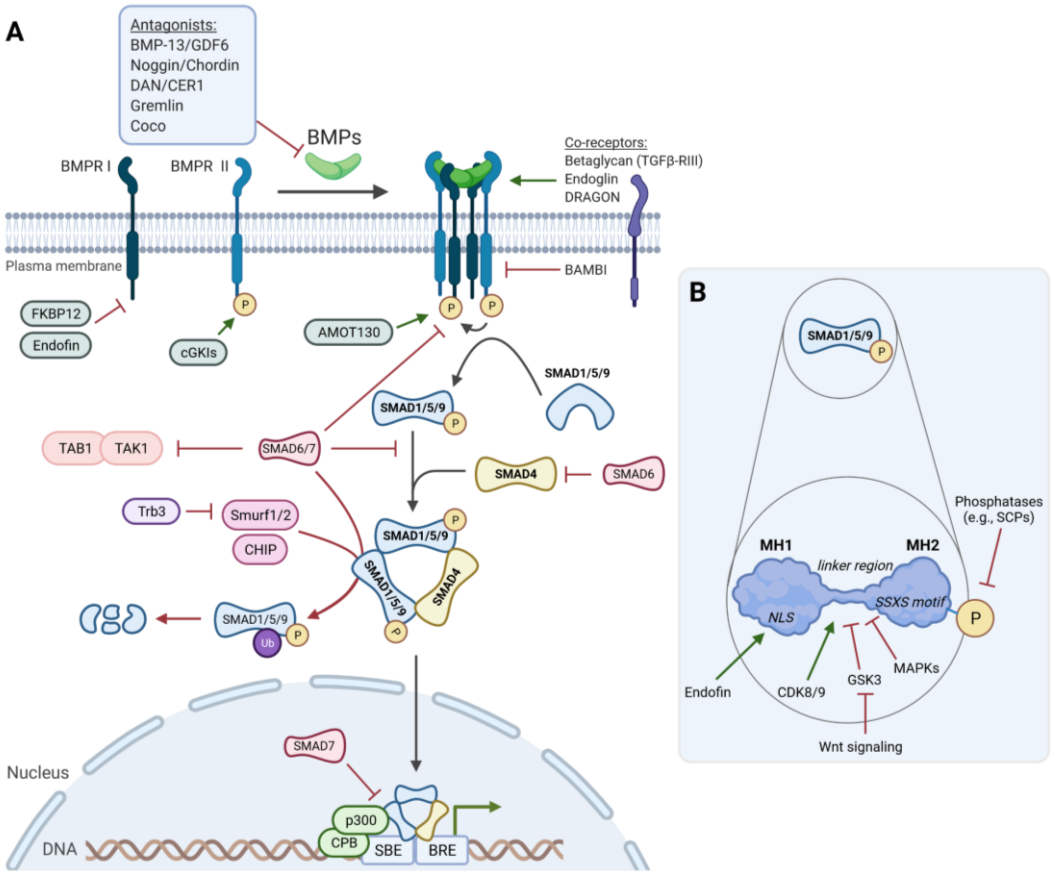

Figure 4: (A) Overview about critical regulatory mechanisms of the BMP signaling pathway. Multiple extracellular secreted antagonists regulate BMP ligand abundance, while receptor activity and stabilization are regulated by different co-receptors and cytoplasmic factors. (B) Schematic representation of structural SMAD regulation. Phosphorylation at the SSXS-motif on the MH2 domain results in conformational activation, which is directly regulated by phosphatases. Moreover, R-SMADs are negatively regulated by phosphorylation and thus ubiquitination at their linker region by various factors such as GSK3α/β and MAPKs.

Additionally, the co-receptor Endoglin interacts with several BMP- and TGFβ-receptors, enhancing complex formation and signaling.[62] The co-receptor DRAGON, a glycosylphosphatidylinositol (GPI)-anchored membrane protein of the repulsive guidance molecule (RGM) family, binds directly to BMP-2 and BMP-4, directing the ligands to BMP receptors, thereby potentiating BMP signaling.[74] Other members of the RGM family like RGMa and RGMc (HFE2) share similar modes of action to DRAGON (RGMb).[112] In contrast, the BMP and activin membrane-bound protein BAMBI, a pseudo-receptor lacking an active serine/threonine kinase domain, competes with type I receptors for heterodimerization and growth factor binding, thereby negatively regulating signal transduction.[74] Other receptor interacting proteins, such as the tight-junction protein angiomotin (AMOT130), a receptor adapter protein, driving cell proliferation and migration at the apical side of polarized cells, at which BMP signaling is enhanced by receptor-induced SMAD1 phosphorylation and increased cellular SMAD response.[113] The immunophilin protein FKBP12 was reported to interact with TGFβ type I receptors and preventing receptor internalization in a negative manner. It was further found to suppress ALK2 and disrupting receptor response to ligand activation.[114]

Cellular sensitivity and response to BMP ligands also depend on the quality and quantity of receptor assembly at the cell surface. Endocytosis and internalization mechanisms of the receptor complexes on the cell surface determine different signaling cascades.[62] In multiple studies, the group of Petra Knaus has shown that BMPs can bind to BMP type I receptors, thereby recruiting complex formation with type II receptors, which is termed the BMP-induced signaling complex (BISC) formation, or by direct binding to preformed receptor complexes (PFC).[115,116] Ligand binding to PFCs induces SMAD1/5 phosphorylation and clathrin-dependent internalization, hence SMAD signaling transduction is initiated. Activated receptor complexes are recruited by the adaptor protein 2 forming a clathrin-coated pit (CCP), inducing receptor endocytosis and recycling, leading to enhanced BMP signaling and continuation.[117] In contrast, the ligand-induced BISC complexes initiate the formation of caveolaes and caveosomes, resulting in signal attenuation through SMAD-independent MAPK/ERK, PI3K and p38 pathways.[115] The latter leads, in part, to the expression of the osteogenic marker alkaline phosphatase (ALP) in C2C12 cells, indicating specific BMP signaling for cell fate decisions.[116] More specifically, type II receptors interact with different components of lipid rafts, such as the scaffold component Caveolin-1 and undergo slow internalization via Caveolae, supported by cholesterol-rich membrane microdomains.[118] This process reduces

BMP type II receptor levels in the membrane, inhibits further activation of BRI in PFCs and attenuates SMAD signaling.[119] Following internalization, BMP receptors are directed to different membrane compartments that determine the signal transduction, whether direct recycling to the cell membrane and signal renewing, lysosomal proteolysis, or endosomal translocation is processed.[115] The different internalization pathways are also determined by receptor mobility and is dependent on the cellular context, cholesterol concentration and caveolin expression.[120] It is assumed, that low concentrations of BMP ligands predominantly bind to PFCs, while increased concentrations re-balance the ratio of PFCs and BISCs, indicating an additional important regulatory mechanism for BMP gradients in embryonic development and differentiation.[121]

Moreover, receptors are directly regulated by SMADs. For example BMP type I receptors ALK3 and ALK6 are negatively regulated by inhibitory SMAD6 via binding of the *N*-terminal lobe to the MH2 domain, thus inhibiting phosphorylation.[122] In contrast, I-SMADs, of which SMAD7 is more selective for TGFβ signaling, function on multiple levels of signal transduction and are transiently upregulated upon BMP and TGFβ activation, thereby initiating a negative-feedback loop, as illustrated in Figure 4.[74,82] Firstly, they inhibit R-SMAD phosphorylation by receptor binding and recruit the Smad ubiquitin regulatory factor 1/2 (Smurf), an E3 ubiquitin ligase, leading to proteasomal degradation and downregulation of the receptors.[123] Both Smurfs differ in their selectivities within the TGFβ superfamily, as Smurf1 mainly interacts with SMAD1/5, whereas Smurf2 interferes with all R-SMADs.[124] Other E3 ligases, such as Hsc70 interacting protein (CHIP) or SCFβ-TrCP1 can ubiquinate SMADs similar to Smurf1.[125] Secondly, I-SMADs act intracellularly by competing with the co-SMAD4 and oligomerization with activated R-SMADs. For instance, SMAD6 can form a complex with SMAD1, thereby enhancing SMAD degradation via Smurf1 recruitment and hence reducing the cellular abundance.[123] In addition, nuclear I-SMADs are also translocated to type I receptors, upon Smurf1 and -2 recruitment, enhancing the receptor suppression.[126] Another study has shown, that SMAD6 interacts with TAK1 to inhibit non-canonical signaling in addition to negatively regulated SMAD signaling.[96] Beside receptor and intracellular SMAD regulation, both I-SMADs were reported to inhibit the transcription of specific genes. In particular, SMAD7 interferes with signaling in the nucleus via binding to the SMAD-binding element of the promoter, thereby disrupting transcription factor complex formation.[127] Generally, this mechanism is mediated by direct binding to specific DNA-binding domains, or indirectly by recruitment of co-repressors such as CtBP and inhibition

of histone deacetylases, thereby repressing transcription factor binding. Regulatory SMADs are also regulated on their linker regions, that contain highly conserved phosphorylation sites for glycogen synthase kinase 3 (GSK3) and MAPKs.[128] Subsequent phosphorylation by MAP kinases of activated SMADs occurs in the nucleus and GSK3 generates a highly phosphorylated SMAD with increased Smurf1 affinity and recognition, thus inducing R-SMAD degradation and downregulation, whereas Wnt activation results in GSK3 inhibition, thereby promoting BMP signaling in many tissues.[128] Specific phosphorylation by nuclear Cyclin-dependent kinases (CDKs) 8 and 9 at the linker region, enables SMAD1-dependet recruitment of YAP and Hippo signaling, thereby enhancing transcription of *Id1*.[129] Generally, the linker region serves as regulatory platform, which can be regulated by different signaling pathways. In addition to the linker region, the *N*-terminal SSXS motif, can be dephosphorylated by phosphatases like PPM1A/PP2Ca or small *C*-terminal domain phosphatases (SCPs).[74]

Despite negative feedback loops, there are several factors that enhance R-SMAD phosphorylation and activation, such as the endosome-associated FYVE domain protein (Endofin), which binds to SMAD1 as an anchor, promoting its nuclear translocation.[130] Interestingly, Endofin can also regulate dephosphorylation of BMP type I receptors in a negative manner (Figure 4). This biphasic mode of action seems to be important for bone formation and skeletal angiogenesis, highlighting the specific cellular sensitivity to BMP signaling.[131] There are also factors that can regulate negative factors like Tribbles-like protein 3 (Trb3), which regulates negative feedback of Smurf1 by driving the degradation of Smurf1, leading to potentiation of transient BMP signaling.[74] Similarly to Trb3, the cyclic guanosine 3′,5′-monophosphate (cGMP)-dependent kinase I (cGKI) is released from the receptor after ligand binding, associates with R-SMADs and enhances BMP target gene expression. This kinase also regulates and maintains type II receptor phosphorylation and activation, indicating a dual mode of action of transient pathway regulation.[132]

Moreover, BMP signaling is crossregulated by other signaling pathways and cytokines, which can additionally control BMP-dependent cell fate decisions, for example osteoblastic differentiation, which is explained in more detail in chapter 1.4.3. One main regulator of SMAD signaling is the Wnt/β-catenin signaling pathway, which stabilizes and potentiates BMP outputs in two ways. Firstly, Wnt inactivates GSK3β, thus reducing R-SMAD ubiquitination and induces stabilization of R-SMADs.[128] Secondly, Wnt activation ultimately leads to β-catenin

accumulation and nuclear translocation, where it can form a cooperative transcription factor complex with SMADs acting as a key module for specific master genes.[133] Both pathways act cooperatively in osteoblastogenesis, inducing target gene expression of BMP and Wnt target genes, leading to subsequent expression of the osteogenic transcription factor Osterix. However, in contrast to the synergistic responses, BMP signaling disturbs β-Catenin nuclear translocation in mesenchymal stem cells (MSCs) by recruiting SMAD1 to the Wnt mediator Dvl1.[134]

Another key modulator of BMP signaling, the Sonic Hedgehog (Shh) pathway, is crucial for embryonic development, bone formation and homeostasis.[135] Once activated by Shh, the transcriptional repressor Gli3 is replaced by the activator Gli2 to induce target gene expression of BMP ligands such as BMP-2, -4 and -7.[135] Conversely, BMP-2 and -4 induced SMAD5 was reported to antagonize Shh signaling via transcriptional repression leading to downregulation of Shh pathway components and inhibition of cell proliferation.[136] In addition, BMPs act in a negative feedback loop to regulate Shh gradients during limb development and in organogenesis, indicating a critical circular regulation of both pathways in cellular differentiation.[137] Another pathway with regulatory roles in cell fate decisions is the Notch signaling pathway, that can interact with BMP in a synergistic manner. Ligand binding induces proteolytic cleavage and release of the Notch intracellular domain of the Notch receptor, which translocates to the nucleus initiating gene expression of Notch target genes like *Hes-1* and *Hey-1*. Expression of these genes has been shown to be enhanced by BMP-4 induced SMAD1 in C2C12 cells.[138]. While these results indicate a clear synergistic effect of Notch and BMP, in endothelial cells Notch and BMP signaling result in functional antagonism.[139] Furthermore, BMP signaling can be regulated by cytokines that induce MAPK signaling and SMAD1/5 linker phosphorylation, thus resulting in SMAD inhibition. These include Ras/MAPK-mediated effects of fibroblast growth factors (FGF).[140] Whether signaling pathway cross-talks result in a BMP synergistic or antagonistic manner strongly depends on the cellular and tissue context.

1.4 Physiological functions of BMPs in development and diseases

1.4.1 Early development

Patterning of the dorso-ventral axis is of great importance in early development of vertebrate embryos. In the blastoderm, BMPs are highly expressed and upon early gastrulation antagonists secreted by the Spemann organizer to establish a BMP gradient across the blastoderm.[141] The Spemann organizer is a dorsal BMP-negative region to control BMP levels, thus forming the dorsal-ventral axis, as shown in Figure 5.[142] Interestingly, in course of the revolution BMP-dependent axis formation was inversed from dorsal to ventral fates, as shown for *Drosophila* and *Xenopus*.[143] The indirect mechanism of dorsal patterning relies on the antagonistic inactivation of highly concentrated auto-activating BMP-2/-4/-7 by Noggin and Chordin.[141] In addition to Noggin and Chordin, nuclear β-catenin, that induces Chordin expression, and the secreted Cerberus are required for BMP inhibition, hence establishing ectoderm fate.

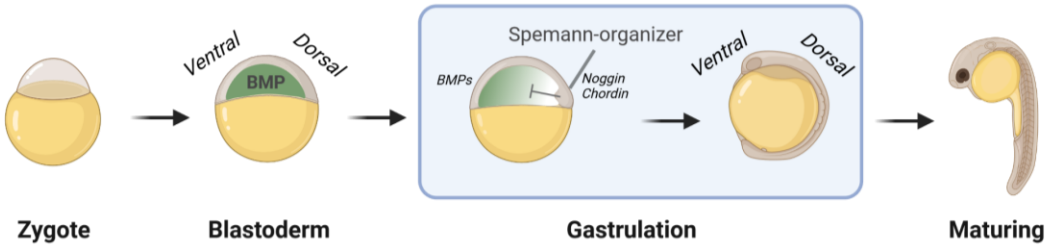

Figure 5: Schematic patterning of dorsal-ventral axis formation in a zebrafish embryo. In the early gastrulation of the blastoderm, the Spemann organizer secrets BMP antagonists to form a BMP gradient and establish the dorsal-ventral axis. The figure was created with BioRender.com and modified from Little et al. and Sieber et al.[62,141]

Besides key roles as morphogens during embryonic patterning, BMPs are critical regulators of self-renewal and mesoderm induction of pluripotent stem cells. The BMP target genes of the Id family were found to encode negative regulators of the bHLH family, thereby suppressing activation of lineage-specific transcription factors to inhibit cell differentiation in murine embryonic stem cells and sustain pluripotency.[77,144] The leukemia inhibitory factor (LIF) is a critical suppressor of differentiation in cooperation with BMP via the LIF-activated transcription factor STAT3. More importantly, LIF/STAT3 signaling alone is not sufficient to maintain pluripotency and LIF withdrawal enhances BMP-induced ESC differentiation to mesoderm. The major effect of BMP-4 in maintaining pluripotency depend on ERK and MAPK pathway inhibition.[145] In addition to combinatorial LIF and BMP activation via growth factor treatment,

a “cocktail” of small molecules consisting of FGF, ERK and GSK3β inhibitors was identified to maintain mESC self-renewal.[146] Furthermore, transient inhibition of BMP signaling induces the differentiation of mesendoderm to cardiomyogenic tissue during gastrulation, that indicated the important role of BMP in cardiogenesis and is explained in more detail in the next chapter.[147]

In contrast to murine ESCs, BMP-4 acts as a mesoderm inducer in human ESCs. In hESCs, inhibition of BMP signaling is required in combination with Activin A, Nodal, FGF and Insulin-dependent pathways.[148] When hESCs are treated with BMP-4, they exit the pluripotent state and irreversibly commit to mesoderm differentiation. This was shown to depend on BMP-4-driven transient induction of GATA3, highlighting the fundamental relevance of BMP-4 in early differentiation.[149] Moreover, BMP signaling is important not only for exit from pluripotency but also for cellular commitment to early mesendodermal stages and subsequent cardiac differentiation of hESCs.[150]

1.4.2 Cardiogenesis

In 2001, the first report was published on the spontaneous differentiation of human ESCs into beating cardiomyocytes.[151] Since then, major efforts were made to study and improve a directed cardiomyogenic protocol in order to increase quantity and quality of generated cardiomyocytes.[152] In general, four main steps are required in order to successfully differentiate ESCs into functional cardiomyocytes. First, induction of primitive streak and mesoderm formation (marked by T/Brachyury) is induced, followed by mesoderm structuring (Goosecoid [Gsc] and Mesoderm posterior-1 [MESP1]), cardiac mesoderm induction (NKX2.5 and MEF2c), and finally, induction of cardiomyocyte formation and maturation (αMHC/MYH6, cTnnT).[11,153]

These processes are largely controlled by three signaling pathway families, i.e. TGFβ/BMP, FGF and Wnt.[153] Their secreted cytokines, such as Activin A, BMP-4 or Wnt3a form gradients and define structural patterning of the cardiac tissue. Further, formed mesoderm posterior cells contribute to the heart structures of the different heart fields, in which the interplay between BMP, FGF, Hedgehog and Wnt at various stages determines cellular expansion and differentiation.[153,154] BMP signaling plays a crucial role in the developing myocardium, where BMP-2 and -4 are essential for atrioventricular (AV) formation and septation of the heart.[155]

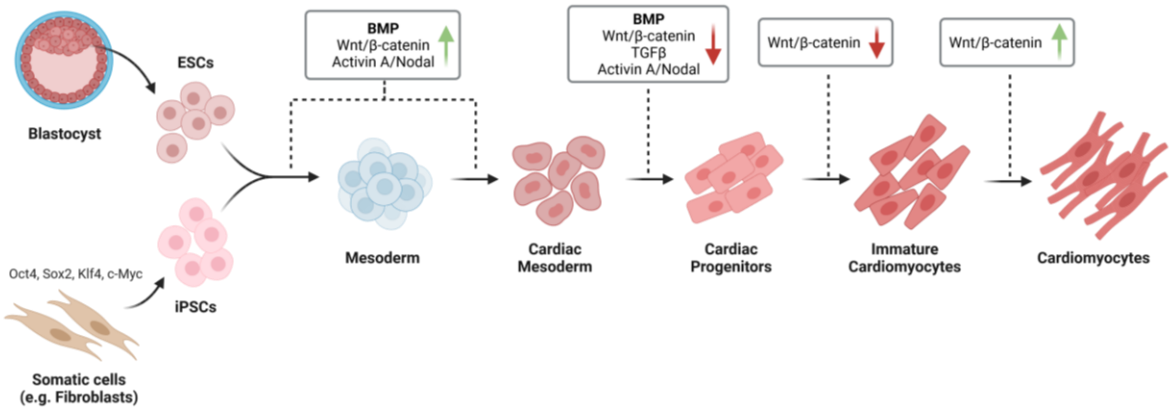

Figure 6: Schematic illustration of the route from stem cell to cardiomyocyte. For directed cardiac differentiation of hESCs or hiPSCs, key signaling pathways need to be modulated during (cardiac-) mesoderm induction, cardiac specification, cardiomyocyte formation and maturation. Highlighted here are the biphasic regulations of BMP and Wnt/β-catenin signaling. Arrows indicate activation or inhibition of the pathways. The figure was created with BioRender.com and modified from Schade and Plowright, 2015 and Später et al., 2014.[11,153]

For the directed differentiation of hiPSCs and hESCs into cardiomyocytes, both BMP and Wnt signaling exhibit multiphasic roles.[11] BMP-4 or Wnt signaling activation drive mesodermal differentiation, followed by inhibition to initiate cardiogenic mesoderm formation.[156] Later differentiation of cardiac progenitor cells depends on DKK1-mediated Wnt downregulation and induction of MESP1, which was considered as the master regulator for cardiac specification, promoting subsequent expression of cardiac mesodermal marker, such as GATA4, NKX2.5, MEF2C and others.[157,158] However, the transcription factor EOMES was found to be the key factor decisive for the formation of cardiac cell lineages from hESCs, mediating MESP1 target gene expression.[159] In addition, Id gene upregulation has been shown to be essential for specifying mesoderm to cardiac cell fate in hESCs.[160] The Greber group conducted a detailed study to determine the key requirements for optimal BMP and Wnt activation for cardiac induction of hESCs.[150] They highlighted the cooperative activation of both signaling pathways at an optimal induction level within a “cardiac corridor" in which EOMES was induced, whereas subsequent cardiac specification was depended on Wnt inhibition. In contrast, in mESCs, each BMP and Nodal signaling must be inhibited to induce differentiation of progenitor into cardiogenic mesoderm, whereas late-stage cardiac progenitor specification is again determined by BMP signaling.[161,162] These findings emphasize the regulatory importance of BMP signaling in cardiac differentiation and specification. It is important to note that differentiation protocols also vary depending on 2D- versus 3D-formats, highlighting the relevance of organism context and complexity in differentiation studies.[163]

In an extensive report, a detailed protocol for hiPSC-derived cardiomyocytes was summarized and discussed, using a cocktail of various factors such as BMP-4, Activin A, FGF and small molecules for optimal mesoderm induction of embryoid bodies.[25] To date, several cardiopoietic small molecules that modulate mesoderm induction and/or determine cardiomyogenic cell fates have been reported and used in cardiac differentiation protocols. In particular, BMP and Wnt signaling modulators were identified as potent cardiomyogenic probes, that also gave new insights in the signaling dependency of certain pathways and their biphasic nature during cardiac differentiation (see Figure 6).[11] In the past decade, potent hESC mesoderm inducers like the GSK3β-targeting Wnt activators CHIR99021 and BIO have been discovered.[150,164] Wnt inhibitors such as XAV939, Wnt-C59, or the inhibitor of the canonical Wnt signaling response 1 (IWR-1) and its analogs, efficiently promoted late-stage cardiomyogenic differentiation.[11,165–168] Moreover, various cardiopoietic inhibitors of the BMP, TGFβ, Wnt and Nodal developmental signaling pathways have been reported, such as Dorsomorphin, SB431542, or A-83-01 (see Figure 7).[162,169,170]

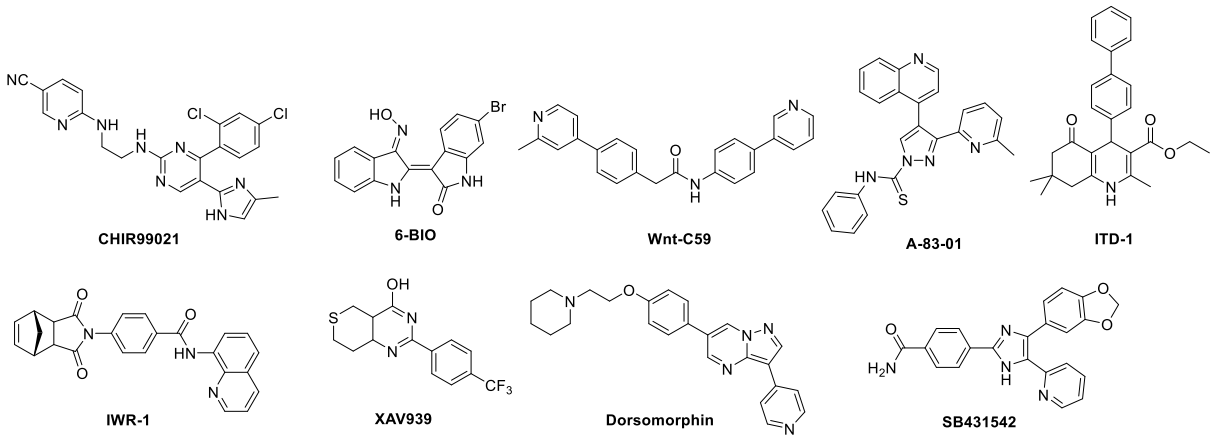

Figure 7: Chemical structures of selected cardiopoietic small molecules for directed differentiation of stem cells via the modulation of distinct developmental signaling pathways.

Remarkably, the potent cardiac inducer ITD-1 was identified as a selective inhibitor of TGFβ signaling by mediating the degradation of TGFβRII.[171,172] Since these cardiac modulators have been found mainly in phenotypic screening assays, they generally lack selectivity among TGFβ superfamily-related receptors, and further optimization studies are needed to overcome selectivity and improve efficacy. Moreover, due to the biphasic behavior of Wnt and BMP signaling, balancing in early cardiac development is critical for specific lineage commitment of hESCs and hiPSCs.[11,150] As a result of the great interest in the chemical modulation of these

cardiopoietic signaling pathways for efficient generation of cardiomyocytes, selective cardiomyogenic small molecules are still being pursued.

Here, recent advances in the growing field of synthetic embryology hold promise for the generation of cardiac organoids. Lineage-specific self-organizing organoids and gastruloids have been successfully formed from hESCs, albeit with limitations in reproducibility.[173] In gastruloid-like systems, BMP-4 was found to enhance the intrinsic tendency of hESCs to form primitive streak and human organizer during early embryonic development.[174,175] Recently, the first iPSC-derived self-organizing gastruloids have been reported to form complex heart-like cardioids.[176] When recapitulating the architecture of cardiac lineage, the Wnt-BMP signaling axis was found to be critical for cavity formation during mesoderm formation and specification for self-morphogenesis. In a similarly established protocol, small aggregates of mESCs formed self-organizing cardiac precursor gastruloids of embryonic hearts with pronounced heart fields and beating domains.[177] While these technologies are limited in terms of reproducibility and are not yet screening-ready, they represent fundamental steps for future drug development and graft formation.

1.4.3 Osteogenesis

The eponymous function of bone morphogenetic proteins is their role as major regulators and inducers of bone morphogenesis, homeostasis, and bone remodeling. Additional signaling pathways are involved in these processes and in differentiation of the mesenchyme, such as Wnt, Hedgehog, MAPK p38, Notch, PI3K/Akt, IGF or Ca^{2+} regulation.[178] Still, the BMP/SMAD-signaling pathway represents most important and associated with diverse and severe bone diseases when dysregulated. In early embryonic development, mesenchymal stem cells (MSCs) are formed from neural crest and mesoderm, and undergo ossification, forming cartilage and osteoblasts for skeletal development.[86,179] Bone tissue consists of different homeostatic cells and an extracellular matrix (ECM), that is formed by hydroxyapatite, collagen fibers, different glycans and bound BMP/TGFβ cytokines. Homeostasis of bone tissue is generally regulated by different cytokines but is has been shown that mechanical inputs from the environment affect bone tissue in a mechano-BMP crosstalk dependent manner.[180] In contrast to BMP, TGFβ signaling has distinct functions in skeletogenesis, including the regulation of osteoclast activity, and thus, bone resorption or cartilage homeostasis.[181] TGFβ

mediates RANKL-induced osteoclast regulation through SMAD2/3-signaling. However, BMP-2/SMAD signaling also stimulates bone resorption activity of osteoclasts but is unable to increase survival rate, indicating a regulatory mechanism of the co-factor SMAD4 in bone homeostasis.[86,182] Osteoblastogenesis of MSCs undergoes different stages with gradual reduction in proliferation potential, subsequent differentiation of osteoblasts and bone matrix formation. While early progenitor cells are still committed to chondrogenic differentiation in response to Sox-9 induction, once pre-osteoblasts are formed they cannot differentiate to chondroblasts anymore.[183] As illustrated in Figure 8, the differentiation is typically defined in three different stages: Firstly, osteoprogenitors start proliferating and growing, followed by maturing process in which they exit cell cycle and secrete components of the extracellular matrix. Subsequently, mature osteoblasts secrete osteocalcin, which promotes mineralization and tissue scaffolding of the osteoblasts.[183,184]

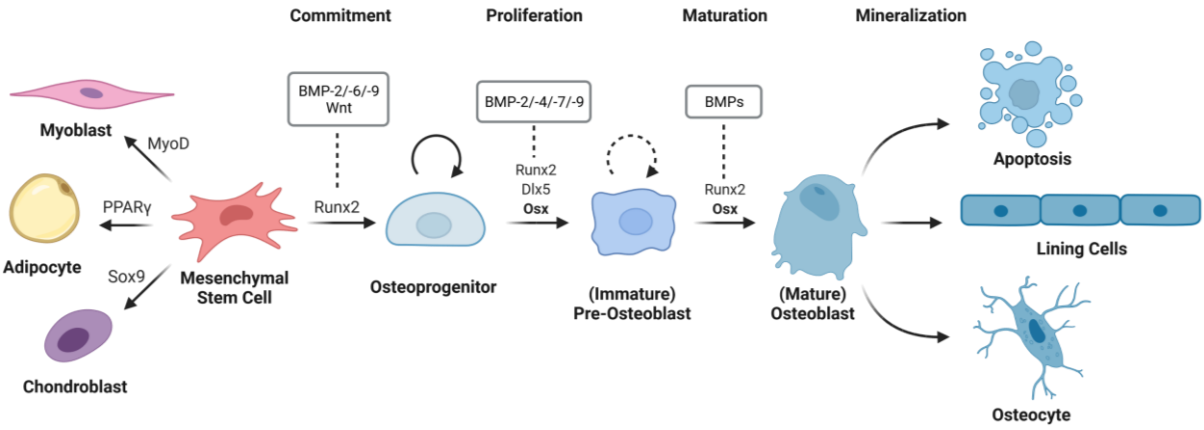

Figure 8: Schematic illustration of BMP-dependent osteoblastogenesis. BMP and Wnt signaling direct MSCs towards osteogenic cell lineage via the key osteogenic regulator Runx2. Successive induction of osteogenic transcription factors Runx2 and Osterix drives osteoblastic differentiation and maturing process of pre-osteoblasts. Until maturation, osteoprogenitors and pre-osteoblasts proliferate, while osteoprogenitors may still have the potential to undergo chondrogenic transition. Terminal mineralization of bone tissue is induced by various non-collagenous proteins and hydroxyapatite, forming the extracellular matrix with incorporated osteoblasts, while some further differentiate into osteoclasts or undergo regulated apoptosis.[183,184]

BMP ligands have diverse roles in regulating lineage commitment of mesenchymal stem cells (MSCs) to different fates by sensitive balancing specific transcription factors like osteogenic Runx2, chondrogenic Sox9, adipogenic PPARγ, and myogenic MyoD, the so-called “master transcription regulators”.[185] Among these, BMP-2, -4, -6, -7, and -9 were shown to induce and enhance osteogenesis and bone formation. In early osteogenesis, BMP-2, -6, and -9 may play a more important role in the induction of osteogenic differentiation, as shown for the MSC-like C3H10T1/2 cell line, whereas BMP-2, -4, -7, and -9 strongly induce the induction of

osteoprogenitors.[186] In contrast, BMP-4 alone promotes adipogenic commitment of MSCs, while BMP-2 was not.[187] Moreover, BMP-2 and -9 can promote *Sox9*-mediated chondrogenic differentiation in mice.[188]

In murine C2C12 myoblasts, osteoblastic MC3T3-E1 and mesenchymal C3H10T1/2 cells, mechanistic studies on BMP-dependent osteogenesis were performed over the last two decades. The myoblast-to-osteoblast transition of C2C12, which are close to osteoprogenitors in their cellular BMP response, was shown to depend on osteogenic induction of *Hey1*, *Tcf7* or *Runx2* and simultaneous suppression of myogenic genes like *myogenin* and *MyoD*.[186,189] BMP-dependent induction leads to the expression of transcription factors that determine osteoblastic fates, such as Runx2, Osx, Dlx3/5 or Msx2, with the subsequent expression of characteristic structural components like Osteocalcin, Osteopontin or bone sialoprotein.[133,183] Runx2 is essential for the induction of several further osteogenic factors, whereas Osx is highly expressed upon osteogenic input, strongly promoting gene expression, which is why both transcription factors are considered as master osteogenic factors.[190] In addition, Runx2 is activated and induced upon BMP addition, but its activation does not solely depend on SMAD1/5 signaling, yet it is necessary to induce osteogenic commitment.[191] The important role of p38-mediated signaling in osteoblastogenesis was shown in C2C12 and MC3T3 cells for critical BMP-2-dependent *Dlx3* expression.[99] Especially in early phases of osteogenic differentiation, SMAD5/p38 signaling is essential, but p38 alone was insufficient to mediate osteogenesis.[192] In MC3T3 pre-osteoblasts, Runx2 transcription is enhanced by p38- and ERK-mediated phosphorylation.[193] Further, ALP expression was found to be induced by BISC-mediated BMP signaling, that initiates the activation of SMAD-independent, but p38-dependent pathways.[194] Moreover, multiple studies on osteoblast differentiation and maturation indicate p38 signaling as a central hub for lineage commitment and subsequent osteoblastogenesis.[193]

Similar to the specific physiological roles of BMP ligands for lineage commitment of MSCs, cellular responses are also determined and mediated by specific receptor densities and compositions. During chondrogenesis, myogenesis, osteogenesis and osteoclastogenesis of MSCs, the three type I BMP receptors ALK2, ALK3 and ALK6 play different roles.[195] Particularly, ALK2 is essential for osteogenic commitment of MSCs and for osteoblastic differentiation of myoblasts, while it is involved in the repression of myogenesis as shown for C2C12 myoblasts.[195] ALK3 exhibits quite similar roles to ALK2, however, its function becomes more relevant in the maturing process of osteoblasts and in the regulation of osteoblast and

osteoclast formation or transition. In osteoblasts, ALK3-mediated signaling regulates osteoclastogenesis and bone resorption depending of Wnt signaling pathway activity.[195,196] The role if ALK6 is more specialized towards regulation of chondrogenesis and proliferation of chondrocytes, while it has minor influence in osteogenesis. Due to the regulatory properties of each individual BMP ligand or receptor, dysregulations cause imbalances in cell commitment and differentiation, leading to severe skeletal diseases.

1.4.4 Pathology and Diseases

The BMP signaling pathway is highly conserved and involved in many cellular processes, tissue development and homeostasis. In this chapter, an overview about prominent human pathologies is given, with a focus on human bone and skeletal diseases, where dysregulated BMP signaling plays a major role. A balanced regulation of BMP signaling in the bone is critical for development and homeostasis. Various mutations in the pathway can cause dysregulation and bone diseases, such as osteoporosis.[14] In osteoporosis, the bone resorption rate is higher than actual bone formation, hence bone matrix is steadily degraded. In general, this is caused by low BMP activity in bone tissue as shown specifically for BMP-2.[197] In line with BMP downregulation, overexpression of endogenous BMP inhibitors Noggin or Gremlin are associated with osteoporosis and spontaneous bone fractures.[198] A similar endogenous balancing mechanism in bone formation is based on BMP-induced expression of *SOST*, a gene encoding for Sclerostin. Mutations in *SOST* lead to an increase in bone density, bone thickening and deformations.[199,200] When overactivated, BMP-2 promotes joint degeneration of articular cartilage osteoarthritis (OA) and high levels of BMP-2 and -4 were found in patients with degenerative joint disease.[201] In contrast, BMP-7 showed stimulative effects in cartilage repair and symptom improvement in a clinical study.[202] *Fibrodysplasia ossificans progressiva* (FOP) is a rare disorder, that causes heterotopic ossification of soft tissues like muscles, tendons and other.[203] The phenotype is associated with mutations in the BMP type I receptor ALK2 transcribing an activating variant, of which a critical and well-characterized mutation is R206H.[204] This gain-of-function mutation is independent from BMPR2 activity, ligand binding, and has a decreased binding affinity to FKBP12. In addition, mutated ALK2 becomes neomorphic for Activin A, which can be rescued by Saracatinib as shown in an iPS-derived FOP model.[205] There are other bone disease causing mutations, such as *Brachydactyly* type

A2/B as a result of inactivating mutation in the ALK6 receptor, a missense mutation of Noggin or a nonsense *Runx2* mutation.[206,207] The expressed truncated Runx2 cannot interact with SMAD anymore, impairing BMP-dependent osteogenic induction. This mutation is associated with the human bone disease *cleidocranial dysplasia* (CCD) and other skeletal disorders and dental abnormalities.[208] Interestingly, a recent study reported a novel Runx2 stabilization pathway through CK2 directed deubiquitylation, whereas pathway attenuation mediates heterotopic ossification and dysregulated mineralization.[209]

Besides osteopathic BMP dysregulations, disrupted BMP signaling is also associated with cardiovascular diseases, such as pulmonary arterial hypertension (PAH).[203,210] Typically, PAH is caused by low BMPR2 levels or mutations in BMPR2, leading to attenuated BMP signaling. It is assumed, that different mutations might lead to altered cellular localizations due to perturbed receptor endocytosis via caveolae or CCPs.[211] PAH is also linked to the autosomal dominant gene disease hereditary hemorrhagic telangiectasia (HHT), also known as Osler-Weber-Rendu syndrome, with fragile blood vessels in skin and organs.[210] Different types are caused by mutations various factors like BMP co-receptor Endoglin, SMAD4 or ALK1 mutants, which are associated with impaired BMP-9 signaling causing HHT in abnormal endothelial cells.[203]

Furthermore, BMP signaling is involved in differentiation of MSCs to adipocytes.[212] In white adipocytes, BMP-4 and -7 were linked to white-to-brown transition in human adipose tissue and may represent a therapeutic target for treating obesity.[213] In addition, alterations in ALK3 expression are linked to nondiabetic human obesity as well as single nucleotide polymorphisms in BMPR2 encoding gene.[203] BMP dysregulation is also associated with glucose homeostasis, diabetes and diabetes-dependent cardiovascular diseases.[214] In particular, BMP ligands have distinct effects on glucose homeostasis and insulin resistance, as BMP-7 was shown to be beneficial for insulin signaling, increasing glucose uptake and body fat reduction, whereas BMP-4 enhanced insulin resistance. In mature adipocytes, BMP-2 and BMP-6 treatment led to an increase of glucose-uptake by sensitizing the cells to insulin.[214] BMP-2 has an interesting role in diabetic retinopathy (DR), where it was shown to be upregulated and the main driver of retinal inflammation, causing progressive vision loss.[215] Along with BMP-4, it destabilizes the blood-retinal barrier, that leads to a pathological environment under diabetic conditions and to the development of microvascular dysfunctions.[216]

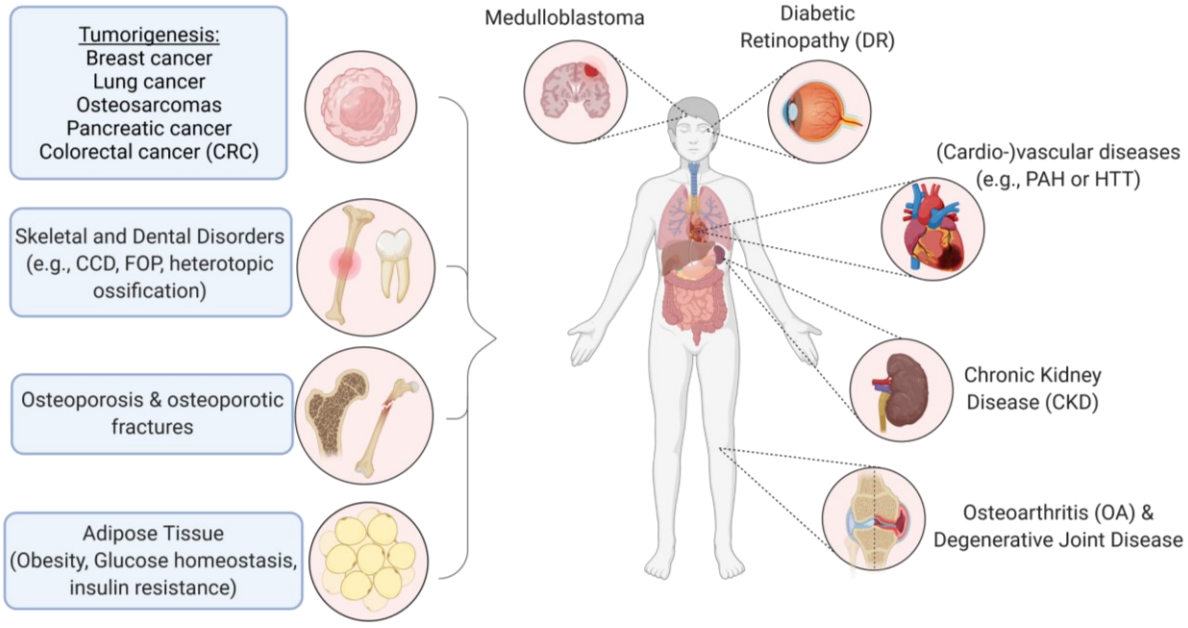

Figure 9: Representative overview about human pathologies and diseases caused by or associated with dysregulated BMP signaling. CCD: *Cleidocranial dysplasia*; FOP: *Fibrodysplasia ossificans progressiva*; HHT: Hereditary hemorrhagic telangiectasia; PAH: pulmonary arterial hypertension.

BMP signaling has divergent roles in cancer development, progression and in affecting tumor microenvironments, as it can promote or suppress tumorigenesis in a context-dependent manner.[217] In breast cancer patients, BMP signaling is generally overactivated, thereby promoting cancer progression and metastasis. For instance, in approximately 50% of primary tumor samples from breast carcinomas, BMP-7 was overexpressed and led to accelerated bone metastasis.[218] Additionally, BMP-4 was identified to enhance epithelial mesenchymal transition (EMT) in combination with activated Notch signaling in cancer stem cells of breast cancer cells, that promotes expression of cancer markers, and ultimately leads to MSC proliferation and cancer metastasis.[219] In hepatocellular carcinoma cells, BMP-9 induced EMT, hence initiated proliferation and metastasis.[217] Aberrant BMP activation through BMPRIB expression in breast cancer contributes to high tumor proliferation and is associated with poor prognosis especially in estrogen receptor-positive carcinomas.[220] BMP ligand overexpression has also been linked to different malignant melanoma cells and they have been found to interact with and activate β-integrins, thereby enhancing human prostate cancer cell or osteosarcoma migration.[221,222] In non-small cell lung cancer (NSCLC), BMP-2 and other ligands are highly overexpressed, due to genetic alterations among all different types of lung adenocarcinomas, whereas BMP receptor mutations are generally rare.[223] For these types of cancer, BMP inhibitors have been shown to be effective.[224,225] In general, it seems that the

degree of BMP overactivation positively correlates with the progression stage and metastatic aggressiveness in lung cancer.[226] However, BMP downregulation can also promote carcinogenesis and metastasis. For instance, very lethal pancreatic cancer is formed by aberrant SMAD4 levels and reduced BMPRIA expression and is highly associated with invasion and poor survival.[227] In addition to these findings, various BMPs were associated with increased proliferation of specific types of human pancreatic cancer cells, indicating diverse roles of dysfunctional BMP signaling in in the pancreas.[203] In colorectal cancer (CRC), nuclear β-catenin is highly accumulated in SMAD4 negative cells, that leads to aberrant BMP signaling and enhanced Wnt signaling.[217]

Taken together, dysregulation of BMP signaling can lead to a variety of diseases underlying an urgent need for novel therapeutic agents that either inhibit or activate BMP signaling, ideally in a cell and disease context-specific manner.

1.5 Clinical use and (potential) therapeutic applications of BMP modulators

1.5.1 Recombinant human BMPs and agonists

BMPs are commonly recognized for their osteoinductive activity, with a high relevance for the development of new therapeutic approaches to address skeletal trauma and osteopenic diseases.[14] The clinical use of BMPs is primarily focused on bone grafting for the treatment of skeletal defects, trauma, degeneration, and other conditions, of which over 0.5 to 1.5 million bone-grafting procedures are performed annually in the U.S. alone.[228] Two recombinant human BMPs, rhBMP-2 (Dibotermin-α) and rhBMP-7 (Eptotermin-α) are approved by the FDA for clinical use, commercially named as InductOS®, InFUSE®, OP-1 Implant®, and OSIGRAFT®.[229] BMP-7 (OP-1, OSIGRAFT®, Opgenra®), is approved for the treatment of tibial diaphyseal fractures with delayed non-unions, long-bone non-unions, and for posterolateral lumbar spinal fusion in patients with spondylolisthesis.[229,230] In addition, Opgenra® has been shown to benefit autologous bone graft for lumbar pseudoarthrosis.[230] Recombinant human BMP-2 (InductOS®, InFUSE®) finds application for a variety of indications, including treatment of acute tibia fractures, long-bone non-unions or anterior lumbar interbody fusion.[229] Furthermore, in dentistry, rhBMPs have been indicated for the

treatment of alveolar ridge augmentation and maxillary sinus lift.[229] Especially for implant placement in dental applications, BMPs have been shown to promote implant wound healing and bone regeneration.[229] For bone remodeling and bone grafting, an osteoconductive microenvironment for rhBMPs is essential, so their application is associated with hydroxyapatite, tricalcium phosphate and calcium phosphate ceramics to increase resorption ratio and bioactivity of calcium phosphates.[228]

Despite the numerous application possibilities, rhBMP approvals are very limited due to occurring side effects and were even associated with increased cancer risk.[231] Moreover, due to their low bioavailability and stability, rhBMPs are administered at supraphysiological levels, that can cause severe adverse side effects (e.g., inflammation and heterotopic ossification). In addition, the impenetrable blood-brain barrier represents another major hurdle for therapeutic delivery of these proteins.[229,232] To overcome these problems, BMP mimetic peptides were designed and tested. In several studies, these peptides could enhance bioactivity *in vitro*, *in vivo* or in dental implants when immobilized on bioactive polymers or titanium surfaces.[233,234] Interestingly, a CK2 inhibiting peptide, CK2.3, was developed as an BMP activator by disrupting the CK2-mediated inhibition of ALK3, thereby activating BMP signaling in the absence of a BMP ligand.[235] Heterodimers, such as BMP-4/-7 with enhanced specificity and bioactivity *in vivo* are another promising strategy, as shown for tissue-engineered constructs.[236] Lack of extensive studies of engineered peptides *in vivo* still limit potential applications. So far, the osteogenic BMP-4 has no application in clinic, but it shares a great potential in bone repair and fracture healing. Moreover, BMP-4 is reported to induce chondrogenesis of mesenchymal stem cells under chondrogenic microenvironment conditions, thus promoting cartilage repair and maintaining regenerated cartilage of traumatic defects.[237] Hence, potential application for BMP-4 (and -2/-7) might be treatment of osteoarthritis (OA) and rheumatoid arthritis (RA), for which patients showed decreased levels of BMPs in chondrogenic synovial tissue.[238]

Another important role is assigned to BMPs in the treatment of cancer. In human osteosarcoma, cancer stem cell pools can be diminished by BMP-induced cell differentiation.[239] Similarly, it was shown that BMP-2 and -4 can induce the differentiation of proliferating primary granule cell precursor (GNP) medulloblastoma cells, the most common malignant brain tumor in children.[136] Constitutively active Shh signaling promotes proliferation, which is antagonized by BMP-2 and -4.[240,241] The irreversible terminal differentiation of these

tumor cells by BMPs might be utilized for potential therapeutic applications in cancer treatment and indicates the broad range of benefits of BMPs in the clinic. Further, in a majority of sporadic colorectal cancers BMP signaling is inactivated and it is assumed that mutations of BMP ligands are linked to higher colon cancer risks.[203,242] As an alternative to recombinant BMPs and related agonists, the inhibition of the antagonizing extracellular factors, such as Noggin or Gremlin, has been pursued. The potential application of an inhibitory antibody was proven for the treatment of pulmonary arterial hypertension and recovery of central nervous system.[233]

In summary, the many (patho)physiological functions of BMPs lead to a wide range of possible therapeutic applications. Recombinant BMPs are in clinical use, but potential small molecule drugs that mimic their physiological effects are rare. Genuine small molecule BMP mimetics or potentiators are highly desirable. Moreover, novel BMP mimetics would also be of great value for biotechnological applications, such as the chemically defined differentiation of human induced PSCs or human ESCs towards mesodermal lineages (e.g., MSCs, CMs).

1.5.2 BMP Modulators

The identification and characterization of highly selective BMP small molecule inhibitors and activators holds great promise for numerous applications in biomedicine. Several potential strategies are feasible to modulate cellular BMP signaling outputs.

In the past decade, few modulators have been identified by different screening approaches. Based on the discovery that Noggin promotes cardiac differentiation of mESC, early attempts were made to screen for cardiogenic BMP inhibitors.[147] The first reported chemical BMP modulator was Dorsomorphin (DM), or Compound C, which was found in a *Zebrafish*-based screen for compounds affecting dorsal-ventral axis formation.[243] DM effectively blocks Smad phosphorylation by inhibiting type I BMP receptors and was found to be a potent inducer of cardiomyogenesis in mESC.[169] To determine off-target effects of DM, subsequent selectivity studies were performed in which DM had significant activities against related receptors, such as TGFβ/Activin A and vascular endothelial growth factor (VEGF) receptors.[244] To date, it is also the only effective AMPK inhibitor, but due to its promiscuous properties, it is less considered for cancer studies.[245] To eliminate off-target activities and improve drug-like properties, structure-activity relationship (SAR) studies were executed. A potent and selective derivative was identified, dorsomorphin homologue 1 (DMH-1), which specifically targets ALK3

over other type I BMP receptors. Moreover, DMH-1 had no effect on VEGF signaling and was unable to inhibit VEGF-dependent Flk1/Kdr phosphorylation.[244] In a follow-up study, DMH-1 was shown to induce cardiomyocyte formation, similar to DM.[246] It was the first selective BMP inhibitor suitable for transient BMP inhibition for directed cardiac differentiation protocols and with *in vivo* efficacy for the suppression of tumor growth and metastasis in mice.[224] Further SAR studies gave insights into receptor selectivities, leading to additional potent BMP inhibitors such as the ALK2/3 selective LDN-193189 (LDN) and ALK2 selective ML-347.[247,248] In C2C12, DM and LDN blocked BMP-induced SMAD phosphorylation and non-canonical signaling via p38 MAPK, ERK and Akt pathway, while DMH-1 had no effect on noncanonical signaling in HEK293 cells.[244,249] In addition, Yu et al. gave first evidence for potential therapeutic applications of these inhibitors, as they showed a significant reduction of heterotopic ossification of FOP in mouse models, by antagonizing the constitutively active ALK2 receptor.[250] In several other studies, the antagonizing effect of LDN was validated *in vivo*, for instance in treating chronic kidney disease in mice via BMPR type I inhibition or BMP-4-driven prostate carcinogenesis.[251,252] LDN also attenuates atherosclerosis and calcification, as demonstrated in mice, but due to the unselective effects on TGFβR2 and VEGF its clinical safety is questionable.[253,254] To address these issues, lead optimization furnished LDN-212854, that showed improved affinity and selectivity for type I BMP receptors, while it remained potent in preventing FOP.[255,256] Further efforts have been made to identify ALK2-selective inhibitors, that led to the identification of K02288 in an ALK2 kinase screening of 2,000 compounds with an improved binding mode in the ATP binding pocket compared with LDN and without affecting TGFβ signaling.[257,258] *In vivo* tests in zebrafish confirmed the typical dorsalization phenotype and subsequent SAR studies delivered LDN-214117, which effectively binds to various ALK2 mutants, suggesting a lead compound for pre-clinical studies.[259] An extensive *in silico* screen provided new ALK2 lead structures and gave insights into the binding modes.[260] Moreover, stable macrocyclic BMP inhibitors were recently found to potently bind to the ATP binding pocket of ALK2 and antagonize ALK2-mutant induced osteogenic and chondrogenic differentiation in FOP *in vitro* models, revealing a new potential strategy for therapeutic BMP inhibition and FOP treatment.[261] Additionally, a decade after the identification of E6201 as a MEK-1 kinase inhibitor, a dual inhibition mode as an ALK2 inhibitor showed high efficacy against ALK2 mutant derived tumor cells.[262,263] Other derivatives of DM, based on the pyrazolo-[1,5-*a*]-pyrimidine core, have been repeatedly optimized, including

DMH-2. Newman et al. developed JL5 with further improved pharmacokinetics compared to DMH-2.[225] Interestingly, other bioactive compounds were found to affect BMP receptor signaling, such as Saracatinib or the PI3K inhibitor BYL719, which were found to inhibit heterotopic ossification caused by ALK2 mutations *in vivo*.[205,264]

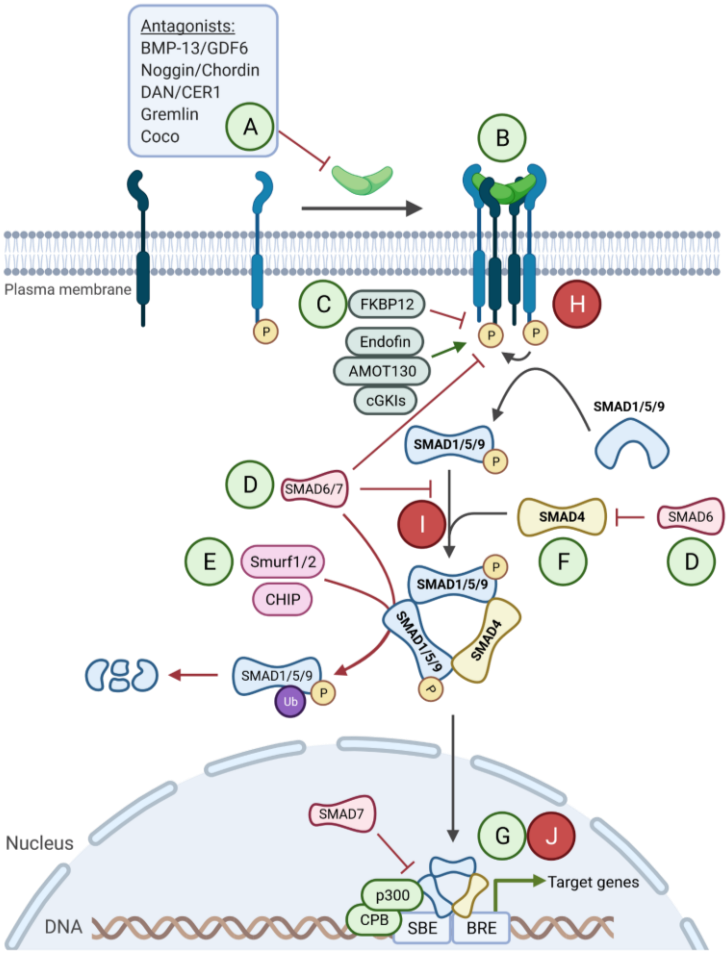

Figure 10: Overview of potential strategies to modulate the BMP signaling pathway. Activation can be modulated via inhibition of extracellular antagonists (A) with antibodies or small molecules and by receptor activation using novel agonists (B) or rhBMPs, alternatively. Further, BMP receptor-mediated activation might be enhanced with receptor stabilizers or downregulation of endogenous negative receptor regulators such as FKBP12 or CK2 (C). Multiple cytoplasmic SMAD regulators can be inhibited with small molecules, thereby enhancing SMAD signaling, such as inhibition of SMAD6/7 or Smurf1/2-mediated ubiquitination (D/E) and by regulating SMAD4 levels (F). In the nucleus various interactions with different transcription factors can be addressed to target selective gene expression (G) and binding to co-factors might be enhanced with small molecules. In contrast, inhibition of BMP signaling might be achieved by receptor kinase inhibitors (H), enhanced activation or expression of negatively SMAD regulators (I) or by inhibition of selective transcription factor complex formation in the nucleus and RNA-induced silencing (J).[233]

While several BMP inhibitors with *in vivo* efficacy have been developed, only few BMP activators have been reported. For instance, the marketed cholesterol-lowering drug Simvastatin, has been shown to promote osteogenic differentiation via enhanced BMP-2 expression.[265,266] The phosphodiesterase inhibitor Sildenafil was shown to potentiate BMP

signaling and is used for treatment of PAH, in which BMP activation is attenuated.[267] Furthermore, two studies recently reported on bacitracin and myricetin to enhance osteogenic differentiation of human stem cells via the BMP-2/SMAD pathway and in part, non-canonical signaling.[268,269]

The first screening approach for the identification of small molecule activators was reported 2013 by Vrijens et al., who discovered four different flavonoid derivatives, with the chalcone Isoliquiritigenin as an effective inducer of osteogenesis in C2C12 differentiation.[270] As the first reported attempt of screening for direct BMP activators, a stably transfected BMP-responsive element (BRE) *Id1*-luciferase reporter assay system in a human carcinoma cell line was utilized. In the following, Isoliquiritigenin was shown to induce p-SMAD1/5 levels and ventralize zebrafish embryos. However, the chalcone scaffold did not suit very well as a lead compound as it had typical properties of a PAIN compound.[56]

Table 1: Overview of identified BMP modulating small molecules in different screening approaches.

Modulator	**Modulation**	**Primary Screen**	**Volume**	***In vivo* functionalization**
Dorsomorphin	Inhibition	Zebrafish	7,500	Embryogenic and iron metabolism studies in zebrafish
K02288	Inhibition	ALK2 kinase screening	2,000	Zebrafish dorsalization
SVAK-12	Activation	*In silico* screen of Smurf-1 binding domain	70,000	-
Isoliquiritigenin	Activation	Stably transfected BRE-*Id1*-Luc in C33A-2D2	~5,600	Zebrafish ventralization
Ventromorphins	Activation	Stably transfected BRE-*Id1*-Luc in C33A-2D2	600,000	Zebrafish ventralization
FK506 (tacrolimus)	Activation	Stably transfected BRE-*Id1*-Luc in C2C12	3,756	Reversion of dysfunctional BMPR2 signaling in endothelial cells from patients with PAH
Benzoxazoles	Activation	Stably transfected BRE-*Id1*-Luc in HEK293	63,608	-
A01/A17	Activation	*In silico* screen of Smurf-1 binding domain	~100,000	-
PD407824	Activation	Transiently transfected BRE-*Id2*-LucGFP in C2C12	4,000	*In vitro* hESC differentiation
DIPQUO	Activation	ALP activity in C2C12	>47,000	Ossification in zebrafish
oxtFK	Activation	Stably transfected BRE-*Id1*-Luc in C2C12	250,000	AKI mouse model

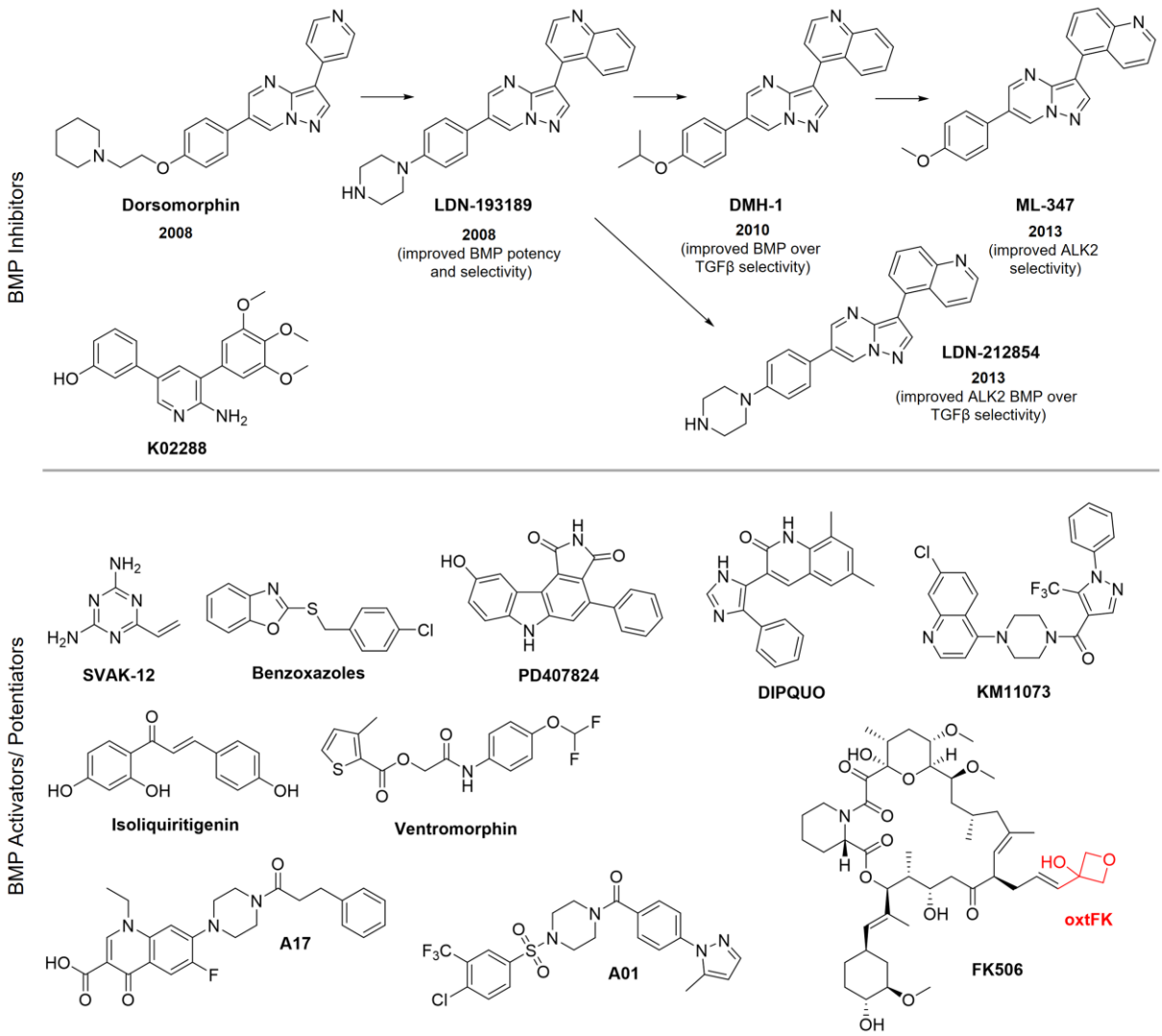

Figure 11: Chemical structures of the identified BMP modulators from different screening assays.

The same assay system was subsequently used for high-throughput screening, that revealed the more promising compound class “Ventromorphins”, which were capable of inducing zebrafish ventralization and osteoblastic differentiation but were lacking potency.[271] Although the authors stated to perform follow-up studies and hit-to-lead optimizations, no further developments have been reported to date.

Another group disclosed a benzoxazole compound class, that was identified as BMP agonists from a high-throughput screen using a BRE-*Id1* luciferase reporter assay system in HEK293 cells.[272] These benzoxazoles were able to induce p-SMAD1/5/9 levels and BMP-4 target gene expression downstream of Noggin and BMP receptor type I levels. To this end, no mechanism-of-action and *in vivo* efficacy have been reported.

The approved immunosuppressant FK506 (tacrolimus), a structural analog of the mTOR inhibitor rapamycin, was identified in a very similar luciferase reporter-based assay system that was shown to activate BMP signaling through FKPB12 inhibition.[273] This led to a stabilization of activated BMP type I receptors, and consequently BMPR2 activation, which was shown to rescue endothelial dysfunction, prevention and reversal of PAH. Thus, BMPR2 activation might be suitable as a therapeutic strategy for PAH, which has also been demonstrated for BMP-9 treatment.[274] In first clinical trials, low-dose FK506 treatments in PAH patients was well tolerated.[275] In addition, a FK506 analog, FKVP was reported to activate BMP signaling by selective inhibition of FKBP12, independently of calcineurin inhibition that lacks the immunosuppressive response of FK506.[276] This unique mechanism demonstrates the dependency on FKBP12 inhibition, that could enhance BMP-2/-4-supported wound healing response of myofibroblasts, as described before.[277] Interestingly, in another study, rapamycin promoted the osteoblastic differentiation of hESCs via activation of BMP dependent SMAD signaling. However, treatment with FK506 and the PI3K inhibitor LY294002 did not lead to osteoblastic differentiation, suggesting a sensitive crosstalk of mTOR/FKBP12 and BMP signaling in these cells.[278] Recently, in a large screen of 250,000 compounds from the Novartis library, a hit cluster of closely related analogs to rapamycin and FK506 were identified in a C2C12-based BRE-*Id1* luciferase reporter gene assay.[279] The team subsequently developed the calcineurin-sparing FKBP12-inhibitor oxtFK, with improved selectivity, *in vivo* pharmacokinetic properties and safety compared with FK506. OxtFK potentiated BMP in renal tissue *in vitro* and *in vivo* and effectively protected mice from acute kidney injury (AKI). Importantly, BMP signaling is downregulated in AKI, that often occurs after cardiac surgery and lacks therapy.[280] In clinical trials for treatment and prevention of AKI, the BMP-7 mimetic peptide THR-184 showed low response and failed. Hence, oxtFK might be a promising, superior therapeutic candidate for AKI treatment.[281] Other BMP activating small molecules that block negative downstream regulators of the pathway were found in very similar screening approaches. In 2014, two Smurf-1 inhibitors were described that attenuate SMAD degradation, thus stabilizing BMP activation.[282] Using an *in silico* screening of the Smurf1-binding domain and subsequent tests in C2C12, A01 and A17 were identified as BMP-active compounds. They enhanced BMP-2-induced osteoblast marker expression in myoblasts and pre-osteoblasts, suggesting Smurf-1 as a potential druggable target for pharmacological BMP activation. Using a similar *in silico* approach, the Smurf-1 inhibitor SVAK-3 was identified, and follow-up studies

reported the more stable SVAK-12 that enhanced the efficacy of BMP-2 in C2C12 transdifferentiation.[283,284] In another study, the pan-kinase inhibitor PD407824 was identified from a high-throughput screening using a BMP-responsive, C2C12-*Id2*-luciferase reporter assay.[285] It was reported to indirectly sensitize BMP-4-driven cellular differentiation, including the formation of cardiac and cytotrophoblast cells from hESCs. PD407824 has been suggested to enhance BMP signaling via checkpoint kinase 1 (CHK1) inhibition leading to a p21-CDK9-mediated degradation of p-SMAD2/3, leaving more SMAD4 for translocating SMAD1 to the nucleus.

Besides blocking negative regulators of canonical BMP signaling, two compounds have been reported to enhance BMP signaling via non-canonical p38 MAPK signaling. BMP-2-induced C2C12 osteogenesis was enhanced by quinoline KM11073 via activation of p38-β. KM11073 induced bone-forming activity in zebrafish and *in vivo* mouse bone formation.[286] Further, Cook et al. reported the potential lead candidate DIPQUO, a BMP activator promoting osteogenesis in human MSCs and zebrafish via selective p38-β activation, yet the direct cellular target and mechanism of p38-β activation is unknown.[287] This study eventually based on previous work of this group who originally reported PD407824 from the conceptually identical screening approach in C2C12 osteoblast differentiation.

Together, the herein summarized examples highlight that it is feasible to identify BMP potentiators and activators from screening. However, many of the currently available agents do not (yet) exhibit an optimal profile regarding their physicochemical, pharmacokinetic and pharmacodynamic features for therapeutic application. In this regard, there is also a need for new technologies beyond artificial reporter assay setups using cell lines. Novel phenotypic assays are desirable that potentially enable the discovery of chemical modalities that expand the druggable space of available BMP signaling modulators.

2 MOTIVATION AND AIMS OF THE THESIS

The BMP signaling pathway is fundamental for embryogenic patterning and cellular differentiation.[63] Modulation of BMP is of great interest for (stem) cell biology, regenerative medicine and basic research of this developmental signaling pathway. High-quality and selective BMP inhibitors, such as the cardiopoietic BMP receptor inhibitor DMH-1, have been developed and are - amongst other activities - reported to modulate embryonic development *in vivo*.[246] In contrast, comparably selective small molecule BMP mimetics are lacking. They would have enormous therapeutic potential since rhBMPs are of great value in regenerative medicine for treating osteopenic diseases and skeletal trauma.[14,288] Several additional therapeutic as well as biotechnological applications exist for BMP activating modalities. However, due to their physicochemical and pharmacokinetic profile, rhBMPs must be administered in supraphysiological doses, which is both costly and associated with adverse effects, including heterotopic ossification or inflammation.[229,288] These deficits could be overcome by selective and potent small molecule alternatives. Despite numerous efforts to identify such BMP activators, there are no drug-like, highly selective chemical modalities available that mimic the physiological action of BMPs. Therapeutic application of BMP activating agents, however, has already been demonstrated using the macrocyclic FK506-based derivative oxtFK in treating acute kidney injury (AKI).[279]

Most reported screening approaches are based on artificial assay systems using immortalized cell lines, which may ultimately miss genuine morphogenic mechanisms, and thus, novel and attractive targets. This may be especially true in hindsight of the cell-context dependence of BMP responses and its complex regulatory mechanisms. Thus, the discovery of small molecules mimicking cytokine activity is intrinsically challenging due to the complexity and diversity of BMP ligand and receptor binding.[62,289] More physiological screening systems such as in zebrafish embryo development might provide attractive BMP-activating molecules but high-throughput formatting is difficult and identified hits prone to polypharmacology. More sophisticated 3D systems such as organoids and gastruloids are not yet suitable for compound screenings.[175–177] Here, *in vitro* embryogenesis was supposed to be bridged with drug discovery by developing a morphogenic phenotypic screening assay that recapitulates BMP signaling during cardiogenic mesoderm patterning from embryonic stem cells (ESCs). The

SCHADE and MERCOLA group previously used a spontaneous 2D cardiac differentiation protocol in murine ESCs, which has already successfully expanded the druggable space of TGFβ inhibitors.[171] Building on this knowledge, Dr. Jonas HALVER identified a BMP-specific time window during cardiogenesis and successfully developed a prototype BMP-mimetic stem cell-based assay.[290,291]

The aim of this thesis is the identification and characterization of novel BMP-activating and/or -potentiating small molecules by integrating principles from phenotypic drug discovery, chemically induced differentiation of stem cells and chemical biology. Therefore, optimization of the prototype mESC assay from HALVER and functional characterization of the BMP- versus TGFβ-specificity during mesoderm structuring needs to be initially addressed. Further, a robust phenotypic assay platform should be established to ultimately identify novel BMP activating small molecules. This platform requires adaption to automation at the Compound Management and Screening Center (COMAS) in Dortmund for high-throughput workflows. For hit validation, a set of orthogonal, secondary assays needs to be established that mimic BMP activation during osteogenic differentiation and allow assessing pathway selectivity.

Furthermore, proof-of-concept of this platform will have to be demonstrated for validated screening hits with the ultimate goal to expand the druggable space of BMP activators and potentiators. Their BMP-activating capacity should subsequently be validated in functional *in vivo* and *in vitro* studies. Structure-activity-relationship (SAR) studies should define pharmacophoric features and provide active as well as inactive derivatives as new tools for the chemical biology of the BMP signaling pathway. Finally, a combination of different biochemical, cell biology methods and target prediction tools is supposed to decipher a plausible mechanism-of-action for the most attractive new BMP mimetics or signaling potentiators.

3 Results and Discussion

3.1 Establishment of a screening platform for BMP activator identification

The differentiation of pluripotent stem cells offers a great opportunity to identify biological mechanisms, and importantly, new chemical modalities that are involved in embryonic development. By harnessing ESC differentiation for phenotypic drug discovery in a 2D-format, throughput and physiological relevance were combined. Therefore, a morphogenic phenotypic screening assay was aimed with focus to probe distinct members of the TGFβ superfamily during cardiogenesis.

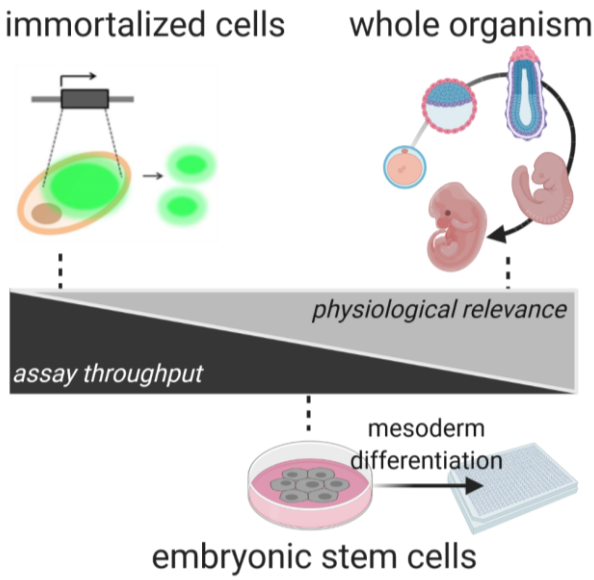

Figure 12: Principle of harnessing ESCs for phenotypic drug discovery by combining throughput and physiological relevance.

Murine embryonic stem cells have been used previously to identify agents and small molecules capable of inducing cardiac differentiation. A *Myh6*-GFP-carrying cell line was firstly described by Takahashi et al., who established and utilized the murine ES cell line to generate embryoid bodies and identified ascorbic acid as a cardiac enhancer.[292] A 2D-approach allows higher and more stable throughput screenings compared to other differentiation techniques, such as 3D-models or embryoid body-based formats and differ in the concrete timings of critical differentiation pathways. Using this cell line in a 2D-assay format, groups from Dr. Mark Mercola and Dr. Dennis Schade discovered a cardiogenic dihydropyridine compound class.[171,172] The identified inducer of TGFβ receptor II degradation, ITD-1, and the further developed DHPs demonstrated proof-of-principle of harnessing ESCs to expand druggable

space of cardiopoietic selective probes. In subsequent studies in this stem cell line, Dr. Jonas HALVER identified and characterized a new pharmacology of hawthorn as a traditional add-on therapy for heart failure treatment.[293]

Next, it was questioned whether it is possible to differentially probe specific members of the TGFβ superfamily during cardiogenesis. Therefore, high-quality chemical probes were tested during different cardiopoietic time frames by image-analysis and quantification of *Myh6*-GFP$^+$ clusters, as schematically shown in Figure 13.

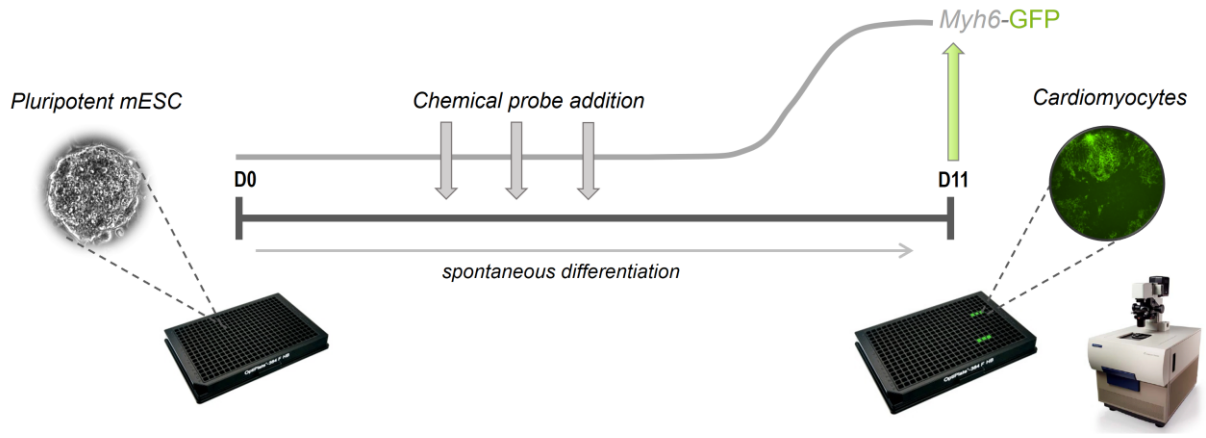

Figure 13: Schematic overview of the cardiac differentiation assay principle using mESCs. Chemical probes are added at different time points during spontaneous mESC differentiation. Cardiogenesis (*Myh6*-GFP+ cardiomyocyte clusters) is quantified after 11 days via high-content imaging.

Considering the known biphasic effect of BMP signaling in cardiac differentiation and its interactions with TGFβ and Wnt signaling, it was important to use selective substances.[11] Therefore, the known BMP inhibitor and cardiac inducer DM and DMH-1 were tested for their cardiopoietic potential for different time frames, in which the ALK1, -2, -3 selective inhibitor DMH-1 specifically induced cardiac cluster formation in between d3-5. These results indicated a BMP-specific window after mesoderm induction during mesoderm structuring at day 3-4 (see Figure 14).[290,291] In addition, the pan-ALK inhibitor Dorsomorphin induced cardiac differentiation at later stages, due to the distinct inhibition of the TGFβ signaling pathway.

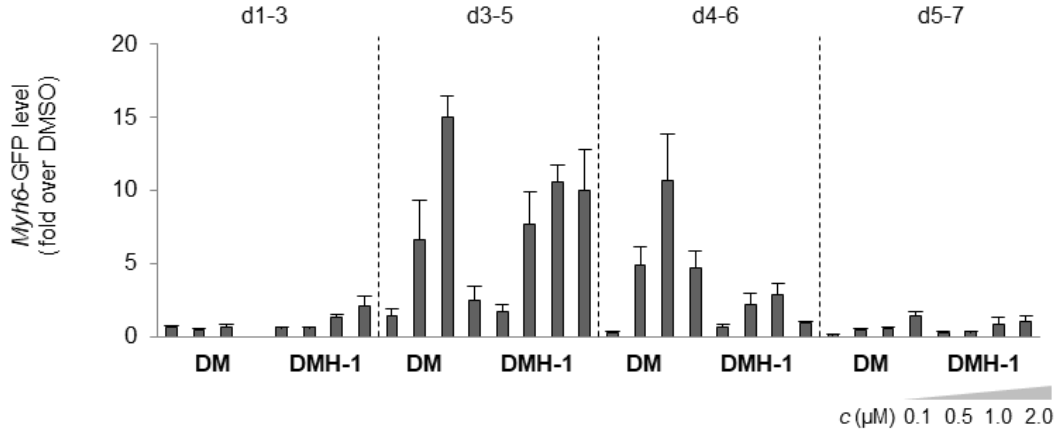

Figure 14: Identification of a BMP-selective time window for cardiac induction of mESC-*Myh6*-GFP. The dose-dependent cardiac induction of DM and DMH-1 indicate a selective BMP time frame during early d3-4 stage. Murine ESCs were treated for 48 h in 384-well format and *Myh6*-GFP+ clusters were analyzed after 11 days, and activities were normalized to DMSO. Bars are represented by the mean of each condition and the respective SEM. Data by Jonas HALVER.[290,291]

In the following, the TGFβ-specific time frame was further confirmed by the highly selective TGFBR-II degrader ITD-1 and the ALK4, -5, -7 inhibitor SB-431542, that induced potent cardiac clusters after treatment during day 4-6, as shown in Figure 15. The cardiogenic and TGFβ-selective (+)-enantiomer of ITD-1 exhibits strong cardiac induction, whereas the (−)-enantiomer completely lacks cardiogenic potential.[172] In agreement with these results, DMH-1 has almost no effect after day 4, where the TGFβ-inhibitors show their maximal effect on cardiac differentiation, which can be seen especially for SB-431542 in later treatments.

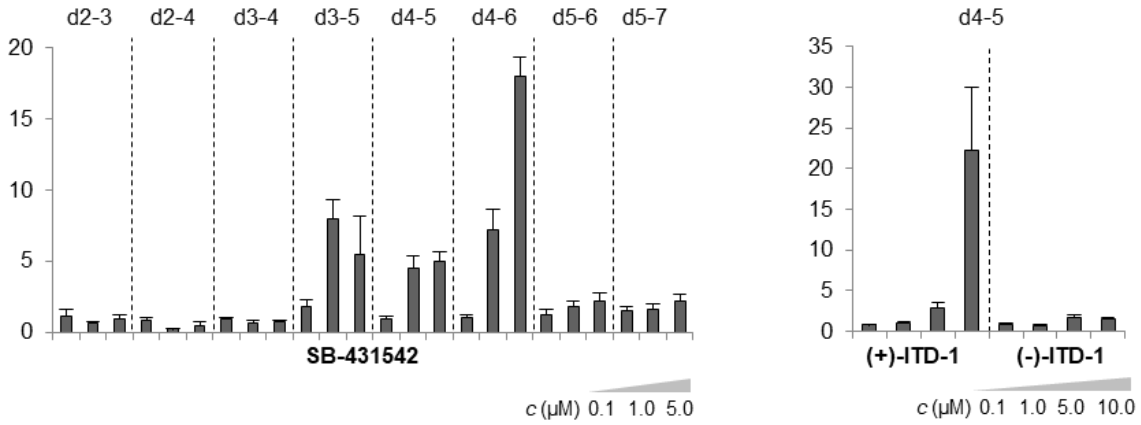

Figure 15: The TGFβ-selective time window can be discriminated from BMP-selective time window. The dose-dependent cardiac induction of SB-431542 and enantiomers of ITD-1 suggests a selective TGFβ time frame during d4-6 after the BMP time frame. Murine ESCs were treated for 24 h or 48 h in 384-well format and *Myh6*-GFP+ clusters were analyzed after 11 days. Bars are represented by the mean of each condition and the respective SEM and are normalized to DMSO.

Overall, utilizing ALK-selective and unselective inhibitors strongly suggested specific time frames for BMP- and TGFβ-signaling during mesoderm structuring of mESCs towards cardiac cell fates, as illustrated in Figure 16.

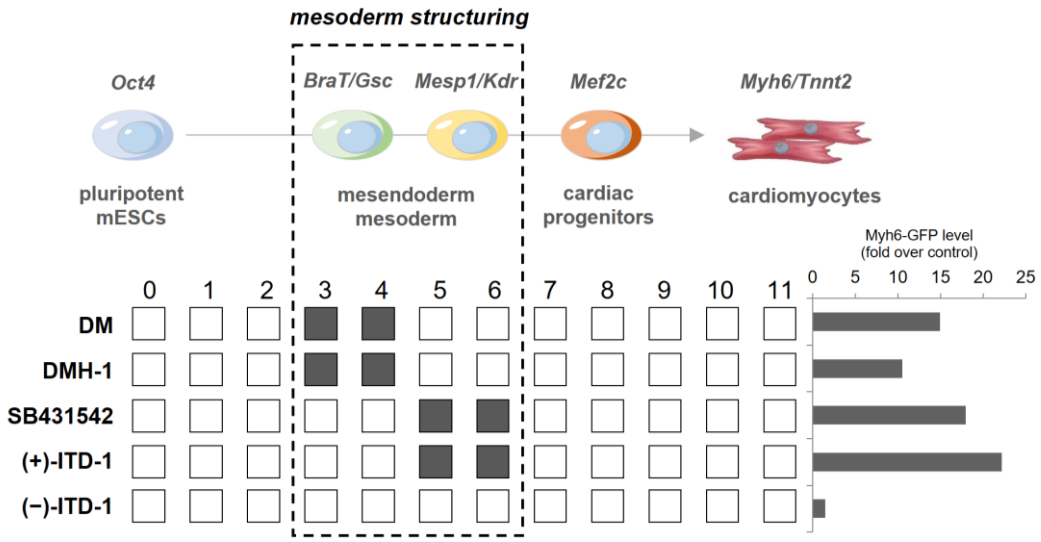

Figure 16: Illustration of cardiac differentiation from pluripotent murine ESCs towards cardiopoietic cell fates. Signaling specificity of mESC-*Myh6*-GFP during mesoderm structuring is indicated by different time frames, as shown for different cardiogenic chemical probes for BMP- and TGFβ-signaling.

In addition, HALVER's studies addressed other embryogenic signaling pathways, in which it was shown that inhibition of Wnt signaling becomes critical at post-mesodermal stages.[290] Based on these initial results, further validation and characterization of the BMP-response towards cardiac cell fates needed to be assessed in this thesis.

3.1.1 Assessment of BMP signaling during mesoderm structuring

3.1.1.1 Characterization of the BMP-specific time frame

Since selective inhibition of BMP signaling during d3-4 led to a cardiac phenotype, it was asked if functional antagonism of DMH-1-mediated blockade by BMPs is possible, which would enable potential screening for BMP-mimetic small molecules. In addition, to characterize the BMP dependence of DMH-1-induced cardiogenesis, functional consequences of BMP perturbation on mesoderm patterning were examined by gene expression analysis of different development stages and cell markers.

To assess functional antagonism, BMP-2 and BMP-4 were tested against 0.5 µM DMH-1 and cluster analysis and quantification revealed a potent and effective antagonism of both rhBMPs

to reverse the DMH-1 induced phenotype (see Figure 17). Here, BMP-4 as a key player in embryonic development was more potent than BMP-2, while both factors were able to completely inhibit cardiogenesis, suggesting the potential to manipulate this particular time frame for assaying BMP activators. However, the observed behavior during d3-4 may ultimately be used as a tool for compound investigation, while cardiac differentiation is suitable as the phenotypic screening readout.

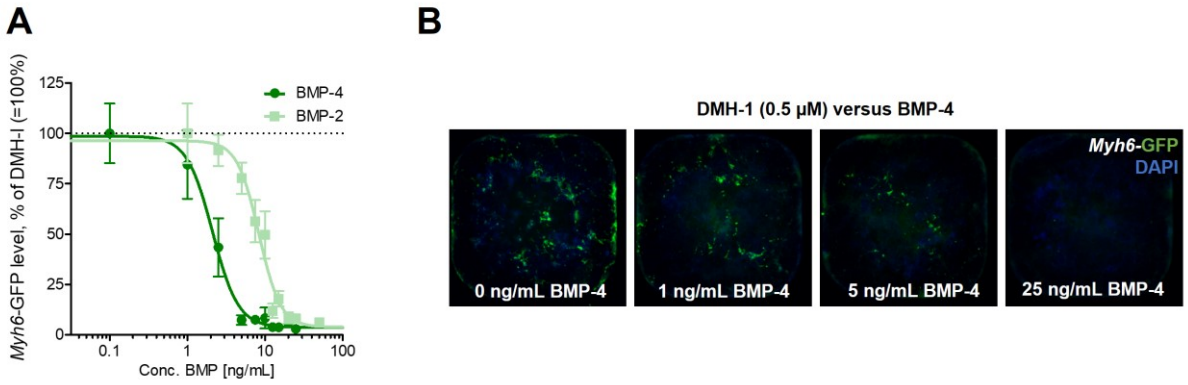

Figure 17: BMP-2/-4 functionally antagonize DMH-1-induced cardiogenesis. Both rhBMPs inhibited DMH-1 induced cardiogenesis in a dose-dependent manner, as shown for cluster formation (B) and quantified *Myh6*-GFP levels (A). The differentiation was induced by DMH-1 (0.5 µM) at d3-4. Representative images of DMH-1 treated mESC after fixation (d11) against BMP-4. Formed cardiomyocytes are indicated by green fluorescence and cell nuclei are visualized by DAPI.

To elucidate whether DMH-1 mediates BMP inhibition through target gene expression, Id gene expression analysis was performed. As shown in Figure 18, DMH-1 inhibited expression of all three *Id1-3* genes, while 10 ng/mL BMP-4 fully rescued gene expression repression, indicating BMP specificity of the identified time frame during cardiac differentiation.

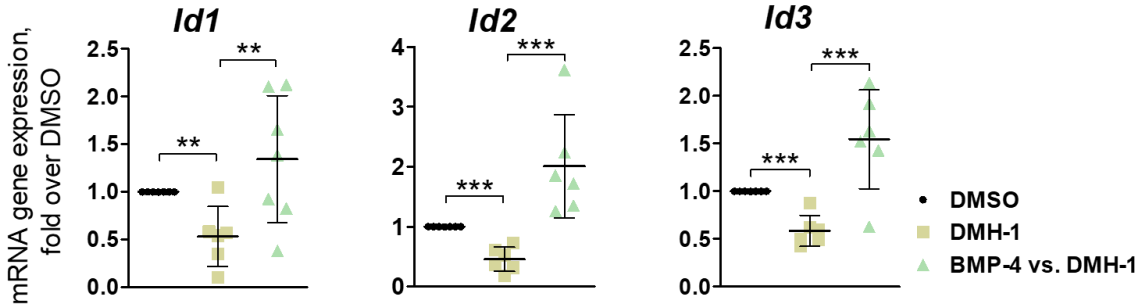

Figure 18: BMP-4 antagonize DMH-1-mediated downregulation of all three BMP target genes. Relative quantification of gene expression for BMP target genes *Id1*, *Id2*, *Id3*.. Murine ESCs were treated with 0.5 µM DMH-1 or 10 ng/mL BMP-4 for 24 h at d3-4. RNA was isolated for each time point and RT-qPCR was conducted. Statistical analysis was performed with an unpaired *t*-test of triplicates and the respective SEM compared to DMSO control and a set confidence level of 95% (*:p <0.05; **:p <0.01; ***:p <0.001) for n=6-7 independent biological experiments.

To ensure that the BMP specificity is in line with expected cardiomyocyte formation, gene expression of certain cell fate markers was conducted during cardiomyogenesis. Therefore, in extensive studies on multiple time points during differentiation, DMSO and DMH-1 was added after 72 h and lysates were taken for each day for reverse transcription qPCR (RT-qPCR). Indeed, DMH-1 promoted timely shifting of mesoderm formation towards *Mef2c* cardiac progenitor cells by reducing *Mesp1* multipotent mesoderm progenitors on day 4, thereby enhancing cardiac differentiation to *Tnnt2*-specific cardiomyocytes after 11 days (Figure 19). Mesoderm-derived *Mesp1*-progenitors can also contribute to other non-cardiac mesodermal lineages, such as muscle cells or hematopoietic precursors, that are repressed by DMH-1 induced BMP inhibition, which is visible by the d4 to d5 shift of *Mesp1*$^{+}$ cells.[160,294] In addition, *Gsc*-dependent formation of mesendodermal progenitors is enlarged, promoting the capacity of the heterogenous cell population to undergo cardiogenic differentiation. *BraT*-specific cells were not affected, as they were already formed at d3.

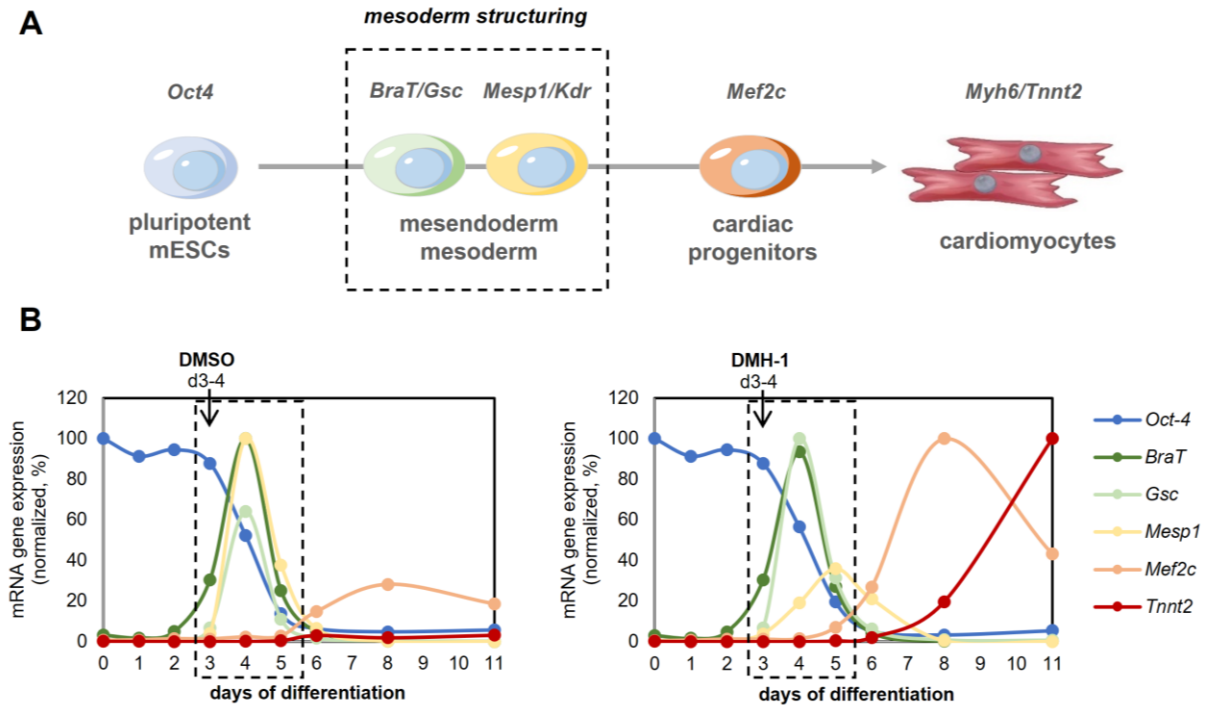

Figure 19: (A) Cardiac differentiation of mESCs illustrated based on marker genes specific for different cell lineages. (B) DMH-1 stimulates mesodermal structuring towards cardiac progenitor cells compared to DMSO treated cells. Cells were treated with DMSO or DMH-1 (0.5 µM) on day 3 for 24 h as indicated by the arrow. RNA was isolated for each time point and RT-qPCR was conducted. Each data point represents the mean and the respective SD of three independent experiments (n = 3) and is normalized to the maximum expression of each gene (=100%).

Interestingly, removal of LIF promotes spontaneous differentiation, however, Oct-4 levels remains stable for 72 h after seeding, which is in line with FACS analysis of Oct-4 protein

levels. Collectively, these data suggest a slow transition from the pluripotent stage with plasticity to commit to differentiation. Remarkably, it has been shown in literature that despite stable Oct-4 levels, cell self-renewal activity decreases upon LIF-withdrawal and colonies start to differentiate.[295] This is consistent with the observed typical flattening of mESC colonies in cell cultures in the absence of LIF.

Because of the characteristic effect of DMH-1 during mesoderm patterning, time-dependency of *Id1* gene expression was monitored during differentiation. As shown in Figure 20 (and in more detail in supporting Figure 95), endogenous levels of Id1 decrease upon spontaneous differentiation and is further suppressed and inhibited by DMH-1 at d3. Removal of DMH-1 at d4 resulted in a drastic increase in its expression, leading to sustained expression over time. These data suggests a critical cellular response during differentiation of the characteristic biphasic BMP-dependent target gene expressions.[160,162] Interestingly, addition of BMP-4 rescued this effect and increased its expression, which steadily decreased over time similar to untreated cells.

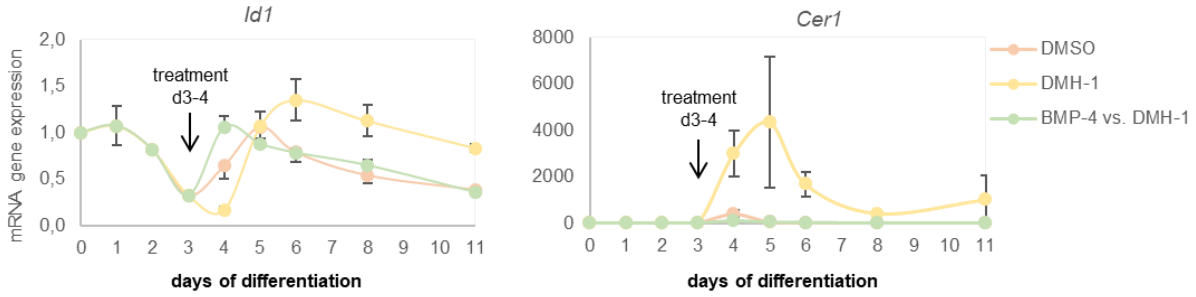

Figure 20: BMP-4 rescues DMH-1-mediated perturbation of *Id1* gene expression and *Cer1* induction. ESCs were treated with DMSO, DMH-1 (0.5 µM) or BMP-4 (10 ng/mL) on day 3 for 24 h as indicated by the arrow. RNA was isolated for each time point and RT-qPCR was conducted. Each data point represents the mean and the respective SD of three independent experiments (n = 3) and is normalized to day 0.

Another critical BMP-antagonistic factor is Cerberus-1 (Cer1), which is a reported endogenous inhibitor of Nodal signaling and a partial driver of committing *Mef2c*-cardiac progenitor cells from *Mesp1* progenitors.[107,162] *Cer1* was substantially induced by DMH-1 and its expression sustained from day 3 to day 6, whereas *Cer1* expression is inhibited and suppressed compared with time-dependent *Id1* expression when *Id1* levels are strongly induced, collectively indicating the potent cardiopoietic effect of DMH-1 in spontaneous differentiation of mESCs. Here again, DMH-1 dependent phenotype was fully reversed by addition of rhBMP-4.

To further emphasize BMP-specificity at d3-4, function of the antagonistic exogenous factor Noggin was determined in response to DMH-1 and BMP-4. Noggin could efficiently antagonize and rescue rhBMP-4-reversed effect on DMH-1 induced cardiac differentiation in a dose-dependent manner, whereas DMH-1 suppressed endogenous Noggin expression when treated on d3 over time but did not further inhibit expression at the time of treatment (Figure 21). However, Noggin alone was incapable to promote cardiogenesis, albeit being reported to gradientally inhibit BMP singling the in heart-forming region during gastrulation and being active on the mesendoderm to promote cardiac differentiation *in vivo*.[147] As Noggin-mediated transient spatial BMP inhibition is required for gastrulation and cardiac tissue formation, the biphasic nature of BMP during cardiogenesis in mouse embryos supports the findings of the identified time frame in the 2D-mESC assay.[296] The incapability of rhNoggin to induce cardiogenesis in the BMP-specific time window (d3-4) may be due to reduced complexity and lack of gradient formation. As expected, and in agreement with the results described above, BMP-4 as an inducer of endogenous Noggin expression, fully reversed the DMH-1-induced phenotype (Figure 21B).

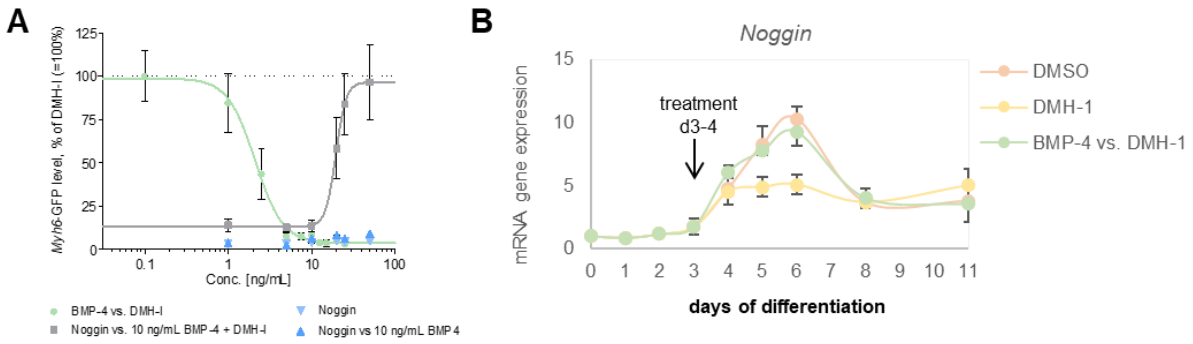

Figure 21: Functional regulation of BMP signaling during d3-4 mesoderm patterning. Exogenous addition of Noggin antagonizes the BMP-4 rescue effect on DMH-1-induced cardiogenesis (A) and its gene expression is repressed by DMH-1 (B). Cardiac differentiation of mESCs was induced by selective BMP inhibitor DMH-1 (0.5 µM) at d3-4 ± rh-Noggin at different concentrations. DMH-1 represses long-term endogenous expression of Noggin after treatment at d3-4. Cells were treated with DMSO, DMH-1 (0.5 µM) or BMP-4 (10 ng/mL) on day 3 for 24 h as indicated by the arrow Each data point represents the mean and the respective SD of three independent experiments (n = 3) and is normalized to day 0.

In conclusion, the characterization of DMH-1 induced cellular commitment towards cardiac cell fates strongly depends on specific and selective BMP inhibition, shifting the mesoderm specification in a small, limited time frame. Importantly, all DMH-1 dependent effects on expression levels and cell fate induction were rescued by BMP-4, which is particularly

significant for the main experimental design of the assay to identify BMP-mimetic or activating compounds.

3.1.1.2 Role of BMP receptor isoforms for mESC mesoderm patterning

Because BMP-4 was in general efficiently reversed DMH-1-mediated BMP receptor blockage whereas Noggin was incapable to induce BMP-dependent cardiogenesis, further investigations were conducted whether specific ALK-inhibitors affect the BMP-selective time frame and thus revealing possible receptor dependency. Different selective BMP inhibitors, which are all developed from the initial found pan-ALK inhibitor Dorsomorphin, were able to induce cardiac differentiation during the validated BMP-selective time from d3-d4 (Figure 22), from which the very potent ALK1/ -3-inhibitor LDN-193189 strongly formed cardiac cluster at very low dosages (50 – 100 nM).

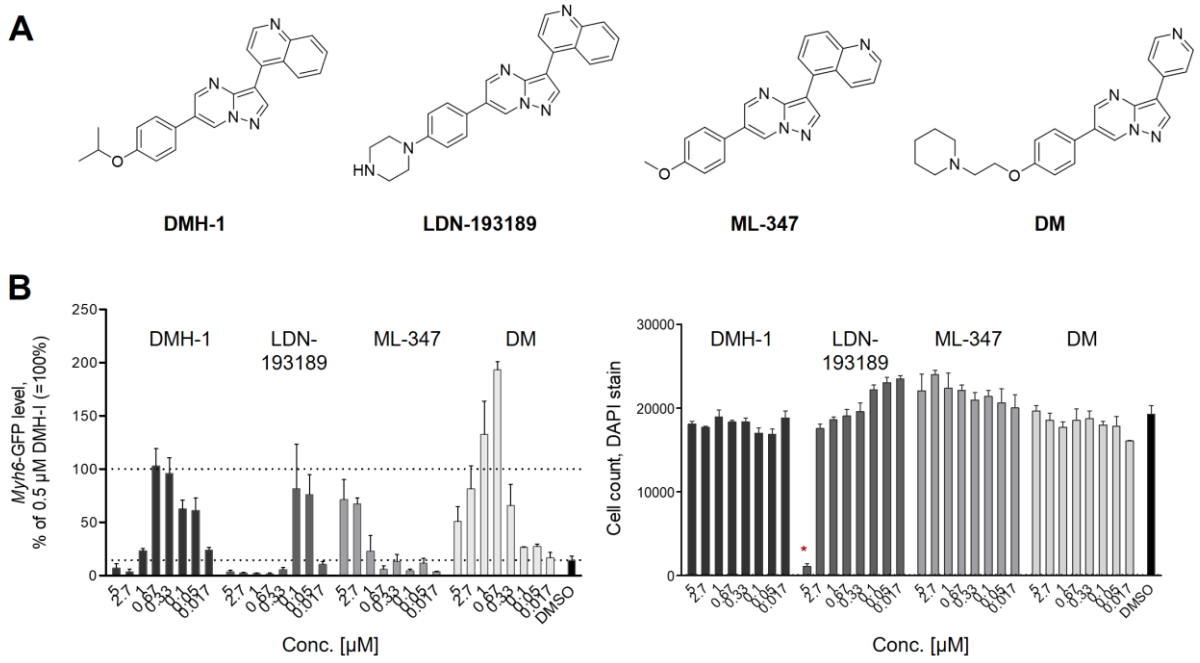

Figure 22: Different ALK-selective inhibitors efficiently induce cardiac cluster formation. (A) Structural overview of used BMP receptor type I inhibitors for evaluation of cardiogenic ALK-selectivity in mESCs. (B) Evaluation of cardiopoietic potential of BMP inhibitors during BMP-dependent time frame of differentiation. Bars are representative for cardiac *Myh6*-GFP levels after 11 days and for total cell count to assess cell viability of mESCs. Red asterisk indicate cytotoxic effects. Compound treatment was performed at d3-4 for 24 h and GFP or DAPI levels are normalized to 0.5 µM DMH-1 (= 100%).

The ALK1/ -2-selective inhibitor ML-347 was less potent in comparison to DMH-1 and LDN-193189, from which only the latter probe drastically reduced cell number after 11 days, indicating cytotoxic effects. Notably, induced cardiogenesis by the unselective ALK-inhibitor

DM exceeds the cardiac potential of the more selective ones, again highlighting potential crosstalk of other affected signaling pathways important for cardiovascular differentiation, such as TGFβ and/or VEGFR.[244]

Furthermore, LDN-193189 also affects TGFβ-relevant and other receptors at higher dosages (see Table 2), which may explain the severe loss of cardiopoietic function at doses greater than 100 nM. Compliant to the literature-reported selectivity of the ALK-inhibitors, the cardiac induction potential of mESCs indicated a predominant dependency on ALK3 over ALK1 and ALK2.[248] This is particularly true for ALK1- and -2-selective ML-347, that only induces cardiogenesis efficiently at dosages > 80-fold higher than its reported IC_{50}, pointing towards an ALK2-independent mechanism. Because ALK2, unlike other receptors, is capable of mediating Activin/Nodal induction of BMP signaling, these findings seem to indicate additional selective dependence of the assay approach in terms of BMP signaling.[297,298]

Table 2: Overview of literature-reported IC_{50}-values for different ALK-selective BMP inhibitors.[248]

IC_{50}'s (nM)	DMH-1	LDN-193189	ML-347	DM
ALK1	27	13	46	106
ALK2	108	41	32	68
ALK3	< 5	< 5	10,800	96
ALK4	>9000	1825	inactive	>25000
ALK5	inactive	565	inactive	17000
ALK6	48	60	9830	235
BMPR2	inactive	3845	inactive	74
TGFβR2	inactive	140	inactive	103
AMPK	inactive	1122	inactive	235
KDR/VEGFR2	inactive	215	19700	22

Taken together, these data are indicative for ALK3-dependency of BMP signaling during mesodermal patterning. However, BMP-4-induced rescue of DMH-1-dependent phenotype may be mediated through alternative type I/ type II receptor complexations, primarily through ALK6 or BMPR2, as BMP-2 and -4 lack binding affinity towards ALK1 and ALK2.[75,104] Suboptimal doses of DMH-1 could also enable compensation mechanisms of BMP-4, which has already been shown in a top-down inhibition xeno-free approach in which sensitive BMP input was specifically generated using exogenous BMP-4 and DMH-1 to induce neural crest

cell formation.[299] The ALK3-dependent phenotype eventually leads to a biased approach in the search for possible targets and mechanisms of BMP-activating effectors in this assay system. Compensation of BMP blockage may be achieved downstream of SMAD signaling or via BMPRs. But due to the low-level blockage of ALK3 by DMH-1 at 0.5 µM and the potential of BMPs to reverse these effects, BMP-activating mechanisms may be identified downstream of receptor-mediated signaling, compensation via BMPR2 or receptor stabilization.

3.1.2 Setup of the stem cell-based phenotypic BMP screening assay

3.1.2.1 Optimization of cardiogenic efficacy

Since the BMP-selective time frame and cell stages during spontaneous cardiac differentiation were validated and characterized, optimization of the developed mESC assay was performed. Given the high variability of undirected spontaneous differentiation of mESCs and the very long incubation time of 11 days, as well as the multiple media changes and handling steps that should generally be avoided in cellular screening assays, further optimization for a more robust assay was required. This included treating or incubation parameters and technical aspects to increase the dynamic range. Firstly, maintenance and pluripotency of mESCs was evaluated with the main goal to store one sensitive batch for medium-throughput screening ensuring maximum reproducibility. Because LIF removal is reported to induce spontaneous differentiation of pluripotent mESCs, continuous FACS analysis of the pluripotent marker gene Oct-4 was performed to ensure high pluripotent quality and integrity of cultured mESCs before assaying.[300] Indeed, Oct-4 was highly expressed in the cell population, indicating a high capacity of pluripotency (see Figure 23A). Upon withdrawal of LIF, Oct-4 levels were mildly reduced but remained stable for 72 h, consistent with the gene expression analysis described above (Figure 19), and with literature.[295]

To further confirm cell plasticity upon removal of LIF, the pluripotent marker Stage-specific embryonic antigen 1 (SSEA1) was quantified. SSEA1 is a carbohydrate antigen that is present on the membrane of mESCs (SSEA4 for human ESCs) and is an early marker for induced pluripotent stem cells.[301] Similar to Oct-4, the quantified $SSEA1^+$ cell population was very high (88%), while the level was moderately reduced under LIF-free conditions but also remained at a high level. This might be typical for LIF-treated pluripotent mESCs, as shown in the literature for LIF-free conditions for Oct-4 and SSEA1 during long-term maintenance, in which marker

slowly decreased.[302] However, the morphological changes of the round colonies, indicative of pluripotent ESCs, provide additional insight into the quality of the cell populations, which was confirmed by confocal imaging of SSEA1- and DAPI-stained colonies, clearly highlighting round-shaped colonies expressing a high amount of SSEA1, whereas LIF-free colonies rapidly expanded and spontaneously differentiated (Figure 23B).[303]

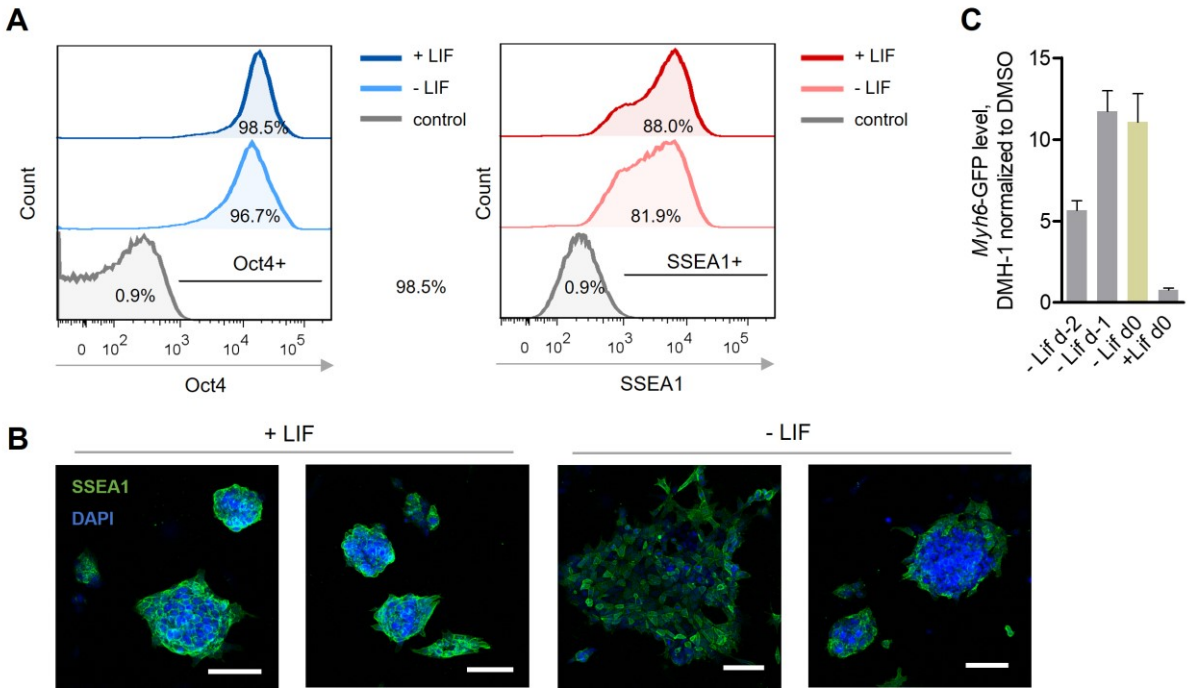

Figure 23: Quality and integrity of pluripotent mESCs. (A) Pluripotent quality of cultured mESCs was verified by FACS analysis of Oct-4 and SSEA1 after 72 h before seeding cells for assaying. Oct-4 and SSEA1 protein levels were quantified by FACS analysis before initiation of differentiation. Analysis was routinely performed by separate immunostaining for Oct4 and SSEA1. Data shown is representative for cultured mESCs in presence or absence of LIF for 72 hours. (B) ESCs were stained and imaged with SSEA1-antibody (green) and DAPI (blue) via confocal imaging and representative images were selected to visualize morphological changes of LIF-untreated and treated cells (scale bar = 100 µm). (C) LIF directly affects DMH-1-induced cardiac differentiation of mESCs. As indicated, LIF removal (d-1/-2) or addition to cells prior seeding (d0), compared to standardized conditions as highlighted in yellow. ESCs were treated under maintenance conditions with 15 ng/mL LIF to keep pluripotency. Bars indicate DMH-1 induced cardiac *Myh6*+-clusters.

To investigate whether LIF directly affects DMH-1-driven cardiogenesis, as it might shift time-dependent induction of differentiation for responsive cells, LIF was removed 24 h (d-1) or 48 h (d-2) before or added prior (d0) seeding cells to induce cardiac differentiation. As expected, transient addition of LIF to seeded cells results in an immediate shift in spontaneous differentiation, disrupting the BMP-sensitive time frame for DMH-1 and inhibiting cardiac induction by delaying mesoderm induction. In addition, LIF removal 48 h before seeding the cells negatively regulated cardiac potential, whereas LIF removal 1 day prior to and on the day of the differentiation assay ensured most efficient cardiopoietic potential by DMH-1. These

results suggest that LIF removal is optimal for mESCs just before cells are seeded, as this reduces further handling, yet no further cardiac induction was obtained.

Given that FBS greatly affects stem cell maintenance and differentiation, different FBS batches were tested during this thesis to ensure the highest quality and viability of cultured mESCs. As FBS also has an influence on compound treatment, FBS concentrations from 0% to 10% during treatment of DMH-1 and effect of heat-inactivated FBS, which might sensitize cells by reducing growth factor activity, were investigated. MESCs treated with heat-inactivated FBS appear to be slightly more sensitized to cardiac differentiation, but the difference was less dominant than expected and generally indicates a stronger dependence on FBS concentration (Figure 24A).

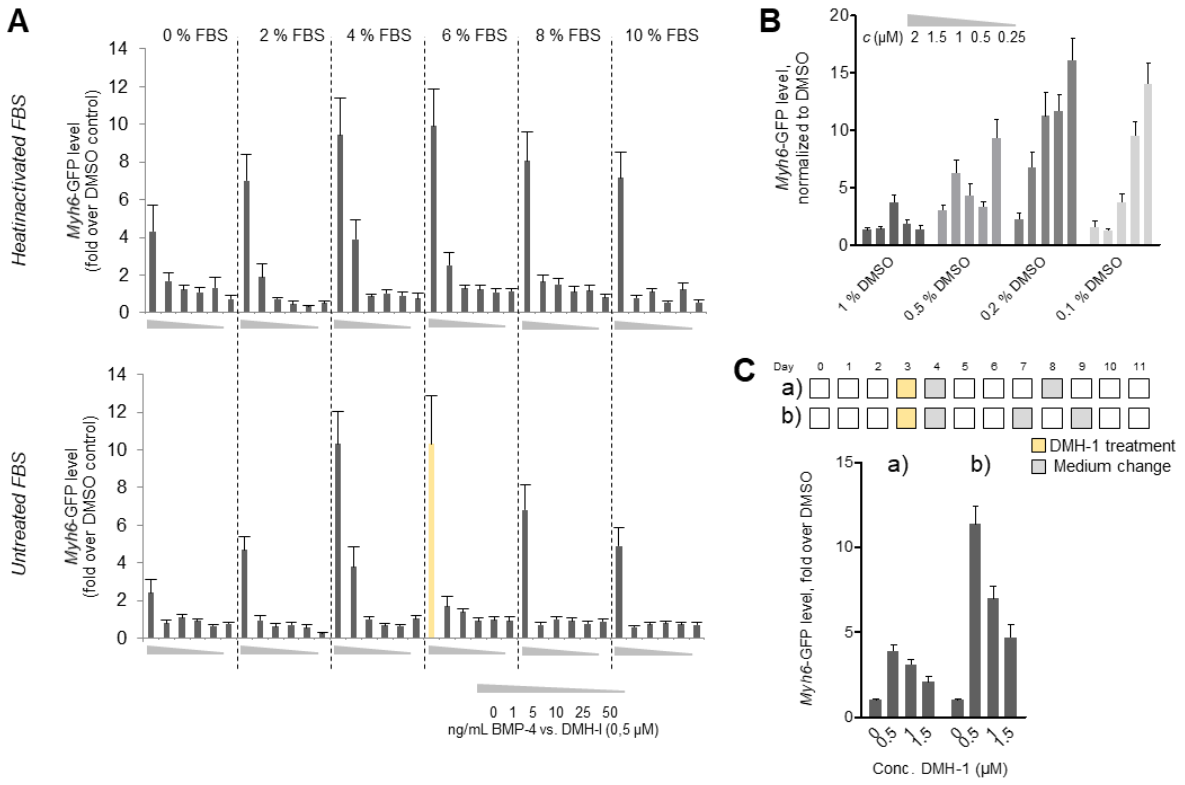

Figure 24: FBS concentration, vehicle and media change affect DMH-1-induced cardiogenesis (A) Assay performance depends on FBS concentration used during DMH-1-treatment window (d3-4). Treatment was performed at day 3-4 for 24 h. Yellow bar highlights standard assay conditions. (B) DMSO effect on cardiac efficacy of DMH-1. Dose-dependent treatment with DMH-1 was performed at d 3-4 for 24 h with different DMSO concentrations. Each concentration was normalized to its respective DMSO control. (C) Medium change frequency affects assay performance, shown by representative induction levels of DMH-1 treated mESC during d3-4.

Moreover, high concentrations similar to FBS concentrations during maintenance result in lower cardiogenic efficacy, indicating a negative influence of FBS on the efficacy of the drug. Hence, the final FBS concentration for treatment should range between 4% and 6% to ensure

maximum cell viability and performance. For further optimization and compound profiling 6% FBS was used.

Next, the effect of the standard compound vehicle DMSO on cardiac efficacy of DMH-1 had to be evaluated, because DMSO might interfere with DMH-1-induced cardiogenesis and ultimately should be reduced to minimum concentration as it also affects cell viability during compound treatments. As shown in Figure 24B, a final assay concentration of DMSO from 0.1% to 1% was tested, indicating a dose-dependent reduction of cardiac cluster formation of DMSO concentrations greater than 0.2% as a result of visible reduction of cell number and proliferation. A reduction of DMSO concentration was desired and stabilization of the cardiogenic phenotype by DMH-1 was indeed measurable. It is important to note the observed synergistic effect on DMH-1-induced cardiogenesis at 0.2% DMSO may be due to the known cardiopoietic efficacy of DMSO itself and decreasing the dynamic range of the assay.[304] Due to technical limitations, a further reduction to 0.1% DMSO was difficult to address, especially when higher compound concentrations (> 5 µM) were tested.

One technical aspect was the amount of media changes during the differentiation over 11 days, that generally should be reduced to a minimal number desirable for high-throughput-screening, in part because of the increased risk of contamination under non-aseptic conditions. Especially for late-stage differentiation of the cells as cardiac cluster might start beating, the differentiation medium was consumed more rapidly, which had a direct negative effect on cell viability and cluster stability, thus negatively affecting assay performance. Even though a single medium chance after compound treatment is preferred, an additional medium change at day 9 drastically enhanced cardiac stability and ensured robust assay performance (Figure 24C).

As observed for negative control wells, autofluorescence of cell accumulations significantly affected dynamic range after signal quantification of cardiac clusters, hence parameters for quantification had to be adjusted for each individual assay run. To minimize quantification of autofluorescence-based edge effects and maximize the dynamic range for DMH-1-induced cardiac efficacy, only 80% of the wells were covered for imaging, which eliminated edge effects, thus significantly improving the ratio of positive clusters to accumulated cells (Figure 25). Since this is a "negative readout", there is a chance of identifying false-positive hits that only affect cell viability (or are cytotoxic). Therefore, during the primary readout for cardiac

clusters, a total cell count was simultaneously included in the image analysis for DAPI-stained cells, and subsequently, false-positive hits and artifacts were eliminated by visual inspection.

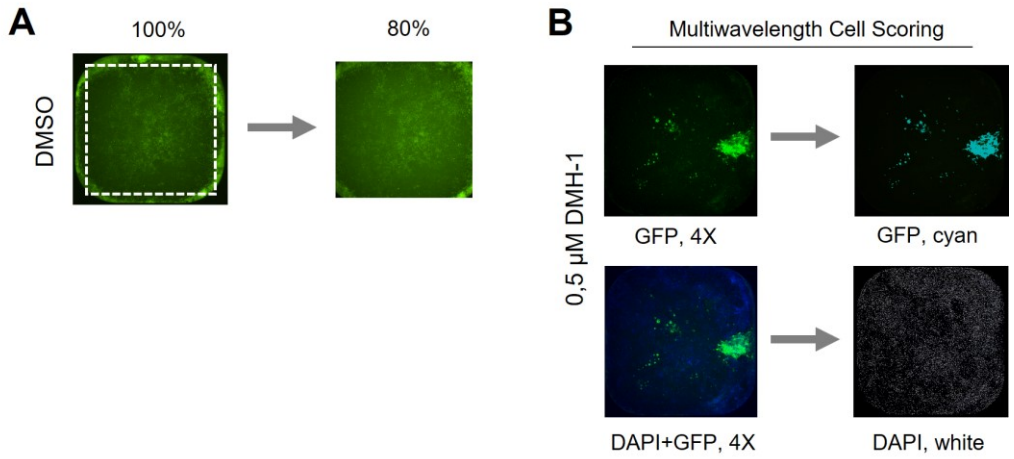

Figure 25: High-content imaging settings. (A) Representative images of DMSO treated cells. For each GFP and DAPI channel one frame per well was taken, covering 80% of the well was analyzed to minimize autofluorescence-based edge effects caused by cell accumulations. (B) Representative images of DMH-1-treated mESC after fixation and illustration of imaging masks after processing for quantification of *Myh6*-GFP and DAPI signals via Multiwavelength Cell Scoring using the MetaXpress software.

While having thoroughly evaluated further technical aspects during differentiation over 11 days including multiple handling steps with different devices such as the automated washer and dispenser in comparison to manual handling of the assay or optimal preparation of the cardiogenic differentiation medium, a screening workflow was established, as shown in Figure 26.

Optimization of technical aspects and assay parameters to address cell viability and cardiac efficacy were shown to successfully enhance assay performance and cardiogenic induction up to 40-fold over control. Nevertheless, due to the nature cell population variability of the assay, technical quadruplicates per plate were used for the primary testing of chemical substances, limiting the compound throughput per plate.

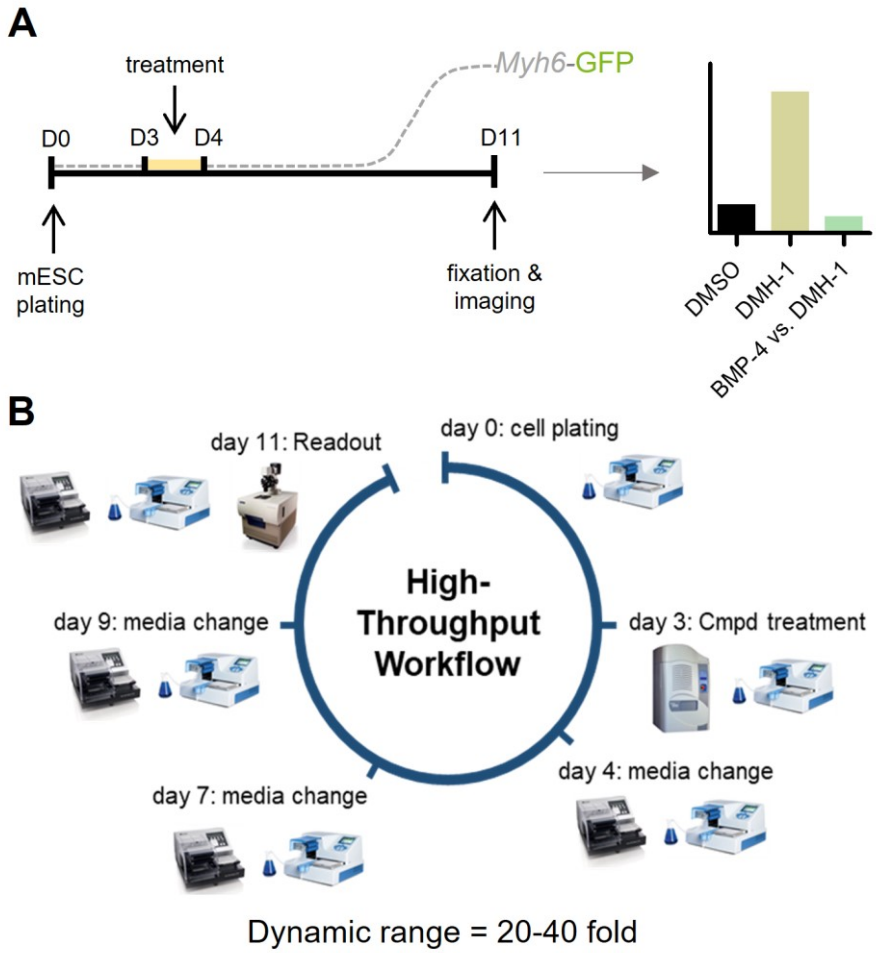

Figure 26: Schematic workflow of the BMP-mimetics assay in a high-throughput format with the assay principle to screen for BMP-mimetic compounds by reversing cardiogenic induction of DMH-1 (A), and technical overview of the screening workflow including the handling steps over the course of 11 days.

3.1.2.2 Assessment of small molecule BMP activators

Based on these findings, the day 3-4 period BMP-specific and selected for screening small molecule BMP mimetics by rescuing a DMH-1-driven cardiomyogenic phenotype in 384-well format. After screening assay parameters were optimized and set up, and BMP-antagonism against cardiac phenotype was validated, a set of literature-known BMP activators was profiled in the assay system to determine their efficacy in the screening setup and to evaluate possible BMP mechanisms in the mESC-assay. For this, reported activators Isoliquiritgenin, Ventromorphin and the CHK1-inhibitor PD407824 were evaluated against 0.5 µM DMH-1.[270,271,285] While Ventromorphin inhibited the cardiogenic phenotype only very moderately at high concentrations above 5 µM, Isoliquiritigenin and PD407824 antagonized DMH-1. Isoliquiritigenin, however, exhibited low efficacy, being active only at very high

concentrations (10-20 µM), whereas the BMP-sensitizer PD407824 drastically inhibited cardiogenesis at 2.5 µM, suggesting strong efficacy but which may be masked by high cytotoxicity, as seen with the reduced cell number at 5 µM (Figure 27).

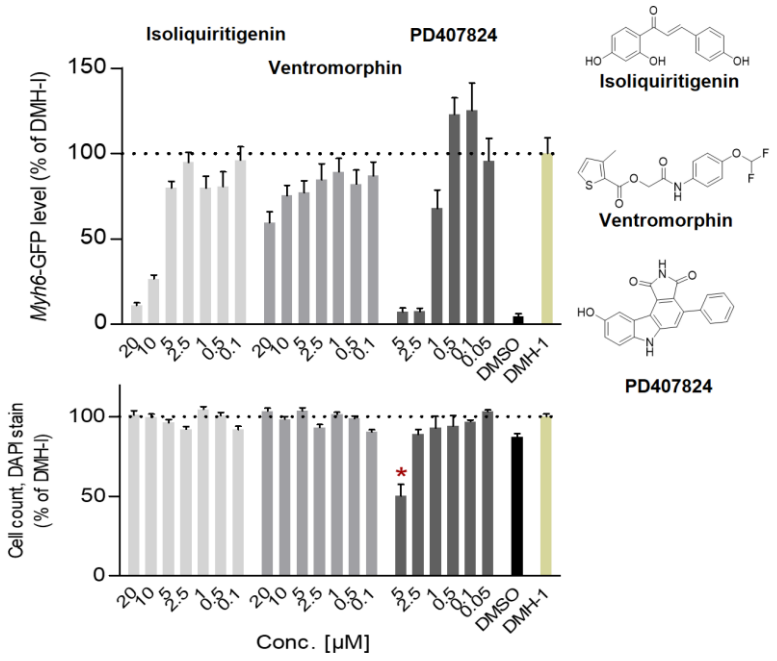

Figure 27: Profiling of Isoliquiritigenin, Ventromorphin and PD407824 exhibit moderate activity in the BMP activator screening assay. Bars graphs illustrate dose-dependent cardiogenic antagonism and cell count of BMP activators against 0.5 µM DMH-I representative for at least three independent experiments. Red asterisks indicate cytotoxic effects.

In general, PD407824 affected cell viability as seen visually after compound treatment, which might be caused by the reported inhibition of the cell cycle regulator checkpoint kinase CHK-1. Its BMP-sensitizing functions through inhibition, leading to progressive activation of the CDK8/9 complex and depletion of SMAD2/3, thus releasing SMAD4 for enhanced BMP signaling.[285] However, inhibition of CHK-1 also leads to cell cycle impairment during regulation of the G2/M checkpoint, and hence cell arrest at this stage.[305] This effect is supported by the reported inhibition of Wee1 by PD407824 and further, moderate pan-kinase activity of PD407824 against the AGC kinase group has been reported, which may explain additional off-target effects in addition to BMP-sensitizing behavior in hESCs.[306] While Isoliquiritigenin efficiently rescued the cardiac phenotype up to 90%, the reported *Zebrafish* ventralizing chemical probe Ventromorphin lacked potent and efficient inhibition, indicating a different BMP-activating mechanism of action that does not appear to be feasible in this assay system. Nevertheless, the moderate activities demonstrate the possibility of small molecule testing to also identify novel mechanisms of BMP pathway activation in embryonic context.

3.1.3 Establishment of an osteoblastic differentiation assay

For further validation of identified non-toxic antagonists of DMH-1-induced cardiac phenotype, an orthogonal secondary BMP-dependent differentiation assay was established. As explained in detail previously, osteoblastic differentiation is highly dependent on BMP signaling and activation. Murine mesenchymal C3H10T1/2 cells, C2C12 myoblasts, osteoblastic MC3T3-E1, or stromal W-20-17 are commonly used for *in vitro* studies on BMP-dependent osteogenesis.[187,189,307,308] They represent distinct stages of osteogenic differentiation and differ in cellular response to BMP stimulation and the respective BMP isoforms.[186] C3H10T1/2 cells are more sensitive to Shh stimulation or co-stimulation of Shh and BMP, while MC3T3 cells are suitable for long-term mineralization studies. The rapid and sensitive transdifferentiation of C2C12 in response to BMP stimulus enables a less complex assay system.[307,308]

Thus, in order to display osteogenic differentiation in dependence of both growth factors BMP-2 and -4, the sensitive C2C12 were employed, which have previously been used for the validation of BMP-activating substances and in which BMP-dependent osteogenic mechanisms were investigated, as summarized in chapter 1.5.2.[189,270] Basically, C2C12 myoblasts were used that undergo spontaneous myogenesis in the confluent stage or by stimulation of Insulin and insulin-like growth factors.[309]

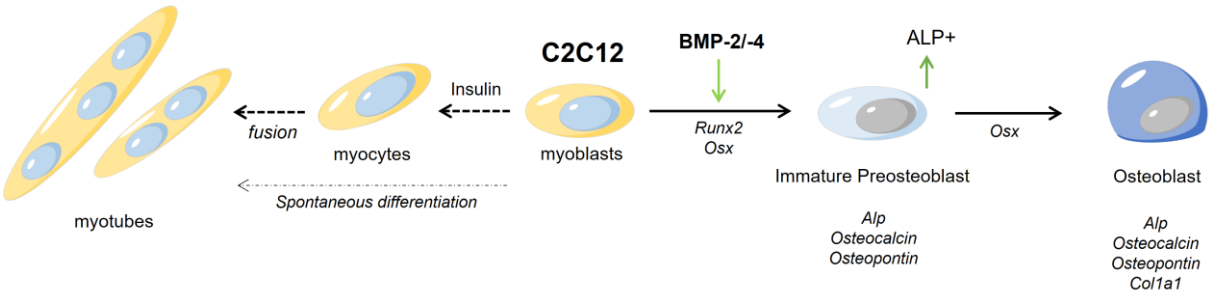

Figure 28: Schematic illustration of myogenic differentiation and BMP-dependent osteogenic induction of C2C12 myoblasts. When C2C12 become confluent, they undergo spontaneous myogenic differentiation into myocytes, which subsequently fuse into multicellular myotubes. In contrast, BMP-dependent osteogenic induction depends strongly on the expression of *Runx2* and *Osx*, forming immature preosteoblasts secreting high levels of ALP and additional cellular osteogenic marker such as Osteocalcin, Osteopontin and Collagen, type I, α1 (Col1a1).

When treated with osteogenic BMPs, C2C12 differentiate into immature preosteoblasts and thereby produce high levels of measurable Alkaline Phosphatase (ALP), as illustrated in Figure

28. This phosphatase is highly expressed and secreted during osteogenesis and is essential for the mineralization of osteogenic tissue through the cleavage of phosphate groups, which are important for the formation of bone-constituting hydroxyapatite.[310]

When establishing the assay for osteogenic differentiation, optimization and transfer to the 384-well format was aimed to allow the possibility of an independent screening of the secondary assays. Firstly, cell number per well, medium volume, readout conditions and FBS concentration was tested. As shown in Figure 29, dose-dependent BMP-4-induced ALP-activity reached its plateau using 2000 cells/well, which ensured contact-free cell layer to reduce myogenic potential of C2C12.

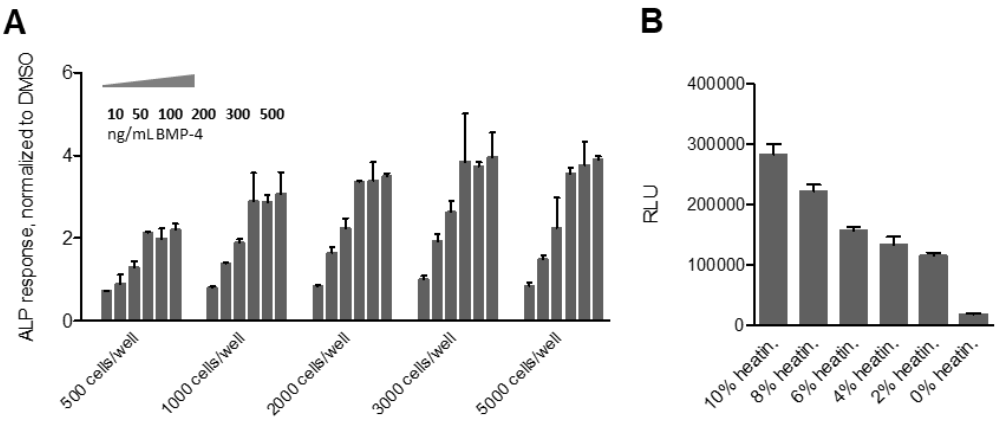

Figure 29: Establishment of the assay in 384-well format resulted in increased sensitivity due to higher cell number (A) and improved ALP performance under medium conditions with heat-inactivated FBS (B). Together with further optimized conditions such as treatment (72 h) and seeding (16 h) time, the assay with 2000 cells/well and 6% heat-inactivated FBS was found to be highly robust for small molecule profiling.

After the cells were seeded for 16 h, BMP-4 was added, and the response was assessed after an additional 72 h to monitor osteogenic differentiation. Activity was measured by robust and stable luminescence reaction of a chemiluminescent substrate for ALP. As FBS may interfere with growth factor-induced differentiation and compound sensitivity, FBS concentration should be minimized without affecting assay performance and cell viability. Heat-inactivated FBS-containing medium showed significant improvement in BMP-dependent cellular response compared with untreated FBS (Figure 29B). Low concentrations (2%-6%) of heat-inactivated FBS still exhibit large dynamic ranges and high RLU, thus, 6% hi-FBS was set to study the response of substances and factors to ensure minimal effects on cell viability during differentiation over 72 h. Under fixed assay conditions, the dose dependence of osteogenic BMP-2 and BMP-4 was assessed, with both reaching a maximum induction level of >400 fold

over control (see Figure 30), but with great difference in potency, in which BMP-2 induced ALP-activity with an EC_{50} of 177 nM, 5.5-times greater than BMP-4 (EC_{50} = 32 nM) and extracellular antagonist Noggin inhibited low concentration of BMP-4. The high potency of BMP-4 is particularly interesting since we were primarily aiming for a BMP-4-mimetic small molecule.

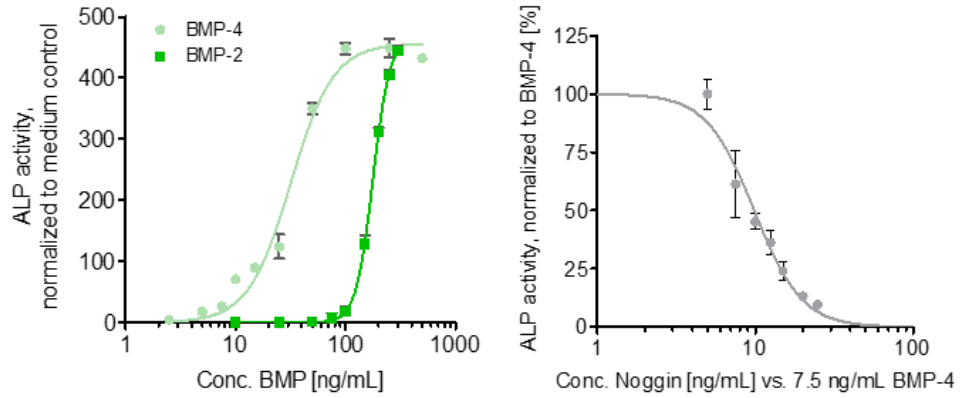

Figure 30: BMP-2 and -4 induce ALP activity of C2C12 in a dose-dependent fashion, indicating a maximum cellular response at 100 ng/mL for BMP-4 and 250 ng/mL for BMP-2, respectively. This effect could be antagonized by rhNoggin as shown for BMP-4. Activities were normalized to medium or DMSO control.

Next, different ALK-selective BMP-inhibitors were tested for their antagonizing activity, as shown in Figure 31. All three chemical probes efficenty inhibited BMP-4-dependent ALP-induction, from which LDN-193189 showed a total inhibition already at 50 nM, 10-times lower than ALK1/-3-selective DMH-1 and > 200-times lower than the ALK1/-2-selective ML-347, indicating a strong ALK3-dependency of C2C12 osteogenic transdifferentiation. These results are consistent with the literature, reporting that BMP-2 and -4-induced osteogenesis is primarily mediated by ALK3, whereas endogenous ALK6 levels in C2C12 are very low.[76,122,311] For this reason, ALK6-selective inducers or agonists identified in the cardiac differentiation assay might be inactive, indicating a mechanistic limitation of the C2C12 assay. However, due to highly conserved binding domain of BMPs and oligomerized receptors, it seems still unlikely to find genuine or even selective receptor agonists.

To investigate, whether DMH-1-induced antagonism could be rescued by increased concentrations of BMP-4 in analogy to the original mESC-based morphogenic BMP activator assay, 500 nM and 50 nM DMH-1 were tested against BMP-4 up to 500 ng/mL, showing complete inhibition of BMP-4-induced ALP-activity at 500 nM (Figure 31B). Indeed, 50 nM DMH-1 antagonism could be rescued by BMP-4 in a dose-dependent manner, whereas

receptor inhibition of DMH-1 in the mESC assay at 0.5 µM could not be abolished. This observation suggests a suboptimal BMP inhibition of DMH-1 in C2C12 analog to the mESC differentiation assay, albeit shifted by a factor of 10 and may be explained by the comparatively homogeneous cell system compared with heterogeneous mESC assay at day 3.

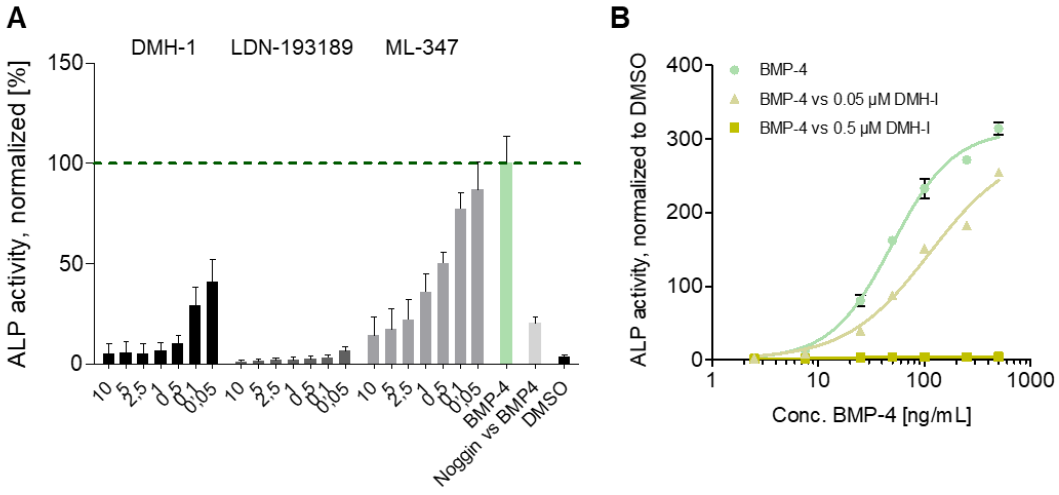

Figure 31: Assessment of BMP-dependent antagonism of selective BMP-inhibitors. (A) Selective ALK-inhibitors potently inhibit 7.5 ng/mL BMP-4-induced osteogenesis up to 99%. Bar graph represents mean ± SD of at least two independent experiments and are normalized to BMP-4/DMSO-control. (B) Dose-dependent osteogenic induction by BMP-4 against DMH-1 treatment at 0.5 and 0.05 µM. Data represents ALP-response normalized to DMSO.

Given the large cellular response to BMP-2 and -4, a sensitive concentration for determining the effects of small molecules had to be determined. To stimulate osteogenic induction of C2C12 cells, small induction with low dose BMPs should be enhanced by a potential small molecule activator and/or sensitizer. For this purpose, two literature-known BMP-activators Isoliquiritigenin and Ventromorphin, which have been reported to induce C2C12-dependent ALP, were tested in a range of low doses of BMP-2 and -4 from 1 to 50 ng/mL. Indeed, as apparent for Isoliquiritigenin, a synergistically sensitive concentration window was revealed between 5 to 20 ng/mL BMP-4, inducing ALP-acitvity at 10 µM up to 5-fold over BMP-4 control (Figure 32). A similar window was seen for BMP-2-induced osteogenic induction, but which was shifted to higher concentrations between 40 to 50 ng/mL BMP-2, consistent with the observed lower efficacy of BMP-2 compared with BMP-4. In contrast, Ventromorphin did not exhibit significant synergistic induction of ALP, nor did it induce ALP without addition of BMP-4, whereas it induced synergistic ALP activity together with BMP-2 in a narrow concentration window of 40 ng/mL.

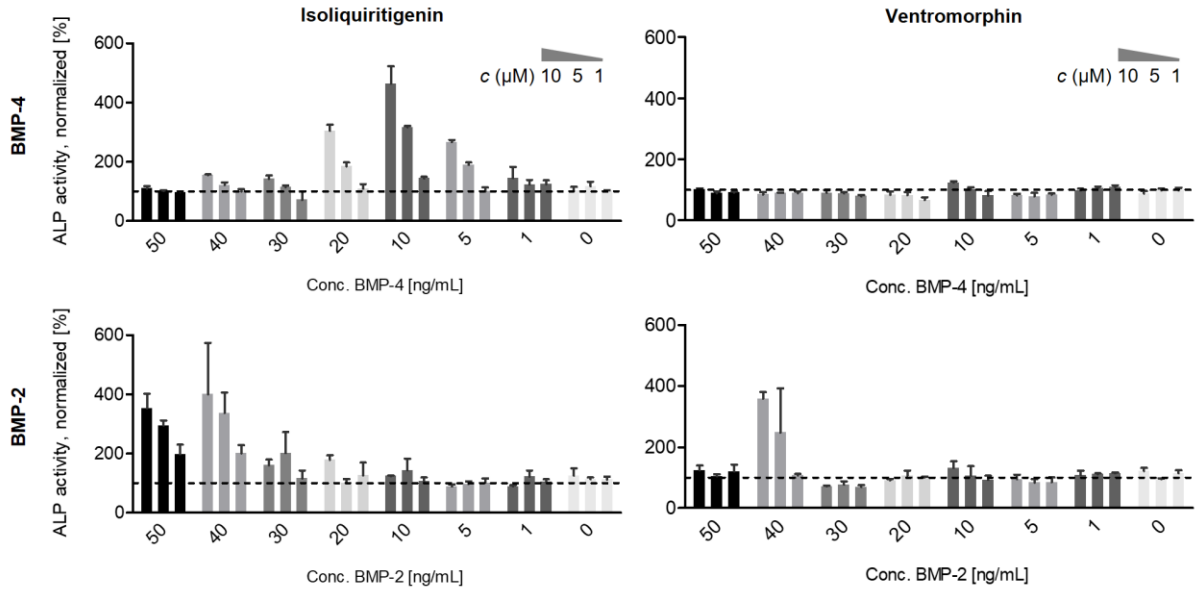

Figure 32: Assessment of BMP-dependent (and -synergistic) ALP induction of Ventromorphin and Isoliquiritigenin to identify responsive concentration window of BMP-2 and -4. BMP-4 concentration of 7.5 ng/mL was considered to be most suitable for investigating synergistic compound activation in a sensitive manner.

These results suggest a synergistic concentration window, but in addition, a certain threshold for osteogenic induction is required, because none of the reference compounds caused synergistic induction at 0-1 ng/mL BMP. For further validation of BMP-potentiating small molecules, the BMP-4 concentration was set at 7.5 ng/ml to provide a compromise between sufficient osteogenic induction and sensitivity to potential BMP activators and sensitizers.

After the optimal dose of BMP-4 to minimally induce osteogenic ALP was identified, full dose-dependency of the known BMP-activators was assessed, as shown in Figure 33. As expected, Isoliquiritgenin induced BMP-induced ALP-activation in a dose-dependent fashion up to 2.5-fold over DMSO vehicle control, indicating a clear synergistic context, whereas Ventromorphin lacked activation in low-dose BMP-4 treated cells. This may be in line with the original publication in which Ventromorphin induced only morphological changes toward osteogenic cell fates of C2C12, but no ALP-induction was demonstrated, in contrast to Isoliquiritgenin published by the same group, indicating a unique mode of action of Ventromorphin for exclusive ventralization of *Zebrafish* embryos.

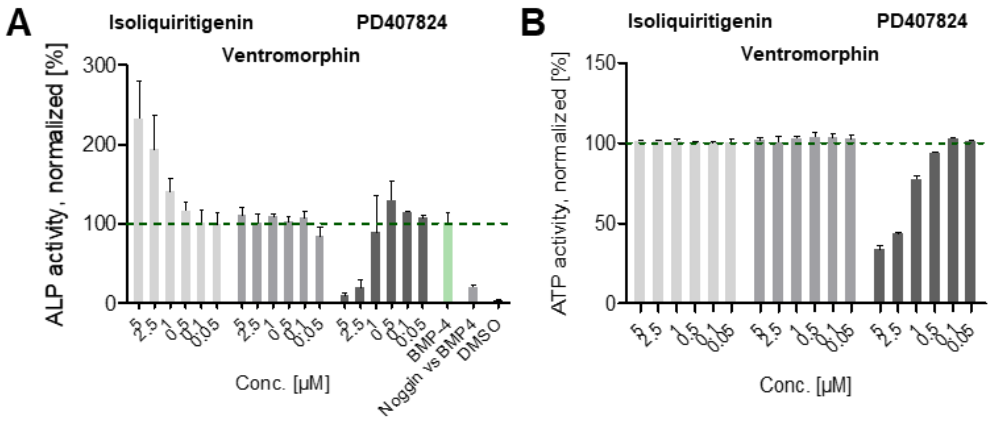

Figure 33: Synergistic dose-dependent ALP induction of BMP activators in C2C12 reveals Isoliquiritigenin as a potent, nontoxic potentiator. (A) Reference compounds were added together with 7.5 ng/mL BMP-4 and ALP-activities were normalized to BMP-4 (= 100%). (B) Cell viability was assessed via a CellTiter-Glo assay. Bars are representative for at least three independent experiments.

The BMP-sensitizer PD407824 showed a very mild synergistic induction at 0.5 µM but strong inhibition of ALP at higher concentrations, which may be due to cytotoxic effects and cell cycle impairment during the course of 72 h of differentiation and also indicated by the reduced cell viability compared with other BMP-activators via ATP-quantification by a CellTiter-Glo assay (Figure 33B). This observation strongly suggests that the described mechanism via inhibition of checkpoint kinase followed by synergistic BMP activation is difficult to reproduce in this assay setup due to the problematic effects on cell viability, as already shown in the cardiac differentiation assay.

Taken together, a C2C12-based BMP-dependent osteoblastogenic differentiaton assay was established to identify synergistic activators with low dose BMP-4 to monitor enhanced ALP-activity, resulting in a stable dynamic induction (30 x) and robust Z'-value of 0.6 to 0.8 (see Figure 34). However, since ALP is not an exclusive marker of BMP-dependent osteogenesis, additional osteogenic gene expression markers critical for cell fate decisions such as Runx2 or Osx and proteins important for tissue patterning like ALP, Osteopontin, Osteocalcin or Collagen, type I, α1 (Col1a1) were established and quantified to profile osteogenic differentiation signature.[312–314] To demonstrate BMP-dependence on these osteogenic marker genes, low dosed BMP-4 (7.5 ng/mL) and high induction with 100 ng/mL BMP-4 was compared with DMSO-treated cells after 72 h (see Figure 34, Readout B).

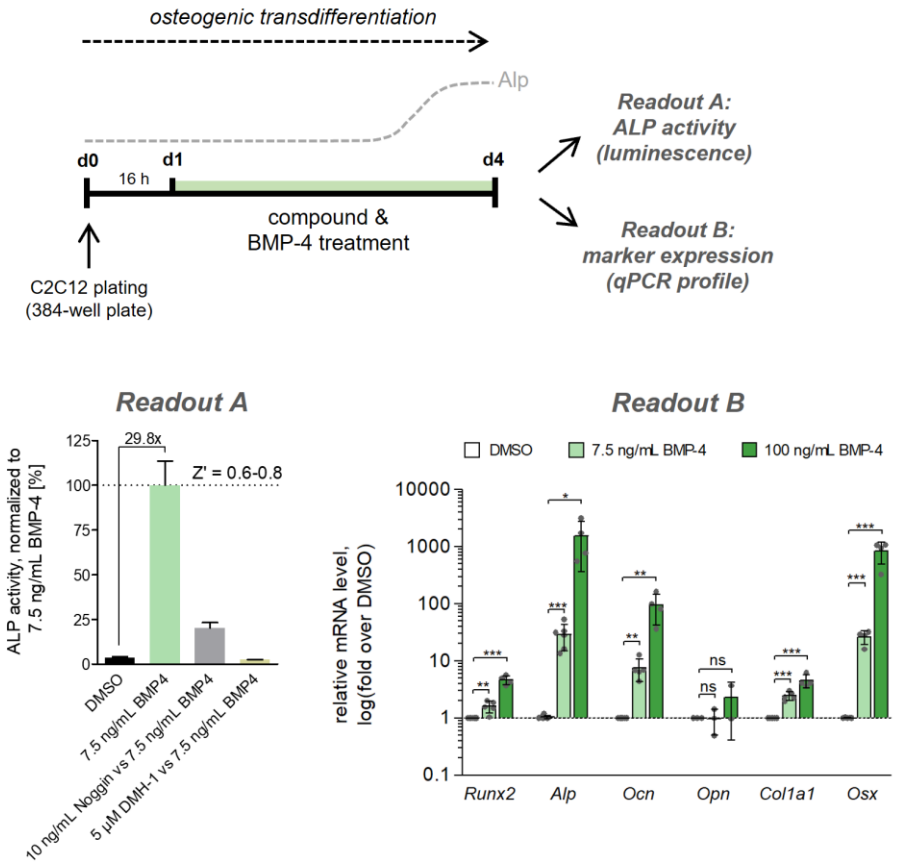

Figure 34: Illustration of assay concept and workflow monitoring osteogenic transdifferentiation of BMP-treated C2C12 myoblasts. Readout A: 16 h after seeding, C2C12 myoblasts were treated with BMP-4 and compounds for 72 h followed by readout and quantification of ALP activity. ALP induction level yields in a ca. 30-fold dynamic range of 7.5 ng/mL BMP-4 for compound treatment and a robust Z'-value of 0.6-0.8. Data is normalized to 100% ALP induction level of 7.5 ng/mL BMP-4 which was effectively inhibited by DMH-1 and rh-Noggin; Readout B: Relative quantification of gene expression for osteogenic target genes. Treatment with vehicle, 7.5 ng/mL BMP-4 or 100 ng/mL BMP-4 was performed for 72 h. Bars represent mean ± SD ($n \geq 3$), normalized to DMSO vehicle control. Statistical analysis was performed with an unpaired two-tailed *t*-test and a set confidence level of 95% (*:p <0.05; **:p <0.01; ***:p <0.001) for n = 3-6 independent experiments for each gene.

As expected, high doses of BMP-4 significantly induced gene expression for all markers except Osteopontin, which generally showed very low expression levels in C2C12 differentiation among the other primers tested. Low concentration of BMP-4 also showed significant induction of osteogenic transcription factors and structural components. Generally, the very high induction of ALP in the assay was successfully confirmed, whereas the transcription of Runx2 was significant but very low. Here, however, Runx2 is also an important regulatory factor, particularly in the early phase of osteogenesis, and is subject to critical regulation for efficient differentiation, thus its expression is tightly controlled.[315] Runx2 promotes *Osx*-expression, another critical transcription factor driving gene expression of osteogenic structural components, and whose expression is potently induced by BMP-4-dependent *Runx2*-expression. The results are promising, as they demonstrate that 7.5 ng/ml BMP-4 is capable

of inducing osteogenesis beyond a certain threshold, while, as shown for all marker genes, further enhancement of BMP signaling can be monitored by a synergistic BMP activator.

Consistent with the measured ALP-activity, Isoliquiritigenin showed significant induction of ALP-expression as shown in Figure 35, but it did not induce any of the other marker genes for osteogenesis in a significant manner. Moderate induction of *Osx* and *Runx2* was observed, but the osteogenic profile indicates a lack of potent osteogenic induction at 5 µM.

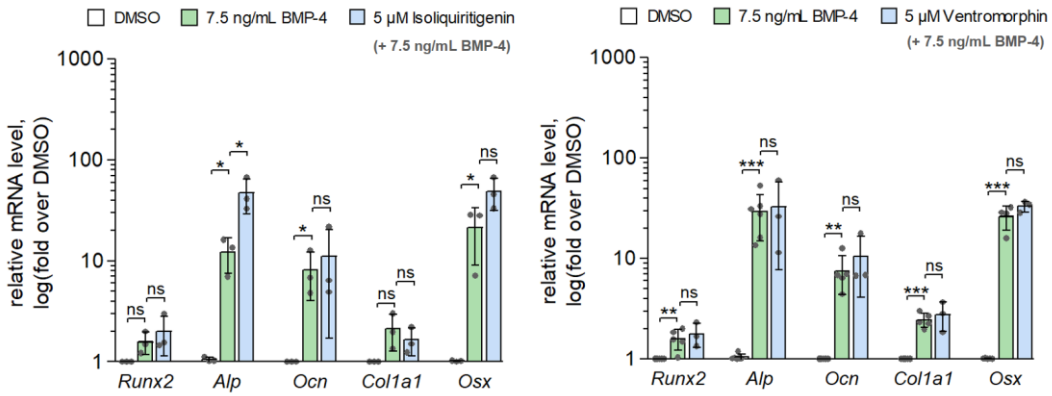

Figure 35: Isoliquiritigenin but not Ventromorphin significantly induced BMP-4-dependent *Alp* expression in C2C12 cells, but no other marker gene for osteogenesis was enhanced by both compounds. Treatment with vehicle, 7.5 ng/mL BMP-4 or 100 ng/mL BMP-4 and compound was performed for 72 h. Data is shown as mean ± SD (n = 3) and normalized to DMSO vehicle (= 1-fold); Statistical analysis was performed with an unpaired two-tailed t-test (* p <0.05; ** p <0.01; *** p <0.001).

As expected, Ventromorphin was incapable of enhancing ALP-expression, compliant to the observed effects on ALP-activity at 5 µM. Contrary to Isoliquiritigenin, no moderate activation of the key transcriptional drivers Runx2 and Osx was induced, thus indicating complete lack of potential to induce BMP-induced osteogenesis in C2C12. Due to its pronounced cytotoxicity of PD407824, no valid expression profile of the BMP-sensitizer PD407824 could be obtained.

Overall, a valid orthogonal assay system was established to depict BMP-dependent osteogenesis and in which further studies on activating and synergistic properties of small molecules can be performed. Moreover, for this purpose, a first gene expression profile complements preliminarily validated substances.

3.1.4 Establishment of BMP-dependent reporter gene assays

To further validate the initial identification of hits that reverse DMH-1-induced cardiac phenotype and exhibit BMP-activating behavior in osteogenesis, reporter gene assays were used to map different signaling pathways that play a role specifically in cardiogenesis. Thus, to exclude possible signaling crosstalks, selectivity of BMP-activating effects was evaluated. While the protocol for transient transfection and compound treatment was established by the SCHADE group previously to investigate small molecule modulation of TGFβ- and Wnt-signaling, transfer to 384-well format was attempted and two different reporters responsive for BMP signaling were tested. Two BMP-responsive elements (BRE) for embryogenic relevant *Vent2* and *Id1* were established to validate BMP-dependent reporter gene activation of small molecules. The BRE-*Id1*-firefly luciferase encoding plasmid was purchased from Addgene and BRE-*Vent2*-firefly luciferase was received from the Mercola group, and its BRE-containing insert was sequenced.[88]

As shown in Figure 36, BMP-4 induced both BMP-specific reporters with a potent EC_{50} of 0.4 ng/mL and 0.5 ng/mL, reaching maximum induction at 10 ng/mL. Similarly, DMH-1 antagonized BMP signaling for both reporters in a dose-dependent manner with an IC_{50} of 90 nM, demonstrating the functional BMP-response of both constructs.

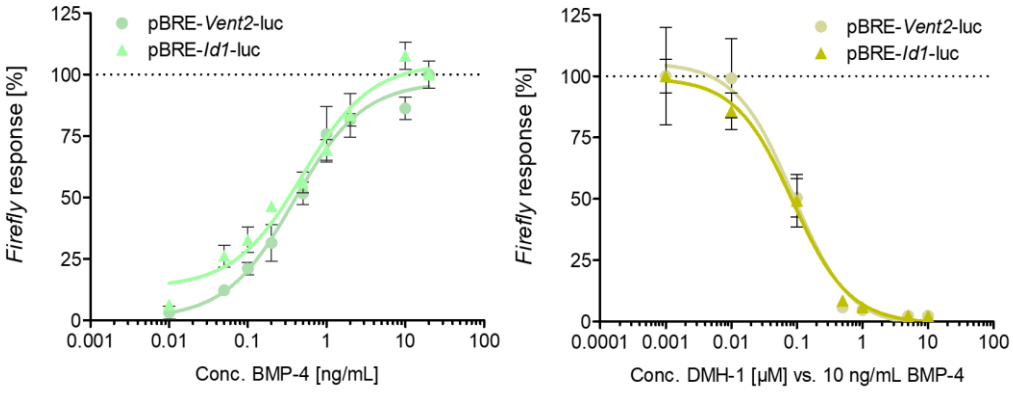

Figure 36: Dose-dependency of BMP-4 on two different BMP-response elements (BRE)-firefly luciferase reporters (BRE-*Vent2*, BRE-*Id1*). BMP-4 was tested from 0.01-20 ng/mL to monitor BMP-dependent activation of BREs, and BMP-4 (10 ng/mL) was antagonized by DMH-1 in a dose-dependent fashion. HEK293T cells were transiently transfected and treated for 22 h before readout. Data is shown as mean ± SD of firefly activity, normalized to DMSO vehicle (= 100%).

It should be noted that both BMP-response elements consist of different BMP-binding domains and differ in their structural constitution, which is why the expression and thus the absolute

luminescence of both reporters differ. Although different transcription cofactors are critical for specific transcription, their functionality behaves identically upon BMP stimulation in this assay.

In order to evaluate the selectivity of the BMP-activating molecules, reference compounds were tested at 5 µM and 1 µM for BMP- and TGFβ-reporters (Figure 37). An additional firefly-luciferase assay was performed to distinguish between firefly modulating and reporter-inducing effects. Isoliquiritigenin and Ventromorphin exhibited high activation of the ventral reporter BRE-*Vent2* and a very moderate activation of BRE-*Id1*, whereas PD407824 strongly inhibited all luciferase expressions at tested concentrations. Interestingly, Isoliquiritigenin showed a highly selective profile for BMP activation, although it modulated the constitutive luciferase control slightly, too. This indicated a more selective BMP-activating profile for this chalcone than expected.

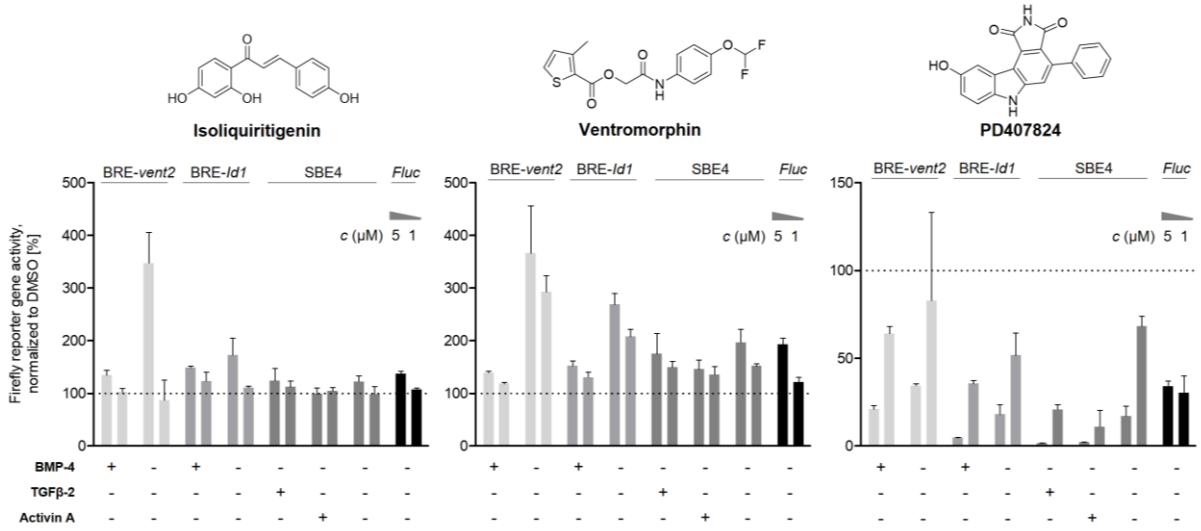

Figure 37: Selectivity profiles of BMP activators showing high activation of BRE-*Vent2* response for Isoliquiritigenin and Ventromorphin, whereas PD407284 inhibited all BMP/TGFβ-reporters. Reporter activation was induced by the respective growth factors at 10 ng/mL and compounds were tested at concentrations of 5 and 1 µM. Additional unspecific Luciferase-control (Fluc) was determined without growth factor under similar conditions. Data is shown as mean ± SD ($n \geq 3$) and normalized to DMSO vehicle (= 100%).

However, Ventromorphin, which is validated for ventralization in zebrafish, was not selective in stimulating all BMP/TGFβ-reporters, which may be due to nonspecific stabilization of luciferase as observed in the constitutively expressed firefly control (Fluc). Similar effects were observed for *Renilla* luciferase (data not shown). Ventromorphin was still able to induce *Vent2*-dependent luciferase expression consistent with the reported induction of ventral phenotype.[271] Nevertheless, BMP activation by Ventromorphin appears to be highly dependent on the cellular context, as no further osteogenic induction was shown in the original

publication and, in a more recent study, Ventromorphins were unable to mimic the BMP-4-induced blockade of TGFβ-induced epithelial-mesenchymal transition (EMT) of lens epithelial cells.[316] However, the study did not examine synergistic effects of BMP-4 and the activators, but only independent effects against TGFβ-2 at very high, unusual concentrations of 40 to 80 µM.

The BMP-sensitizer PD407824 inhibited all reporters with or without growth factor stimulation, which was due to cytotoxic effect in HEK293T cells, as they were strongly rounded and decreased in cell number. These observations and associated results suggest a dominant effect of the off-target effects of PD407824 on CHK-1 and Wee1 in inhibiting cell cycle regulation, and thus reflect an inadequate mapping of BMP activity in this assay system. Since PD407824 consistently exhibited high toxicity and inhibition of cell proliferation in all BMP assays, the problematic nature of negative modulation of the on- and off-target effects suggests a very narrow concentration-response window for BMP sensitization of PD407824, suggesting that the complex mechanism is unattractive and not suitable to mimic physiological BMP activation.

3.1.5 Summary of the developed screening platform

Starting from the idea of establishing a phenotypic screening assay using embryogenic stem cell development to mimic a more physiological cellular/tissue-relevant context compared to rather artificial cell assays, extensive characterization and validation of the BMP-dependent time window during cardiogenesis was performed and a broad assay pipeline for efficient validation and selectivity studies was established. Furthermore, it was shown that the orchestration of BMP signaling cues during mesodermal differentiation and specification can be recapitulated for the discovery of BMP-activating chemical modalities. Validation was performed in a newly established platform, consisting of an osteoblastic differentiation assay, in which the synergistic activation of BMP-4 was examined and a reporter gene assay panel for TGFβ-superfamily and Wnt-signaling pathways to assess signaling crosstalks and pathway selectivity (see Figure 38).

A special feature of the two differentiation assays is also the different morphological changes and readouts. While rescue effects on DMH-1-induced cardiogenesis are investigated in the phenotypic assay in stem cells, validation in an orthogonal differentiation assay to study BMP-

activating effects in an actual induction readout is an excellent complementary setup. A good example of this is the BMP-sensitizer PD407824, which is suspected to inhibited cardiac differentiation by disrupting cell cycle regulation and these effects are also evident in the orthogonal assay and in the activity profile of reporter genes that play important roles in cardiogenesis and osteogenesis. The partial lack of activity in the selection of reference compounds highlights the general problem in identifying growth factor-activating or -mimetic factors due to the complexity and interplay of various mechanistic regulations of BMP signaling depending on the cellular and developmental context, hence, a broad and comprehensive test system with multiple cellular contexts is preferred.

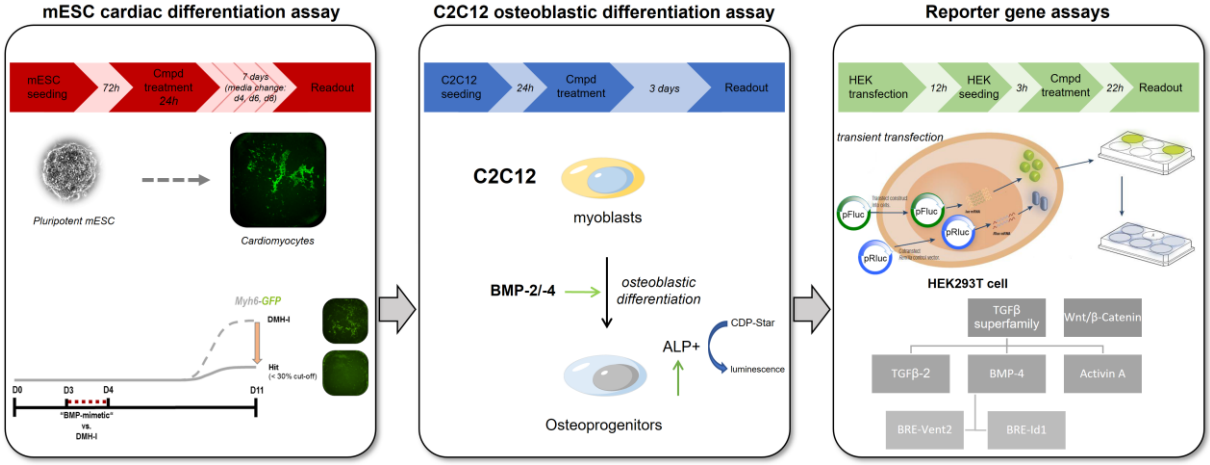

Figure 38: Schematic overview of the assay pipeline developed to identify and further validate novel BMP-activating small molecules via primary screening in a mESC-based cardiogenic differentiation assay, followed by validation in an orthogonal osteoblastic differentiation assay to study BMP-dependent ALP-induction and finally assessment of BMP signaling-responsive reporter activities and selectivity studies of TGFβ-superfamily.

For future testing, established gene expression profiles might be applied and mechanistic studies would round out the understanding induced osteogenic differentiation of chemical probes. However, since the main goal is to identify a chemical modality that could be used in therapeutic applications, the capacity to promote mineralization and thus ossification is more attractive. Therefore, mineralization studies in the human osteosarcoma cell line hSaOS-2 were established and carried out by the BERTRAND group in Magdeburg, the results of which are presented in validation studies in this thesis.

3.2 Identification and characterization of Chromenone 1 as a novel BMP potentiator

3.2.1 Phenotypic screening of an in-house diversity set of small molecules

The established and well-characterized BMP phenotypic screening assay was used to screen an in-house diversity-focused and natural product-inspired small molecule library of almost 7,000 compounds. Therefore, compounds were subjected to mESC-*Myh6*-GFP cells at a single dose of 5 µM to identify hits that would antagonize BMP-dependent DMH-1-induced cardiogenesis. Due to the sensitivity of stem cells, compounds were tested only at 5 µM, primarily to exclude hits that could negatively affect cell viability and thus be identified as false-positive hits, but also to avoid excluding potential modulators of novel mechanisms by off-target effects or crosstalks affecting cell proliferation and metabolism. Hits were defined as compounds able to reduce DMH-1-induced cardiogenesis below 30% of its average 10-fold dynamic range, which is below 2-fold the SD of mean induction without decreasing cell number by maximum 30% after 11 days of differentiation. As visualized in Figure 39B, the compounds varied in their activity, with 322 passing the initial criteria and 97 compounds (hit rate of 1.4%) confirmed by retesting that had a purity of at least 70% as determined by COMAS for the respective compounds. Remarkably, there are many outliers that probably even promoted cardiogenesis, but this quantified effect is due to accumulated cell colonies and disrupted cell monolayer that can form autofluorescent artifacts, as previously described and observed for DMSO. Since these substances had a decisive negative influence on the vitality of the cells, they were automatically excluded from the evaluation. The 97 compound hits were further tested to verify dose-dependent activity in the mESC assay and to validate possible BMP-dependent modulation. Of these, 35 hits were evaluated as potent compounds with an IC_{50} below 1.5 µM, resulting in a final hit rate of 0.5%, which can be considered a valid value for phenotypic screening. The 35 most potent hits were further subjected to the orthogonal osteoblastic differentiation assay in C2C12 to determine their BMP-enhancing efficacy and potency in the presence of a low dose of BMP to induce BMP-dependent osteogenesis.

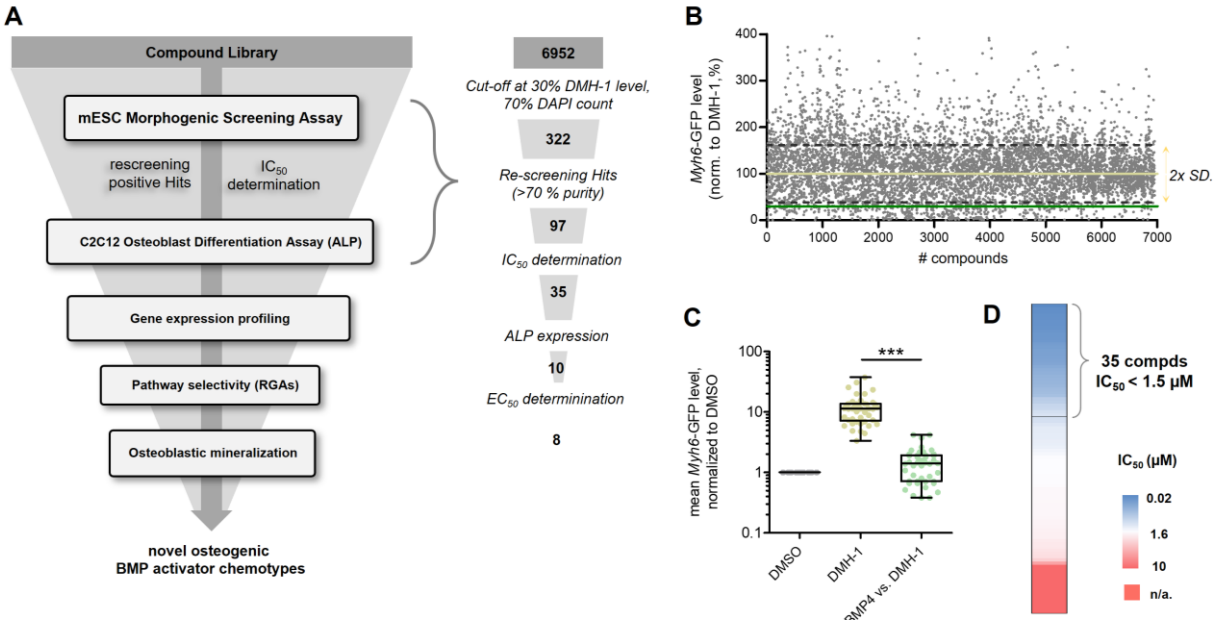

Figure 39: Screening of an in-house diversity-focused compound library yielded 35 potent hits that antagonize DMH-1-induced cardiogenesis. (A) Illustration of screening and validation workflow to identify novel osteogenic BMP activators: Primary screening was performed in mESC-based phenotypic screening assay and IC_{50}-validated hits moved forward to secondary screening in osteoblastic differentiation of C2C12 cells and subsequent mechanistic validation via gene expression analysis (C2C12), pathway selectivity (reporter gene assays, RGAs) and osteoblast mineralization (human SaOS-2 cells). (B) Summary of medium-throughput screening results in mESC-*Myh6*-GFP. Stem cells were treated with compounds (at 5 µM) and cardiogenesis was induced by 0.5 µM DMH-1 for 24 h at d3-4 of differentiation. Cardiac cluster levels are normalized to DMH-1 (= 100%, yellow line) and compounds antagonizing cardiogenesis below set threshold of 30% *Myh6*-GFP level of DMH-1 (green line) were selected. (C) Dynamic range of phenotypic screening assay averaged 10-fold the mean antagonism (DMH-1/ BMP-4) and induction (DMH-1). Data is shown as mean ± SD of *Myh6*-GFP levels under screening conditions for $n = 45$ plates. Statistical analysis was performed with an unpaired *t*-test (*** $p < 0.001$). (D) Dose-dependent hit validation of 97 initial hits yielded 35 potent inhibitors with IC_{50}-values below 1.5 µM (n/a = not applicable).

3.2.1.1 Primary hit validation and clustering

The established secondary orthogonal differentiation assay in C2C12 was employed to validate the BMP-dependent activation of identified potent primary hits. A total set of 10 compounds promoted low-dose BMP-induced osteogenic ALP-expression (Figure 40A,B), which could be primarily classified into three distinct chemotypes, a quinolinoles-based class, one 4*H*-chromen-4-one (Chromenone 1) and a subset of seven 2-aminopyrimidines including the reported autophagy-inhibitor Autophinib that highly induced ALP-activity.[317] Both quinolinoles stimulated osteogenesis in a similar manner as Isoliquiritigenin at 5 µM, however, the activity of both compounds could not be robustly reproduced, which will be discussed in the next chapter. One cluster that appeared to be potent antagonists of cardiogenesis in the primary screening assay included several glucose uptake inhibitors with different chemotypes

collectively targeting the GLUT1-4 glucose transporters with different selectivity profiles.[318–320] However, this highly potent cluster inhibited BMP-dependent osteogenesis in C2C12 in a very similar manner to the profile observed in phenotypic screening assay and correlated strongly with their GLUT inhibitory response (see appendix, Figure 96). Thus, these data suggest a BMP-independent and antagonistic response mainly due to the perturbation of the cellular glucose flux and homeostasis, which has been shown to be of great importance for the differentiation process, since a high amount of glucose is required, and the cells undergo a major change in their metabolic profile during differentiation.[321,322] The other two hit classes with Autophinib as the most potent autophagy inhibitor from the 2-aminopyrimidine subclass and the 4*H*-chromen-4-one completely reversed DMH-1-induced cardiac cluster formation in a dose-dependent manner with an equally potent IC_{50} of 200 nM displaying high potency and efficacy (Figure 40C).

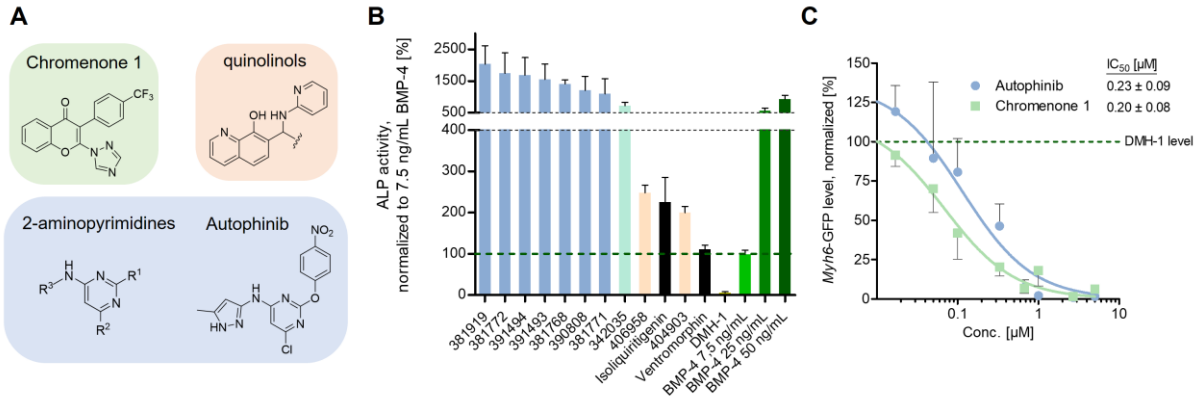

Figure 40: Orthogonal assay furnished three distinct chemotypes of putative osteogenic BMP activators. (A) Chemical structures of the three identified active BMP activator chemotypes. (B) ALP-induction of screening hits on C2C12 osteoblastic differentiation at single doses (5 µM) in presence of 7.5 ng/mL BMP-4 after initial orthogonal screening. Bars are represented as means ± SD of ALP activity after 72 h, normalized to 7.5 ng/mL BMP-4. (C) Proof of dose-response profiles of Autophinib and Chromenone 1 on DMH-1-induced (0.5 µM) mESC-*Myh6*-GFP cardiogenesis display high potencies as BMP-4-mimetics. Data is shown as means ± SEM for *n* = 3 experiments.

Next, the dose-dependent stimulation of BMP-driven ALP-induction in C2C12 myoblasts was determined in absence and presence of BMP-4 to evaluate the potential of BMP-4-mimetics or enhancers, respectively. Autophinib and Chromenone 1 exhibited quite distinct activity profiles in C2C12 osteoblast differentiation (Figure 41A), with Autophinib overactivating ALP induction in a very potent manner compared with high-dose BMP-4 (50 ng/mL) in a relatively very small dosing window (0.2-1 µM), whereas Chromenone 1 showed a milder dose-dependence from 0.013-1 µM with high efficacy and a calculated EC_{50} of 0.34 µM, which is close to the IC_{50}-value from its potent reduction in cardiogenic cluster formation (1.7-fold

higher). Interestingly, Autophinib also stimulated ALP-induction independently of synergistic low-dose BMP-addition with similar efficacy but lower potency, indicating a ligand binding-independent mode of action. In contrast, Chromenone 1 was inactive in the absence of BMP-4, suggesting a BMP-activating dependency and thus a BMP-potentiating mechanism in osteogenic differentiation. Due to the very strong induction and the different modes of action of the two chemotypes, the morphology typical for transdifferentiated C2C12 myoblasts was examined and the characteristic "cobblestone" phenotype for high-dose BMP-4 was observed (Figure 41B).[271] Even low-dose BMP-4 (7.5 ng/mL) used to induce basal osteogenesis showed the typical morphology, but less-developed, and an intact cell monolayer. Notably, synergistically treated C2C12 with low-dose BMP-4 and Chromenone 1 at 1 µM indeed showed a significant morphological shift toward osteoblastic C2C12, as observed for 100 ng/mL BMP-4, consistent with the observed ALP-activity of 1 µM and high-dosed BMP-4.

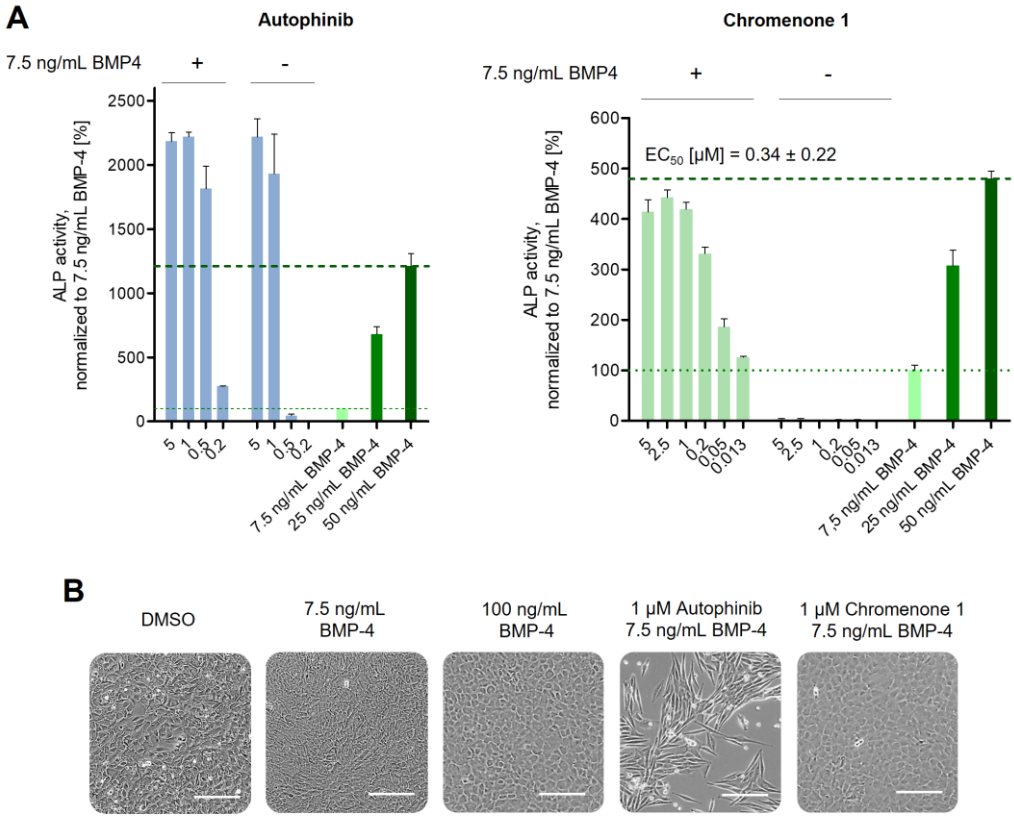

Figure 41: Orthogonal hit validation in C2C12 established Chromenone 1 as a novel osteogenic BMP potentiator. (A) Dose-dependency of screening hits on ALP-induction in presence of absence of 7.5 ng/mL BMP-4, compared to low- (7.5 ng/mL), medium- (50 ng/mL) and high-dosed (100 ng/mL) BMP-4; Data is shown as means ± SD of ALP activity ($n \geq 3$), normalized to 7.5 ng/mL BMP-4 (= 100%). (B) Representative micrographs reveal distinct morphologies of BMP-4 and Chromenone 1/BMP-4 treated C2C12 cells after 72 h compared to Autophinib (scale bar = 200 µm).

However, the morphology observed in C2C12 treated with 1 µM Autophinib differed from the expected phenotype showing a predominantly myotube-like phenotype and significantly reduced cell number, indicating that the formed cells are incapable of proliferation, contrary to formed osteoprogenitors. This morphological change was also observed at lower doses of Autophinib and it was suggested to be associated to the potent stimulation of ALP. To exclude artificial ALP-activating effects and to assess the differentiation process, osteogenic transcript levels were determined by qRT-PCR and compared with 7.5 ng/mL BMP-4-induced mRNA levels. As shown in Figure 42, ALP-induction could be confirmed for Autophinib, which increased relative transcript levels >80-fold over BMP-stimulated expression, but the autophagy inhibitor was unable to induce any other osteogenic marker and even appeared to suppress BMP-dependent gene induction. Various signaling pathways that crosstalk with BMP signaling may be a crucial factor here, such as Wnt or SCF signaling, which can strongly promote ALP production, but their function is only present with basal BMP stimulus.[312,313] In addition, Autophinib may have a regulatory impact on noncanonical BMP signaling due to the known modulation of Akt signaling. Since Autophinib mediates downregulation of autophagy through inhibition of class III PI3K lipid kinase, this potential mechanism for ALP induction required further investigation.

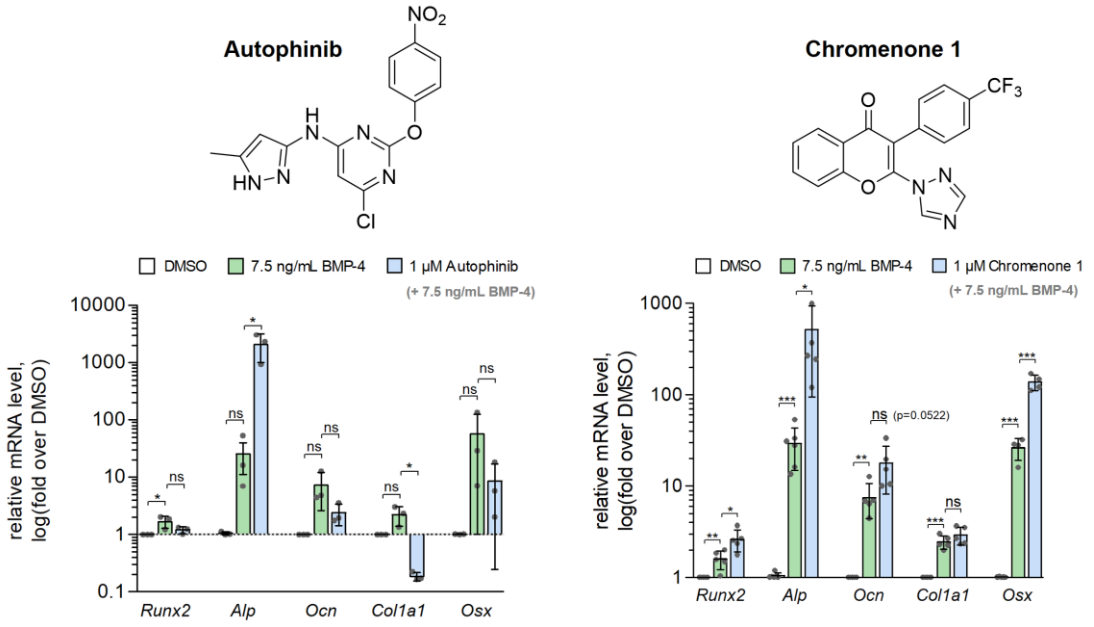

Figure 42: Relative quantification of BMP-dependent osteogenic gene expression transcripts confirmed Chromenone 1 as a BMP-4 potentiator and suggests Autophinib as a BMP-independent ALP-inducer. C2C12 cells were treated with DMSO and/or BMP-4 (7.5 ng/mL) in the presence or absence of compound (1 µM) for 72 h. Data is shown as mean ± SD ($n \geq 3$) and normalized to DMSO. Statistical analysis was performed with an unpaired two-tailed *t*-test (* $p < 0.05$; ** $p < 0.01$; *** $p < 0.001$).

In contrast to Autophinib, Chromenone 1 showed an osteogenic and BMP-dependent profile, confirming the observed morphology and measured ALP-induction in C2C12. Although important structural markers such as *Osteocalcin* and *Col1a1* could not be significantly increased despite moderate stimulation, the key osteogenic driver and transcription factors Runx2 and Osx were markedly induced, yielding Chromenone 1 as the only potent positive BMP-stimulating or amplifying chemotype from this screen.

3.2.1.2 De-validation of VPS34/GSK3-targeting 2-aminopyrimidines

Since Autophinib passed the primary screening assay and orthogonal differentiation assay, further experiments were conducted to evaluate the activity and mode of action of the reported autophagy inhibitor targeting VPS34 lipid kinase and to understand the potent and effective induction of the observed BMP-independent ALP-activation. Therefore, an in-house panel of 14 2-aminopyrimidine derivatives, from which six derivatives were also identified after secondary evaluation in C2C12, were profiled in both differentiation assays and their IC_{50} and EC_{50} values were calculated (Figure 43).

The activities of the derivatives were compared with the literature-reported IC_{50}-values for autophagy and VPS34, as illustrated in a heatmap, which indicate a strong correlation between inhibition of VPS34 and activity in both BMP-dependent differentiation assays. Lack of the pyrazole substitution resulted in a complete loss of function in inhibiting the catalytic activity of VPS34 and also in its ability to induce ALP activity in C2C12. Interestingly, the isoxazole-derivative (11) of Autophinib, was completely inactive against VPS34 and neither showed any morphogenic activity in osteogenic and cardiogenic differentiation assays. Derivative 14 was the only BMP-active VPS34 inhibitor that was inactive in C2C12, which is a known TBK1-inhibitor and was the starting point for the development of Autophinib as a potent autophagy inhibitor.[323] These data strongly suggest a correlation between VPS34 inhibition and ALP-induction.

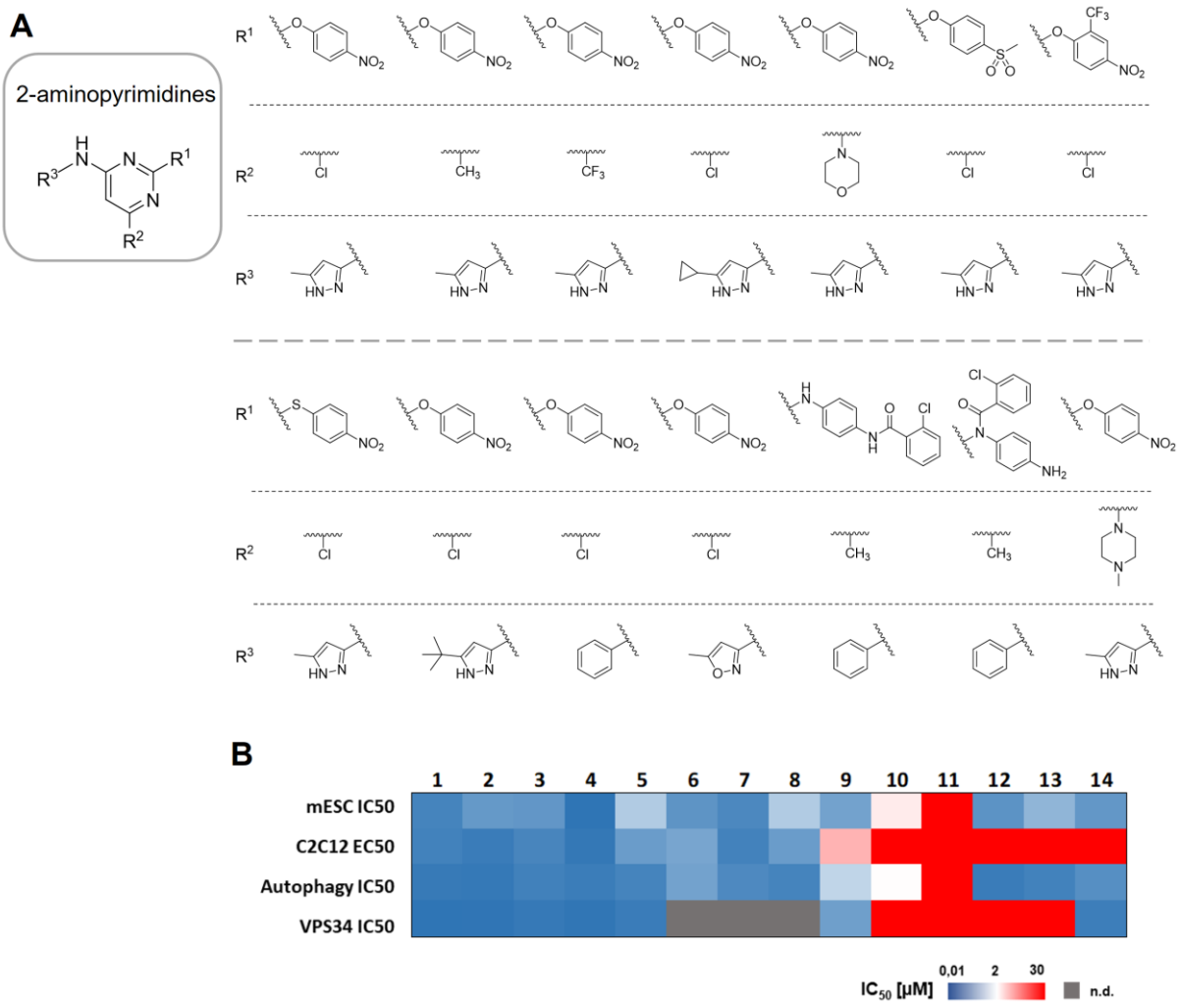

Figure 43: Structure-activity relationship analysis and de-validation of VPS34-targeting 2-aminopyrimidine hit class. (A) Chemical structures of the in-house series of 2-aminopyrimidines tested for structure-activity relationships (SARs). (B) Correlation of calculated and literature-reported activities of autophagy and VPS34-inhibitors for a selected panel of aminopyrimidines in BMP-dependent differentiation assays.[317]

To further rule out autophagy regulation as an underlying cause of ALP induction, two other literature-known autophagy inhibitors with different chemotypes targeting mitochondrial complex I were tested in both differentiation assays.[324,325] Both Aumitin and Authipyrin have been shown to inhibit mitochondrial complex I, leading to dysregulated autophagy and mitochondrial respiration, thus negatively affecting cellular homeostasis. While Authipyrin showed only moderate activity in the cardiogenic assay, Aumitin strongly antagonized DMH-1-induced cardiogenesis at higher concentration above 2.7 µM, but notably, a decrease in cell number was observed (Figure 44A).

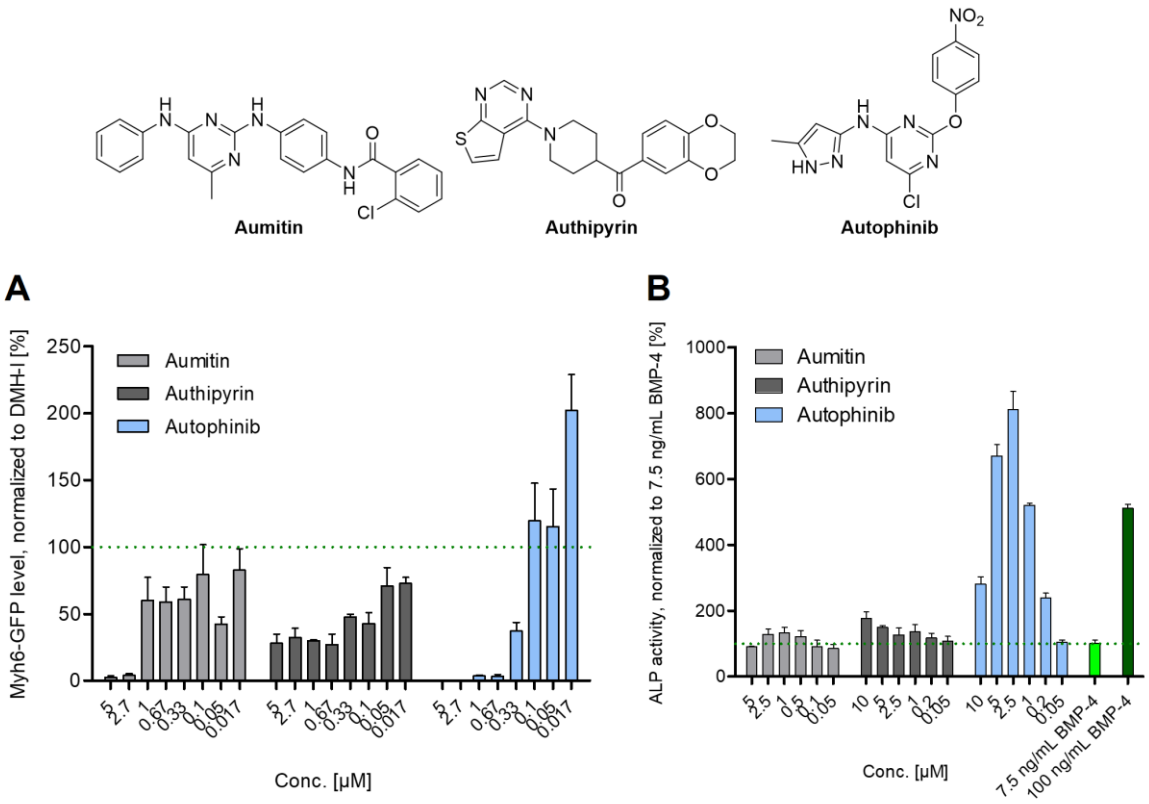

Figure 44: Inhibition of mitochondrial complex I leading to disrupted autophagy did not correlate with VPS34-induced ALP induction. (A) Dose-response antagonism of in-house literature-known autophagy inhibitors with distinct chemotypes in cardiac differentiation induced by selective BMP inhibitor DMH-1 (0.5 µM). Bar graph is representative for the mean ± SEM of two independent experiments. *Myh6*-GFP levels were normalized to DMH-1 with vehicle (DMSO). (B) Potent autophagy inhibitors did not enhance ALP-induction in C2C12. Compounds were incubated along with 7.5 ng/mL BMP-4 in C2C12 and treated for 72 h. ALP activities were normalized to DMSO and bars are represented as mean ± SD for at least two independent experiments.

In comparison to Autophinib, both compounds lacked potency and showed distinct activity profiles. A similar profile was observed in the BMP-dependent osteoblastic assay, where only Authipyrin moderately induced ALP activity (1.7-fold over basal BMP-level, Figure 44B). Since both compounds share a similar profile in both assays that differs from the one observed with Autophinib, downregulation of autophagy by inhibition of mitochondrial complex I is most probably not a mechanism of action, indicating an autophagy-independent effect of Autophinib through VPS34 modulation.

Given the known role of PI3K signaling on BMP signaling, selective VPS34 inhibition might affect non-canonical and thus secondary expression of typical BMP-dependent target genes such as ALP.[101,102] To elucidate whether modulation of lipid kinase class III is indeed responsible for its expression, two literature-known distinct VPS34-inhibitor chemotypes (SAR405 and VPS34-IN1) were profiled in the differentiation assays.[326,327] Both potent VPS34

inhibitors displayed very similar profiles, as they inhibited DMH-1-dependent cardiomyocyte formation and moderately induced ALP-activity up to 2.5-fold above low-dose BMP-levels (Figure 45B, C). However, they showed a significant decrease in cell number at higher concentrations in both assays, and their efficacy differed substantially from that of Autophinib. To evaluate the ALP-activation, osteogenic differentiation marker levels of SAR405 at a non-toxic and effective concentration (1 µM) were quantified, showing no effects on BMP-dependent expression (see Figure 45D), suggesting a unique mode of action of Autophinib's potent effects on differentiation, that is not solely due to selective VPS34 inhibition.

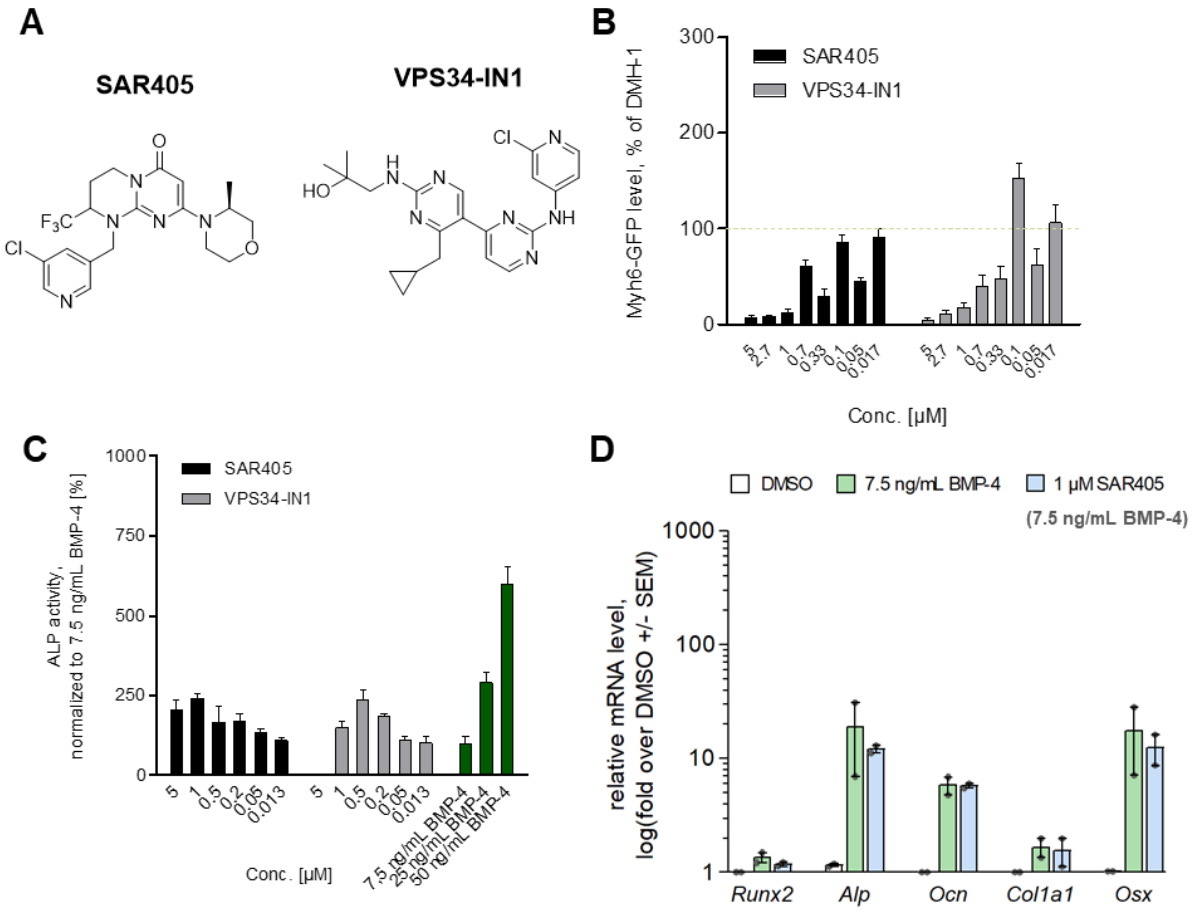

Figure 45: Evaluation of VPS34-dependent BMP-induction indicate no enhanced osteogenic differentiation. (A) Chemical structures of two distinct, highly potent VPS34 inhibitor chemotypes (SAR-405, VPS34-IN1). (B) Dose-response antagonism of VPS34 inhibitors in cardiac differentiation induced by selective BMP inhibitor DMH-1 (0.5 µM). Bar graph is representative for the mean of triplicates and the respective SEM of two independent experiments. *Myh6*-GFP level were normalized to DMH-1 with vehicle (DMSO). (C) Potent VPS34 inhibitors moderately enhance BMP-dependent ALP induction in C2C12. Compounds were incubated along with 7.5 ng/mL BMP-4 in C2C12 and treated for 72 h. ALP activities were normalized to DMSO and bars are represented as mean ± SD for at least two independent experiments. (D) SAR405 did not induce synergistic gene expression of osteogenic transcripts compared to BMP-4-treated and untreated C2C12. Treatment with vehicle, 7.5 ng/mL BMP-4 or 7.5 ng/mL BMP-4 and compound was performed for 72 h. Statistical analysis was performed with an unpaired two-tailed *t*-test of the mean of triplicates and the respective SD compared to DMSO control and a set confidence level of 95% (*:p <0.05; **:p <0.01; ***:p <0.001) for n = 2 independent experiments for each gene.

Based on the unique profile in both assays, it is reasonable to assume that autophagy inhibition by both modulation of mitochondrial respiration and inhibition of PI3K class III kinase does not show crosstalk with BMP activating or amplifying effects in the differentiation assays. These are also interesting results considering that Akt-induced mTOR signaling can also be activated by noncanonical BMP signaling and may represent a potential mechanism via a positive feedback loop. However, it should be noted that cells undergoing differentiation demand high energy, so an intact metabolism is essential, and impaired autophagy critical for cellular homeostasis, could promote metabolic stress and thus cell viability and proliferation. This was also observed for the most potent autophagy/VPS34-inhibitors at highest concentrations in the stem cell-based cardiac differentiation assay, as cell number decreased.

Another possible reason for the potent activity of Autophinib could be its pronounced GSK3β activity (IC_{50} = 1.3 nM), a kinase involved in regulation of Wnt/β-catenin signaling. Activation of canonical Wnt/β-catenin signaling via GSK3β-inhibition is a known synergistic contribution to BMP-driven osteoblastogenesis and expression of Runx2 and ALP.[133,312] To prove this hypothesis, two potent GSK3β-inhibitors 6-BIO and CHIR99021 were tested similar to the VPS34-inhibitors, as shown in Figure 46.

Both reference compounds antagonized BMP-dependent cardiogenesis only at very high concentrations, with significantly lower potency compared with Autophinib, indicating a predominant response to VPS34 inhibition, which is consistent with the observed profile of potent VPS34 inhibitors in the mESC assay (Figure 46A). However, as observed for ALP-activity and morphology in C2C12, GSK3β inhibition resulted in a highly similar profile. The data strongly suggest a GSK3β-dependence of ALP-induction both in the presence and absence of low-dose BMP-4 up to maximum cellular BMP-response as both reference compounds exhibited only a slightly less potent profile, which would be expected given their slightly less potent literature-reported IC_{50} of 5-6 nM.[328,329] This effect was also supported by representative micrographs, revealing similar cell morphologies of BIO (5 µM) and Autophinib/BMP-4-treated C2C12 cells after 72 h that differ from BMP-4-dependent phenotype, as shown in Figure 46D.

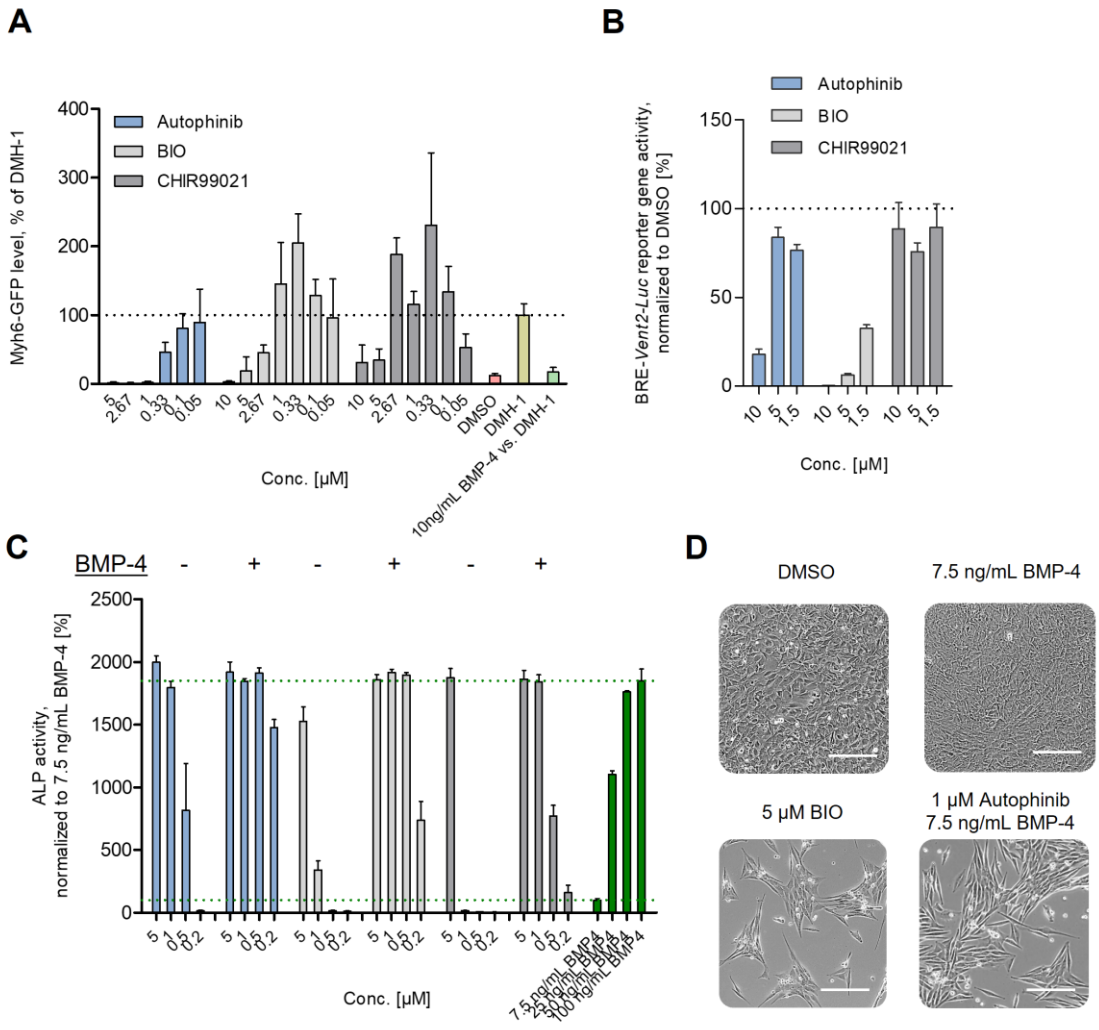

Figure 46: The potent VPS34/GSK3 inhibitor Autophinib reveals a GSK3-dependent ALP-induction in C2C12 differentiation. (A) Comparison of VPS34/GSK3 inhibitor Autophinib with two distinct, selective and potent GSK3β-inhibitors (BIO, CHIR99021) in mESC-BMP assay indicates a predominant cellular response to VPS34 inhibition. Data graph is representative for the mean of triplicates and the respective SEM of two independent experiments. *Myh6*-GFP level were normalized to DMH-1 (= 100%). (B) Autophinib and the GSK3β inhibitors (BIO, CHIR) did not induce BMP-dependent reporter activity (BRE-*Vent2*) in HEK293T cells. 293T were transiently transfected and treated with BMP-4 (10 ng/mL) and compounds at indicated doses for 22 h before readout. Data is shown as mean ± SD ($n \geq 2$) and normalized to DMSO vehicle (= 100%). (C) In the C2C12 osteoblast assay, Autophinib and known potent GSK3β inhibitors induced ALP activity both in the presence or absence of 7.5 ng/mL BMP-4. Activities are normalized to 7.5 ng/mL BMP-4 (= 100%). (D) Representative micrographs reveal similar cell morphologies of BIO (5 µM) and Autophinib/BMP-4-treated C2C12 cells after 72 h (scale bar = 200 µm).

To investigate whether GSK3β-inhibition, and thus Wnt/β-catenin stimulation, also leads to an increase in reporter activity, the set of compounds was tested on the BMP-dependent reporter BRE-*Vent2* and BRE-*Id1*. Contrary to the contributing stimulation of GSK3β-inhibition in osteogenesis of differentiated C2C12, no enhancing effect of BMP reporter activity was observed (Figure 46B), suggesting a quite exclusive crosstalk depending on the cellular context. Collectively, these data demonstrated that inhibition of VPS34 may result in a false-

positive hit in the mESC assay but shows only weak activity in the C2C12 transdifferentiation assay. This profile is reversed for GSK3β inhibition, in which classical inhibitors are inactive in the mESC assay and mediate non-osteogenic ALP induction in C2C12.

To assess how such a mechanism or similar Wnt activating effects would affect the validation assays, since Wnt and BMP signaling cross-regulations are known to be common in differentiation processes, an overall selectivity profile of Autophinib was included. Here, Autophinib (1 µM) showed no activity on TGFβ-superfamily signaling including TGFβ-2 and Activin A (Figure 47A), but a strong induction of the β-catenin-sensitive SuperTOPflash (STF) luciferase reporter was observed (up to 2-fold above basal Wnt stimulation of transfected cells).

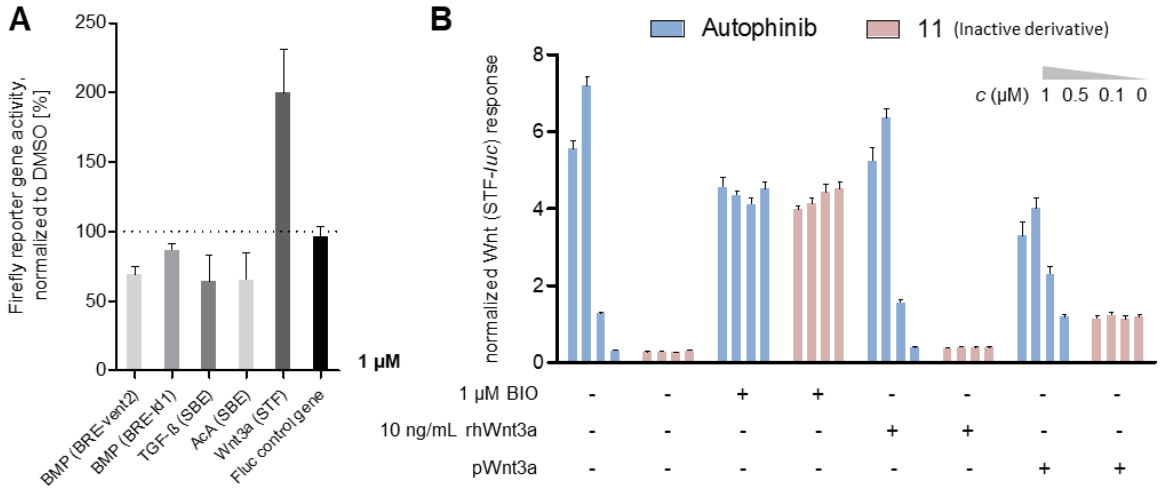

Figure 47: Autophinib strongly induced selective Wnt/β-catenin signaling via GSK3-modulation. (A) Pathway selectivity profile of Autophinib at 1 µM. The specific pathways were activated with their respective GF at 10 ng/mL. Wnt-activation was induced with co-transfection of pWnt3a for autocrine Wnt3a expression. Additional unspecific Luciferase modulation was determined without growth factor under similar conditions via the constitutively active Fluc-reporter. Data is shown as mean ± SD ($n \geq 3$) and normalized to DMSO vehicle (= 100%). These results based on experiments performed by Tanja Schuh during her Bachelor thesis.[330] (B) Activation of Wnt/β-catenin signaling by Autophinib and C2C12/ALP-inactive derivative 11 in the presence or absence of different Wnt stimuli. HEK293T were transiently transfected with a SuperTOPflash (STF) luciferase reporter and treated with compounds at indicated doses for 22 h. Wnt stimulation was induced by either 6-BIO or rhWnt3a or by co-transfection of a Wnt3a expression plasmid for autocrine activation. Bar graph represents mean ± SD ($n \geq 2$) and normalized to DMSO vehicle (= 100%).

Autophinib could effectively induce Wnt reporter gene activity up to 7-fold over basal reporter activity in the presence and absence of autocrine Wnt3a-stimulus or exogenous rhWnt3a, suggesting a strong cellular response to GSK3β-modulation of Autophinib (Figure 47B). This dependence was further proven by Wnt induction of 1 µM 6-BIO and addition of Autophinib, which was unable to increase Wnt activity in the presence of the reference compound. Interestingly, the inactive isoxazole-substituted 2-aminopyrimidine derivative 11 was incapable

of inducing reporter activity, indicating a possible correlation between VPS34- and GSK3β-inhibition of pyrazole-substituted derivatives of Autophinib.

These data will be beneficial for future evaluation of Wnt-stimulating compounds in the differentiation assays, as Wnt stimulation can interfere with BMP-dependent ALP-induction during osteoblastogenesis but had only a moderate effect on DMH-1 antagonism in mESC cells. Notably, neither GSK3β-reference compound would have been identified as a potent hit from the primary screening assay. Furthermore, evaluation of the strong activity of Autophinib also showed the expected effect on cellular viability and homeostasis, which could specifically lead to false-positive hits in the mESC assay. Taken together, although the VPS34/GSK3β-targeting Autophinib remained as a potent hit alongside the chromenone chemotype from screening, it was ultimately de-validated as a BMP-mimetic compound, and further was a useful tool compound to validate and prove the screening workflow, thus supported the proof-of-principle of the assay strategy and provided insight into upcoming issues in future screening campaigns.

3.2.1.2 De-validation of quinolinols

One of the identified hit clusters identified during orthogonal validation was the quinolinol chemotype, from which two compounds were identified to synergistically induce ALP activity during osteogenic differentiation of C2C12. In contrast to the 2-aminopyrimidine and chromenone-based scaffolds, the activity was moderate at best and could not be reproduced. Interestingly, the chemotype have been reported to activate TEAD-YAP interaction, thus leading to Hippo pathway activation.[331] Since the compound class was identified from an internally synthesized library, a rapid re-screening of a variety of quinolinol derivatives was performed to identify potential more active compounds and to generate a small SAR profile. As shown in Figure 48, nine derivatives were tested in both differentiation assays, showing a dose-dependent effect in the cardiogenic mESC-assay, with quinolinole 1 being the most potent inhibitor (IC_{50} = 1 µM). However, subsequent evaluation of quinolinol derivatives in osteogenesis could not confirm this hit class, as they lacked robust and efficient potential to induce ALP activity.

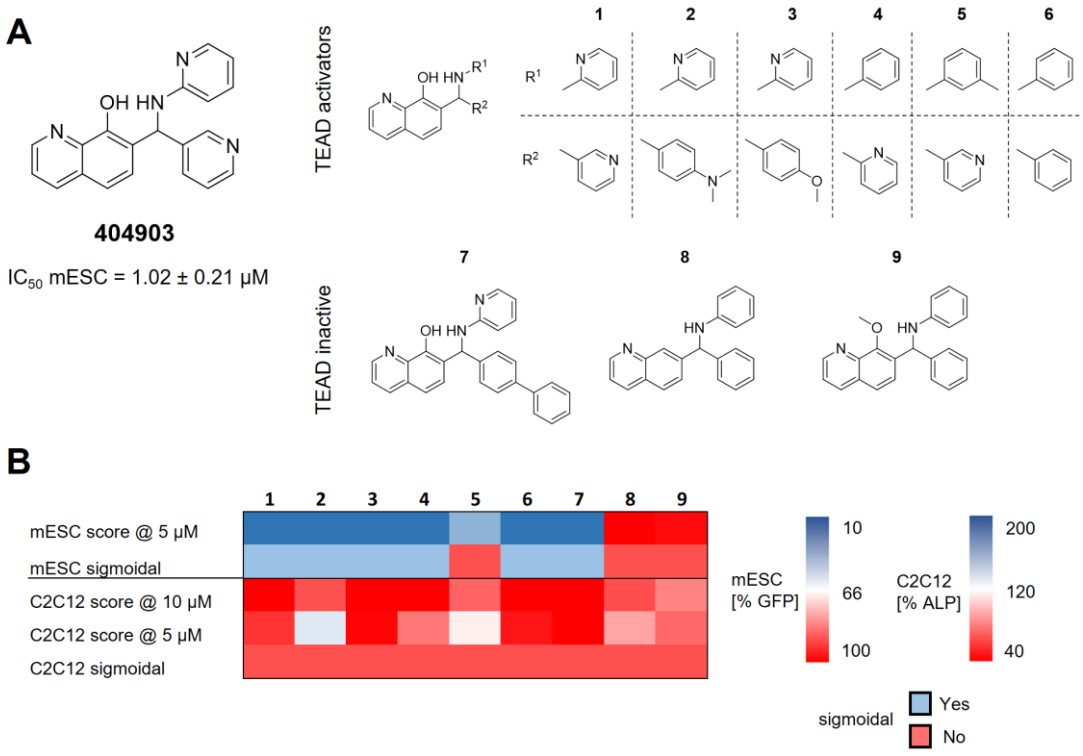

Figure 48: De-validation of the hit chemotype of quinolinols. (A) Chemical structures of quinolinol derivates tested for SAR-based validation. (B) SAR did not confirm BMP-dependent activity of quinolinols in C2C12 cells. Compounds were sorted according to their reported activity as TEAD activators (from left to right, increasing potency).[331]

Given that the ALP-enhancing activity could not be reproduced or was very weakly, no further studies were performed, in part because the hydroxyquinoline-based scaffold is a known metal-chelating scaffold that may affect cellular homeostasis, suggesting cellular artefacts thus affecting reproducibility during differentiation.[332]

3.2.2 Structure-Activity-Relationships of chromenone derivatives

A structure-activity-relationship study was performed to evaluate critical structural substituents for BMP activity and to improve cellular BMP-response of the chromenone chemotype. For this purpose, a combination of derivatives from the in-house library based on the previously reported compound class and analogues newly synthesized by Mahesh Puthanveedu focusing on the 2- and 3-positions (i.e., R^2 and R^1) of the 4*H*-chromen-4-one scaffold were used. A total of 29 pure derivatives were profiled in both morphogenic differentiation assays and their BMP-dependent activation was visualized in a heatmap (Figure 49).[333]

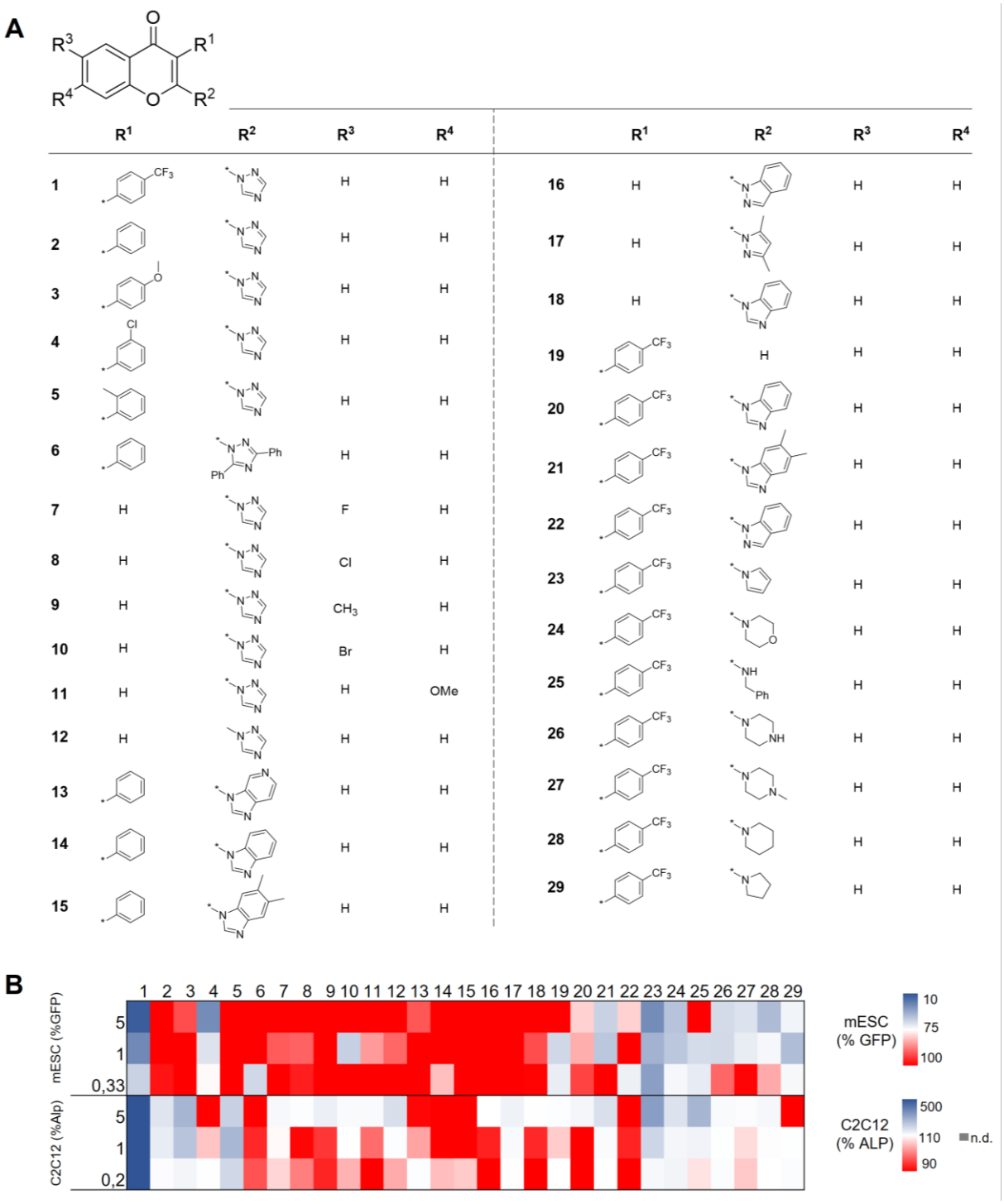

Figure 49: Structure-activity relationship study reveals chromenone 1 as chemical probe to induce BMP signaling in differentiation assays. (A) Chemical structures of the series of chromenones **1-29** tested and synthesized for SAR study. (B) Comparative structure−activity profiling of chromenone derivatives in BMP-dependent mESC- and C2C12-differentiation assays in a dose-dependent manner. Heatmap illustrates activity as mean values of $n \geq 3$ independent experiments.

At a first glance, no derivative exhibited an effective BMP-synergistic profile as the initial hit, Chromenone 1 (1). In general, substitution on 3-position was essential for activity, as unsubstituted analogues like 12 and 16-18 showed no effect. Interestingly, analogue 2

(Chromenone 2), only lacking the *p*-trifluoromethyl moiety, was also inactive in the differentiation assays, indicating a strong dependence on the electron-rich pharmacophore that might cause a critical reduction in the electron-density of the chromenone-scaffold. Replacement of the *p*-trifluoromethyl with an electron-donating group such as *para*-OMe (3), or incorporation of a *meta*-chloro (4) or *ortho*-methyl (5) group resulted in loss of cellular response. Notably, 4 showed activity in the mESC-assay, but this was due to a reduction in cell number thus suggesting a cytotoxic effect of the chlorine-substituent. Modification at the 2-position were also not well tolerated, as alterations showed significant decrease in activity in the cardiogenic differentiation assay, but generally were inactive in osteogenesis (6, 13-29). Only the pyrrol-substituted analogue 23 showed a BMP-dependent response in both morphological assays, albeit with lower potency compared with Chromenone 1. Moreover, neither saturated 2-heteroalicyclic (24, 26-29) nor larger 2-heteroarylic derivatives (20-22) exhibited increased activity, thus indicating a preference for small heteroaromatic groups. Since all these modifications at the 2-position resulted in a significant reduction in biological activity, the 2-(1,2,4-triazolyl) group turned out to be critical for the BMP-dependent response. Various combinations including modifications at the 6- and 7-position (7-11) did not enhance activity, but all of these derivatives lacked essential substitution in 3-position. These results highlight the importance of pharmacophoric features at the 2- and 3-position of the 4*H*-chromen-4-one scaffold with a small heteroaryl group in 2-position and an electron-deficient aromatic substituent in 3-position. Overall, the set used for the SAR provided initial insights into key elements critical for BMP activity, and thus providing a suitable starting point for extensive hit-to-lead optimization. Considering that the 6- and 7-position at the chromenone scaffold were not further investigated due to the more difficult accessibility of the synthesis, there may be great potential for further modifications and optimization.

To further validate the critical triazole- and trifluoromethyl-substitutions for cellular BMP response as valuable negative controls for biological profiling, the structural closely related 3-(*p*-phenyl)- derivative (Chromenone 2) and the 2-(1,2,4-triazolyl)-lacking derivative (Chromenone 3) were tested for their ability to induce ALP activity and their effect on the BMP-responsive reporters *Vent2* and *Id1* compared with Chromenone 1. When profiling ALP activity in C2C12 in the range of 0.05-10 µM, Chromenone 1 enhanced cellular ALP to the maximum BMP response (100 ng/mL), whereas replacement of the triazole (Chromenone 3) resulted in complete loss of function (Figure 50B), underlining high potency (EC_{50} = 0.34 µM) and efficacy

of Chromenone 1 compared to the inactive Chromenones. A mild induction up to 5-fold over low-dose BMP-4 at 10 µM was observed for Chromenone 2, which exhibited moderate BMP-induced osteogenesis, demonstrating the essentialism of the *p*-trifluoromethyl group. These effects were confirmed by quantification of *Alp* expression levels after 72 h, consistent with the observed activation range of measured catalytic ALP (Figure 50C).

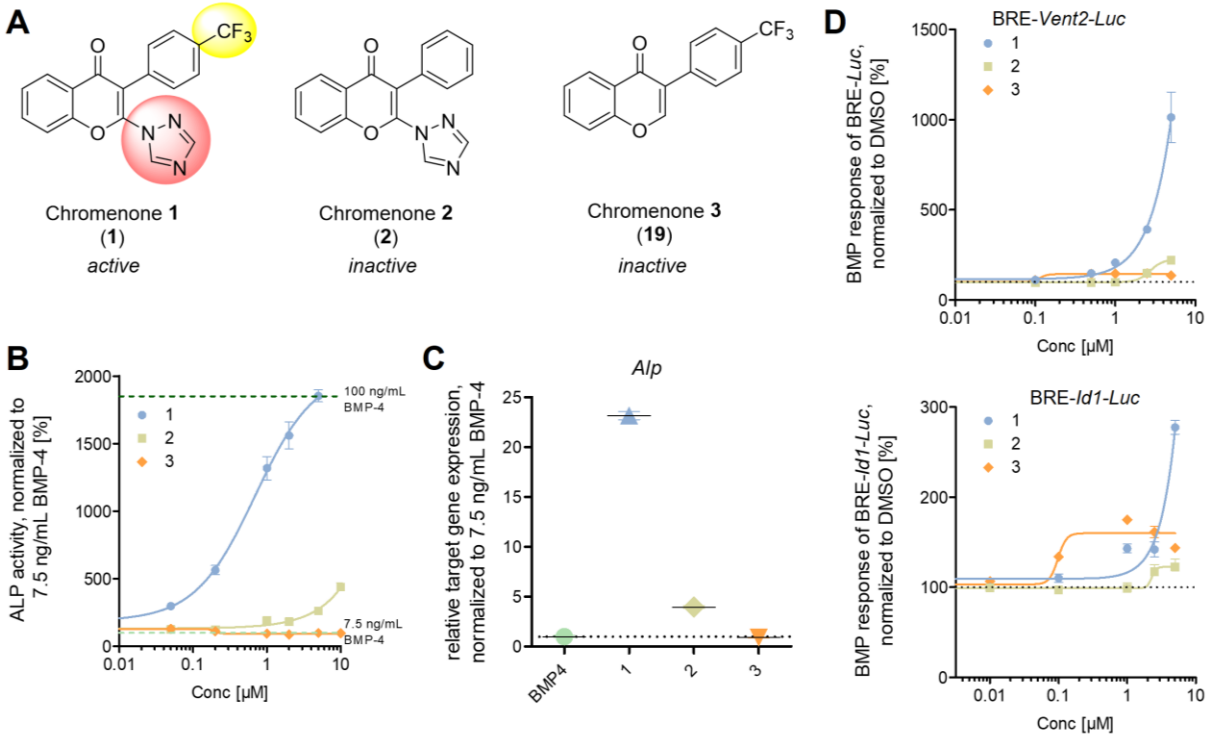

Figure 50: Chromenone 1-3 highlight key pharmacophoric features in 2- and 3-position required for BMP activity. (A) Chemical structures of Chromenone 1-3 illustrating key pharmacophoric features. (B) Dose-dependent BMP-synergistic ALP-induction of Chromenones 1-3 in C2C12 together with 7.5 ng/mL BMP-4. ALP activities are normalized to 7.5 ng/mL BMP-4 and represents mean ± SD for *n* = 3 independent experiments. (C) Quantification of *ALP* transcript level normalized to BMP-4-induced expression. Treatment with vehicle, 7.5 ng/mL BMP-4 or 7.5 ng/mL BMP-4 and compound was performed for 72 h. (D) Dose-dependent profiles of Chromenones 1-3 on BMP response element (BRE) firefly luciferase reporters using the *Vent2* and *Id1* promoters. HEK293T cells were transiently transfected with BRE-luc reporter and co-treatment with compounds and BMP-4 (10 ng/mL) was performed for 22 h. Luciferase activity was analyzed and normalized to DMSO (= 100%). Data is representative for *n* = 3 independent experiments.

A very similar dose-response relationship for this set of chromenones was observed for the induction of BMP-dependent luciferase reporter expressions *Id1* and *Vent2* (Figure 50D). Chromenone 1 induced both luciferase expressions synergistically with applied BMP-4 (10 ng/mL), showing high efficacy up to 3-10-fold over BMP-4 induced expression levels. The moderate ALP-inducer Chromenone 2 enhanced luciferase expression at 2.5-5 µM on both reporters, indicating a similar dose-response to the observed ALP activity, whereas Chromenone 3 was inactive on *Vent2*-expression, but exhibited a bell-like activation profile on

the *Id1*-reporter. This effect was also observed in *Renilla* induction (not shown), suggesting artificial activation of the reporter. However, the profile of active and inactive chromenones was consistent across these validation assays, indicating pharmacophoric features essential for BMP activity. Taken together, the SAR study furnished a set of BMP activating and inactive 4*H*-chromen-4-one-based closely related derivatives that can be used as valuable negative controls for biological profiling and subsequent mechanistic studies.

3.2.3 Functional validation of Chromenone 1 as an osteogenic BMP potentiator

After successful screening and filtering of potential hits in a workflow of orthogonal validation assays and observed BMP-amplifying behavior, *in vitro* mineralization studies were carried out in BMP-sensitive osteosarcoma cells to validate osteogenic BMP-activators. As the only remaining hit capable of inducing ALP activity and BMP-dependent osteogenic transcript levels, quick profiling of a pair of close derivatives from the in-house library revealed a close and inactive analogue of Chromenone 1 lacking the triazole, and both chromenone-based compounds were tested on human SaOS-2 cells to evaluate their BMP-dependent potential to promote mineralization in a more physiologically relevant and BMP-sensitive cell line. The assay was set up in collaboration with Prof. Jessica Bertrand and her students at the University Hospital in Magdeburg. In principle, during osteoblastogenesis, cells undergo different cellular stages in a maturation process with gradually decreasing proliferating potential and increased secretion of structuring factors that are important for the formation of an osteogenic milieu and thus accumulate calcium and phosphates, form hydroxyapatite and contribute to terminal mineralization of osteoblasts.[183] The human osteosarcoma cell line SaOS-2 is well-characterized in osteoblastogenesis and mineralization. Similar to the basal BMP stimulus required for C2C12 osteoblast induction (7.5 ng/mL), it was observed that minimal induction of BMP signaling (2 ng/mL) was required to induce osteosarcoma cell mineralization for investigating small molecule induction. Both, the active Chromenone 1 and its inactive analogue, as well as the characterized BMP-activator Ventromorphin were subjected to the cells along with low-dose osteogenic BMP-2 and BMP-4 and incubated for 11 days. Notably, due to the sensitivity of the cells during differentiation and regular medium refreshment, higher concentrations of compound and DMSO negatively affected maturation and matrix mineralization. As shown in Figure 51, the stained calcium deposits show an increase upon

addition of BMPs, while Chromenone 1 indeed promoted mineralization of the cells by almost 1.5-fold, forming large local deposits, suggesting a strong induction of the osteogenic environment during maturing process in combination with both BMPs. Moreover, Chromenone 1 was incapable of inducing mineralization in absence of BMPs, which is consistent with the lack of potential to induce ALP levels independently of BMP-4 in C2C12. Considering that the inactive derivative showed no enhancement in the absence and presence of BMPs, the data overall suggest a BMP-dependent synergistic contribution of Chromenone 1 that is also significant for BMP-4, as calculated for the quantified stained calcium levels.

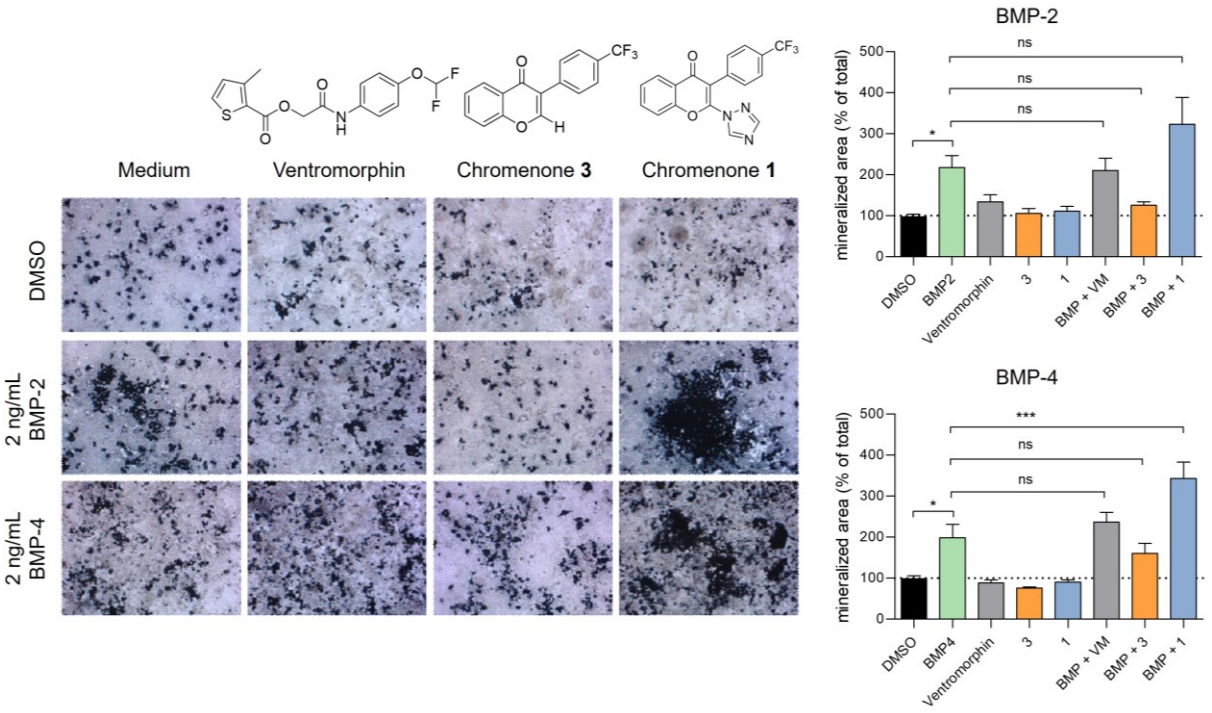

Figure 51: Chromenone 1 significantly induced synergistic osteoblastic mineralization in human osteosarcoma cell line SaOS-2 after 11 days of differentiation. The active compound, its inactive derivative 3 and Ventromorphin (VM) were incubated in absence or presence of BMP-2/-4 (2 ng/mL) at 0.025 µM for 11 days and *in vitro* mineralization was visualized by Kossa staining of calcium and image-based quantification of mineralized area was performed. Bar graphs represent data as mean ± SEM (n = 9); Statistical analysis was performed using one-way ANOVA test (* $p < 0.05$, ** $p < 0.01$, *** $p < 0.001$). Data from BERTRAND group.

As expected, the reference compound Ventromorphin did not exhibit synergistic induction of mineralized area with neither BMP, which is consistent with its osteogenic profile in C2C12, but notably, but noteworthy, the applied concentration may be outside its osteogenic range.

Overall, Chromenone 1 could be fully validated by *in vitro* mineralization as a novel osteogenic BMP activator chemotype. It functions as a probe potentiating basal BMP signaling in mouse and human cells and proves to be a valuable chemical biology tool for modulating BMP signaling with a superior profile compared to reference BMP-activators.

3.2.4 Mechanistic studies for Chromenone 1 as a BMP potentiator

3.2.4.1 Characterization of BMP/Smad- and TGFβ/Smad-signaling outputs

After confirming the osteogenic activity of chromenone 1, the next step was to investigate the underlying mechanism. Since an effective induction on both BMP reporter (*Id1* and *Vent2*) was observed, possible crosstalk of TGFβ signaling was evaluated by the reporter gene response of the TGFβ-dependent Smad-binding element (SBE) in presence and absence of TGFβ-2 or Activin A.

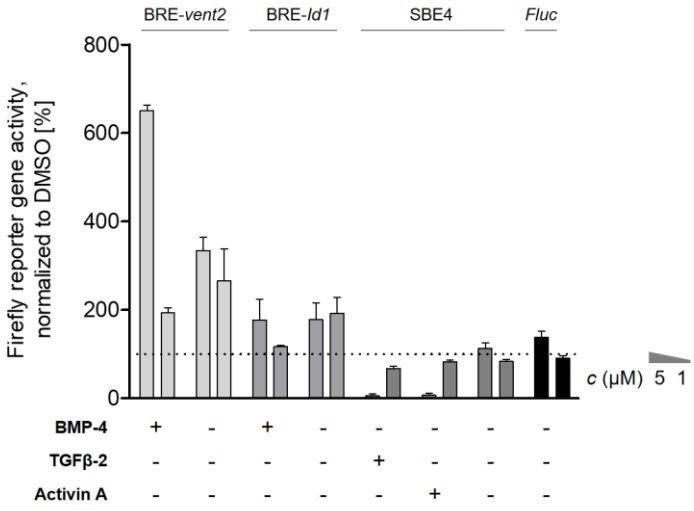

Figure 52: Pathway selectivity profile of Chromenone 1 showing contrary modulation of BMP and TGFβ signaling. HEK293T cells were transiently transfected and treated with compound in presence or absence of growth factor for 22 h. Reporter activation on BRE-luc and SBE4-luc reporters was induced by the respective growth factors at 10 ng/mL and compounds were tested at concentrations of 5 and 1 µM. Additional unspecific Luciferase modulation was determined without growth factor under similar conditions via the constitutively active Fluc-reporter. Data is shown as mean ± SD ($n \geq 3$) and normalized to DMSO vehicle (= 100%). These results based on experiments performed by Tanja Schuh during her Bachelor thesis.[330]

As shown in Figure 52, Chromenone 1 induced both BMP reporter, whereas it efficiently inhibited TGFβ-signaling up to 95% upon stimulation with TGFβ-2 and Activin A at 5 µM. An insignificant activation of the basal activity of SBE was observed, which is similar to the non-specific effect on the constitutively active Fluc-reporter control and is therefore considered artificial. These data indicate a BMP-TGFβ-feedback mechanism, as BMP-4 is inactive on the TGFβ-dependent SBE reporter, suggesting a possible crosstalk via the Smad4 cofactor shared by both signaling pathways. Interestingly, such a mechanism via SMAD4 has been described for the BMP-sensitizer PD407824 by CHK-1 inhibition leading to subsequent p21-CDK9-mediated degradation of Smad2/3.[285] However, PD407824 was found to be inactive in

osteogenic differentiation and BMP-reporter activation, suggesting a distinct mode of action of Chromenone 1, that could also lead to Smad2/3 downregulation, which in turn leads to an increase in BMP signaling outputs. To test this hypothesis, Daniel RIEGE monitored and quantified cytosolic and nuclear levels of Smad2 and Smad4 after transient addition of exogenous BMP-4 or TGFβ-2. Indeed, cytosolic Smad2 levels decreased to levels similar to the reference compound when treated simultaneously with Chromenone 1 and TGFβ-2 for 24 h in C2C12 myoblasts (Figure 53B).

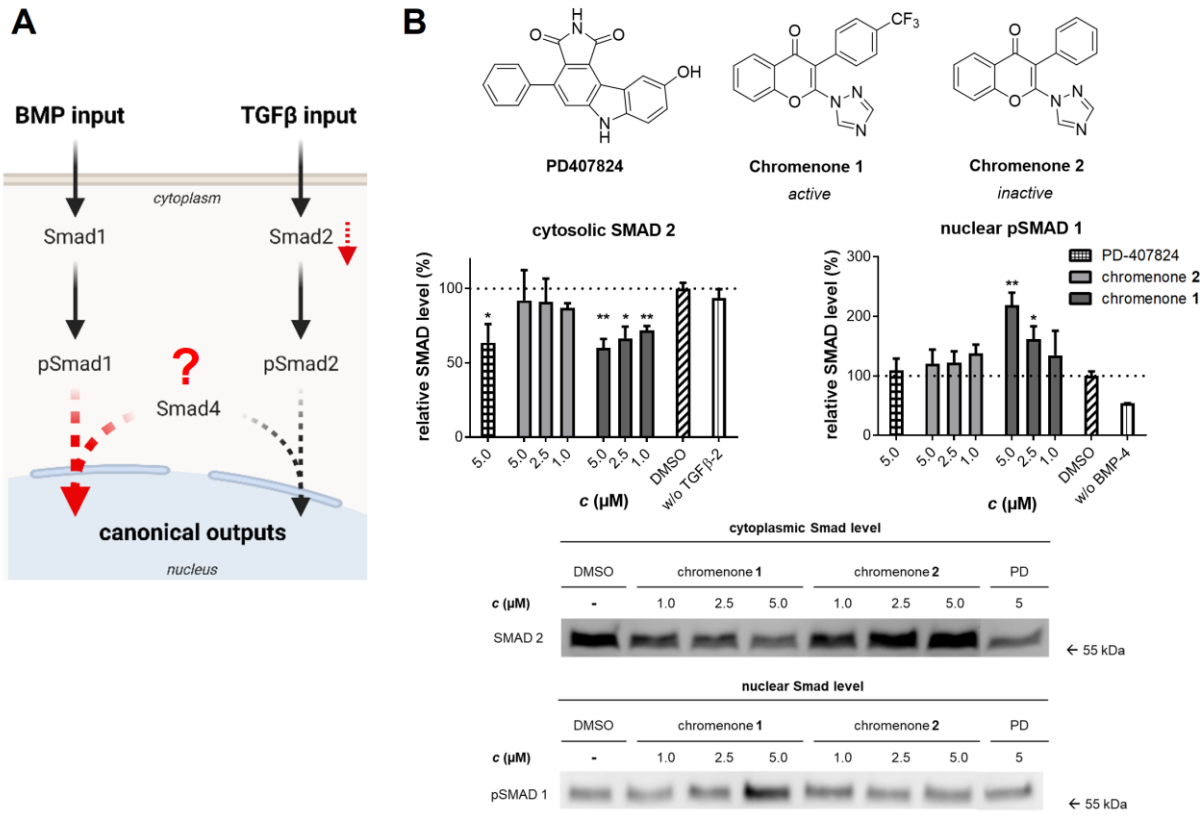

Figure 53: TGFβ/BMP-Smad level quantification reveals a negative TGFβ feedback loop for Chromenone 1 via TGFβ-Smad2 downregulation resulting in increased nuclear SMAD1. (A) Schematic illustration of proposed mode of action in TGFβ/BMP-Smad regulation through Smad4. (B) Fractionation and quantification (Western Blot) of cytosolic Smads in C2C12 cells after 24 hours compound exposure along with TGFβ-2 (10 ng/mL). Nuclear (phospho)-Smad1 levels were analyzed after an additional 30 min low-dosed BMP-4 stimulus (2 ng/mL); Bar data is normalized to DMSO and shown as means ± SD; Statistical analysis: unpaired, one-tailed t-test (* $p < 0.01$, ** $p < 0.001$). Data by Daniel RIEGE.

To distinguish between cytoplasmic and nuclear Smad levels, the latter of which activates target gene expression in a Smad4-dependent manner, cellular lysates were fractionated. Since BMP signaling is transiently induced upon addition of BMP-4, compounds were pre-incubated for 24 h followed by transient treatment with BMP-4 for 30 min. Activated nuclear phospho-Smad1 levels were increased by 2-fold upon co-treatment with BMP-4 and TGFβ-2

in a dose-dependent manner, while PD407824 remained inactive under these conditions. Notably, the inactive analogue Chromenone 2 did not significantly affect either cytoplasmic Smad2 or nuclear pSmad1 levels. These data suggest a predominant BMP-potentiating effect through downregulation of TGFβ-Smad levels, leaving free Smad4 that enhances Smad1 translocation into the nucleus. Given that PD407824 did not induce osteogenesis but mESC-based mesoderm structuring and showed no effect on Smad1-levels, Chromenone 1 appeared to potentiate BMP signaling in a distinct manner compared with PD407824 through a novel mechanism of selective regulation of Smad2/3 levels.

To rule out possible unexpected interactions of TGFβ inhibition, the dose-dependent response of specific TGFβ inhibitors in C2C12 osteoblastogenesis was assessed.

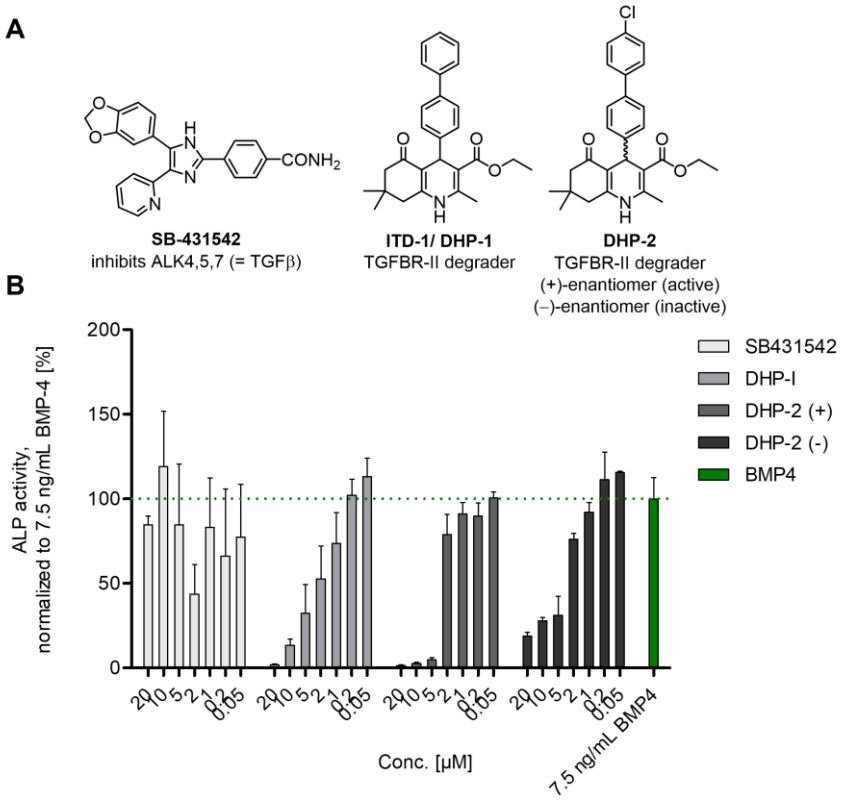

Figure 54: TGFβ inhibition did not induce BMP-dependent osteogenesis. Potent TGFβ-inhibitors SB431542, DHP-1 and its more selective and more potent derivative DHP-2 were not able to enhance BMP-dependent activation on ALP and BRE-*Vent2*-Luc reporter. (A) Chemical structures of tested TGFβ inhibitors. (B) ALP-activity of treated C2C12 with inhibitors and BMP-4 (7.5 ng/mL) for 72 h. Data is shown as mean ± SD ($n \geq 2$) and normalized to DMSO vehicle (= 100%).

The ALK4/5/7-selective inhibitor SB431542 did not induce BMP-dependent ALP, whereas DHP-1 and DHP-2 antagonized BMP-dependent osteogenesis in a dose-response manner, indicating negative feedback of TGFβ receptor-mediated inhibition on BMP signaling outputs

(Figure 54). This is particularly interesting, since Chromenone 1 may act through TGFβ inhibition, strongly suggesting an intracellular and receptor-independent mode of action by regulating available Smad4-levels. Notably, Chromenone 1 showed a unique profile across the BMP-assays that could not be recapitulated by classical TGFβ-inhibitors such as SB431542 and ITD-1, as observed with the distinct profiles in DMH-1-mediated mesodermal specification during d3-4 in the phenotypic mESC-BMP-assay (Figure 15).

To obtain a more comprehensive view of how Chromenone 1 modulates the TGFβ superfamily, particularly in the initial phase of BMP-dependent C2C12 differentiation, an expression profile of 84 transcripts was performed, including direct target genes and various factors relevant to the regulation and signal transduction of this network. As illustrated in a heatmap indicating up- or downregulation of gene expressions relative to BMP-4-treated C2C12, Chromenone 1 did not drastically alter the overall expression profile of low-dose BMP-4 treated cells (Figure 55A), but rather augmented BMP-4 induced expression patterns.

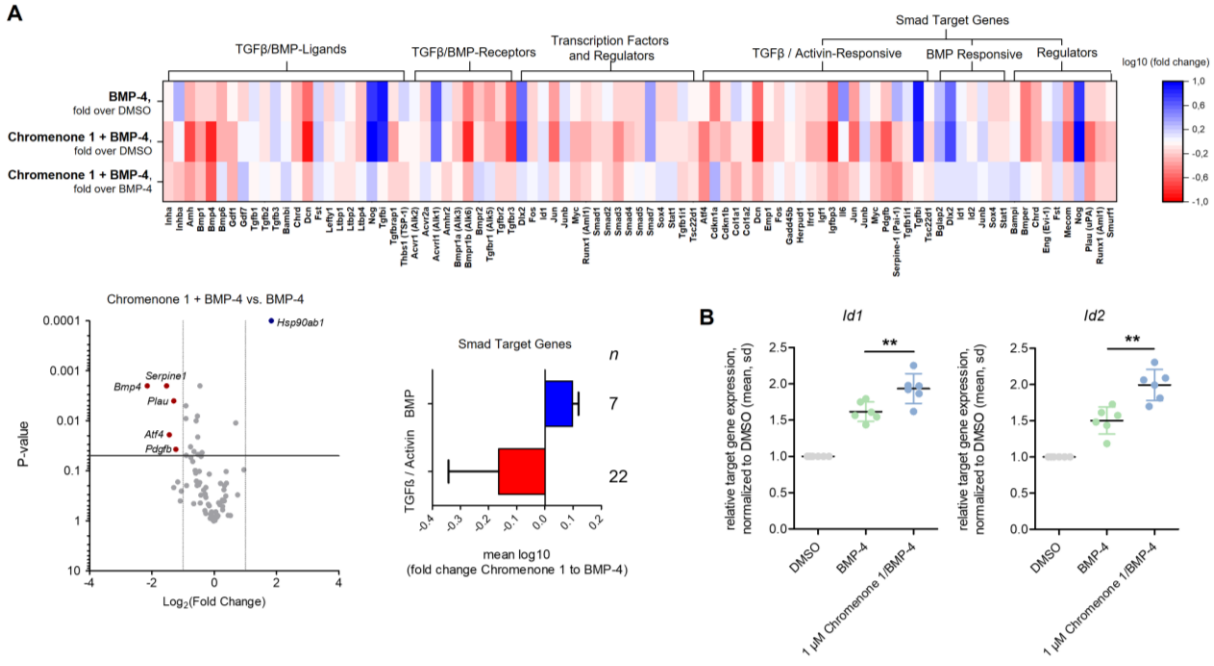

Figure 55: PCR-array analysis highlights negative TGFβ-feedback loop for Chromenone 1 via TGFβ-Smad downregulation. (A) TGFβ/BMP-pathway gene expression analysis was conducted with RT^2 Profiler PCR-Array (Qiagen) in C2C12 cells. After 24 h treatments with DMSO, BMP-4 (7.5 ng/mL) or Chromenone 1/BMP-4 (1 µM/7.5 ng/mL), cells were lysed, and RNA was isolated for microarray analysis. Heatmap visualization shows gene expression data of 84 transcripts, sorted according to their pathway functions (log10-fold changes, n = 3). Volcano plot compares Chromenone 1/BMP-4 co-treatment with BMP-4 alone and indicates significantly regulated transcripts according to their p-values calculated with a student's t-test. Bar graph summarizes the mean up- and down-regulation of all BMP- (blue) and TGFβ/Activin- (red) dependent Smad target genes. (B) Quantification of relative gene expression of *Id1* and *Id2* upon BMP-4 (7.5 ng/mL) and Chromenone 1/BMP-4 (1 µM/7.5 ng/mL) treatments of C2C12 cells for 24 h. Data is shown as means ± SD (n = 6) and normalized to DMSO vehicle. Statistical analysis was performed with an unpaired two-tailed t-test (* $p < 0.05$, ** $p < 0.01$; *** $p < 0.001$).

As shown in a volcano plot, synergistic treatment resulted in significant downregulation of TGFβ-related transcripts (*Atf4*, *Plau*, *Serpine1*, *Pdgfb*), which are positive regulators of balancing TGFβ-mediated signaling and whose impairment is associated with reduced Smad-activity.[334–336] Moreover, Atf4 induction by TGFβ ligands was reported to suppress osteogenesis.[337] Interestingly, BMP-4 expression was significantly reduced, which is a typical response to BMP-4-induced signaling as negative feedback, and further downregulation upon simultaneous treatment most likely reflects the cellular response to regulate the strong amplifying effect of Chromenone 1. Similarly, the pronounced activation of *Hsp90* expression might represent another feedback mechanism to compensate for the predominant negative regulation of TGFβ-Smad signaling by synergistic treatment with Chromenone 1 and BMP-4, since the chaperone has been reported to protect TGFβR-I and TGFβR-II from ubiquitination and proteasomal degradation.[338,339]Based on the proposed mechanism of downregulation of TGFβ-Smad2 and thus enhanced BMP-Smad1 activity, Smad-dependent target gene expression was also expected to be affected by Chromenone 1. As shown in the bar graph, a significant downregulation of mean expression change was indeed observed for TGFβ-Smad-specific target genes (22 responsive genes) compared with BMP-4-treated cellular expression patterns. This hypothesis was further confirmed by the collective upregulation of seven BMP-dependent Smad target genes. To further confirm this observation, the target genes *Id1* and *Id2* were examined in detail in separate qRT-PCR experiments and a successful and significant induction was validated relative to low-dose BMP-4-treated C2C12 (Figure 55B).

These data collectively provided evidence that Chromenone 1 triggers a BMP stimulus-dependent negative TGFβ feedback loop by downregulating Smad2 levels and Smad2/3-dependent target gene expression while activating nuclear BMP-Smad1, resulting in increased Smad target gene expression. It should be noted that due to the strong regulator connection via canonical and non-canonical signaling of TGFβ and BMP and thus regulatory feedback loops, it may be difficult to identify exclusively BMP-activating chemical probes, especially if the BMP-potentiating response is mediated by an intracellular factor that is directly or passively involved in this signaling network. The data collected so far strongly indicate such a feedback mechanism for Chromenone 1, possibly through kinase network signaling.

3.2.4.2 Kinome-wide activity profiling of Chromenone 1

Since Chromenone 1 decreased cytosolic TGFβ-Smad2, thereby enhanced nuclear BMP-Smad1 leading to potentiating BMP signaling response in a distinct manner compared with PD407824, a kinome-wide profile was determined to obtain novel insights into relevant kinases involved in signaling network regulations of BMP signaling. Therefore, Chromenone 1 was screened at 1 µM (~5x above cellular IC_{50}/EC_{50}) and showed a clean kinome profile as none of the catalytic activities of the 484 tested kinases were significantly modulated by more than 25% compared to the vehicle control (see appendix, Figure 97). Looking at the activity of canonical and noncanonical BMP regulators, Chromenone 1 was completely inactive against cell cycling regulators (CHKs, CDKs) and GSK3 isoforms, which were proposed to be targeted by PD407824 and Autophinib (Figure 56).

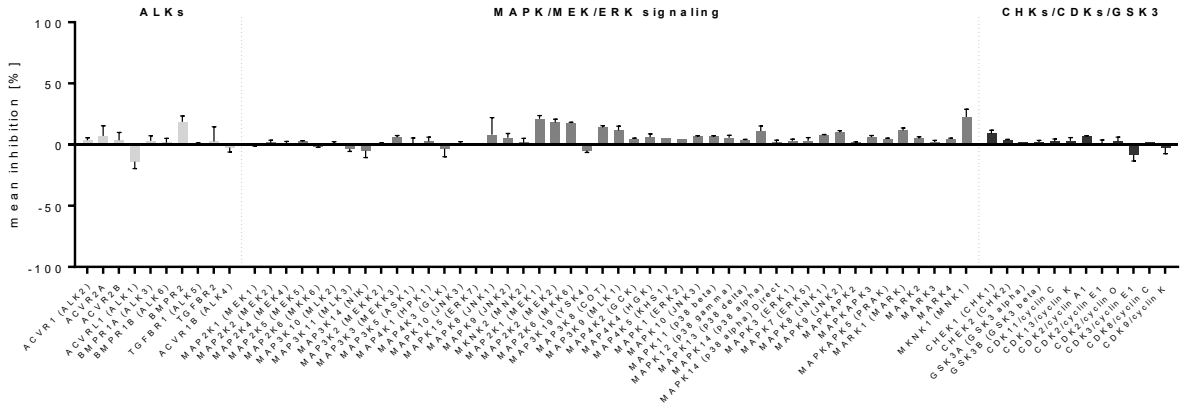

Figure 56: Kinase profiling of Chromenone 1 against kinases associated with canonical or non-canonical BMP signaling regulation. Chromenone 1 did not modulate the catalytic activity of any kinase above 20%. Activities were monitored by biochemical inhibition of selected kinases of 1 µM Chromenone 1 by Life Technologies in three biochemical assay formats (Adapta, Z-Lyte, Lantha). Data is shown as the mean ± SD of two replicates (*n* = 2) for each kinase.

Further, no kinase involved in MAPK/ERK signaling was inhibited, suggesting a regulation of Smad4-mediated BMP/TGFβ signaling independent of noncanonical signaling. In this regard, also no receptor kinase (e.g., ALKs) was modulated, showing only the type II receptor BMPR2, which was inhibited by 20%, suggesting a rather non-specific modulation at tested concentration at 1 µM in biochemical context.

A clean kinome profile suggests low polypharmacology of Chromenone 1, especially in hindsight to the other kinase-modulating compounds tested such as PD407824 or the herein targeted developmental signaling pathways, which are linked and regulated by kinase

networks.[340] Overall, Chromenone 1 did not modulate the catalytic activity of any kinase family known to regulate canonical or non-canonical BMP signaling or through closely related signaling pathways. These results point towards a novel mechanism distinct from the proposed one for PD407824, which predominantly sensitizes cells towards BMP signaling by affecting various cell cycle regulating kinases. However, due to its described pan-kinase activity, PD407824 affected cell viability and could interfere with the sensitive and selective induction of BMP signaling. Thus, since no kinase was affected by Chromenone 1, Smad4 availability is regulated in a distinct manner compared to PD407824, likely not via direct and instant kinase-driven events. The responsible target or effector for this mechanism remains to be identified by target deconvolution approaches.

3.2.5 Summary and Outlook

A novel screening workflow has been developed that successfully harnessed embryonic development in a morphogenic cardiac differentiation assay to identify novel small molecule BMP activators. As proof-of-concept, a diversity-focused library of almost 7,000 compounds was screened, yielding 35 hits with a hit rate of 0.5% that showed a strong dose-response. From subsequent validation assays and hit cluster analysis, two chemotypes were de-validated due to lack of activity and structural issues, as shown for the quinolinole compound class. The 2-aminopyrimidine Autophinib exhibited a false-positive BMP-independent response through dual VPS34- and GSK3β-inhibition. Follow-up studies revealed that VPS34 inhibition may yield potent false-positive hits in the mESC-based screening assay, whereas GSK3β inhibition leads to non-osteogenic ALP induction in the secondary C2C12 assay. Remarkably, neither selective inhibition would have resulted in a false-positive BMP mimetic. Thus, de-validation of Autophinib demonstrated proof-of-concept of the screening campaign workflow and underpinned the importance of combining both phenotypic BMP assays as a screening platform.

Stringent hit filtering left the chromenone-based chemotype, which was further proven as a potent osteogenic BMP potentiator. Moreover, validation of Chromenone 1 demonstrated the feasibility of successful identification of BMP-activating chemicals via orthogonal validation, induction of osteogenic protein and transcript levels, and phenotypic evaluation. By *in vitro* mineralization of human osteosarcoma cells, Chromenone 1 could be fully validated as a novel

osteogenic BMP activator chemotype, functioning as a probe potentiating basal BMP signaling in mouse and human cell lines and proves to be a valuable chemical biological tool for modulating BMP signaling. In SAR studies, a probe set of Chromenone-type BMP potentiators was successfully established, highlighting key pharmacophoric features that provide a well-characterized starting point for extensive hit-to-lead optimization studies and integration of functional groups for target identification approaches. For this, functional groups, such as a photo crosslinking or coupling group could be incorporated onto 6- or 7-position of the 4*H*-chromenone-scaffold, since slight modifications at the chromon-based heterocycle on 2- and 3-position resulted in significant loss of activity.

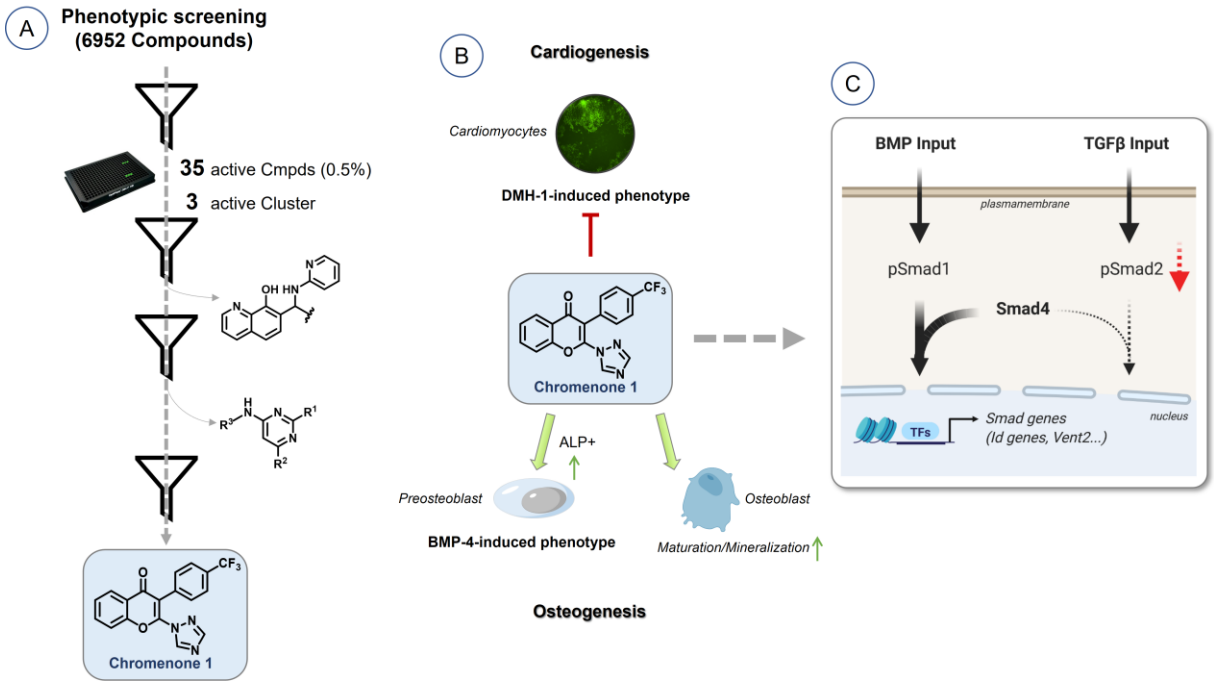

Figure 57: Screening of 6952 compounds in a stem cell-based phenotypic screening approach and subsequent (de-)validation resulted in identification of a novel BMP-potentiating chemical probe, Chromenone 1. Initial mechanistic studies revealed that BMP-potentiation might be mediated by TGFβ-downregulation via balancing Smad-canonical signaling.

Furthermore, reporter gene assays, BMP/TGFβ-dependent gene expression analysis, Smad level dynamic studies and kinase profiling substantiated the BMP-dependent osteogenic response, suggesting a unique mode of action by downregulating TGFβ-Smad signaling and thereby enhancing nuclear BMP-Smad translocation and signaling outputs. Contrary to a very similar mechanism reported for PD407824, negative TGFβ feedback was shown to be kinase-independent, leading to a chemical modality with lower promiscuity as well as lower cell toxicity.[285] Indeed, Chromenone 1 potentiated BMP signaling with high potency and efficacy,

exhibiting cytotoxic effects only at concentrations above 10 µM, which were 30-50-fold higher than the observed IC_{50} and EC_{50} values, thus showing a superior profile than the CHK-1/Wee1 inhibitor PD407824. In addition, even though Chromenone 1 does not act as an actual BMP mimetic but rather potentiates the signaling output, the identified unique mode of action allows for applications where basal BMP signaling or low rhBMP levels can be locally targeted contributing to a cell/tissue-specificity and an overall beneficial safety profile.

Taken together, proof-of-concept was demonstrated for the developed assay platform by the successful identification of a genuine BMP-potentiating small molecule, thereby demonstrating the potential to expand the chemical space of previously published BMP activators and sensitizers whose activity is particularly dependent on the cellular context. To assess therapeutic potential, further studies in zebrafish, bone marrow derived MSCs, or human-derived osteopenia model systems may be considered.[14,287] Since validation of Chromenone 1 was mainly focused on its osteogenic potential, broader applications are required to evaluate BMP-potentiating efficacy in hESC-based mesoderm induction or cardiac specification, which ultimately would contribute to more robust chemically-defined differentiation protocols in 2D- and 3D-culture systems.[149,173]

3.3 Characterization of triazolo[1,5-*c*]quinazolines as novel BMP potentiators

3.3.1 Identification of CGS-15943 as a highly potent and selective BMP potentiator

Based on the initial identification of the BMP-sensitive time frame during cardiogenesis in mESCs and the development of the BMP-mimetic morphogenic assay, a very first pilot screen was performed by Jonas HALVER in the SCHADE group (2017).[290] For this, screening of 1408 compounds was conducted that consisted mainly of the LOPAC/Prestwick libraries which contain pharmacologically active and well validated compounds that span all major target classes of approved drugs on the market. Thus, phenotypic screening hits from such libraries have a great potential to quickly identify relevant targets and mechanisms. These small molecules represent a tool for demonstrating *in vivo* efficacy of observed activities, and ultimately the repurposing of clinically tested or approved drugs may be attractive. Briefly, compounds were subjected at 5 µM to the mESC-*Myh6*-GFP cells simultaneously with cardiogenic DMH-1 (0.5 µM) at the BMP-specific time window (d3-4) to evaluate the antagonistic potential of each compound after 11 days of differentiation. After quantification of cardiac cluster intensity, compounds that antagonized DMH-1-induced *Myh6*-GFP cluster by at least 50% were considered primary hits. From these 33 nontoxic hits, 12 remained that showed a dose-dependent response in a concentration range of 0.01-5 µM (Figure 58A-C), indicating a primary hit rate of 0.9%. Interestingly, among the identified active hits, eight compounds were reported to target different G protein-coupled receptors (GPCRs), some of which are associated with or related to BMP signaling or growth factor expression (e.g., Domperidone, Loxapine).[290] For further hit validation, a BMP reporter gene assay and other reporter constructs for TGFβ and Wnt signaling were used for all identified positive hits to determine selectivity within key developmental signaling pathways. Here, only one compound stimulated both synergistic and non-synergistic BMP reporter gene expression of *Vent2*-luciferase (Figure 58D): the triazolo[1,5-*c*]quinazoline CGS-15943.[291] CGS-15943 is a potent non-selective adenosine receptor antagonist, inhibiting the binding of adenosine to its receptors (A_1, A_{2A}, A_{2B}, A_3) in the nanomolar range.[341,342] It was one of the first reported non-xanthine adenosine receptor antagonists without activity toward phosphodiesterases, indicating a more specific pharmacological signature. In animal studies it exhibited similar

effects to caffeine, being more potent and effective.[343,344] However, the orally active research compound did not advance beyond preclinical stages and did not exhibit selectivity for human adenosine receptors compared with other non-xanthine compounds (e.g., ZM241385 or SCH58261).[345] Interestingly, Adenosine receptor blockade is already recognized as a therapeutic approach for osteopenic diseases as it has been linked to the inhibition of osteoclast differentiation.[346,347]

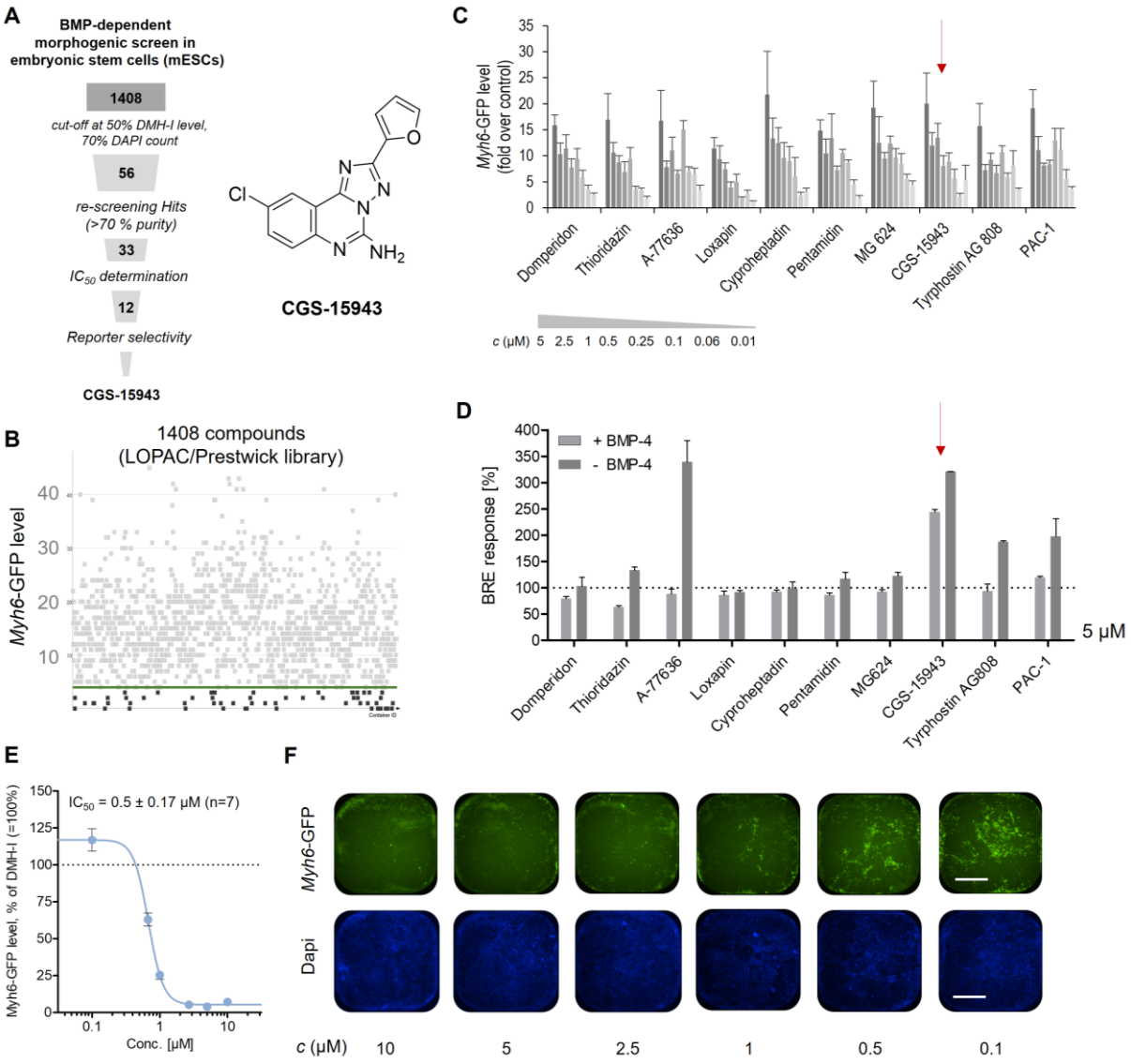

Figure 58: Overview of a mESC mesoderm patterning screen for BMP activators from the LOPAC/Prestwick library of pharmacologically active compounds, which identified CGS-15943. (A) Illustrative workflow of screening and validation workflow to identify novel BMP activators in a 384-well format. (B) Primary screening was performed in mESC-*Myh6*-GFP-based phenotypic screening assay which were treated with compounds (at 5 µM) and cardiogenesis was induced by 0.5 µM DMH-1 for 24 h at d3-4 of differentiation, leading to 33 non-toxic and IC_{50}-validated hits (C) that moved forward to secondary validation by testing BMP response on the BMP-responsive reporter *Vent2*-luciferase in HEK293T cells in presence or absence of BMP-4 (10 ng/mL) (D) Bar graphs are represented by luciferase activity, normalized to *Renilla* control plasmid and DMSO vehicle. (E) Quantified *Myh6*-GFP levels of CGS-15943, normalized to DMH-1 levels (= 100%). (F) Representative images (4x) of fluorescent *Myh6*-GFP+ clusters and visualized cell nuclei by DAPI (scale bar = 1 mm) after fixation (d11).

As shown in Figure 58F by fluorescence images, CGS-15943 inhibited cardiac cluster formation in a dose-dependent manner, with high efficacy at doses above 2.5 µM and potency indicated by the IC_{50}-value of 0.5 µM.

In order to characterize and validate the BMP-specificity during the sensitive BMP time frame in cardiogenesis, *Id* gene expression of CGS-15943 was determined.

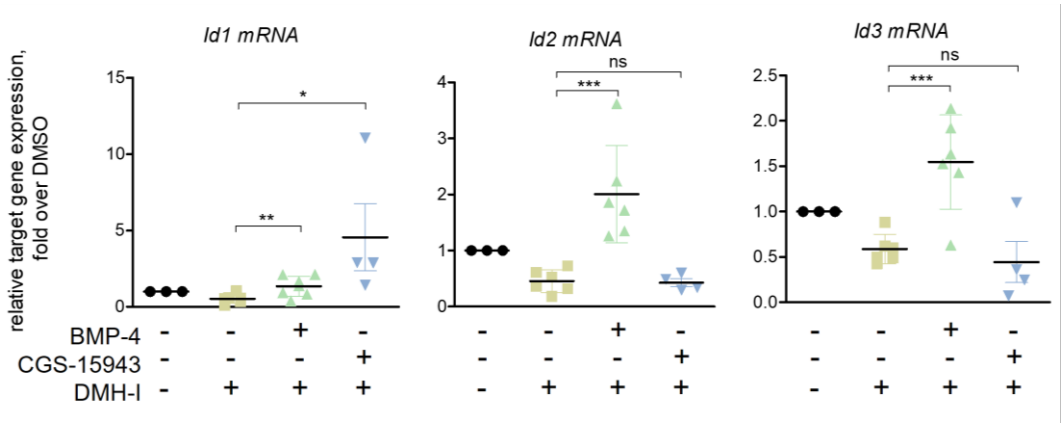

Figure 59: Antagonistic effect of CGS-15943 on DMH-1-repressed *Id* gene expression during cardiogenesis. Relative quantification of gene expression for BMP target genes *Id1*, *Id2*, *Id3* during BMP-sensitive time frame (d3-4). Murine ESCs were treated with 2.5 µM CGS.15943, 0.5 µM DMH-1 or 10 ng/mL BMP-4 for 24 h at d3-4. RNA was isolated at day 4 and RT-qPCR was conducted. Statistical analysis was performed with an unpaired *t*-test of triplicates and the respective SEM compared to DMSO control and a set confidence level of 95% (*:p <0.05; **:p <0.01; ***:p <0.001) for $n \geq 4$ independent biological experiments.

Indeed, CGS-15943 was able to significantly rescue the DMH-1-triggered repression of *Id1* gene expression (Figure 59) at 2.5 µM, similar to BMP-4 (10 ng/mL). However, in contrast to BMP-4, the expression of *Id2* and *Id3* was not rescued by CGS-15943, suggesting a distinct and specific mechanism to control *Id1*. Id genes differ in their specificity during different developmental stages and differentiations as has been shown for *Id1*, which is critical for early heart formation.[160] According to these data, CGS-15943 exhibit a distinct cellular response to BMP-4 on BMP target gene expression. The underlying mechanism causing the morphogenetic phenotype may depend on targeting target gene regulators, leading to selective gene expression, which needs to be elucidated.

Since four compounds stimulated reporter activity in the absence but not in presence of BMP-4, while only CGS-15943 induced both, this initially suggested a unique mode of action (Figure 58B). Moreover, the other three chemotypes (i.e., A-77636, Tyrphostin AG808, PAC-1) showed structural elements typical of PAINS and non-selective modulation of TGFβ superfamily was observed.[290] Only CGS-15943 displayed a highly selective profile within the

TGFβ superfamily as demonstrated by employing various pathway-specific response elements (Figure 60A). Here, CGS-15943 (5 µM) exhibited a selective profile on BMP-dependent *Vent2*-expression with a significant induction over 100% of the basal reporter expression in presence of BMP-4. It should be noted that the reporter activity was more prone to artificial effects in the absence of growth factor, since the basal luminescence signal was very low, Therefore, growth factor-independent reporter gene induction or activation should be viewed with caution. The *Vent2* reporter was in place for the pre-validation of all hits identified from the pilot screen. However, during the course of this thesis the BRE-*Id1* reporter has been additionally established to provide a broader picture of the compounds' BMP-activity. Moreover, as previously described and discussed, the *Renilla* control luciferase signal oftentimes resulted in artificial luciferase perturbation. Therefore, firefly luciferase reporter activities were also compared in the absence of an internal *Renilla* control, but under close observation of cell number and morphology. To further exclude unspecific effects of test compounds on the firefly luciferase reporter expression and activity, a constitutively active firefly luciferase system in 293T cells was used as a control.

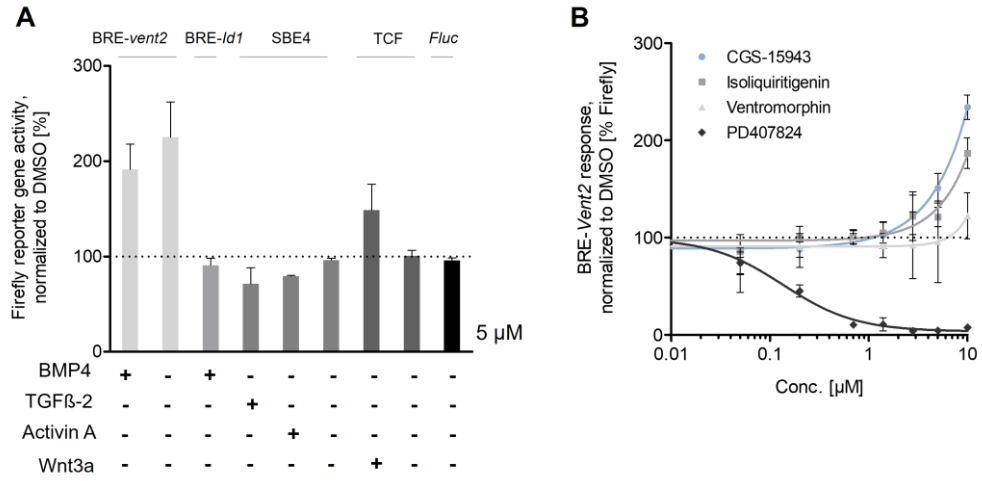

Figure 60: The pathway selectivity profile of CGS-15943 showed specificity for BMP-dependent Vent2 expression but not for Id1. (A) HEK293T cells were transiently transfected and treated with compound in presence or absence of growth factor for 22 h and firefly luciferase response was normalized to the basal activity. Reporter activation on BRE-luc, SBE4-luc and STF-luc reporters was induced by the respective growth factors at 10 ng/mL or co-transfection with pWnt3a for autocrine Wnt-signaling, and compound was tested at concentrations of 5 µM. Data is shown as mean ± SD ($n \geq 3$) and normalized to DMSO vehicle (= 100%). (B) Dose-dependent profiles of CGS-15943 in comparison with reference compounds on BRE-*vent2*-luc reporter. HEK293T cells were transiently transfected with BRE-luc reporter and co-treatment with compounds and BMP-4 (10 ng/mL) or Noggin (10 ng/mL) was performed for 22 h. Luciferase activity was normalized to DMSO (= 100%) and data is shown as mean ± SD of $n = 3$ independent experiments.

Furthermore, a mild inhibition (< 25%) of TGFβ-2 and Activin A was observed, but no inhibition of the basal activity of TGFβ-responsive reporter was mediated and thus, TGFβ modulation was considered to be negligible (Figure 60A). These data were very promising, as avoiding crosstalks between BMP and TGFβ signaling was already recognized as challenging. The herein presented Chromenone 1 (see Chapter 3.2) eventually enhanced canonical BMP signaling outputs via a negative TGFβ feedback mechanism. Moderate induction of up to 48% was observed for Wnt3a-induced signaling, suggesting a possible crosstalk via Wnt-induced signaling. However, CGS-15943 did not enhance basal Wnt signaling activity. Importantly, the expression of the constitutively active firefly luciferase was not affected, indicating that luciferase induction was not caused by artificial luciferase modulation. Crosstalks with Wnt/β-Catenin have been observed via targeting GSK3β (see Autophinib, Chapter 3.2.1.2). In contrast, Autophinib effectively induced Wnt reporter gene activity up to 7-fold over basal reporter activity in both presence and absence of autocrine Wnt3a-stimulus (see Figure 47). In fact, all of the known BMP activators/sensitizers profiled in this work affected more or less these pathways. Therefore, CGS-15943 appears to exhibit a superior selectivity for BMP. Moreover, it showed a superior dose-dependent activity profile on reporter activity when treated simultaneously with BMP-4 up to 10 µM compared to the tested known BMP potentiators (Isoliquiritigenin, Ventromorphin, PD407824) as reference compounds (Figure 60B; for selectivity, see Figure 37).

Interestingly, in contrast to the observed enhancement of *Id1* gene expression by CGS-15943 in the cardiogenic differentiation assay, it did not result in synergistic *Id1*-reporter luciferase expression in HEK293T cells. Initial test experiments in C2C12 confirmed this observation (data not shown), so the effect cannot be attributed solely to the lack of complexity of the HEK reporter gene assay. In contrast to the quantified induction of *Id1* gene transcripts in the context of complex differentiation, which involves critical interactions and regulatory feedback as described, these mechanisms may be absent in the artificial Id1 reporter. Id1-dependent expression of luciferase could therefore be very linear and is mainly dependent on the pure Smad1/4-signaling cascade.[348] This would also imply limitation of the general use of reporter gene assays and underscore the established approach to identifying novel BMP-activating small molecules. Another possible explanation for the lack of reporter activation, in contrast to the induction of the embryonically important developmental biology marker *Vent2*, could be compound-mediated repression of certain transcription factors involved in the selective

expression of target genes, as various factors and cofactors have been reported to impair or enhance gene binding and thus expression activity. This is particularly the case with BMP signaling, given that BMP drives cellular commitment to various cell lineages by inducing transcriptional regulation of early genes transcribing lineage-specific transcription factors and cofactors that in turn promote differentiation.[349] Since both assays differ greatly in their cellular complexity to depict BMP signaling and because regulatory networks may be beneficial on the phenotype of interest in embryonic biology, mere observation of reporter activity in HEK293T cells is not sufficient to conclude a physiological BMP-mimetic effect, especially since Id1 was not affected here. Therefore, the *Vent2* reporter was used for further characterization of the underlying BMP activity of CGS-15943.

To examine whether CGS-15943 induces reporter activity independently of exogenous BMP and whether it synergistically enhances BMP signaling output at a sensitive BMP concentration similar to the observed profile of references in C2C12 (see Figure 32), BMP-4 was titrated from 0.01 to 10 ng/mL and the dose-response of CGS-15943 was determined. To eliminate endogenous and exogenous BMP activity, cells were treated with rhNoggin (10 ng/mL), which showed basal activity of CGS-15943 on Vent2 expression (Figure 61).

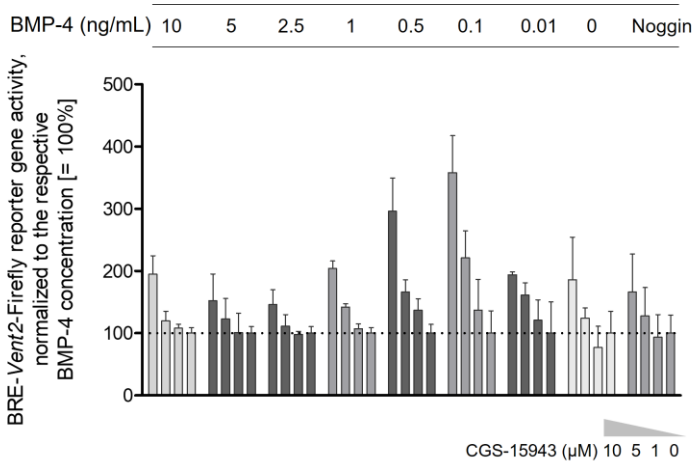

Figure 61: CGS-15943 activates Vent2 expression independent of BMP-4 but synergistically enhances reporter activity at low BMP-4 doses. BMP-4 was titrated from 0.01-10 ng/mL along with CGS-15943 for 22 h and bar graphs indicate *Vent2*-luc-induction normalized to the respective BMP-4 concentration. Noggin (10 ng/mL) was added as control to eliminate exogenous and endogenous BMP-4. These results based in part on experiments performed by Tanja Schuh during her Bachelor thesis.[330]

Consistent with previously collected data, the hit compound enhanced reporter response in a sensitive concentration window between 0.1-0.5 ng/mL BMP-4 by up to 3.5-fold above BMP-4-mediated level, which is within the range of calculated EC_{50}-values of BMP-4 (0.5 ng/mL, see

Figure 36). These data suggest an amplifying effect of *Vent2* expression on low synergistic BMP levels, resulting in a more sensitive cellular response. As previously discussed, such a sensitive concentration window for BMP activating reference compounds was observed in C2C12 cells. This was also shown for CGS-15943 in HEK293T cells, thus a reduction of exogenous BMP could be considered for further validation of BMP-enhancing compounds. It is important to note that the cofactor OAZ is essential for *Vent2* expression, but not expressed in C2C12 cells. Consequently, the BRE-*Vent2*-luc reporter did not work in these cells for compound profiling (data not shown).[88]

Taken together, an initial test screen of bioactive compounds yielded 12 compounds (hit rate of 0.9%) that exhibited dose-dependent antagonism of DMH-1. Only CGS-15943 was able to induce *Vent2*-dependent expression either in the presence or absence of BMP-4 and was capable of partially reversing DMH-1-induced gene expression. These data indicate a regulatory enhancement of BMP-dependent signaling outputs. Promisingly, CGS-15943 showed a distinct and superior selective profile to all reference compounds and to the herein characterized hit compound Chromenone 1. Next, CGS-15943 was further validated in BMP-dependent osteogenic differentiation to examine its BMP-potentiating capacity.

3.3.2 Functional validation of CGS-15943 as an osteogenic BMP potentiator

Next, the osteogenic potential of the hit compound CGS-15943 in both C2C12 differentiation and human SaOS-2 mineralization was investigated to further validate a BMP-potentiating or activating mode-of-action. As shown previously, a minimum induction of BMP-4 is usually required to induce transdifferentiation in C2C12 and to overcome a certain BMP output threshold to display a BMP-inducing response. Interestingly, this behavior was also observed for CGS-15943, as it induced synergistic ALP activity at concentrations of 5-20 ng/mL BMP-4 with efficient signal amplification up to 5.4-fold of the BMP-4 level (Figure 62A). However, a BMP-independent induction was not observed, in contrast to the reporter response on the BRE-*vent2* promoter in 293T cells. This may suggest a specific mechanism potentiating BMP-signaling or underlying basal BMP activity that cannot be excluded in this 239T-based setup. Similar to Ventromorphin and Isoliquiritigenin (see Figure 32), the osteogenic potential of the hit compound was suppressed at very high physiological levels of BMP-4 above 30 ng/mL, as maximum signaling upregulation may be reached. When tested along with 7.5 ng/mL BMP-4

under standard assay conditions, CGS-15943 exhibited a synergistic dose-response, starting with low doses at 0.1 µM (Figure 62B).

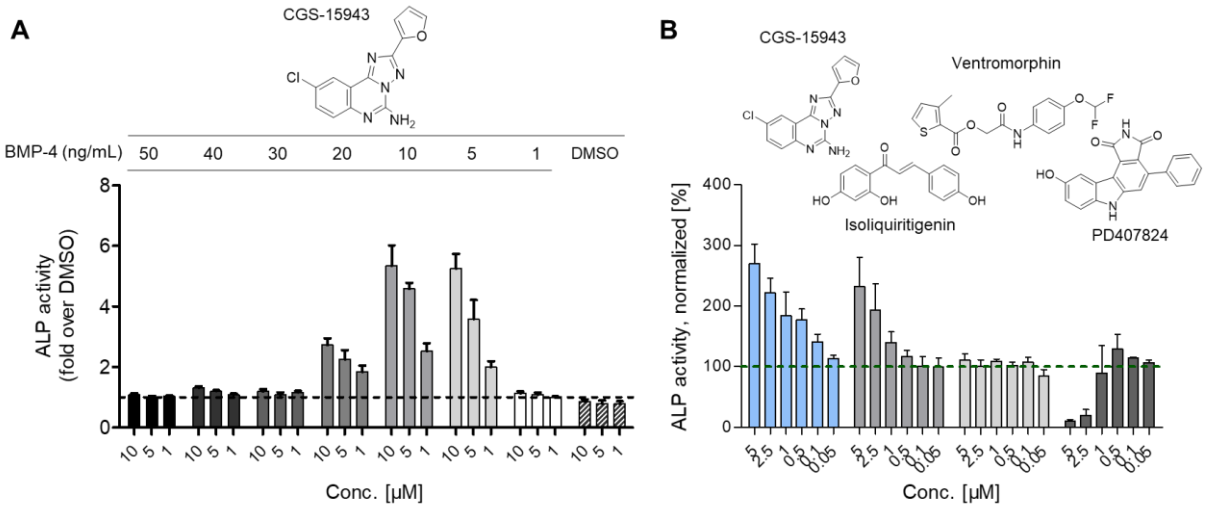

Figure 62: Assessment of BMP-dependent (and -synergistic) ALP induction of CGS-15943 displaying a sensitive ALP-enhanced dose-dependent relationship in co-treatment with 5-20 ng/mL BMP-4. (A) BMP-4 was titrated from 1-50 ng/mL along with CGS-15943 for 72 h and bar graph indicate ALP-induction normalized to the respective BMP-4 concentration. (B) CGS-15943 and reference compounds were added together with 7.5 ng/mL BMP-4 for 72 h and ALP-activities were normalized to BMP-4 (= 100%).

Compared with the tested BMP-active reference compounds, CGS-15943 displayed a very similar activation profile on reporter activity and ALP-induced activation as Isoliquiritigenin, albeit the latter was not as effective in antagonizing cardiogenesis in mESCs. To validate the observed ALP-activity, gene expression was monitored, and an osteogenic transcript profile was determined. Here, similar to Isoliquiritigenin, synergistic ALP induction was successfully validated by significantly induced *Alp* expression after 72 h (Figure 63).

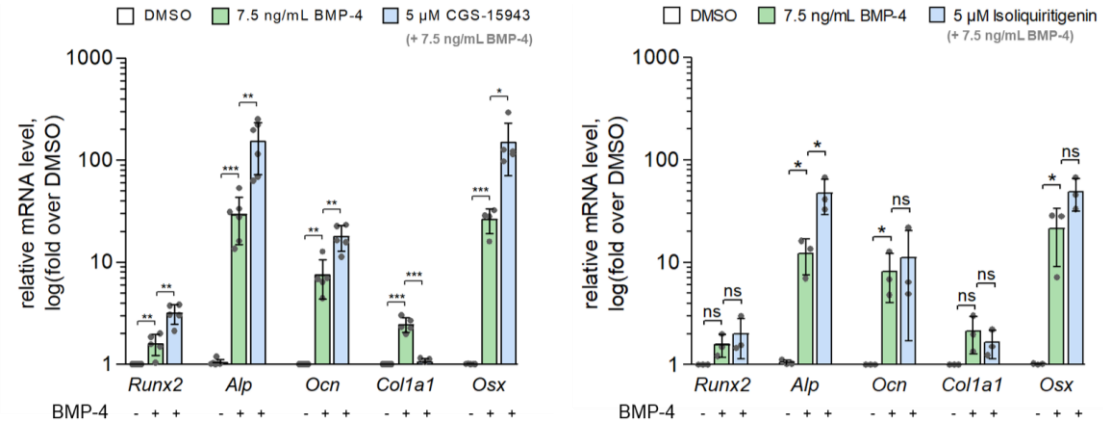

Figure 63: Relative quantification of BMP-dependent osteogenic gene expression transcripts confirmed CGS-15943 as a BMP-4 potentiator. C2C12 cells were treated with DMSO and/or BMP-4 (7.5 ng/mL) in the presence or absence of compound (5 µM) for 72 h. Data is shown as mean ± SD ($n \geq 5$) and normalized to DMSO. Statistical analysis was performed with an unpaired two-tailed *t*-test (* $p < 0.05$; ** $p < 0.01$; *** $p < 0.001$).

In contrast to Isoliquiritigenin, the entire set of osteogenic markers was significantly stimulated, especially the osteogenic transcriptional drivers *Runx2* and *Osterix*. The only exception was a repression of *Col1a1,* which may be explained by a delayed expression. This marker gene is particularly important for later stages of osteoblastic maturation.[183]

To validate long-term differentiation and osteoblastic maturation in a human context, CGS-15943 was tested in the *in vitro* hSaOS-2-based mineralization assay. As shown by normalization to DMSO, CGS-15943 was incapable of increasing basal mineralization in absence of BMPs, whereas low-dose BMP-2 and BMP-4 (2 ng/mL) stimulated osteogenesis by up to 50%. Simultaneous treatment resulted in an increase in BMP-dependent mineralization by up to 150% for BMP-2 and 100% for BMP-4, suggesting an enhancement of BMP-dependent signaling during osteoblastogenesis (Figure 64).

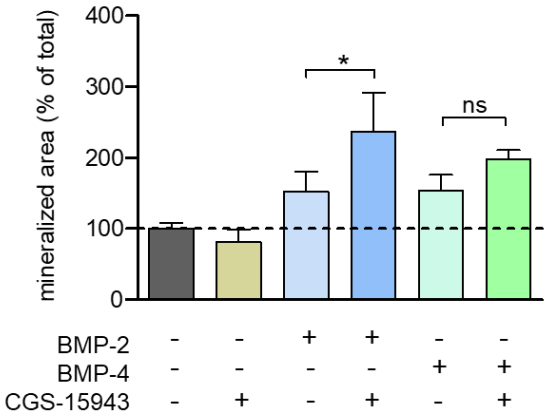

Figure 64: CGS-15943 significantly induced synergistic osteoblastic mineralization in human osteosarcoma cell line SaOS-2 after 11 days of differentiation as shown by quantified calcium deposits of mineralized area. Incubation in absence or presence of BMP-2/-4 (2 ng/mL) at 0.025 µM was performed for 11 days and *in vitro* mineralization was visualized by Kossa staining of calcium and image-based quantification of mineralized area was performed. Bar graphs represent data as mean ± SEM ($n \geq 3$); Statistical analysis was performed using paired one-tailed *t*-tests (* $p < 0.05$). These experiments were performed by the BERTRAND group (Magdeburg).

With these data, CGS-15943 was shown to enhance BMP-induced osteogenesis in both mouse and human cell lines. Overall, CGS-15943 was not able to induce osteogenesis in the complete absence of BMP-4, supporting an amplifying activity on BMP signaling. This observation was further confirmed by mineralization studies, where CGS-15943 did stimulate calcium deposits moderately in a synergistic manner when treated with osteogenic BMP-2 or BMP-4. Thus, it was hypothesized that CGS-15943 mediates a BMP-amplifying mechanism of action that differs depending on the cellular context, as opposite observations were made for reporter gene activity and osteogenesis. As demonstrated for the reference compound

Isoliquiritigenin, however, C2C12-dependent osteogenic induction requires minimal BMP induction for myoblasts to undergo osteoblastogenesis. The C2C12 assays have been used in several screening campaigns to search for BMP activators. However, despite the large number of small molecules screened in these assays, it is becoming increasingly apparent that drug-like small molecules that mimic the physiological activity of BMP are unlikely to be found, which is why this assay is reaching its limits.[273,279,285,287] This is also likely due to the complex heterodimeric complexation of the receptors, their different binding affinities towards specific ligands such as BMP-2 and -4, and their highly conserved binding mode, supporting efforts made in this thesis to establish alternative phenotypic assays in this field.

3.3.3 *In vivo* validation in a zebrafish embryo development model

Since *Zebrafish* models have been used to evaluate BMP-activating chemical probes, zebrafish embryos were utilized and tested during early gastrulation and dorso-ventral axis patterning. Early gastrula stage can be visualized by marker gene expression for phenotypic analysis of embryonic dorsalization and ventralization.[270,271] To recapitulate the potential of CGS-15943 to modulate BMP-dependent embryonic development, given the critical response of CGS-15943 during mesodermal specification in mESCs, it was questioned whether the compound also induces ventralization during early gastrulation (3 hpf) leading to ventrally matured embryos (24 hpf) by enhancing BMP-mediated response of BMP-gradient areas during axis patterning (Figure 65A). These experiments were performed by collaboration partners at the Karlsruhe Institute of Technology (KIT, Dr. Sepand RASTEGAR). CGS-15943 was tested at 1 µM, and the expression of dorsal (*goosecoid*) and ventral (*vox*, *eve1*) markers was visualized by *in situ*-hybridization as shown in Figure 65B. The BMP-dependent target genes *Vox/vent* and *eve1* are counterparts of the dorsal gene *goosecoid* that prevent its expression, thus causing defects in head regions.[350–352] As expected for a BMP activating compound, expression of the ventral markers *vox/vent* and *eve1* were induced, whereas *goosecoid* expression was suppressed by CGS-15943 at 2 µM. These data underscored that CGS-15943 increases BMP signaling during gastrulation, thereby shifting the morphogenic BMP gradient-dependent dorsal-ventral axis patterning. To further validate this activity, a large number of embryos were treated with DMSO or CGS-15943 (1-50 µM) and dorso-ventral-specific phenotypes evaluated (Figure 65C,D).

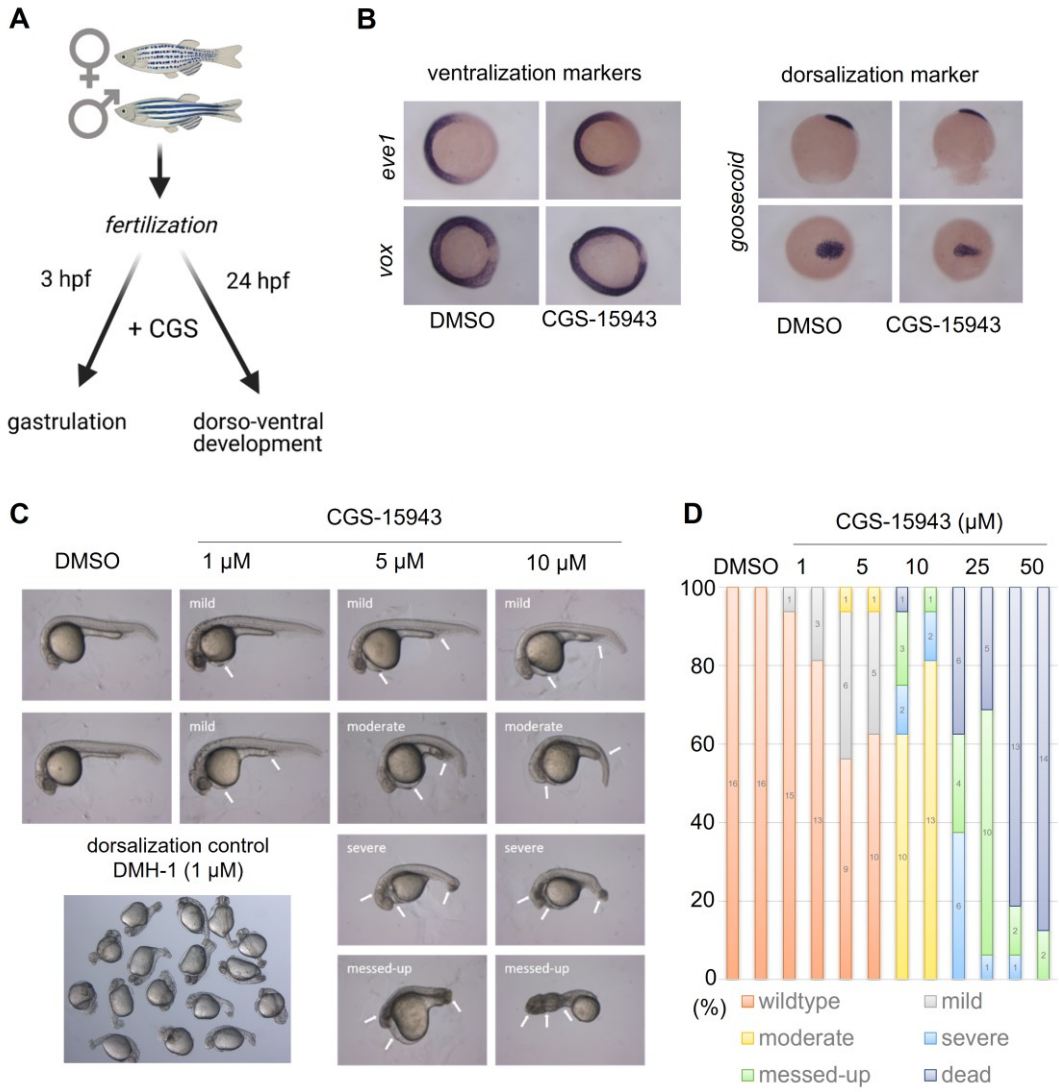

Figure 65: CGS-15943 recapitulates BMP-triggered zebrafish ventralization. (A) Schematic illustration of the experimental setup to evaluate ventralization during grastrulation after 3 h and dorso-ventral axis formation 24 h post fertilization (hpf). (B) Visualization of gastrula stage marker gene expression by in situ hybridization at 3 hpf of embryos treated with DMSO vehicle or CGS-15943 (2 µM). (C) Representative images of dose-dependent ventral induction by CGS-15943 from 1-10 µM and dorsalizing phenotype induced by control DMH-1 (1 µM). Images of treated embryos were taken 24 hpf. Arrows indicate ventralized areas (D) Embryos develop distinct phenotypes at different CGS-15943 concentrations (1-50 µM) for at least 15 embryos per condition. Experiments were conducted and analyzed by Sabrina WEBER and Dr. Sepand RASTEGAR (KIT, Karlsruhe).

Representative images illustrate ventral phenotypes (24 hpf) induced by concentrations of 1-10 µM, typical morphological ventral defects were observed, such as mild cyclopia, a reduction in brain size or more severe heedlessness on the ventral tissue (Figure 65C). In addition, growth of ventral mesoderm tissue at the yolk sac and its terminal extension, as well as abnormal cellular accumulation at the urogenital pore, was observed, which was visible in mild and moderate ventral phenotypes. This was particularly noticeable in embryos treated with 1-5 µM CGS-15943, while increasing the concentration resulted in more severe phenotypes with

loss of dorsoanterior tissue in the tail region. As controls, zebrafish embryos treated with DMSO showed an intact wild-type phenotype, whereas embryos treated with DMH-1 showed a dorsal phenotype with impaired tail patterning, as previously reported.[244] When sorting and quantifying ventral-specific phenotypes, a dose-dependent relationship was observed, albeit high concentrations (25-50 µM) were toxic.

Next, the ventral capacity of the BMP-sensitizer PD407824 was examined, as it exhibited moderate antagonism of DMH-1-induced cardiogenesis in mESC up to 2.5 µM (see Figure 27) before becoming toxic. Since the tested references Isoliquiritigenin and Ventromorphin have already been shown to mediate ventral phenotypes, they were not included further.[270,271] The ventralization potential of PD407824 was assessed at 24 h post fertilization (Figure 66).

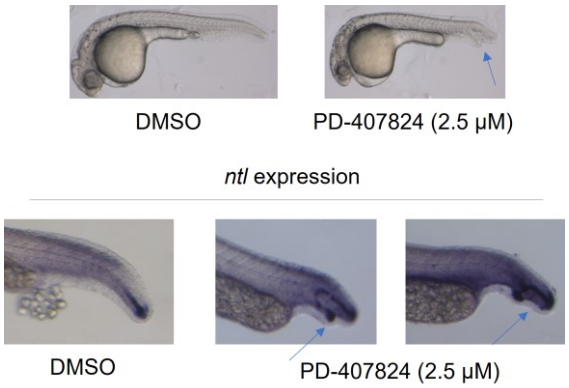

Figure 66: Representative images of embryos treated with the BMP-sensitizer PD407824 at 24 hpf indicate a dorsalization phenotype. Dorsal marker *ntl* (no tail) is visualized by in situ hybridization 24 hpf (see blue arrows). Experiments were conducted and analysed by Sabrina WEBER and Dr. Sepand RASTEGAR (KIT, Karlsruhe).

Indeed, PD407824 induced the characteristic secondary tail fin morphology described as dorsalization phenotype, indicating an antagonistic BMP response in zebrafish embryonic development. This observation was further confirmed by additional in situ hybridization of the *ntl* gene expression, which is a critical gene for the development of the mesoderm during gastrulation and subsequent tail fin formation.[350] As indicated by the blue arrows (Figure 66), PD407824 mediated an impaired tail phenotype, further questioning its described activity and utility as a BMP sensitizer. Moreover, PD407824 exhibited pronounced cytotoxic effects, likely mediated by its pan-kinase inhibitor activity, specifically on cell cycle regulators, leading to many off-target effects in a more complex *in vivo* model such as zebrafish development.

Overall, CGS-15943 induces a moderate ventralization phenotype consistent with an activation or enhancement of BMP signaling. Furthermore, it exhibits comparable ventral phenotypes

compared to those reported for Isoliquiritigenin and Ventromorphins. Notably, studying synergistic response in *Zebrafish* embryogenesis is difficult due to the low bioavailability of exogenously supplemented proteins, so no direct synergism could be tested in this setup.

3.3.4 Structure-activity-relationship studies

Following validation of CGS-15943 in several *in vitro* and *in vivo* assays, a systematic structure-activity-relationship study was performed to identify critical pharmacophoric features and opportunities to introduce functional groups for target identification approaches. Stefan LOHMANN (SCHADE group, Kiel) designed and synthesized a series of CGS derivatives for this purpose. For biological characterization, the osteogenic potential of the synthesized derivatives was assessed in C2C12 differentiation in a BMP-synergistic manner, as the secondary assay represents a suitable compromise between subsequent extensive SAR studies and physiological relevance by recapitulating the potential to induce cellular commitment. The major focus was on an array of substituents at the 2-, 5- and 9-position while the triazoloquinazoline scaffold was kept. Replacement and modifications of the primary amino group in 5-position was examined in detail to explore potential hydrogen-bond formations. In addition, initial attempts were made to test the potential of a scaffold-hopping approach to overcome the rigid nature of the scaffold by replacing the triazolo-quinazoline with an imidazo-quinoline.

Figure 67 summarizes the activity data of all newly synthesized CGS derivatives in C2C12 cells. ALP activity is represented relative to BMP-4 levels using a color code that indicates an enhanced activity in blue or no activity in red.

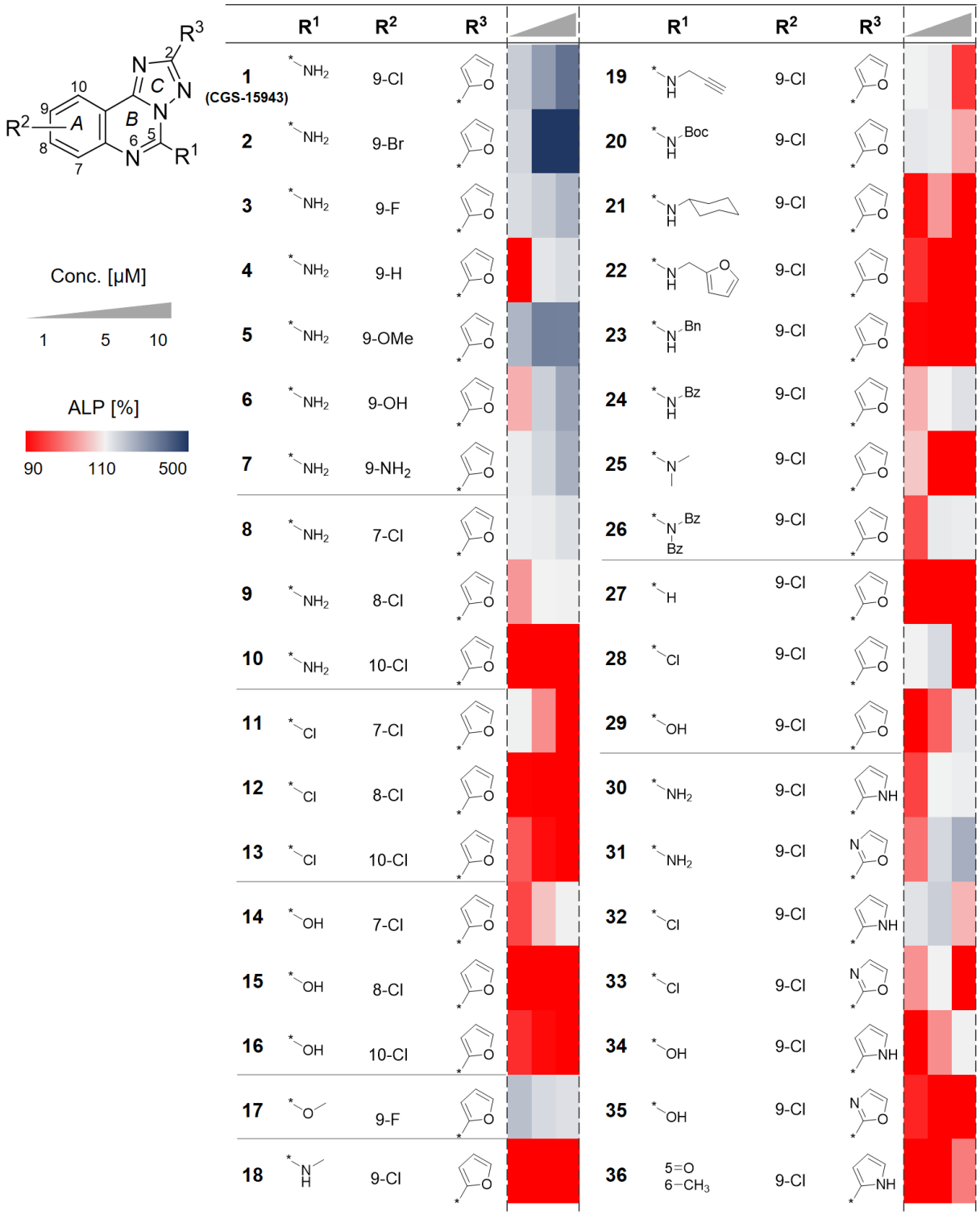

Figure 67: The Structure-activity-relationship study illustrates potential to modulate the osteogenic BMP activity of CGS-15943 by different substituents in 9-position. All derivatives were synthesized by Stefan LOHMANN and tested in the C2C12 osteogenic differentiation assay at three different doses (1, 5, 10 µM). The color code illustrates activity as mean values of $n \geq 3$ independent experiments, with enhanced ALP activity in blue.

First, the necessity of the chlorine substituent in the 9-position on the A-ring of triazolo-quinoline (R^2) was investigated to determine the relevance of a halogen in this position and to identify opportunities to replace chlorine with other halogens and substituents. Significant shifts

in activity were observed with variations. By removing the 9-chlorine (4), a significant decrease in activity was observed, indicating an interaction of the halogen with its respective target, e.g., via possible halogen-π-stacking or electrostatic interaction. Consistent with this assumption, bromination at the 9-position resulted in the strongest ALP-induction (2), while the fluorinated analog (3) was less active than 1 and 2, suggesting an interaction that is enhanced with increasing atomic size and decreasing –*I*-effect of the tested halogens (Br>Cl>F). With the incorporation of oxygen at the 9-position, moderate activity for the hydroxyl group (6) similar to the amino group (7) and potent activity of the methoxy substitution (5) relative to CGS-15943 (1) were observed, indicating a beneficial -*I*- and +*M*-effect (OMe>OH>NH_2) for the BMP-response on 9-position. Thus, electron-rich substitutions at the 9-position of quinazoline that do not have significant electron-withdrawing influence on the tricyclic heteroaromatic backbone are favorable. When shift in the position of the mono-substitution (7-, 8-, 10-Cl) on the A-ring was assessed, it revealed a loss of activity for nearly all derivatives (8-10, 11-13, 14-16), with 7-Cl (8) exhibiting moderate activity but being less active than the 9-Cl-substitution, suggesting a steric clash at the 7-, 8-, 10-positions in the binding site.

Further, to investigate the importance of the NH_2 group in the 5-position, its possible importance as a functional group for the formation of H-bridges by exchange with other substituents was evaluated. Different substituents were incorporated at the amino-group in the 5-position (R^1), which resulted in an overall reduction or complete loss of ALP-activity. Given that small methyl groups (18, 25) and larger substituents such as benzoyl (24, 26) or benzyl (23) were inactive, indicated very little space in the binding site and critical hydrogen-bond formations of the amine to the target. The latter hypothesis is supported by the replacement of the 5-amino group by a chlorine substituent or hydroxy group (28, 29), which resulted in a significant decrease in activity. In general, replacement of the amino group by chlorine resulted in significantly lower solubility and increased cytotoxicity in the assay.

Next, the possibility of replacing different heterocycles at position 2 was investigated. The furan group in the 2-position was modified (R^3) by incorporating an additional nitrogen (30, 32, 34, 36) or by replacing the furan with an oxazole (31, 33, 35) to introduce an additional hydrogen-donor for a hydrogen-bond-interaction and to preserve the H-accepting properties of the oxygen. Replacement of the furan with a pyrrole (30) resulted in loss of activity, indicating incompatible introduction of a hydrogen-donator, whereas the oxazole-derivative (31) exhibited moderate ALP induction but was less active than the 2-furan (1) showing an activity

≥ 5 µM. However, this correlation showed no beneficial properties from introducing an additional heteroatom, but there may still be room for optimization in the 2-position.

Finally, the scaffold was analyzed to assess the rigidity of the triazoloquinazoline backbone. Here, attempts were made to open up the tricyclic structure at the B-heterocycle (37, 38) as well as converting the scaffold to an imidazoquinoline (40). Interestingly, the ring-opened derivatives 37 and 38 were similarly active as CGS-15943 (4a) as shown in Figure 68.

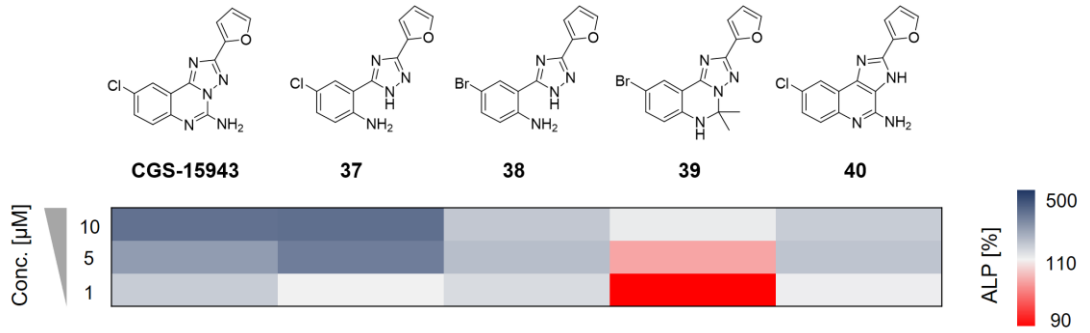

Figure 68: Structure-activity-relationship study of different scaffold-changing approaches reveals limited potential to enhance BMP-response of CGS-15943 in C2C12 osteogenic differentiation assay. Dose-response of the derivatives synthesized by Stefan Lohmann is visualized in a heatmap. The color code illustrates activity as mean values of n ≥ 3 independent experiments, with blue activity indicating ALP-increase.

It is tempting to speculate that ring opening allowed for intramolecular H-bonds that stabilized the molecule in a conformation similar to the triazolo-quinazoline scaffold. However, the 9-bromo derivative 38 was less active than its 9-chloro congener as well as CGS-15943 (1). This may hint towards a distinct binding mode and raises the question whether the observed activity is due to the same mechanism of action. Fixation of a putative cyclic conformation as speculated for 37/38 via an *N,N*-acetonide (40) again diminished biological activity. This finding again underscores the necessity of an unsubstituted amino group in this part of the molecule.

Imidazoquinoline 40 was designed and synthesized as an early attempt to assess the relevance of the nitrogen-rich scaffold for osteogenic BMP activity. In particular, replacement of the 4-nitrogen at the annulation site by a carbon atom would result in dramatic changes of the scaffolds' ability to form hydrogen-bond acceptor/donor interactions within a given target. Although the imidazoquinoline (40) stimulated osteogenic C2C12 differentiation, its activity reached a plateau at 5 µM and was inferior compared to the triazoloquinazoline CGS-15943. The observed activity suggests that the imidazole ring is either losing critical H-bond acceptor interactions or gains counterproductive H-bond donor features, leading to an impaired H-bridge network and thus decreased target binding affinity.

As summarized for the most active derivatives in Figure 69, the SAR consisting of 39 synthesized derivatives revealed several key pharmacophoric elements regarding the desired osteogenic BMP response. Key substituents were identified, including the free 5-amino group and an electron-rich functionality in 9-position, preferably bromine, but hydroxyl- and methoxy-substitutions were also tolerated with a reduction in activity. Replacement of the furan at 2-position with an oxazole was tolerated, while a pyrrole resulted in further loss of activity. Scaffold changes due to nitrogen shift and reduction in the rigidity of the triazoloquinazoline backbone were tolerated but did not outperform maximum response induced by CGS-15943 (Figure 69A). In addition, compared with (1), these derivatives exhibited moderate to no activity on *Vent2* expression, suggesting critical hydrogen-bond acceptor formations of the incorporated 4-nitrogen (Figure 69B). In general, the dose-response of the derivatives was consistent with that observed with *Vent2* expression, proving cellular activity in both assays. Both 37 and 40 reached a plateau at 5 µM on ALP activation and were lacking activity or efficacy in the reporter gene assay (Figure 69C), respectively.

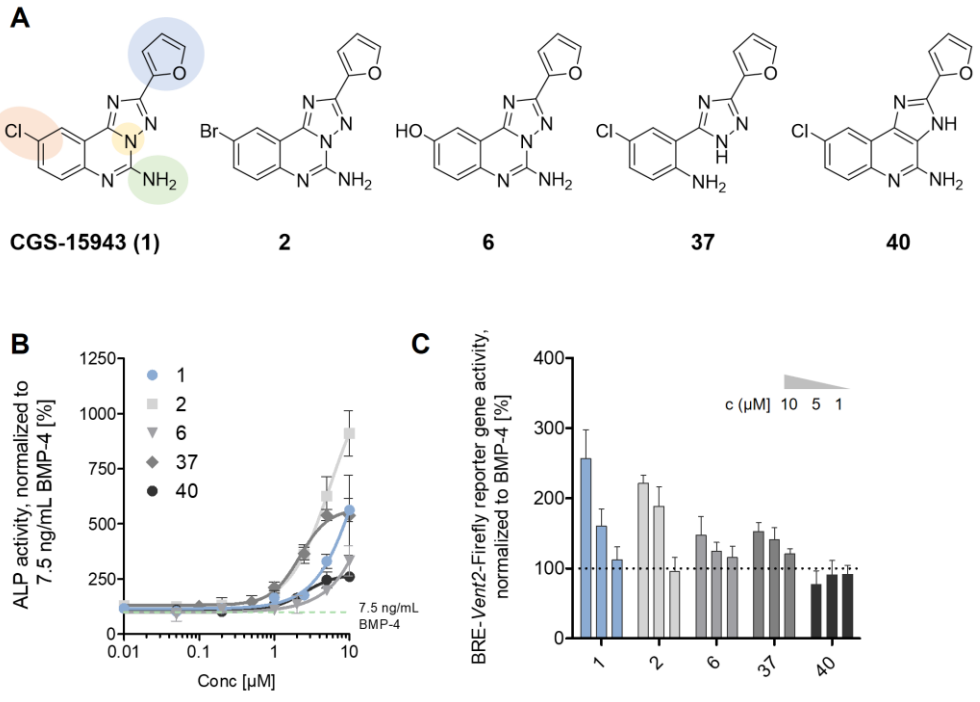

Figure 69: SAR summary of key pharmacophoric elements of the triazoloquinazoline CGS-15943 as an osteogenic BMP potentiator. (A) Chemical structures of derivatives exhibiting the most efficient ALP activity and key pharmacophoric features of the SAR study are highlighted: 2-, 5-, and 9-position required for BMP activity. (B) Dose-dependent BMP synergistic ALP induction of selected derivatives in C2C12 along with 7.5 ng/mL BMP-4. ALP activities are normalized to 7.5 ng/mL BMP-4 and are representative for mean ± SD for $n \geq 3$. (C) Dose-dependent activity on BMP *Vent2* response element (BRE) firefly luciferase. HEK293T cells were transiently transfected with BRE-*Vent2*-luc reporter and co-treatment with compounds and BMP-4 (10 ng/mL) was performed for 22 h. Luciferase activity was analyzed and normalized to DMSO (= 100%). Data represent the mean ± SD for $n \geq 3$.

The hydroxyl derivative (6) was tolerated and exhibited a moderate activity in both assays, which is particularly promising as it would allow the incorporation of functional phosphate esters as prodrugs. Notably, incorporation of an amino group at the 9-position (7) also appeared to be moderately tolerated in osteogenesis but did not affect *Vent2* expression (data not shown). With (2), one derivative was identified with improved capacity to enhance BMP-dependent ALP activity, with slightly induced activity on *Vent2* gene expression. Remarkably, in comparison with CGS-15943, (2) had no negative effects on cell viability, resulting in an improved viable and active analog.

Taken together, the study revealed a rather narrow SAR profile. Halogenation at the 9-position appeared to be essential, and modifications of the furan group on 2-position resulted in a significant reduction in activity. Collectively, the SAR study revealed key elements for the observed osteogenic BMP activity, providing insights into potential steric clashes of CGS-15943 with its target. Further target-agnostic optimization may lead to more precise structural improvements that may enable new derivatives with improved bioavailability as valid chemical probes for osteogenic studies.

3.3.5 Mechanistic studies and target deconvolution

Following the functional validation of CGS-15943 and the evaluation of the structure-activity relationship study, efforts were made to illuminate the mechanism of action underlying its potentiating efficacy on BMP signaling. Since functional validation and SAR were carried out in C2C12 cells, this cell line was also used for most of the mechanistic studies. A combination of gene expression analyses and assessment of BMP/TGFβ-Smad regulation was used to decipher the quality, quantity, and dynamics of BMP signaling outputs. These efforts were complemented by kinome and cell imaging profiling and several hypothesis-driven approaches to explain the BMP-potentiating mode of action of CGS-15943.

3.3.5.1 Characterization of BMP signaling dynamics

Cellular responses to growth factor-induced signaling are often transient, and target gene expression can occur within minutes upon growth factor binding, leading to rapid and irreversible cellular commitment.[149] Since the long-term effect of CGS-15943 on osteogenic

gene expression has been validated (after 72 h), the short-term response on BMP target genes was further evaluated to assess mechanistic dynamics and eliminate long-term feedback loops. It was questioned, how fast minimal low-dose BMP-4 (7.5 ng/mL) promotes irreversible induction of osteogenic differentiation and whether CGS-15943 sustains or amplifies the BMP4-induced signals. Based on these findings, the optimal time window for follow-up studies such as TGFβ/BMP-wide qPCR array analysis should be determined.

First, the BMP target genes *Id1*, *Id2*, *Id3* and the osteogenic transcription factors *Runx2* and *Osx*, as well as the expression level of *Bmp-4* in response to exogenous BMP-4 were quantified (Figure 70).

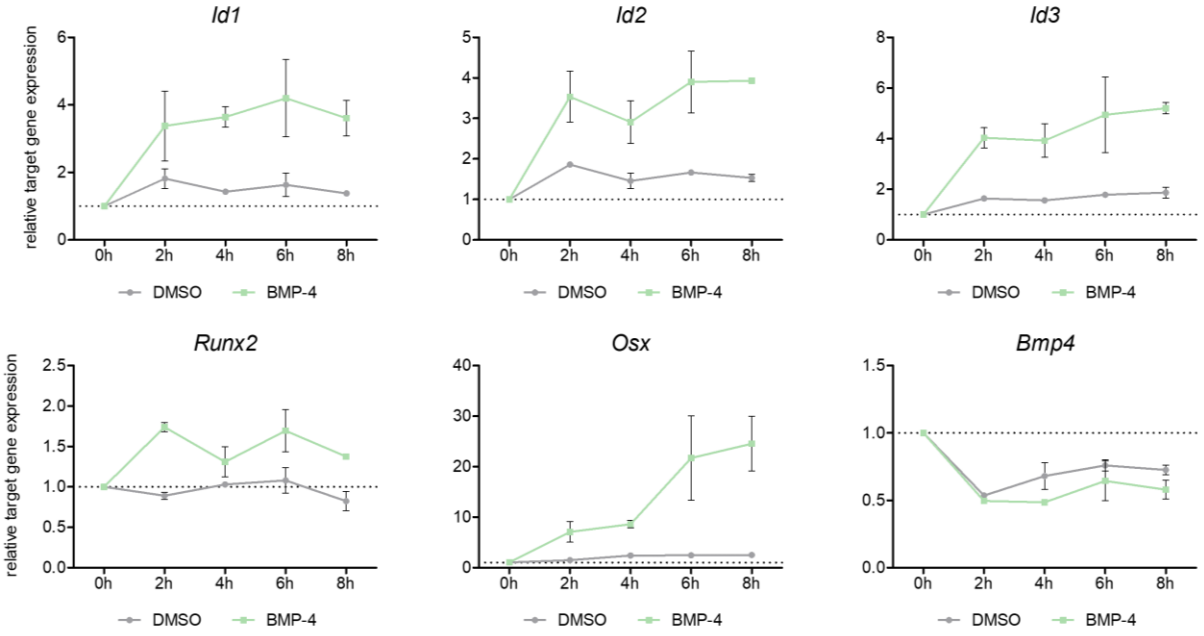

Figure 70: Relative quantification of gene expression for BMP target genes and osteogenic transcription factors. Treatment with vehicle or 7.5 ng/mL BMP-4 was performed for 8 h and cell lysates were taken for each time point and qRT-PCR was conducted. Data points represent mean ± SD (n = 2), normalized to 0 h (t_0).

As expected, strong transcriptional induction of *Id* genes was observed after 2 h, reaching a robust and consistent level (4-fold induction) after 8 h of treatment, while DMSO-treated expression remained at a very low basal level. Interestingly, all *Id* genes displayed quite similar profiles and transcript levels, suggesting nonselective induction of *Id* genes. In addition to *Id* gene expression, transcript levels of the osteogenic relevant factors *Runx2* and *Osx* were induced upon stimulation of BMP signaling after 2 h. *Runx2* in particular showed an expression pattern with higher fluctuations, but within the margin of error. However, its gene expression was induced only up to 1.8-fold relative to DMSO, consistent with its reported tight regulation

even after osteogenic induction is triggered. In contrast to the regulation of *Runx2* expression, *Osx* as a downstream transcriptional regulator of Runx2, was strongly induced after 2 h and was consistently induced up to 25-fold of basal activity, substantiating initiated and ongoing osteoblastic differentiation of C2C12. The only downregulated gene expression quantified was observed for *Bmp-4*, which was stably downregulated by 50% upon BMP induction, which may be a cellular response to regulate BMP activation via an early negative feedback mechanism. Remarkably, this negative cellular response also occurred rapidly after 2 h. Overall, these results provided evidence that rapid transcriptional activation occurred already after 2 h of exposure to minimal osteogenic BMP-4 levels.

Next, the synergistic effect of CGS-15943 was examined to determine whether it stabilizes and sustains signal transduction at an early stage of differentiation. A maximum duration of 24 h was chosen since instant amplification of BMP-dependent induction appeared unlikely. Indeed, BMP-4-induced expression of the selection of genes showed a sustained and stable level of activity from 2-24 h, whereas *Osx* expression was again continuously activated, which is overall consistent with the observed early rapid response (Figure 71). When BMP-4 was treated simultaneously with 5 µM CGS-15943, a BMP-enhanced activity was observed only for *Id1* with a continuous increase of cellular transcript levels, while *Runx2* mRNA levels remained unaffected and *Osx* gene activity was attenuated.

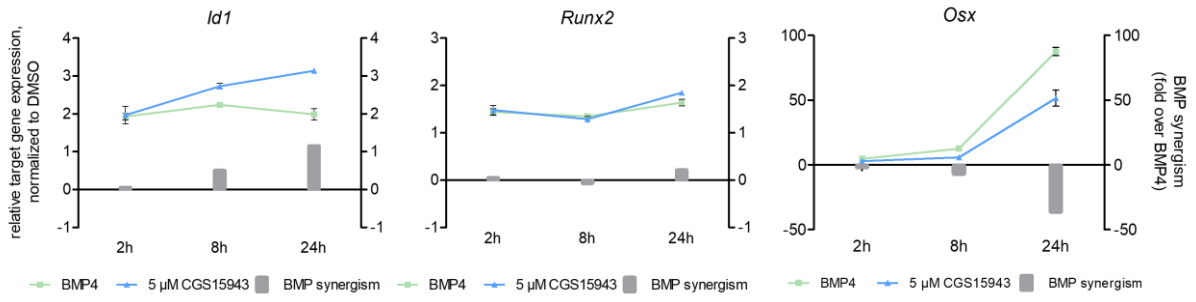

Figure 71: Relative quantification of gene expression for BMP target genes and osteogenic transcription factors. Treatment with vehicle, 7.5 ng/mL BMP-4 w/ or w/o 5 µM CGS-15943 was performed for 24 h and cell lysates were taken after 2 h, 8 h and 24 h and qRT-PCR was conducted. Data points represent mean ± SD (n = 2), normalized to t_0.

Remarkably, CGS-15943 exhibited an amplifying effect on *Id1* expression in C2C12 osteogenesis, which was also detected in mESC cardiogenesis after being exposed to the compound for 24 h, suggesting the important role of *Id1* transcriptional activity during differentiation (see Figure 71, Id1). Since *Runx2* expression was not increased within 24 h but

strong activation of the downstream transcription factor *Osx* was observed, these data suggest a BMP-enhancing effect of CGS-15943 on direct BMP-enhancing target gene regulations that might sustain BMP signaling outputs over time. This may lead to a substantiated osteogenic differentiation, that is not due to direct induction of the key osteogenic drivers. Because *Osx* is a downstream osteogenic driver of tightly regulated *Runx2* for efficient osteogenic differentiation, early induction might not be apparent when treated with CGS-15943, albeit long-term positive regulation of osteogenic factors may be mediated, as CGS-15943 induced *Osx* expression more than 4-fold above basal BMP levels after 72 h.

Next, it was examined how BMP signaling is amplified when cells are exposed to CGS-15943 prior to BMP stimuli. Since CGS-15943 was shown to stimulate *Id1* gene expression, the transcriptional activation of *Id1-3* gene expression was investigated. As depicted in Figure 72, BMP-4-induced mRNA levels were quantified after 2 h and 24 h in presence or absence of simultaneous treatment with 5 µM CGS-15943 in combination with pretreated cells for 2 h and 16 h exposure to CGS-15943.

After treating C2C12 for 2 h, no synergistic enhancement of *Id1* expression was observed compared with BMP-4 treated cells. In addition, pre-incubation with CGS-15943 (for 2 h and 16 h) did not result in synergistic induction but enhanced BMP signaling output of BMP-4 by 23–25% after 2 h, as shown in the curve plot. When BMP-4 was incubated for 24 h, the synergistic treatment resulted in a significant induction of *Id1* gene expression by nearly 40%, consistent with the observed effects of CGS-15943 after 24 h. Here, short-term preincubation (2 h) of C2C12 with CGS-15943 did not further enhance synergistic induction, whereas longer preincubation (16 h) enhanced expression under both synergistic and non-synergistic conditions. Remarkably, similar but still significantly weaker effects were observed in the transcript levels of *Id2* and *Id3*, consistent with the lack of ability of CGS-15943 to induce *Id2* and *Id3* in both C2C12 and mESC cells after 24 h. (see appendix, Figure 98).

These observed effects on the regulation of *Id1* expression indicate a predominant synergistic induction of CGS-15943 after 24 hours, suggesting interference with regulatory mechanisms to maintain and prolong the downstream activity of BMP-4.

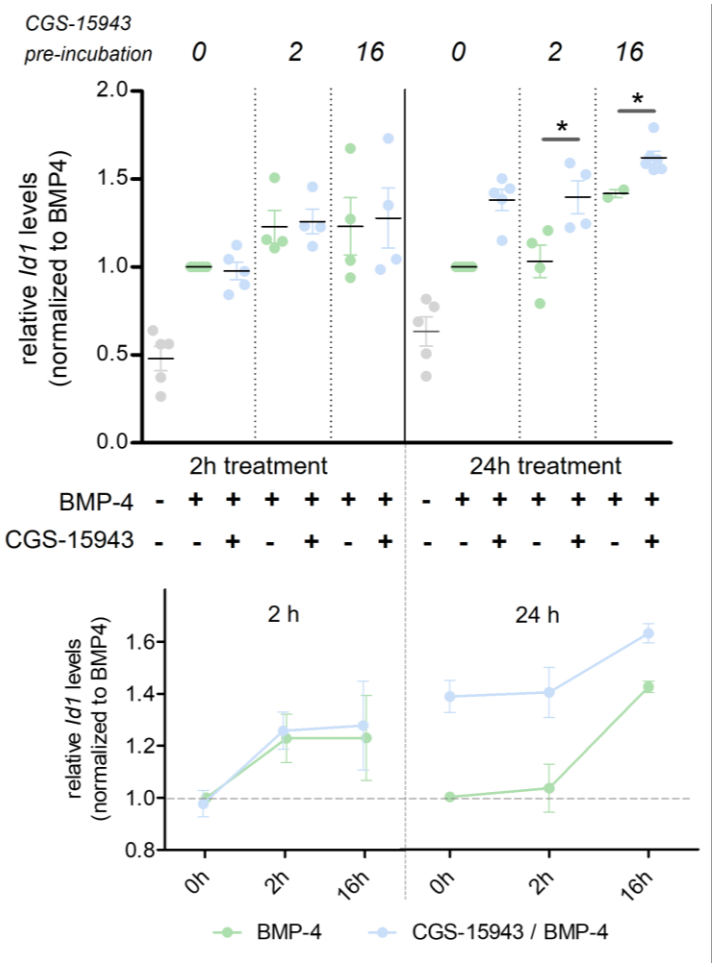

Figure 72: BMP-dependent *Id1* expression dynamics upon CGS-15943 exposure reveal a long-term upregulation after 24 h. Relative quantification of gene expression for BMP target gene *Id1* was determined by qRT-PCR. Treatment with DMSO vehicle (grey dot), 7.5 ng/mL BMP-4 (green) and/or 5 µM CGS-15943 (blue) was performed for 24 h with different pre-incubation times of CGS-15943 for 2 h and 16 h. Cell lysates were taken after 2 h and 24 h. Data points represent mean ± SD (n = 4), normalized to 7.5 ng/mL BMP-4. Statistical analysis was performed with an unpaired two-tailed t-test (*: p <0.05).

Beyond that, the short-term positive effect (within 2 h of BMP-4 exposure) after preincubation with CGS-15943 suggests increased cellular sensitivity towards BMP stimulation that might depend on a rapid *Id1*-mediated pre-regulatory effect on differentiation by directing myoblasts to osteogenic differentiation prior to the BMP stimulus. Such a “priming effect” could promote cellular plasticity, which in turn increases subsequent osteogenic potential. Indeed, *Id1* has been proposed to be an important inhibitory factor in preventing myogenic differentiation of C2C12 myoblasts.[353] Given that CGS-15943 did not directly enhance synergistic BMP signaling outputs, whereas preincubation positively affected them, this could point at a mechanism that does not require prior BMP stimulation but positively influences and maintains long-term cellular BMP output.

To further address these signaling dynamics, Smad protein levels were monitored. This work was performed by Daniel RIEGE (SCHADE group, Kiel). Nuclear and cytosolic fractions of BMP-4- and CGS-15943-treated C2C12 were generated and canonical Smad levels quantified to investigate phosphorylation and translocation dynamics.

As shown in Figure 73, levels of nuclear Smad1 and phospho-Smads were rapidly induced upon stimulation with 7.5 ng/mL BMP-4, reaching a peak level of translocated Smads in the nucleus within 10-30 min. This activation slowly decayed, reaching a basal level of Smads after 60-120 min and thus a restored activity level of BMP-Smad-mediated signaling. This was also observed for a decrease in band intensity over 24 h and a characteristic band indicating ubiquitinylated Smad proteins in test experiments (not shown).

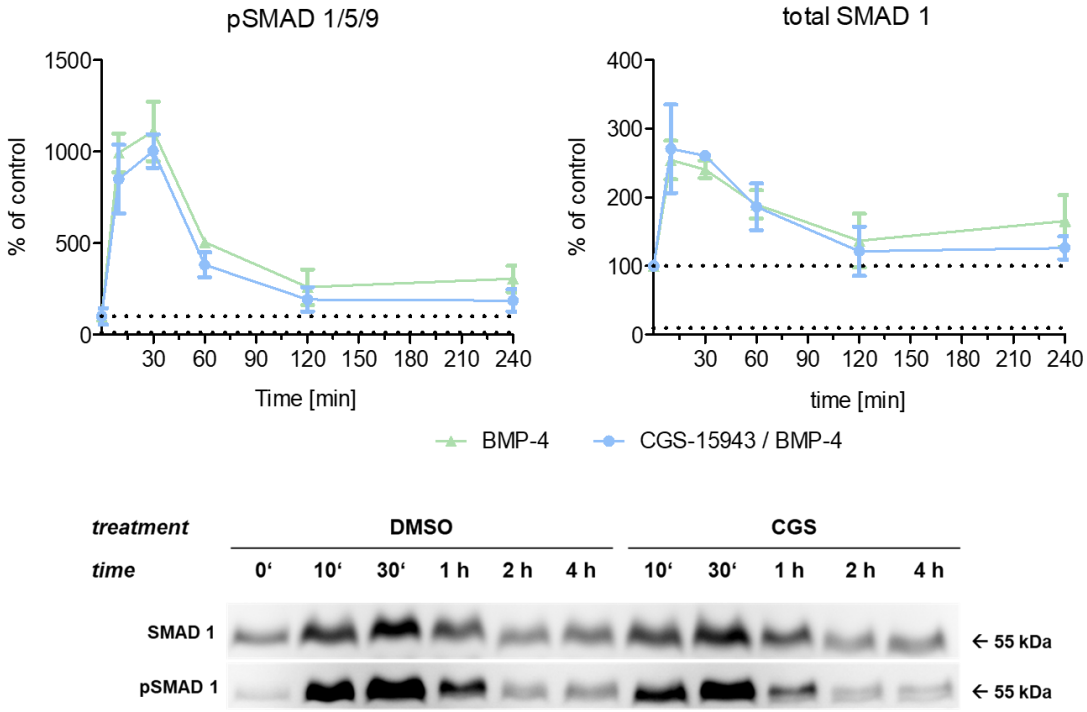

Figure 73: Smad nuclear levels increased rapidly in response to BMP-4 but remained unchanged upon stimulation with CGS-15943. Fractionation and quantification (Western Blot) of nuclear activated p-Smads and total Smad1 was performed in C2C12 cells. DMSO vehicle, 7.5 ng/mL BMP-4 or 5 µM CGS-15943 were incubated for 240 minutes and lysates were collected after different time points, followed by subcellular fractionation and western blotting. Data is shown as means ± SD and normalized to t_0. The experiment was conducted by Daniel Riege.

Importantly, co-treatment with 5 µM CGS-15943 did not enhance early transient Smad activation and translocation in comparison with BMP-4-mediated activity. This is in agreement with the observed early downstream regulation of *Id1* within 2 h of treatment (Figure 72). Remarkably, no difference in the response profile was observed between pSmad1/5/9 and total Smad1 proteins.

Since CGS-15943 did not enhance early Smad signaling outputs, a pre-incubation was examined to elicit Smad dynamics after reapplied BMP stimulation. A second stimulus was induced with low-dose BMP-4 (2 ng/mL) for 30 min after 24 h of treatment to detect CGS-15943/BMP-synergism (Figure 74A). Again, stimulation with 7.5 ng/mL BMP-4 resulted in a rapid induction (1.8-3.1-fold) of total nuclear Smad1 and activated nuclear p-Smads levels, but no further increased nuclear translocation was observed when cells were treated synergistically with CGS-15943 (Figure 74B).

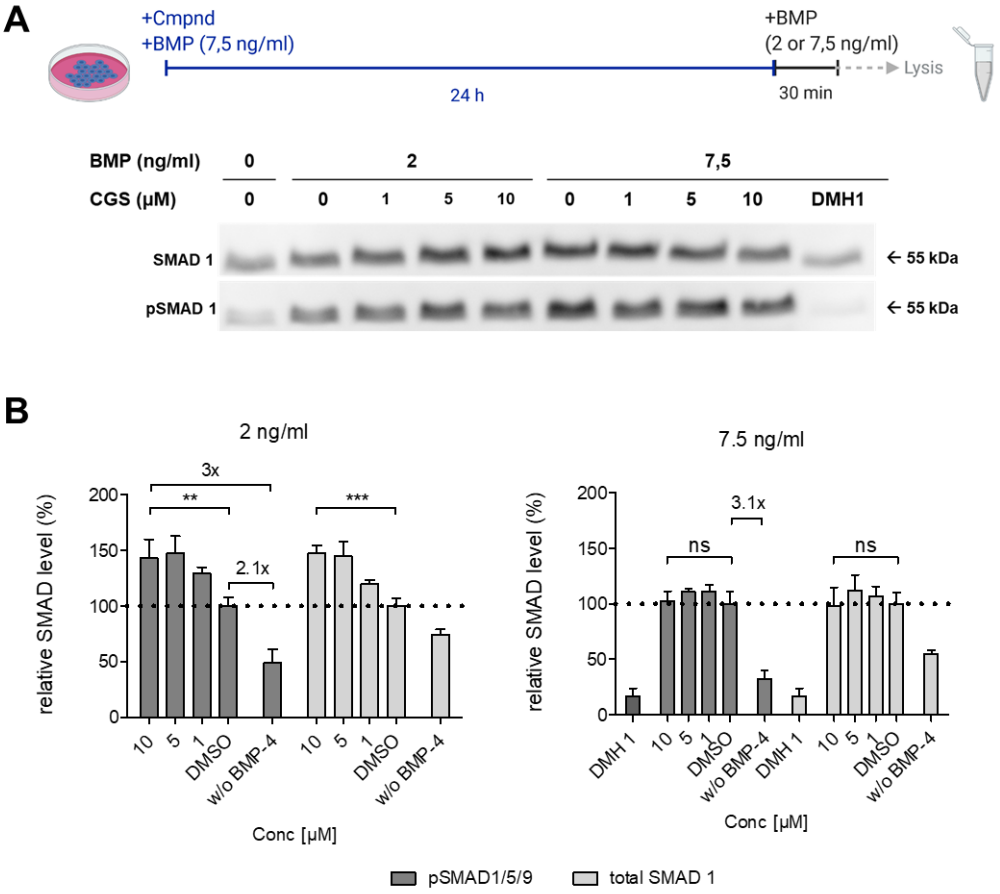

Figure 74: Smad nuclear levels increased rapidly in response to BMP-4 but remained unchanged upon stimulation with CGS-15943. Fractionation and quantification (Western Blot) of nuclear activated p-Smads and total Smad1 was performed in C2C12 cells. DMSO vehicle, 7.5 ng/mL BMP-4 and 5 µM CGS-15943 were incubated for 24 h, followed by additional stimulation with 2 or 7.5 ng/mL for 30 min. After transient stimulation of the cells, lysates were collected, fractionated and western blotting was performed. (A) Smad-characteristic bands were visualized by western blot and quantified intensity (B) was determined by total protein staining. Data is shown as means ± SD (n = 4) and normalized to BMP-4. Statistical analysis was calculated with an unpaired, one-tailed *t*-test (* p <0.05; ** p <0.01; *** p <0.001). The experiment was conducted by Daniel Riege.

When BMP input was reduced by stimulating the system with 2 ng/mL BMP-4 for 30 min, a reduction in the dynamic range of enhanced translocation was detected for both total Smad (1.5-fold) and p-Smad levels (2-fold) relative to the basal levels, proving the hypothesized

maximal cellular response to 7.5 ng/mL BMP-4 within 30 min. Here, a dose-dependent induction of CGS-15943 was shown from 1-10 µM relative to BMP-4-treated cells with significance indicated for 10 µM. Remarkably, synergistic treatment of CGS-15943 and 2 ng/mL BMP-4 increased p-Smad levels by 3-fold over basal activity, consistent with the calculated maximum induction of 7.5 ng/mL on Smad phosphorylation (3.1-fold), providing evidence for an amplified effect on Smad phosphorylation and translocation to the nucleus by CGS-15943, subsequently leading to enhanced target gene expression such as *Id1*.

In summary, the data comprehensively describe a rapid BMP-induced Smad-phosphorylation within 30-60 min, leading to maximal BMP-target gene transcription that became apparent after 2 h. Moreover, the collective data from *Id* gene expression analysis and pSmad1 protein level quantification indicated that CGS-15943 activity requires BMP stimulation to be fully effective. Collectively, this profile suggests a mechanism for CGS-15943 that counteracts or blocks negative regulatory feedback on canonical BMP signaling outputs.

3.3.5.2 Global perturbation of the BMP/TGFβ superfamily

To identify potential negative regulators of BMP signaling whose expression is inhibited by CGS-15943, a global TGFβ/BMP gene expression profiling was performed. Considering that CGS-15943 enhanced BMP-Smad dependent signaling outputs after 24 h, an expression profile screen of 84 transcripts was performed, including direct target genes and various factors relevant to the regulation and signal transduction of this signaling network. Global TGFβ/BMP gene expression with 7.5 ng/mL BMP-4 and 5 µM CGS-15943 was visualized by a heatmap showing up- or downregulation of gene expressions relative to BMP-4-treated C2C12 (Figure 75), revealing nonsystematic perturbation of TGFβ-dependent target genes, whereas induction was observed for BMP-responsive Smad target genes. This signature of CGS-15943 is consistent with the exhibited selectivity profile towards BMP signaling in reporter gene assays. In general, no global disruption of TGFβ/BMP signaling was observed, suggesting that BMP signaling is enhanced by CGS-15943 in a similar manner as basal, physiological BMP signaling. Furthermore, CGS-15943 did not inhibit the tested TGFβ-dependent *Smad* genes and had no effect on *Smad2* and *Smad3* expression levels in contrast to Chromenone 1, which attenuated TGFβ-Smad-dependent target gene expression, whereas, remarkably, moderate induction of *Smad4* and *Smad5* transcript levels was detected.

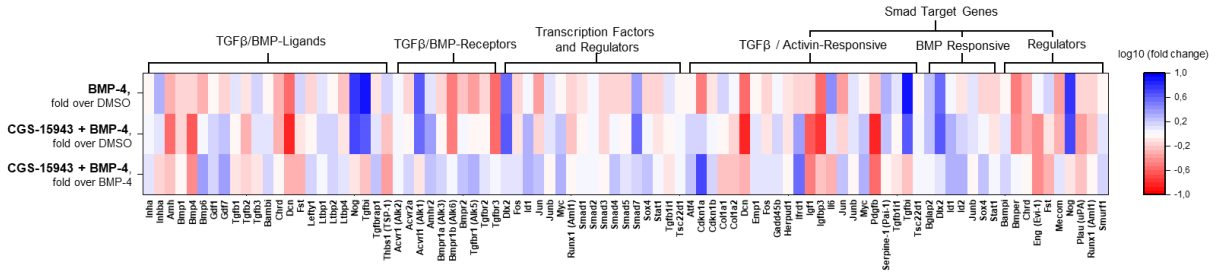

Figure 75: TGFβ/BMP superfamily-focused qPCR-array revealed that CGS-15943 has an enhanced BMP signaling pattern similar to physiological BMP-4. Gene expression analysis of the TGFβ/BMP pathway was performed using the RT2 Profiler PCR array (Qiagen) in C2C12 cells. C2C12 were treated with DMSO, BMP-4 (7.5 ng/mL) or CGS-15943/BMP-4 (5 µM/7.5 ng/mL) for 24 h, lysates were taken, and RNA was isolated for microarray analysis. Heatmap shows gene expression data of 84 transcripts, sorted according to their pathway functions (log10-fold changes, *n* = 3).

More pronounced effects were observed when significant modulation of genes was taken into account, as illustrated by a volcano diagram (Figure 76). Strongly perturbed genes are highlighted that exhibited a 2-fold change upon treatment with CGS-15943 after 24 h in presence of BMP-4 (over BMP-4-induced gene expression).

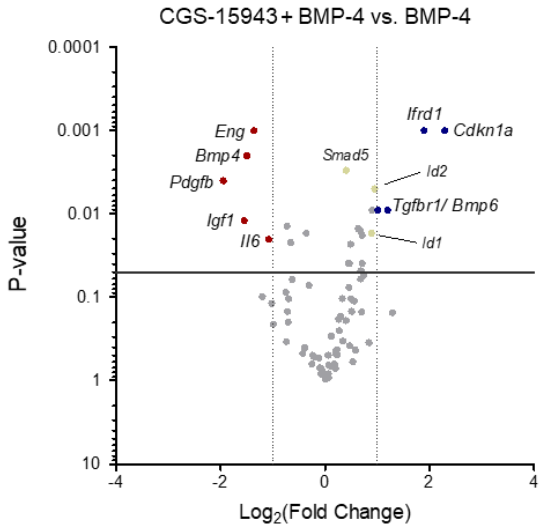

Figure 76: Significantly perturbed transcript levels of CGS-15943/BMP-4-treated cells compared with physiological expression levels of BMP-4. Volcano plot showing significantly regulated transcripts of TGFβ/BMP superfamily-focused qPCR-array (84 genes) according to their *p*-values (> 0.5) calculated with a student's *t*-test (*n* = 3). Red/blue/yellow dots indicate significantly downregulated/upregulated/BMP-responsive genes.

Here again, as observed for BMP-4 and Chromenone 1-treated cells, *Bmp-4* expression was significantly reduced in response to signal activation as a negative feedback response to enhanced BMP signaling. Remarkably, the gene expression of *Id1* and *Id2* was increased by 1.9-fold, showing high significance and being consistent with the observed effects discussed previously and therefore suitable as positive controls in this array analysis.

Other upregulated genes such as *Ifrd1* and *Cdkn1a* (*p21*) were highly increased by 3.7- and 4.9-fold, respectively, in CGS-15943-treated cells. Remarkably, *Cdkn1a* (*p21*) was shown to be downregulated by PD407824, thereby subsequently attenuating TGFβ downregulation.[285] However, CGS-15943 showed a distinct cellular response throughout the BMP-assays and did not inhibit TGFβ signaling, indicating a different mode of action for inducing *p21* expression. Indeed, the expression of *p21* (*p21*$^{CIP1/WAF1}$), as well as *p27* (here 1.4-fold induction) has been shown to be induced by BMP-4 in osteoblast-like cells and to contribute to osteoblast proliferation and differentiation and being a target gene activated by Smad1.[354–356] It should be noted that general downregulation of cell cycle regulators results in dysregulation and impairment of cell homeostasis and proliferation, and thus is often found to be dysregulated in cancer cells, so off-target attenuation should be avoided.[357] The other strongly induced gene, *Ifrd1*, is a transcriptional coactivator involved in promoting muscle gene expression and is highly expressed in myoblasts such as C2C12 and myofibroblasts.[358] The strong upregulation induced by CGS-15943 might be another cellular response to compensate for the enhanced commitment to osteogenic differentiation, as shown for BMP-2 in primary osteoblasts, in which induced BMP signaling enhanced *Ifrd1* expression as negative regulation of osteoblastogenesis.[359]

Several genes that were significantly downregulated in response to CGS-15943 are involved in the regulation of myogenic differentiation or are expressed in muscle cells, such as *Igf1*/*Igfr*, *Interleukin-6* (*Il6*) and the TGFβ-receptor-associated protein Endoglin, whereas the gene transcribing the growth factor Pdgfb is involved in TGFβ-mediated modulation of myofibroblasts, which all together strongly suggests a specific downregulation of muscle development by CGS-15943.[360–363]

Collectively, these data further support that synergistic treatment with CGS-15943 strongly sensitizes cells to BMP-4-induced signaling, as shown by gene expression perturbation of regulatory proteins involved in myogenic and osteogenic differentiation as well as direct amplification of BMP-Smad signaling target genes. Studies on reporter genes and on BMP/TGFβ gene expression profiling demonstrated unprecedented pathway selectivity of CGS-15943. This is particularly interesting, since regulatory crosstalks with TGFβ are common (e.g., Chromenone 1, PD407824), while CGS-15943 exhibit a unique and selective BMP amplifier mode-of-action.

3.3.5.3 Kinome profiling of CGS-15943

Since BMP signaling is crossregulated by other network kinase signaling pathways, a kinome-wide profiling was performed at Reaction Biology. Here, the casein kinase 1 (CK1) α1, δ, ε-isoforms, were found to be prominent targets that are regulatory factors of various cellular processes (see Figure 77).[364] They showed the most efficient inhibition among the 391 tested kinases with an efficient activity of up to 18% residual activity for CK1δ and around 60% residual activity for CK1α1 and ε. None of the other typical kinases were inhibited by more than 50%, indicating a very clean kinome profile for CGS-15943.

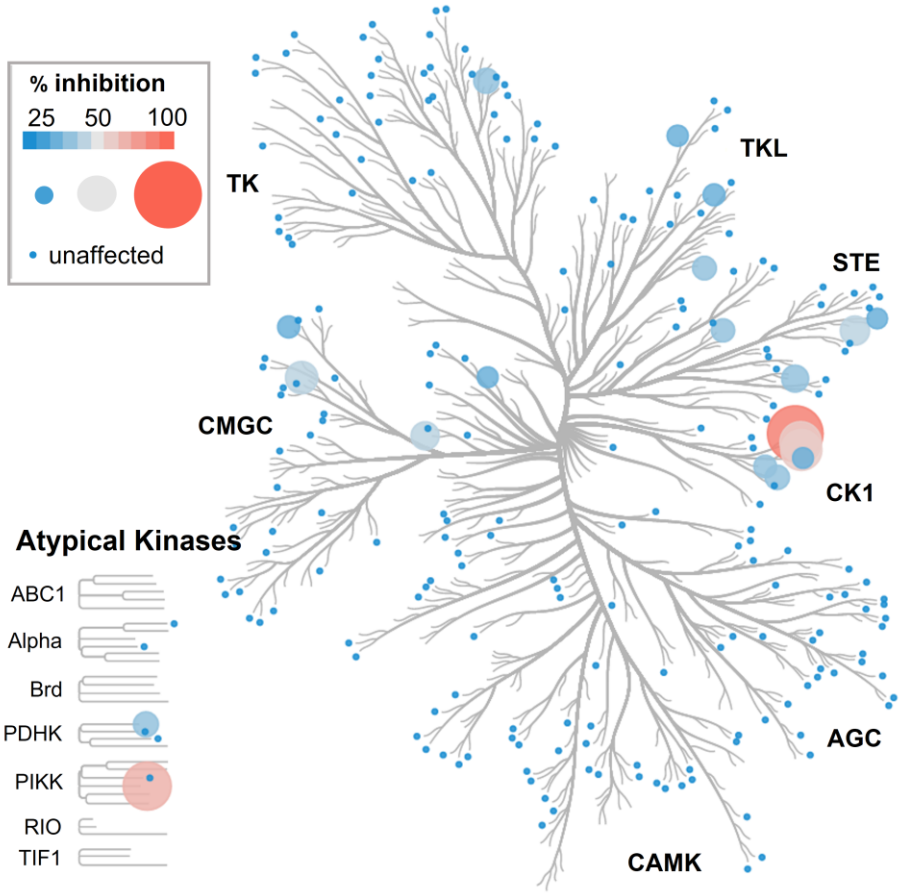

Figure 77: Kinome screen versus 408 kinases revealed CK1 isoforms as a target of CGS-15943. Dendogram represents residual activities of 391 screened kinases (without lipid kinases) against 1 µM CGS-15943. Activities were determined by biochemical inhibition at Reaction Biology. Data is shown as percentage relative to DMSO control and results were plotted using CORAL. Data analysis was performed by Stefan LOHMANN.

Among the 17 lipid kinases tested, only the γ-isoform of class IB PI3K (p110γ) kinases was significantly inhibited by 70% at 1 µM CGS-15943. In the course of a study of cancer treatment with caffeine, the analog CGS-15943 was shown to selectively inhibit the p110γ catalytic subunit among other lipid kinases, leading to attenuation of PI3K/Akt signaling.[365] in addition,

the DNA-dependent protein kinase (DNA-PK) was inhibited by 70% similar to p110γ. DNA-PK is a regulatory factor involved in transcriptional regulation of certain signal transduction-associated genes related to proliferation and differentiation. Of the identified kinases that were modulated by at least 50%, a dose-response curve was determined to validate the observed perturbation on the catalytic activity. Compound 29 was profiled against these kinases as a structurally closely related analog of CGS-15943 lacking osteogenic BMP activity.

A

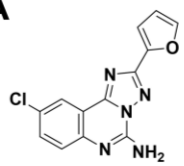

kinases (> 50 % inhibition)	inh. (%) @ 1 µM	IC_{50} (µM)
CK1δ	82	0.23
CK1ε	59	0.49
CK1α1	58	0.84
DNA-PK	70	0.21
PI3Kγ (p110γ)	74	0.12
PI3K (p110α/p65α)	65	n.t.
PI3K (p110α(E545K)/p85α)	58	n.t.

B

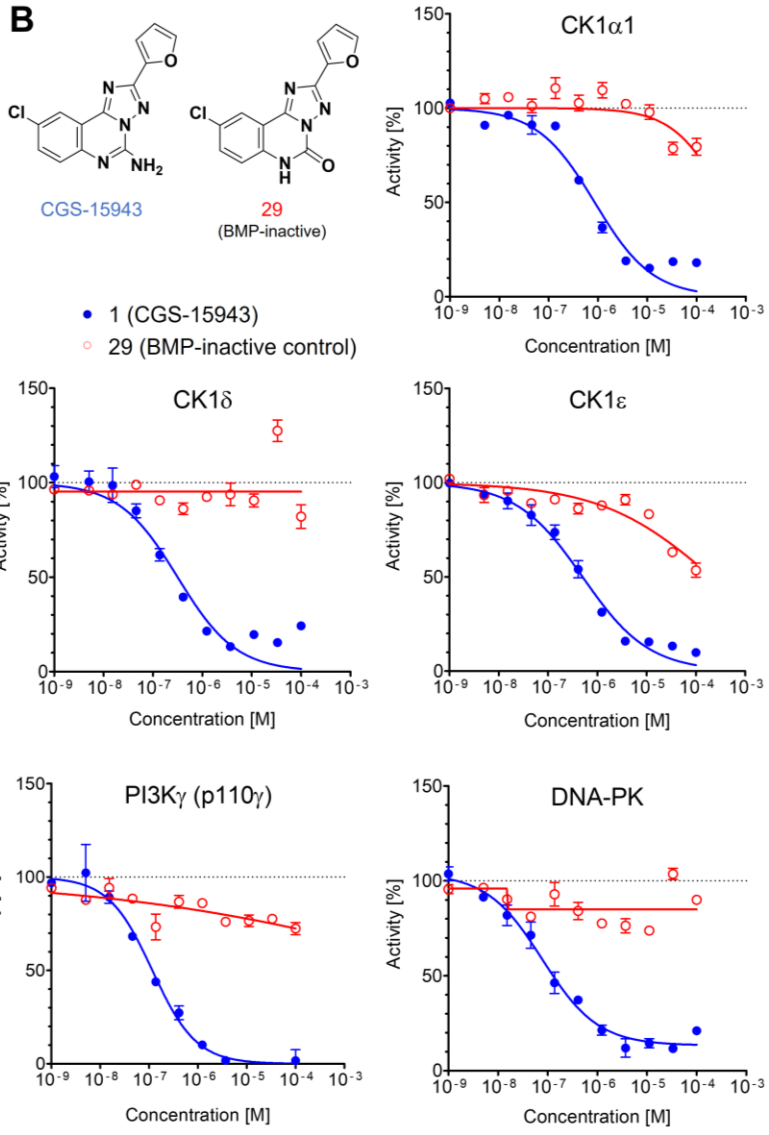

Figure 78: Validation of kinome screening hits confirmed CK1 isoforms, PI3K isoforms and DNA-PK as targets of CGS-15943. (A) Calculated IC_{50}-values of validated targets showing ≥ 50% inhibition. N.t. = not tested (de-validated in the literature).[365] (B) Dose-response curve of inhibition of CK1 isoforms against CGS-15943 and BMP-inactive analog 2a at the ATP concentration at K_m of the tested kinases.

As depicted in Figure 78, CGS-15943 inhibited the kinase activity of all three CK1 isoforms, DNA-PK and p110γ in a dose-dependent manner, thus confirming the targeting of these kinases. The calculated IC_{50}-values of CK1 isoforms were consistent with the measured

inhibition of each kinase at 1 µM, with selectivity toward the δ-isoform being expressed by potent inhibition of 50% at 230 nM. The dose-response relationship of CK1α1 and ε showed less potent inhibition with IC_{50}'s of 0.84 µM and 0.49 µM, displaying a 3.7- and 2.1-fold lower activity than the δ-isoform. Interestingly, the BMP-inactive derivative was inactive toward CK1δ and showed weak inhibition of CK1α1 and ε at high concentrations above 10 µM. As expected, potent inhibition of p110γ (IC_{50} = 120 nM) as well as inhibition of DNA-PK activity (IC_{50} = 210 nM) were confirmed, demonstrating efficient perturbation by CGS-15943, whereas the BMP-inactive quinazolinone analog 29 showed no inhibition. Given that 29 did not inhibit any of the validated kinases, all of them might represent potential target candidates for CGS-15943, underlying its mechanism of BMP amplification.

In summary, CGS-15943 affected only three types of kinases, representing a unique signature of the kinome with high selectively. All of these kinases were modulated in a dose-dependent manner but remained unaffected by the BMP-inactive analog. Subsequently, biological characterization and (de-)validation should be performed using biochemical and pharmacological inhibition studies.

3.3.5.4 Characterization of CK1δ/ε as a new target for CGS-15943

After CGS-15943 revealed a clean profile of kinase modulation and inhibition of CK1 isoforms was validated, the role of CK1 isoforms as BMP-relevant targets of CGS-15943 was assessed and potential off-target contributions evaluated. First, SAR studies on the catalytic activity of CK1 isoforms were performed by Aileen ROTH (KNIPPSCHILD group, Ulm), who tested a selection of derivatives against full-length CK1 isoforms, as opposed to the catalytic fragments used in kinome screening. Testing against full-length proteins provides higher quality inhibitor profiles as all possible binding modes, including allosteric mechanisms, are taken into account. New insights into structural modifications for the rational design of optimized and selective derivatives could be obtained. Two potent CK1 inhibitors, SR-3029 and PF-670462, were included for the direct comparison of the CK1 inhibitory capacity of CGS-15943. Residual activities were monitored and visualized in a heatmap, indicating a very steep SAR on all three CK1 isoforms (Figure 79A). This limited SAR is in line with activity data derived for BMP-dependent C2C12 differentiation, suggesting a possible correlation of CK1 isoform inhibition and BMP activation. Notably, an improved activity was detected for the bromo-derivative 4b.

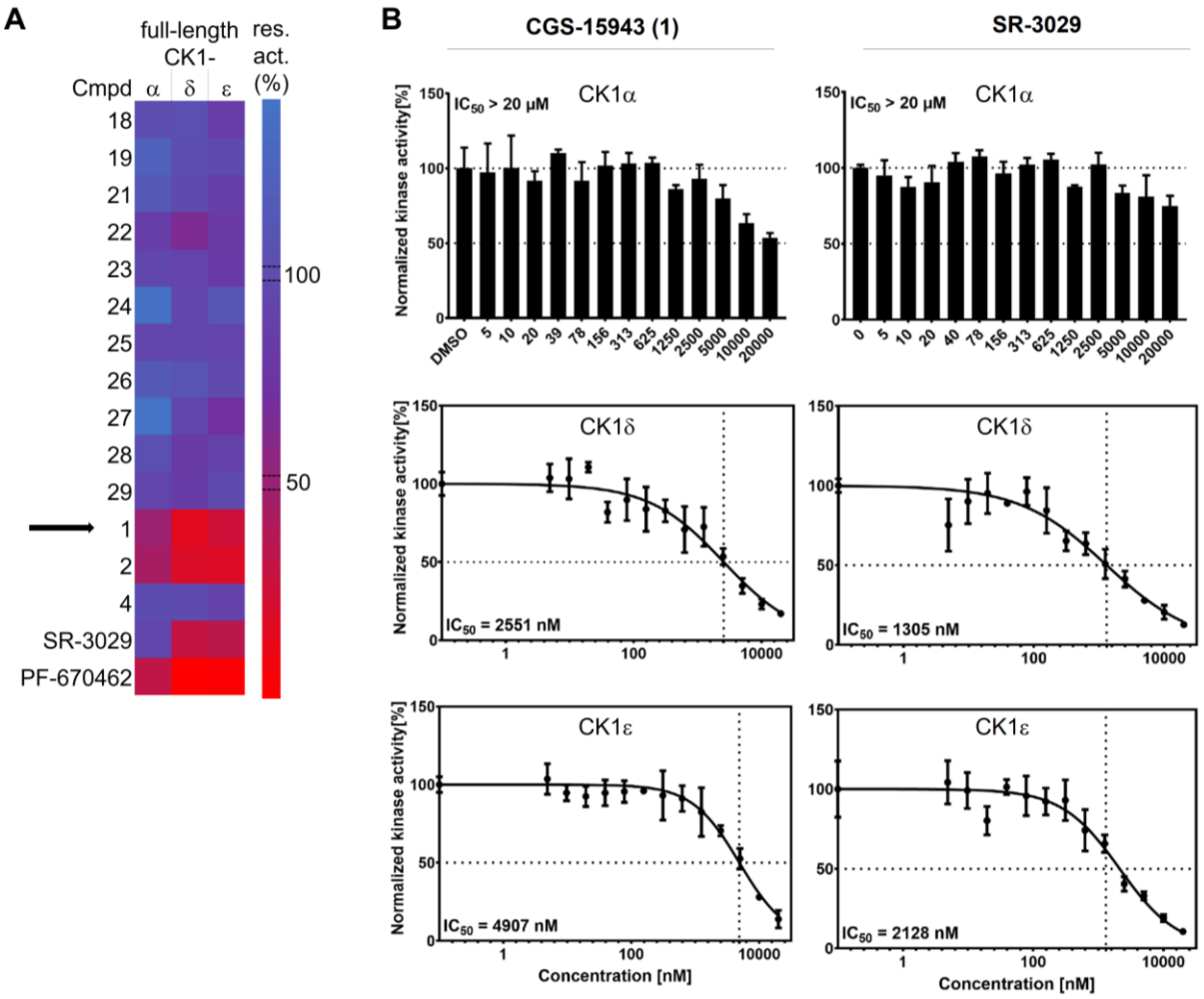

Figure 79: CGS-15943 inhibits full-length CK1δ and CK1ε selectively. (A) Biochemical screening of SAR-derivatives (10 µM) for their effect on full-length CK1-isoenzymes. Heatmap visualized as percentage of mean residual activity (n = 3), normalized to DMSO control. (B) Corresponding representative dose-response curves and IC_{50}-values of CGS-15943 and CK1δ/ε-selective reference inhibitor SR-3029. Experiments were conducted by Aileen Roth.

Moreover, as expected and described for full-length CK1 kinases, the overall activities were lower than those calculated for the catalytic fragments of the enzymes, approximately one order of magnitude lower (Figure 79B). Similar behavior was observed for the CK1δ/ε-selective inhibitor SR-3029 with reported IC_{50}'s of 44 nM and 460 nM, respectively.[366] However, both compounds were incapable of inhibiting CK1α at relevant concentrations, with CGS-15943 being more active than the selective inhibitor SR-3029. The unselective CK1 inhibitor PF-670462 exhibited higher activity on all CK1 isoforms.

Subsequently, the mode of inhibition was further investigated by varying the substrate concentrations (i.e., radiolabeled ATP) from 0-100 µM. CGS-15943 was tested at its calculated IC_{50} and IC_{25} concentrations against CK1δ and ε and the reaction rates were plotted as Michaelis-Menten and Lineweaver-Burk diagrams (Figure 80).

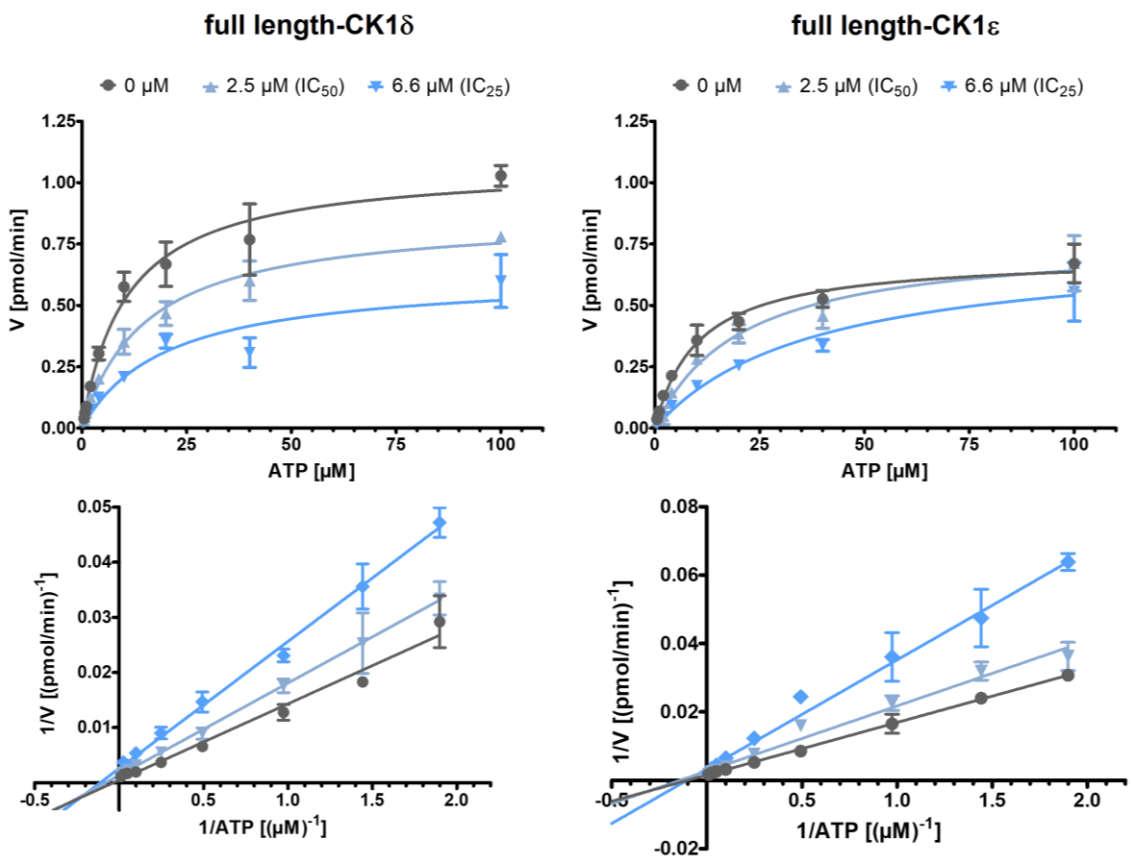

CGS-15943 [µM]	K_m [µM]	V_{max} [pmol/min]
0	10.72	1.07
2.5	15.3	0.87
6.6	20.22	0.63

CGS-15943 [µM]	K_m [µM]	V_{max} [pmol/min]
0	10.25	0.70
4.9	20.41	0.77
16.2	38.09	0.75

Figure 80: Michaelis-Menten kinetic studies revealed a mixed inhibition (competitive and uncompetitive inhibition) profile of CGS-15943 on CK1δ. Kinase assays were conducted with 6xHis-tagged full-length CK1 enzyme, 40 pmol α-casein substrate, [γ-^{32}P]-ATP (0-100 µM) versus IC_{25} and IC_{50}-concentraions of CGS-15943 in H2O at 30 °C for 30 min. The reactions were stopped by addition of SDS and samples were separated by SDS-PAGE followed by quantification of radioactive signal strength by Cherenkov counting. Enzyme kinetics were displayed using Lineweaver-Burk plots. Experiments were conducted by Aileen Roth. K_m = Michaelis-Menten constant; V_{max} = maximum conversion rate.

As shown for CK1δ and ε, an increase in the Michaelis-Menten constant K_m was observed for both kinases at elevated concentrations of CGS-15943, as indicated by an increase in the slope in the Lineweaver-Burk plots. Interestingly, a decrease in maximum rate (V_{max}) of the reaction was observed versus CK1δ, with increased K_m indicating a mixed inhibition of competitive and non-competitive inhibition of ATP.[367] This type of inhibition differs from that of a purely competitive inhibitor (unaffected V_{max}), which typically competes with ATP for binding and thus inhibits enzyme activity. A mixed inhibition suggests a combination of ATP-competition and potential allosteric binding to CK1 mediated by a conformational change or by

direct binding to the enzyme-bound substrate.[368,369] A different effect on CK1ε-activity was observed for CGS-15943 at the calculated IC_{50}- and IC_{25}-concentrations, displaying an increase in K_m but an unaffected V_{max}, suggesting a competitive inhibition of CGS-15943 on CK1ε. This is particularly interesting since distinct types of inhibition between CK1 isoforms are not very common. These data suggest a quite unique isoform-specific mechanism of CK1 perturbation for CGS-15943.[366]

In order to confirm binding to the CK1 active site and to gain further insights into ligand-protein interaction, a soak-in experiment in a CK1δ crystal was performed by the group of Prof. BAUMANN. The co-crystal structure was resolved at 1.85-1.92 Å (Figure 81).

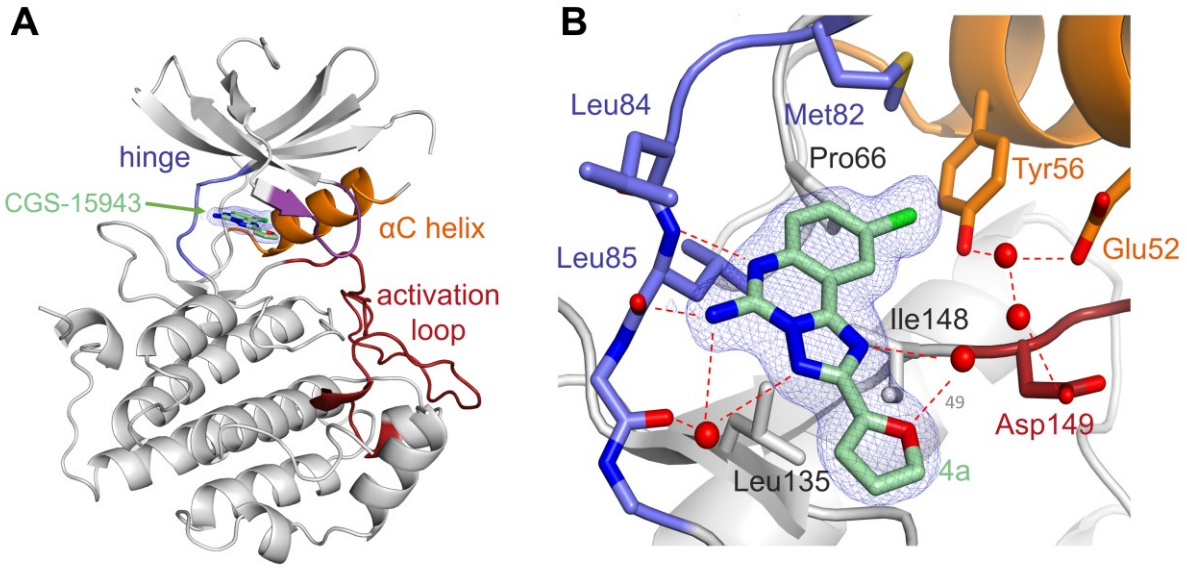

Figure 81: Binding mode of CGS-15943 in the ATP pocket of CK1δ. (A) Overview about the resolved CK1δ/CGS-15943 co-crystal structure. A truncated crystal structure of CK1δ (PDB: 4TWC) was used as a search model (B) Close-up pose of CGS-15943 in the ATP-binding pocket of the enzyme (Electron density of CGS-15943 is depicted as blue mesh with a contour level of 1σ; red dashed lines symbolize stabilizing hydrogen-bond interactions; Coordinated water molecules are shown as red spheres). Illustration of binding pose was made by Christian PICHLO and BAUMANN group, Cologne.

Similar to the adenine of bound ATP, the quinazoline scaffold of CGS-15943 forms multiple hydrogen bonds with the flexible hinge in the cleft region between both lobes of CK1. The amino group in 5-position, which is very critical for BMP activity, is stabilized by hydrogen bonds within the hinge region and a coordinated water molecule. The 9-chloro substituted part of CGS-15943 extends into the deeper hydrophobic cavity at the gatekeeper residues of the ATP binding pocket. Here, the halogen appears to interact with Tyr56 via π-halogen-stacking over a distance of 3 Å, which could be enhanced by exchange with bromine at the 9-position

of CGS-15943. Intriguingly, this derivative has been shown to improve cellular BMP responses in the SAR study. Moreover, the chloro-quinazoline might also coordinate the gatekeeper residue Met82, mediating a significant conformational change to ligand-free CK1δ.[370] Further, van der Waals interactions of the triazolo-quinazoline scaffold with the side chains of Leu135 and Ile148 could contribute to the binding mode. The furan-2-yl coordinates another water molecule in cooperation with the 1-triazolo-moiety of CGS-15943, and thus, stabilizes the solvent exposed part of the molecule in the pocket. However, no binding or stabilization via hydrogen-bond-interactions with the catalytically active Lys38 and Asp149 was observed, which are typically strongly engaged by CK1δ/ε-inhibitors such as PF670462 or 4,5-diarylimidazoles.[371,372] The lack of interaction with these residues might provide opportunities for further optimization of binding affinity. Another option for improvement might be achieved by a more complex functionalization in the future, replacing the 2-furyl group and thereby increasing the structural flexibility of CGS-15943, binding affinity and/or selectivity, respectively. Considering that the SAR of CGS-15943 was also very narrow and that various modifications to the amino group resulted in almost complete loss of activity, this may be further evidence of CK1 inhibition-dependent BMP activity. The binding pose of CGS-15943 in CK1δ supports the notion that any *N*-alkyl or *N*-acyl substituent would diminish inhibitory activity as steric clash in the hinge region is expected to occur. Interestingly, the reduction in BMP activity by replacing the triazoloquinazoline with an imidazoquinoline could be due to an impaired propensity to coordinate several water molecules as observed for the nitrogen atoms of the triazole-moiety, all which function as hydrogen-bond acceptors. This H-bond network might be disturbed by an imidazole that functions both as an H-bond donor and acceptor, depending on the tautomeric form within the CK1 active site. It should be noted that the quite selective kinome signature of CGS-15943 suggests a unique binding mode that may not be shared with other kinases. This would also be consistent with the narrow structure-activity-relationship, where minimal changes or functional modifications lead to a loss of activity that may depend on the specific mixed inhibition on CK1δ. In particular, the structural basis and functional consequences of the putative allosteric modulation of this CK1 isoform will be very interesting and important to elucidate in future studies.

To further assess whether the unique, mixed CK1 inhibition mechanism is relevant for BMP activity, the CK1δ/ε-selective SR-3029 and the less selective CK1 inhibitors PF-670462 were systematically profiled in all morphogenic BMP assays. In general, CK1 inhibitors differ in terms

of isoform selectivity, leading to distinct cellular responses.[370] To assess the differentiation ability of both mESC and C2C12, the dose-response relationship was monitored, as depicted in Figure 82.

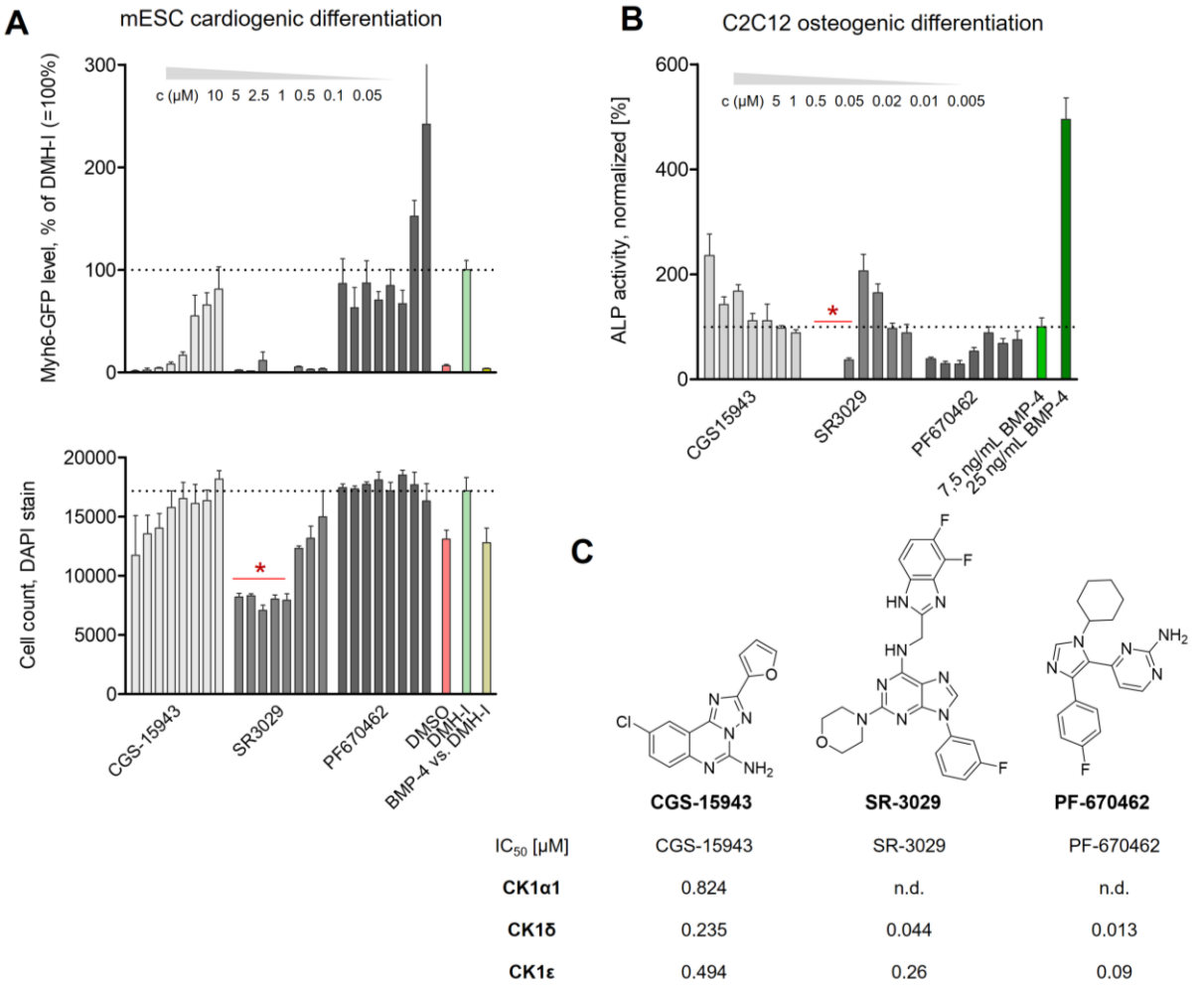

IC_{50} [µM]	CGS-15943	SR-3029	PF-670462
CK1α1	0.824	n.d.	n.d.
CK1δ	0.235	0.044	0.013
CK1ε	0.494	0.26	0.09

Figure 82: Characterization of CK1 inhibitors in BMP-dependent differentiation assays suggests a unique CK1-related contribution by CGS-15943 compared to classic inhibitors. (A) Dose-response antagonism of CK1 inhibitors in cardiac differentiation induced by the selective BMP inhibitor DMH-1 (0.5 µM). Bar graph is representative of the mean of triplicates and the respective SEM (n = 3). *Myh6*-GFP levels were normalized to DMH-1 with vehicle (DMSO). Impaired cell viability is indicated by red dots (B) Dose-response relationship of CK1 inhibitors on ALP activity during BMP-induced osteogenesis in C2C12. Compounds were incubated along with 7.5 ng/mL BMP-4 in C2C12 and treated for 72 h. ALP activities were normalized to DMSO and bars are shown as mean ± SD for at least three independent experiments. (C) Chemical structures of used CK1 inhibitors and their reported biochemical IC_{50}-values in comparison with the calculated IC_{50}'s of CGS-15943.[366]

In mESC-*Myh6*-GFP, SR-3029 potently inhibited BMP-dependent DMH-1-induced cardiac cluster formations, albeit exhibiting high cytotoxicity, as revealed by the significant decrease in cell number at concentrations greater than 0.5 µM (Figure 82A). However, due to impaired cell viability, the "rescue effect" on DMH-1 was no evidence of a BMP-specific response. SR-3029 would not have passed the set standard assay filter for potential hits in the cardiac mESC

assay. In osteogenic differentiation of C2C12 myoblasts, SR-3029 also impaired cell viability above 50-100 nM, as indicated, but induced ALP-activity within a narrow dose range from 20-50 nM to a similar extent as CGS-15943, as shown in Figure 82B. Together, these data imply a CK1-dependence in both differentiation assays that may also be mediated by CGS-15943. In contrast, the more potent CK1 inhibitor PF-670462 showed no activity and did not affect cellular viability in either differentiation assay, which is surprising at first glance. The lack of activity may be due to lower cell permeability of PF-670462.[366] Moreover, PF-670462 lacked the anti-carcinogenic activity of SR-3029, which exhibited highly antiproliferative effects in comparison to PF-670462 in several tumor types, such as CK1δ-high breast cancer cells.[373] This may also be due to a less selective kinome profile of PF-670462 relative to SR-3029, which was more effective against various kinases including p38 or EGFR, indicating a pan-kinase activity of PF-670462 and a distinct pharmacological effect due to non-selective targeting.[366,374] Again, it should be noted that SR-3029 showed potent inhibition of various CDKs with IC_{50}'s from 400-600 nM, which could lead to the observed cytotoxicity at higher concentrations and contribute to its combinatorial pharmacological profile and improved pharmacokinetic properties leading to the reported efficacy in cancer treatment as an anti-cancer drug.[366,375] Based on these reported characteristics, the different profile of the CK1 inhibitors SR-3029 compared with PF-670462 may have been observed in both differentiation assays.

When CK1 inhibitors were tested to further verify activity on the BMP reporter genes BRE-*Vent2* and BRE-*Id1*, a different response was again observed, with SR-3029 showing specific induction of *Vent2*-luciferase expression, whereas PF-670462 showed no activity on either reporter (Figure 83). Remarkably, SR-3029 exhibited a moderate dose response on *Vent2*-expression of up to 200%, but no induction of *Id1*-luciferase was observed, which is comparable to the very selective induction of *Vent2* by CGS-15943 (see Figure 61). However, SR-3029 showed a bell-shape dose-response on *Vent2*-expression with artefacts at higher concentrations, as typically described for firefly luciferase stabilizers.[376] Since *Id1*-dependent expression of firefly luciferase was not increased, it was hypothesized that enhancement of BMP-induced *Vent2*-expression may be mediated by selective CK1δ/ε-inhibition. The observed effects at higher concentrations in both C2C12 and HEK293 are likely due to global CK1 inhibition leading to attenuated cell viability and biosynthesis.

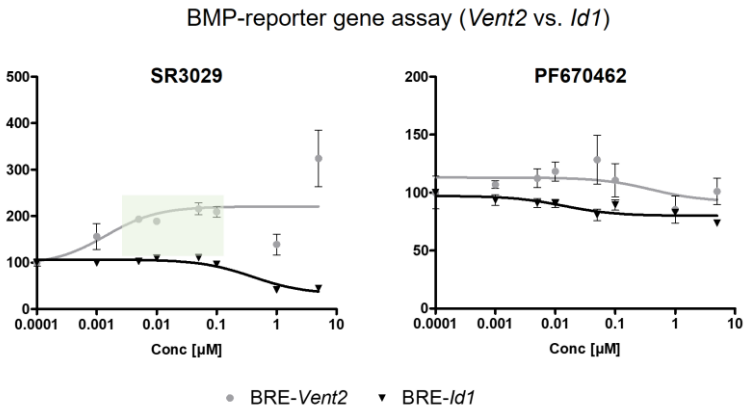

Figure 83: Characterization of CK1-inhibitors on BMP-responsive reporters reveal bell-like shape specifically on *Vent2* expression. Dose-dependent profiles of reference compounds on BRE-*Vent2*-luc and BRE-*Id1*-luc reporter was determined. HEK293T cells were transiently transfected and treated with compounds and BMP-4 (10 ng/mL) for 22 h. Luciferase activity was normalized to *Renilla* activity expressed by a control plasmid and data is shown as mean ± SD of *n* = 2 experiments relative to DMSO (= 100%).

Because SR-3029 showed a very similar profile to the one of CGS-15943 in the BMP-specific assays and to prove the tiny concentration range in which both CK1 inhibitors induce ALP-activity, the osteogenic expression levels of established marker were determined. Given the narrow activation window of SR-3029 on BMP-dependent ALP activity (20-50 nM, see Figure 82), osteogenic transcript levels were calculated for 50 nM. However, no significant synergistic induction of SR-3029 was observed for any marker gene, indicating a lack of osteogenic potential (Figure 84). Only *Runx2* and *Alp* were moderately induced by up to 2-fold over BMP-4-dependent expression levels, but this was significantly less relative to CGS-15943.

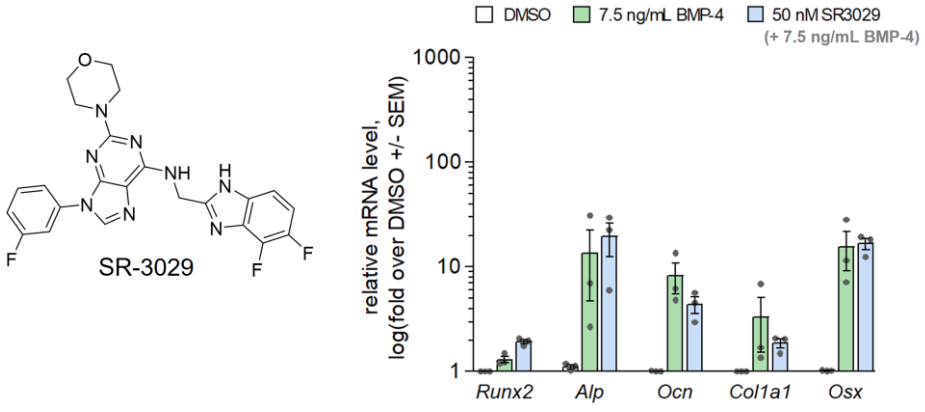

Figure 84: Relative quantification of BMP-dependent osteogenic gene expression transcripts did not confirm efficient osteogenic induction by SR-3029. C2C12 cells were treated with DMSO and/or BMP-4 (7.5 ng/mL) in the presence or absence of compound for 72 h. Data is shown as mean ± SEM (*n* ≥ 3) and normalized to 7.5 ng/mL BMP-4 (base line = 1).

These data did not provide evidence for a CK1-dependent activation of osteogenic ALP-induction, which may also depend on the tiny activation frame for both inhibitors, thus recapitulation of the osteogenic potential in C2C12 might be problematic. In addition, these data may imply a different mechanism for CGS-15943 based on additional targets.

To further delineate a CK1 isoform-specific dependency of CGS-15943-mediated BMP amplification, functional genetics experiments were considered. CK1 isoforms could be overexpressed using constitutively active expression constructs. In combination with the BMP-responsive *Vent2*-luc reporter, dose-response were determined for CGS-15943 when individual CK1 isoforms were overexpressed. As shown in Figure 85, overexpression of CK1δ resulted in a complete loss of BMP activity, while overexpression of CK1ε did not completely rescue the activity of CGS-15943. Notably, overexpression of CK1α did not affect the performance of CGS-15943. These data are consistent with the determined selectivity profile of CGS-15943 for the CK1 isoforms, with δ/ε being potently inhibited and are also in agreement with the insignificant reduction of CK1α by 17% at 10 µM relative to basal CK1 levels and are within the range of the determined IC_{50} (δ/ε = 2.6/4.9 µM) versus full-length CK1.

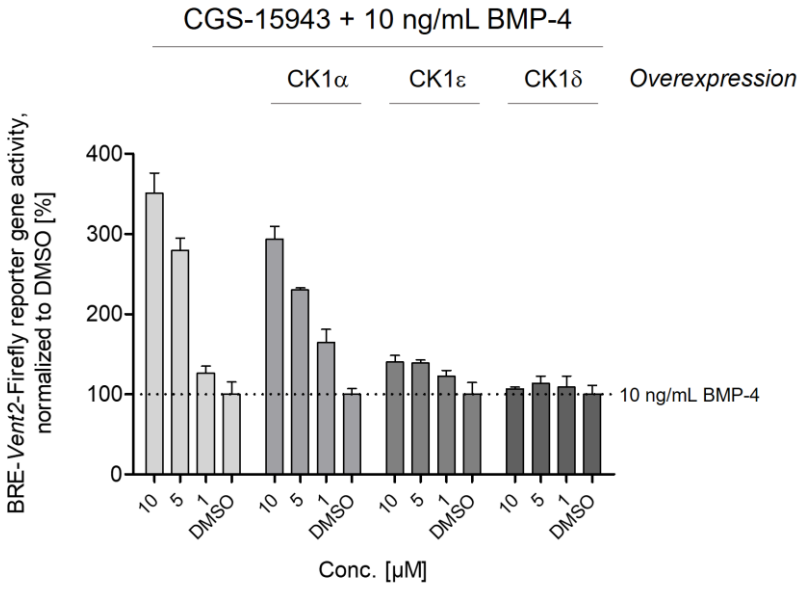

Figure 85: Overexpression of CK1δ and ε rescued the BMP amplifier activity of CGS-15943. HEK293T cells were transiently transfected with BRE-*Vent2*-luc and different plasmids with constitutively active expression constructs encoding CK1 isoforms for 16 h, followed by treatment with compound and 10 ng/mL BMP-4 for 22 h. Bar graphs represent luciferase activity as mean ± SD (*n* = 2), normalized to DMSO vehicle (= 100%).

Since the transcription factor OAZ, which is essential for *Vent2*-expression, is not expressed in C2C12 cells, the CK1-dependence might be demonstrated by ALP activity rescue of CGS-

15943. In addition, upcoming genetic validation by knockdown of CK1 isoforms should provide further insight into CK1-dependent ALP induction. Considering that CGS-15943 exhibited a much lower cytotoxicity, it could also be considered as a novel chemical probe to address CK1-dependent cancer pathologies with a mitigated safety risk than SR-3029.[366,373]

3.3.5.5 Investigation of a dual CK1/PI3K inhibition mechanism

Since SR-3029 did not enhance osteogenic transcript levels in a significant manner, the underlying mechanism of CGS-15943 may differ from that of classical CK1 inhibitors. This was evidenced by its differential efficacy in enhancing BMP signaling outputs and enzymatically by its mixed inhibition profile, which appeared to rely on inhibiting CK1δ and ε isoform in a competitive and noncompetitive manner.

Interestingly, profiling of morphological changes by chemical probes in an unbiased approach, provided further insight into potential cellular targets. Recently, the COMAS established a cell painting assay (CPA) to evaluate bioactivity of compounds relative to annotated references, in order to identify cellular targets and devise target hypotheses.[332] In this assay, cells were treated with compounds, followed by staining of different cell compartments and acquired automated imaging. Using comprehensive image analyses, 579 morphological features are captured, providing a unique fingerprint for each small molecule. Each fingerprint represents a mean induction value indicating overall significant changes of the observed phenotype relative to DMSO vehicle, with a threshold induction of ≥5% reflecting significant morphological changes. By adjusting the concentrations of overactive (induction >75%) or inactive compounds, valid fingerprints can be generated that are comparable to each other. Taking into account the correlation distances between the individual profiles, a biological similarity value (in %) can be calculated, which is empirically considered significant if the value is greater than 75% between compounds.

When analyzing CGS-15943 in the CPA, its low induction value (9%) provided no insight into biosimilar references. In general, low induction indicates morphological changes of only a few features, but does not mean that a compound is inactive. With increasing concentration, the changes of the features in the fingerprint became more dominant without altering the overall signature of the phenotype (Figure 86). The highest biological similarity compared to 50 µM CGS-15943 was exhibited by the reference compounds PIK-93 (10 µM), BYL-719 (10 µM),

and NU6027 (30 µM), which had no structural similarity. Interestingly, PIK-93 exhibited the most similar profile and is a known class I PI3K inhibitor with selectivity for the γ over α isoform (IC_{50} = 16/ 39 nM).[377] BYL-719, also known as Alpelisib, was identified as another PI3K inhibitor that exhibits >50-fold selectivity for p110α relative to other isoforms.[378] The other identified compound, NU6027, is a reported inhibitor of various cyclin dependent kinases such as CDK1 and 2, for which no inhibition by CGS-15943 was observed in the kinome profile and therefore not considered a hypothetical target.[379]

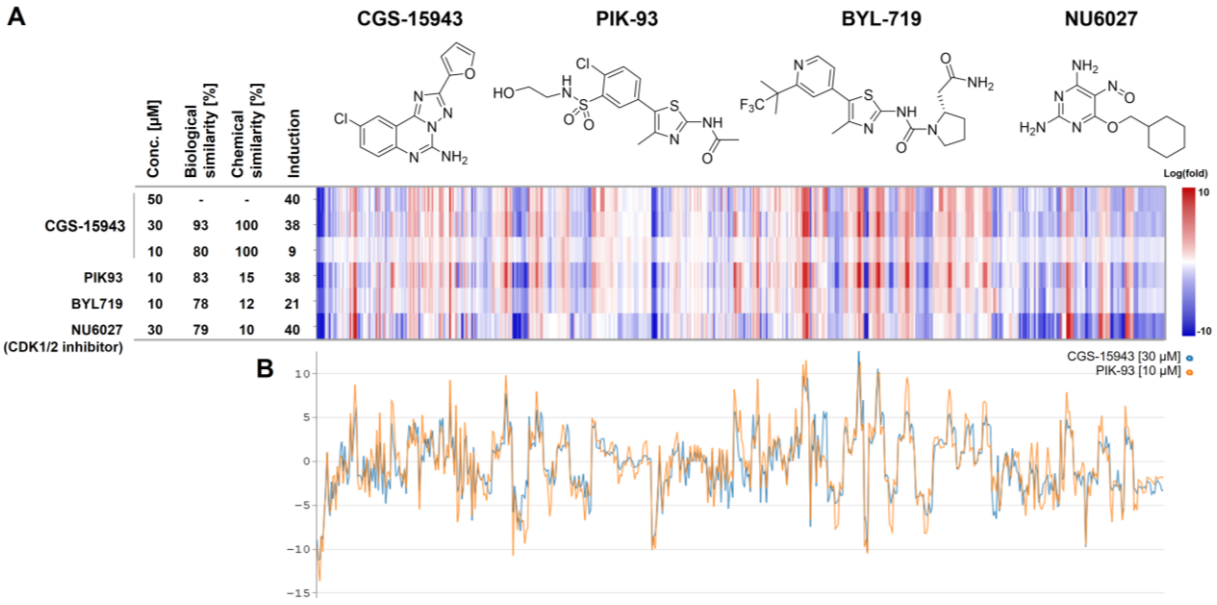

Figure 86: Morphological profiling of CGS-15943 in the Cell Painting Assay reveals high biosimilarity to selective PI3K class I inhibitors. Compounds exhibiting high biological similarity greater than 75% to CGS-15943 (50 µM) were considered significant. Assay and analysis were conducted by the COMAS team. (A) Heatmap visualizes morphological fingerprints consisting of 579 morphological features divided into cellular (1-229), cytoplasmic (230-461) and nucleic (462-579) parameters. Induction represents overall increase (red) and decrease (blue) of features relative to DMSO. (B) Morphological fingerprint of CGS-15943 (30 µM) and PIK-93 (10 µM) visualized as line plot, indicates high biological similarity.

The identification of selective PI3K inhibitors in this unbiased morphological approach provided evidence for a PI3K-mediated cellular response of CGS-15943. In fact, CGS-15943 inhibited p110γ up to 70% at 1 µM and was validated with an IC_{50} of 120 nM with selectivity toward the γ-isoform, consistent with previously reported selectivity.[365] Remarkably, CGS-15943 inhibited VPS34 at 1 µM only very mildly (by 28%) in kinome profiling, highlighting its selectivity over class I PI3Kγ.

Next, it was questioned if specific inhibition of PI3Ks could enhance BMP-dependent ALP induction in C2C12 transdifferentiation. Inhibition of PI3K class I lipid kinases has been shown to benefit osteogenic differentiation by enhancing the cellular response of BMP-2.[102] This was

demonstrated by the non-selective PI3K class I inhibitor LY294002 (IC_{50} = 500-970 nM), which inhibits PI3K$\alpha/\beta/\delta$-mediated Akt/mTOR signaling and enhances ALP activity similar as the mTOR inhibitor rapamycin.[380] However, it was also reported that the observed effects did not depend on BMP-mediated Smad1 phosphorylation, which would be contrary to the effects observed for CGS-15943. Therefore, the VPS34-selective inhibitors VPS34-IN1 and SAR405 as well as the PI3K class I inhibitors PIK-93 and BYL-719 were investigated in greater detail in the two morphogenic BMP assays. As depicted in Figure 87, only the two distinct VPS34 inhibitor chemotypes potently rescued DMH-1-induced cardiogenesis, turned out toxic at higher concentrations and only moderately enhanced ALP-induction in the C2C12 assay. However, the latter effect did not depend on BMP as discussed earlier (see Figure 45, chapter 3.2.1.2). In fact, VPS34 Inhibitor treatment eventually induced distinct phenotypes and a highly apoptotic cell population of C2C12 (data not shown).

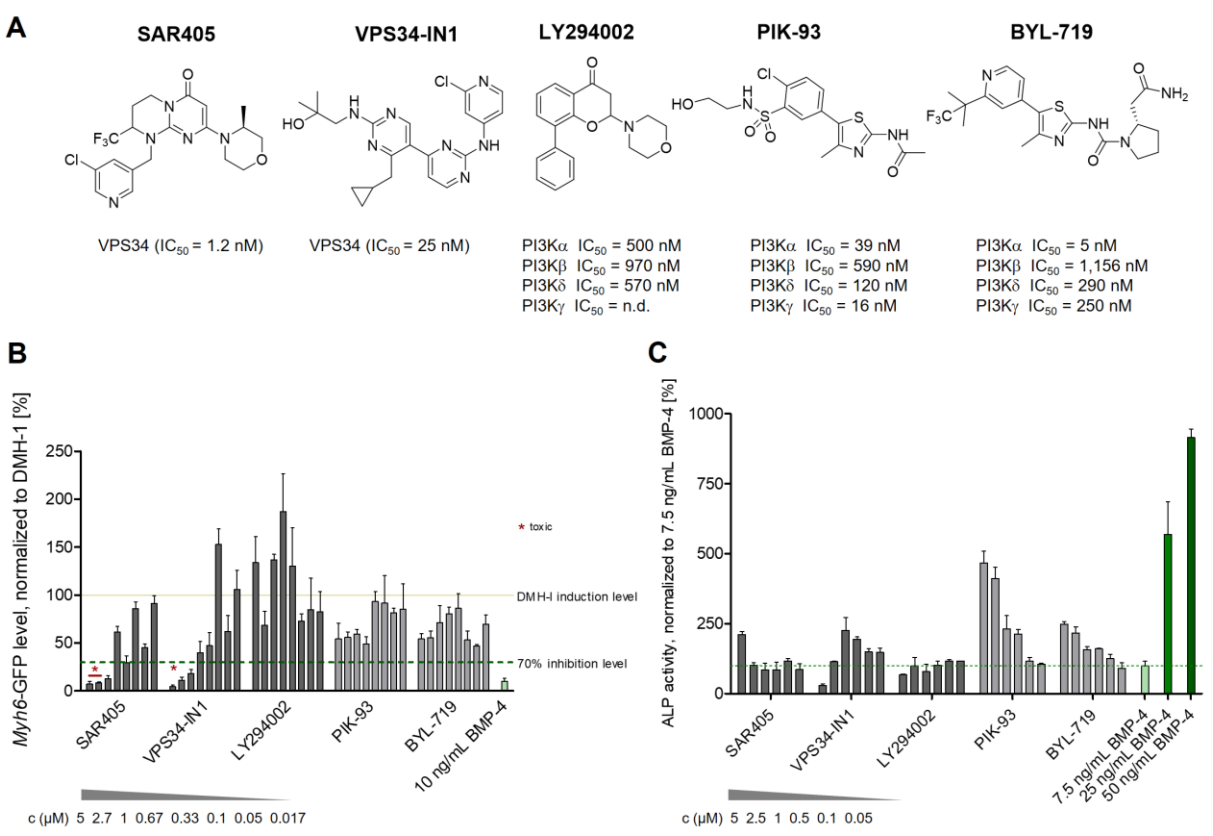

Figure 87: Selective class I PI3K inhibitors exhibit predominant ALP induction relative to class III inhibitors. (A) Chemical structures of selective compounds for PI3K subclasses and isoforms and their reported IC_{50}'s.[326,327,377,380,381] (B) Dose-response antagonism in cardiac differentiation induced by the selective BMP inhibitor DMH-1 (0.5 μM). The bar graph is representative of the mean of triplicates and the respective SEM of two independent experiments. *Myh6*-GFP level were normalized to DMH-1 with vehicle (DMSO). (C) Potent VPS34 inhibitors moderately enhanced ALP induction, while p110γ-selective PIK-93 enhanced BMP response with high potency. The compounds were incubated along with 7.5 ng/mL BMP-4 in C2C12 and treated for 72 h. ALP activities were normalized to DMSO and bars are represented as mean ± SD for $n \geq 2$ experiments.

The non-selective inhibitor LY294002 was inactive in both differentiation assays, indicating an Akt/mTOR-independent mechanism of BMP amplification and contradicting to the reported enhancement of ALP induction. In particular, it lacks potency (>20-fold less active) compared to PIK-93, especially towards the γ-isoform, and selectivity among class I PI3Ks.[380] Interestingly, the γ- and α-selective PI3K inhibitors PIK-93 and BYL-719 induced ALP activity in a dose-dependent fashion, whereas PIK-93 enhanced synergistic activity up to 5-fold compared to the basal BMP level. Despite enhancing ALP activity, no efficient dose-response was observed in cardiogenesis (Figure 87B), with similar antagonism detected with a residual Myh6-signal of 54%, clarifying the distinct response of the different lipid kinases during differentiation. Thus, it appears that inhibition of specific class I PI3K isoforms is insufficient to recapitulate the activation of BMP signaling in mESCs.

Since PIK-93 showed greater similarity to CGS-15943 in the CPA as well as in the C2C12 osteogenic differentiation assays, it was selected for further characterization. Interestingly, CGS-15943 was also more selective for the γ-isoform, unlike BYL-719 that reportedly inhibits α- and γ-isoforms about equally potent. In this regard, selective inhibition of PI3K class I α has been shown to impair osteoblastic function and homeostasis, thus preventing heterotopic ossification, suggesting an opposite mechanism to the hypothesized p110γ-mediated BMP signal amplification and highlighting the cellular specificity of distinct PI3K isoforms.[264,382]

Because osteogenic ALP induction of PI3K class III inhibitors has been de-validated previously (see Figure 45), a similar osteogenic transcript profile was examined in presence of 5 µM PIK-93 and 7.5 ng/mL BMP-4 to evaluate BMP-dependent ALP activity of p110γ inhibition. As shown in Figure 88, PIK-93 significantly enhanced BMP-mediated gene expression of *Runx2*, *Osteocalcin*, and *Osx*, while no significance was confirmed for *Alp* mRNA. This effect was possibly due to the high biological variability of the BMP-4-induced response for these generated samples. However, the pronounced enhancement of ALP activity was significant and has been validated before (Figure 87). With respect to CGS-15943, enhanced expression of the osteogenic drivers *Runx2* and *Osx* was induced at very similar levels (2- and 6-fold induction) compared with low-dose BMP-4. The induction of the late-stage marker of osteoblastogenesis, *Col1a1*, was not observed, but was similarly inactive to CGS-15943 treatment. This osteogenic gene expression profile during C2C12 differentiation suggests that PI3K p110γ is a BMP-dependent target in this context.

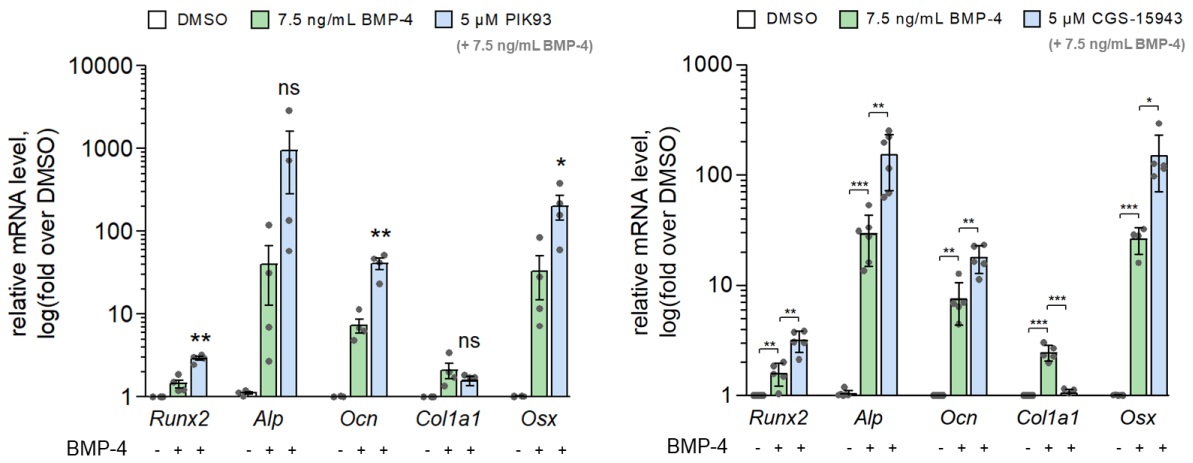

Figure 88: Relative quantification of BMP-dependent osteogenic gene expression transcripts confirmed enhanced osteogenesis by PIK-93. C2C12 cells were treated with DMSO and/or BMP-4 (7.5 ng/mL) in the presence or absence of compound (5 µM) for 72 h. Data is shown as mean ± SEM ($n \geq 4$) and normalized to DMSO (=1). Statistical analysis was performed with an unpaired two-tailed t-test (* p <0.05; ** p <0.01; *** p <0.001).

Since selective chemical probes for CK1δ/ε and PI3K-p110γ were able to stimulate BMP-dependent ALP induction, a possible mechanistic synergism was postulated to account for the unique efficacy of CGS-15943. To investigate a potential synergistic capacity of dual CK1δε/p110γ inhibition, combinations of the well-characterized inhibitors were assessed. Combinatorial 2D-screening of a large dose-range was deemed most suitable for this purpose. As shown in Figure 89, with potent ALP induction depicted in deep green, no additive effect was observed for PIK-93 and SR-3029 at higher concentrations of PIK-93 (a), while mild synergism occurred at 20-50 nM SR-3029 and 1-2 µM PIK-93, indicating a “synergistic dose-response corridor”. Further, a modest shift in synergistic activity was visible toward low nM-levels of the CK1-inhibitor, indicating positive contribution of CK1δ/ε and p110γ inhibition.

Treatment of CGS-15943 with the selective p110γ inhibitor PIK-93 and CK1δ/ε-selective SR-3029 resulting in insufficient enhancement of CGS-15943-mediated ALP induction would indicate saturation of the respective kinase targeted by CGS-15943. As shown for b) and c), synergistic treatment of CGS-15943 with PIK-93 and SR-3029 did not contribute to enhanced ALP formation at higher concentrations, suggesting saturation of the respective p110γ and CK1δ/ε targets by CGS-15943. At lower concentrations of CGS-15943 below 50 nM, a mild synergism is observed, which may indicate incomplete saturation of the kinases that is captured by the respective inhibitor.

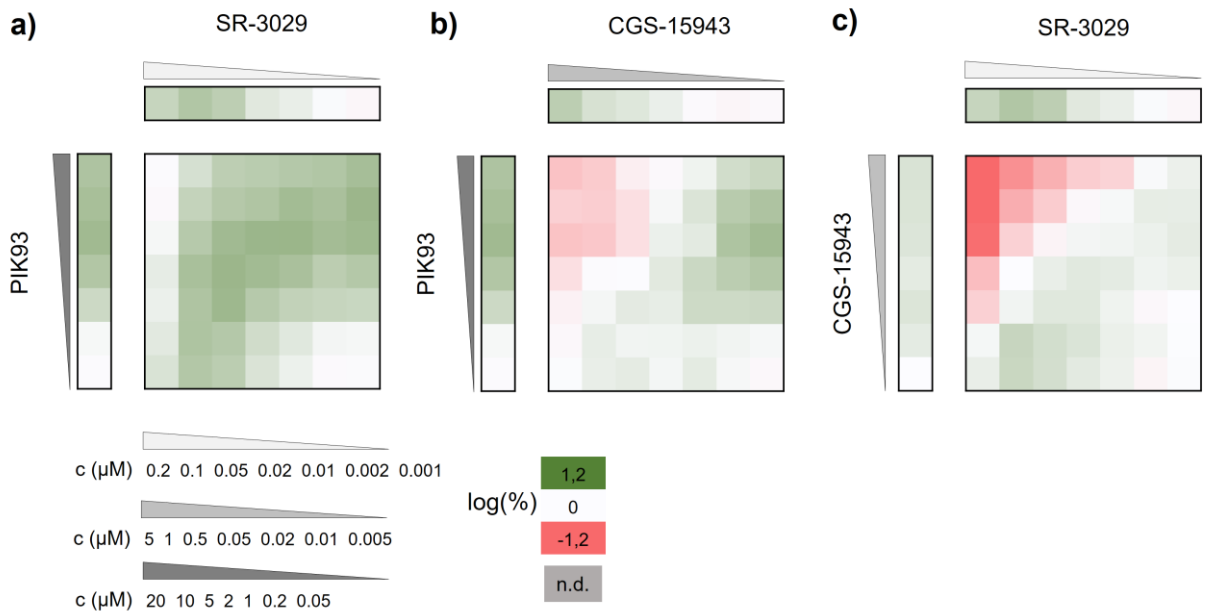

Figure 89: Analysis of CK1 and p110γ inhibition by combination treatment in the C2C12 osteogenesis assay. ALP induction was detected after 72 h of treatment with compounds in presence of 7.5 ng/mL BMP-4. Total DMSO vehicle concentration was set to 0.4% for each condition. ALP activities were normalized to 7.5 ng/mL BMP-4 and log(% induction) was calculated and visualized, representing induction and/or synergism with green squares.

These data suggest the titratability of CK1δ/ε and p110γ inhibition (a vs. b/c) to generate an optimal osteogenic profile, which is no longer possible when attempting to titrate CGS-15943 with either inhibitor. Both combinatorial screens showed a reduction or inhibition in ALP activity at high concentrations that could be caused by oversaturation of these regulatory kinases in the long-term and cause cellular stress or be counterproductive in terms of BMP-enhanced signaling.

Taken together, the 2D-Screen further supports a synergistic mode-of-action via combined CK1δε/-PI3Kγ inhibition. At this point, however, the presented pharmacological approach reaches its limits and additional functional genomics and biochemical experiments will have to shed light on the underlying mechanistic consequences for BMP-driven osteoblastogenesis.

3.3.5.6 Proposed mechanism of action

In this work, CK1δ/ε was identified and further validated as a novel target for CGS-15943 by kinome screening. Furthermore, utilizing the newly established COMAS morphological cell painting assay, a correlation of phenotypic PI3Kγ inhibition with CGS-15943 was observed. In subsequent studies, a BMP inducing activity was observed when these specific isoforms were

inhibited, whereas global CK1 and PI3K class I inhibition was counterproductive. These observations suggest a successful recapitulation of CGS-15943's capacity to induce BMP signaling via CK1δε/PI3Kγ-dependent downregulation. Furthermore, CGS-15943 exhibits a unique selectivity profile CK1, particularly affecting CK1δ and ε-isoforms in a competitive (δ and ε) and non-competitive (δ) manner, with very low activity on CK1α. It also shows an interesting selective profile to the γ-isoform of class I PI3Ks. Together, this profile contributes to the hypothesis of a novel dual mode-of-action on selective targeting of CK1 and PI3K isoforms, as particularly shown in C2C12 osteogenesis.

Global silencing of PI3K/mTOR signaling has been shown to attenuate nuclear translocation and accumulation of Smads.[101] PI3K/Akt signaling is part of the non-canonical BMP signaling pathways and is well-recognized to support osteoblastogenesis, in part by regulating low basal levels of Smad1 via a PI3Kα/β-GSK3-Smad axis.[382] In particular, p110α/β-deletion resulted in increased GSK3 and reduced Smad1 levels, leading to reduced bone formation. This is consistent with the demonstrated selective p110α inhibition by BYL-719 that leads in impaired BMP signaling and thus indicated useful pharmacology for the treatment of heterotopic ossification.[264] These findings show isoform specificity of PI3K class I with specific roles for distinct signaling outputs in BMP signaling and osteogenic differentiation or homeostasis. Selective inhibition of p110γ might have another specific role in osteogenic regulation that would explain the observed activity of CGS-15943 and PIK-93 in C2C12. However, the selective modulation of PI3K isoforms on Smad activity requires further investigation. In fact, Smads are tightly regulated, even after their activation by phosphorylation at multiple sites in the linker region by regulatory kinases such as GSK3.[62] However, as shown in this thesis, selective inhibition of GSK3 does not result in specific induction of osteogenic BMP signaling in C2C12. Here, selective inhibition of specific isoform appears to promote the cellular BMP response, whereas global inhibition of PI3K/mTOR signaling was less pronounced. This suggests an indirect regulatory mechanism of p110γ resulting in enhanced BMP signaling, e.g., by downregulation of a negative feedback loop of BMP. Interestingly, CGS-15943 has been shown to sensitize the cellular response when treated prior BMP input, supporting this hypothesis. In addition, inhibition of PI3K isoforms in C2C12 myoblasts has been shown to block myogenic differentiation, which in turn supports BMP-driven osteogenic commitment.[102]

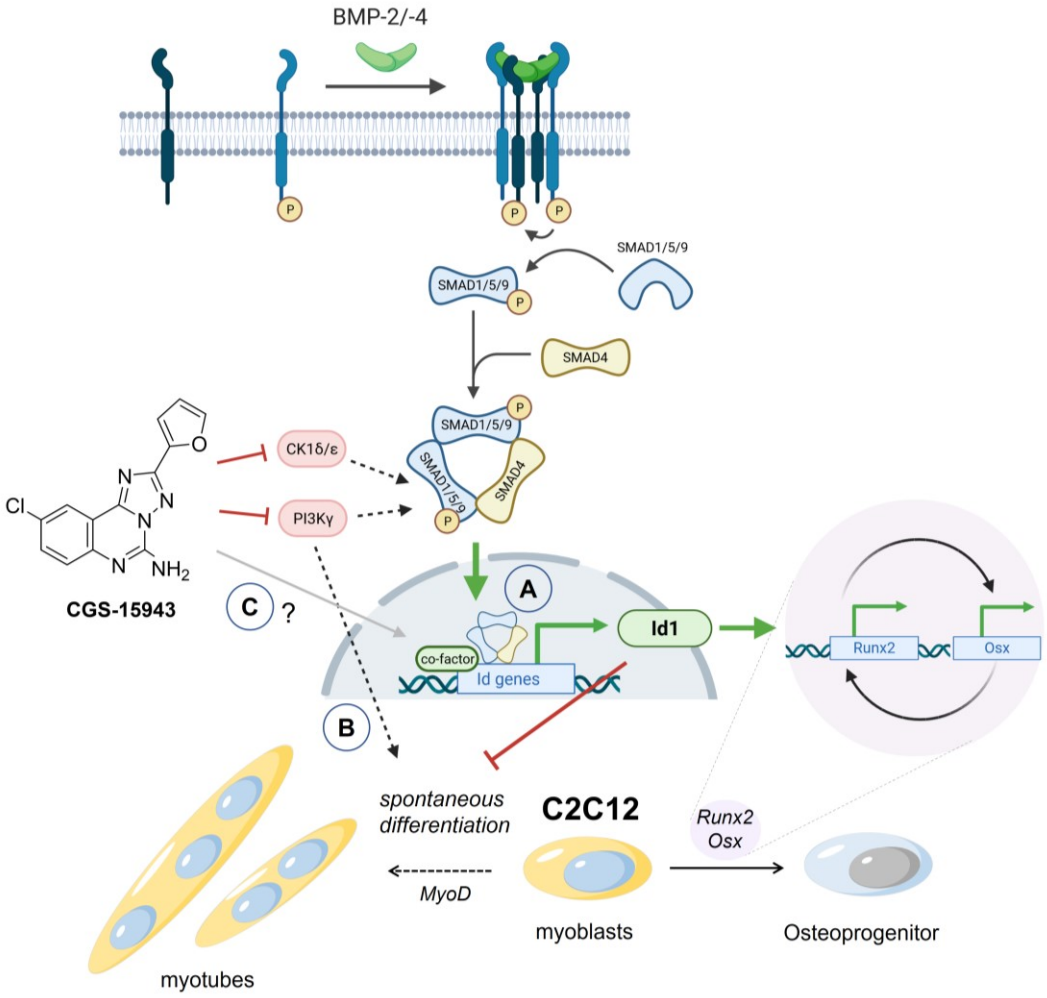

Figure 90: Proposed mechanism of action of CGS-15943 in potentiating BMP signaling via dual inhibition of selective kinase isoforms CK1δ/ε and PI3Kγ. CK1δ/ε and PI3Kγ may regulate Smad signaling directly via phosphorylation or via crosstalk regulation. Selective inhibition leads to enhanced nuclear translocation and sustained or stabilized nuclear Smad signaling (A). Enhanced BMP-Smad target gene expression of Id1 promotes upregulation of Runx2 and subsequently osteogenic target gene expression. Further Id1 inhibits myogenic capacity of C2C12. Specifically, in C2C12, inhibition of PI3K class I blocks myogenesis, maintains cellular plasticity, and thus sensitizes osteogenic differentiation at low BMP input (B). Moreover, the underlying mechanism of selectively increased target gene expression depend on CK1δ/ε inhibition, that may depend on specific transcription factor regulation or repression (C). Dashed arrows indicate attenuated activity.

Moreover, induction of expression of the BMP target gene *Id1* is essential for cellular osteogenic differentiation and leads to transient induction of the major osteogenic master regulator Runx2, which in turn promotes expression of *Osterix*. Stable Id1 levels support osteogenesis by additionally suppressing myogenesis by directly affecting the transcriptional activity of the myogenic driver MyoD.[353] This could explain the observed activity of CGS-15943, since it induced and sustained *Id1* expression levels within 24 h upon BMP administration, thereby promoting short-term inhibition of myogenesis and long-term induction of osteoblastic commitment.[383]

Regarding the observed activity in mESC cells, CK1-dependent activity may be more essential for mimicking BMP activation and *Id1* expression, as PI3Kγ modulation did not express similar activity but may be beneficial in the hypothesized dual CK1δε/-PI3Kγ inhibition of CGS-15943. Both kinases may be directly involved in regulating activated Smads by controlling its phosphorylation, as pretreatment with CGS-15943 enhanced BMP sensitivity, as shown by Smad levels. To date, no clear regulation of Smad signaling by CK1 isoforms has been reported. This would suggest novel functions of CK1 on BMP-Smad biology, albeit there is evidence that the CK1ε isoform may interact directly with various Smads and act as a ligand-dependent regulator.[384] Due to the crucial involvement of CK1 isoforms in Wnt signaling, various crosstalks with BMP signaling have been discussed, such as GSK3 inhibition and Wnt-mediated amplification of BMP signaling.[128] Given the distinct properties of CK1 isoforms in Wnt signaling, contrary effects with respect to Wnt inhibition are mediated by CK1δ/ε-selective inhibitors such as SR-3029. Moreover, since CK1 isoforms are found only in the cytoplasm, they do not mediate direct nuclear regulation of transcription factors, but upstream regulation of such factors cannot be excluded. However, further extensive studies should be considered to substantiate this dual mode of action to gain new insights into the underlying mechanism of the regulatory function of CK1 isoforms on BMP-Smads on the proposed CK1-dependent BMP enhancement.

3.3.5.7 Miscellaneous target hypotheses

To assess and (de)validate the BMP dependence of the most important reported and identified off-targets of CGS-15943, modulators of ADORA signaling, DNA-PK and AhR were subsequently tested in the BMP assays.

CGS-15943 was first discovered and developed as a potent non-selective adenosine receptor antagonist with low nanomolar activity against all four receptor types.[341,342] Therefore, an obvious and necessary step to delineate a plausible mechanism of action for CGS-15943 as a new BMP potentiator was to assess a broad range of adenosine signaling modulators for this activity. The selection consisted of 45 compounds, including receptor agonists, antagonists, and modulators of adenosine metabolism to investigate a possible adenosine-dependent response in BMP signaling during osteogenic differentiation of C2C12 cells, mESC mesoderm patterning as well as the BRE-*Vent2*-luc reporter assay. As shown in Figure 91,

none of the 45 modulators exhibited a similar BMP response to CGS-15943 (1), whose BMP-dependent enhancing effect is shown in blue. Interestingly, the xanthine caffeine (3), which has been frequently compared with the pharmacological profile of CGS-15943, was inactive in all three assays.

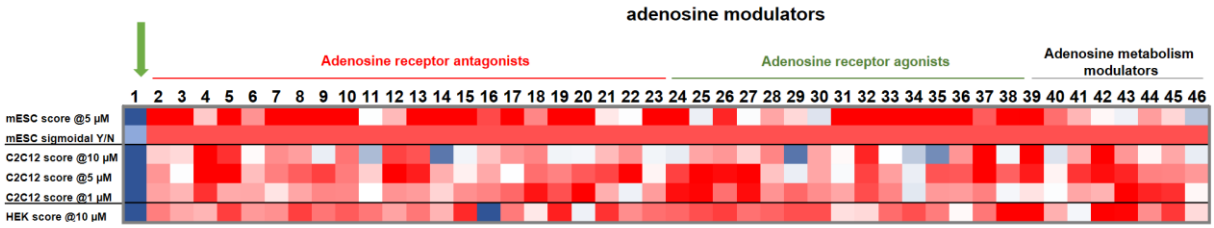

Index	Supplier_ID / Enso name	trivial name
1	C199	CGS-15943
2	A-242	Alloxazine, Isoalloxazine
3	Prestw-1256	Caffeine
4	Prestw-820	Aminophylline ethylenediamine, Theophylline ethylenediamine
5	Prestw-874	Theobromine
6	MRS 1754	"MRS 1754"
7	A-013	8-(p-Sulfophenyl)theophylline
8	A-022	1,3-Dipropyl-8-(p-sulfophenyl)xanthine
9	A-145	1-Allyl-3,7-dimethyl-8-p-sulfophenylxanthine
10	A1755	Aminophylline ethylenediamine, Theophylline ethylenediamine
11	0439, C-101	"DPCPX, PD 116,948"
12	C-102, C102	"8-Cyclopentyltheophylline, CPT"
13	3306, C-197	"8-(3-Chlorostyryl)caffeine, CSC"
14	D-108	1,3-Dipropyl-7-methylxanthine
15	D-134, D134	"DMPX, 3,7-Dimethyl-1-", (2-propynyl)xanthine
16	F7927	FSCPX
17	M1809	"MRS 1523"
18	P2278	8-Phenyltheophylline
19	P5679	3-n-Propylxanthine, Enprofylline
20	P9689	Propentofylline, HWA 285
21	T1633	Theophylline
22	2010	"PSB-10 hydrochloride"
23	1036, S8105	"ZM 241385"
24	H3288	HEMADO
25	G5794	GR 79236X
26	A-202	APNEA
27	A-236	AB-MECA
28	C-141	CGS-21680 hydrochloride
29	C-277	Chloro-IB-MECA
30	C5134	2-CADO
31	C8031	N6-Cyclopentyladenosine, CPA
32	C9901	CHA
33	I-146	IB-MECA
34	M-225	Metrifudil
35	P-101	2-Phenylaminoadenosine, CV-1808
36	P-108	N6-Phenyladenosine
37	1104	2-Cl-IB-MECA
38	4472	"BAY 60-6583"
39	Prestw-236	Dilazep dihydrochloride
40	A7987	5'-Amino-5'-deoxyadenosine p-toluenesulfonate salt
41	861669	S-(4-Nitrobenzyl)-6-thioguanosine
42	D5294	Dilazep hydrochloride, Cormelian
43	D5385	Paraxanthine
44	M5501	N6-Methyladenosine
45	N2255	S-(4-Nitrobenzyl)-6-thioinosine, NBTI
46	A8626	"Adenine, Vitamin B4"

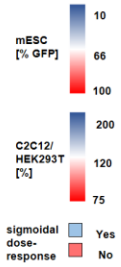

Figure 91: Adenosine (receptor) modulators do not share BMP amplifying activity of the triazolo[1,5-*c*]quinazoline CGS-15943. BMP-dependent response in differentiation assays (mESC and C2C12) and response on *Vent2*-expression of a selection of adenosine receptor and metabolic modulators from the COMAS library revealed no systematic correlation between BMP response of CGS-15943 (1) and adenosine modulation. Heatmap illustrates activity as mean values of $n \geq 2$ independent experiments. BMP-dependent activity is indicated in blue.

Generally, agonistic chemical probes were moderately active at best. Remarkably, the known Toll-like receptor agonist Imiquimod, whose imidazoquinoline-based scaffold is closely related

to CGS-15943, also inhibits Sonic hedgehog signaling through ADORA-mediated GLI-phosphorylation and suppression of target gene expression, revealing a novel poly-pharmacological profile.[385] In contrast to CGS-15943, it acts as an adenosine receptor agonist but was entirely inactive in all BMP-dependent assays (data not shown), hence a similar mechanism is also unlikely. Several known receptor modulators had already been screened in the initial LOPAC screen with only CGS-15943 identified as a hit. Since no comparable pharmacological profile to CGS-15943 was observed, ADORA-signaling was considered as a BMP-irrelevant off-target.

The atypical DNA-dependent protein kinase (DNA-PK) has been identified as a kinase target for CGS-15943. It is critically involved in regulation of cellular homeostasis and DNA repair by recognizing and repairing double-strand DNA breaks, and thus, ensures genomic stability.[386] Inhibition of DNA-PK has been shown to be beneficial in combination with radiation and chemotherapy to enhance drug response by interrupting DNA damage repair mechanisms. However, it is generally challenging to discriminate between selective DNA-PK and PI3K inhibition due to the close structural similarity of these kinases.[387] Recently, the very potent DNA-PK inhibitor AZD7648 has been reported to have superior selectivity and an improved pharmacokinetic properties with a good safety profile and potential for combinatorial drug therapies.[388] Interestingly, although it showed strong biochemical inhibition of PI3K type I isoform fragments (e.g., IC_{50} of p110γ = 50 nM), it lacked cellular activity against PI3Ks, while retaining high efficiency against DNA-PK.[388] Notably, a 100-fold selectivity against 396 other kinases was described for AZD7648.[389] Considering the lack of selectivity among all currently available DNA-PK inhibitors, AZD7648 also represents a valid tool compound for assessing putative DNA-PK-dependent effects on BMP signaling in our differentiation assays. As shown in Figure 92, AZD7648 showed a very weak rescue of DMH-1 during mESC mesoderm patterning at concentrations ≥ 1 µM. This finding points at a DNA-PK-independent response, given that the biochemically determined potency of AZD7648 on DNA-PK is 350-fold higher than the one calculated for CGS-15943. Consistent with this data, AZD7648 also did not induce ALP activity during osteogenic C2C12 differentiation at concentrations up to 5 µM and no enhancement of osteogenic transcript levels was observed (see Appendix, Figure 99). Since the cellular activity of AZD7648 on p110γ has been confirmed by Fok et al. with a reported, high IC_{50} of 1.37 µM, an amplifying effect on ALP and osteogenesis may be observed at much higher concentrations.[388]

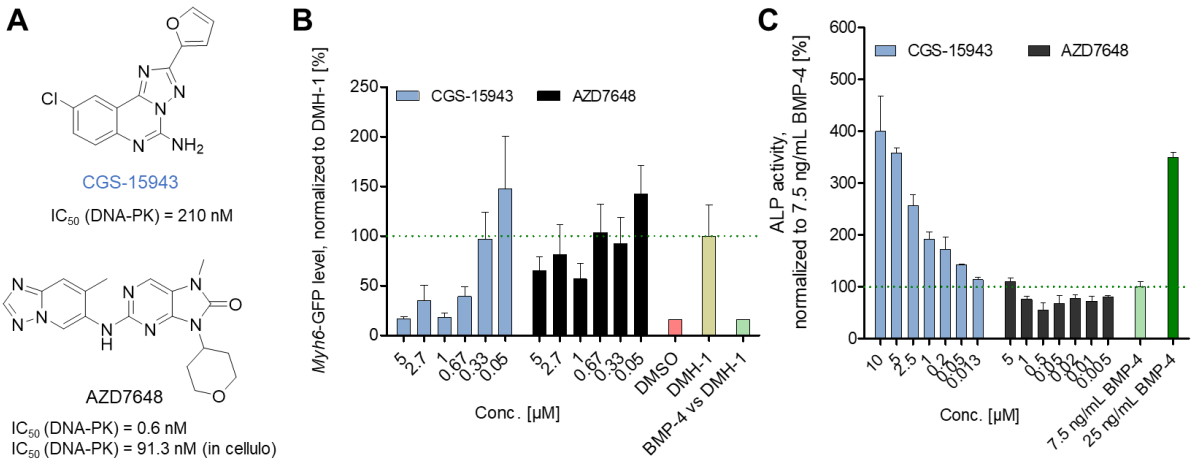

Figure 92: Evaluation of DNA-PK-dependent BMP induction indicates no correlation with BMP signal activation. (A) Chemical structure of AZD7648 and its reported IC_{50}-values on DNA-PK *in vitro* and *in cellulo*. (B) Dose-response antagonism of CGS-15943 and AZD7648 in cardiac differentiation induced by selective BMP inhibitor DMH-1 (0.5 µM). Bar graph is representative for the mean of triplicates and the respective SEM for n ≥ 3. *Myh6*-GFP level were normalized to DMH-1 with vehicle (DMSO). (C) Osteogenic induction of ALP by CGS-15943 and AZD7648. Compounds were incubated along with 7.5 ng/mL BMP-4 in C2C12 and treated for 72 h. ALP activities were normalized to BMP-4/DMSO and bars are represented as mean ± SD for *n* ≥ 3.[388,389]

Albeit the distinction between selective targeting of DNA-PK and lipid kinases is challenging, assessment of the selective inhibitor AZD7648 did not result in significant BMP-dependent activation in either morphological assay. Moreover, due to the endogenous activity and specific role of DNA-PK, it is unlikely to be involved in the observed specificity with respect to BMP signaling and collectively considered as an off-target. In view of the high selectivity of CGS-15943 versus CK1δ/ε, p110γ and DNA-PK on the kinome, it should be noted that it is generally difficult to distinguish between PI3K and DNA-PK selective inhibitors. This is why commonly used reference compounds, such as PIK-93, despite being reported as selective, also show high potency toward DNA-PK.

Furthermore, during the course of this thesis, a new report and patent was published describing the aryl hydrocarbon receptor (AhR) as a putative target of CGS-15943. The AhR is a ligand-activated transcription factor that translocates to the nucleus inducing expression of target genes involved in cellular proliferation.[390] It also mediates the toxicity of compounds such as 2,3,7,8-Tetrachlorodibenzo-p-dioxin (TCDD). Its modulation has implications for anti-cancer therapy. By binding to and activating AhR, CGS-15943 has been shown to induce apoptosis of breast and liver cancer cells via upregulation of the Fas-ligand.[391] Jana FLEGEL (WALDMANN group, MPI Dortmund) established an AhR-reporter gene assay and characterized CGS-15943 to confirm its activity on *XRE*-reporter in comparison to its BMP-inactive derivative 29 and the

highly potent known AhR inducer FICZ. As depicted in Figure 93A, FICZ induced *XRE* expression with high potency and efficacy up to nearly 100-fold. As expected, CSG-15943 also showed up to 62-fold induction, reaching a maximum at 10 µM. The BMP-inactive analog 29 was less active as CGS-15943, but still able to drive AhR-dependent transcription (31-fold). These profiles suggest an AhR-independent correlation to BMP signaling.

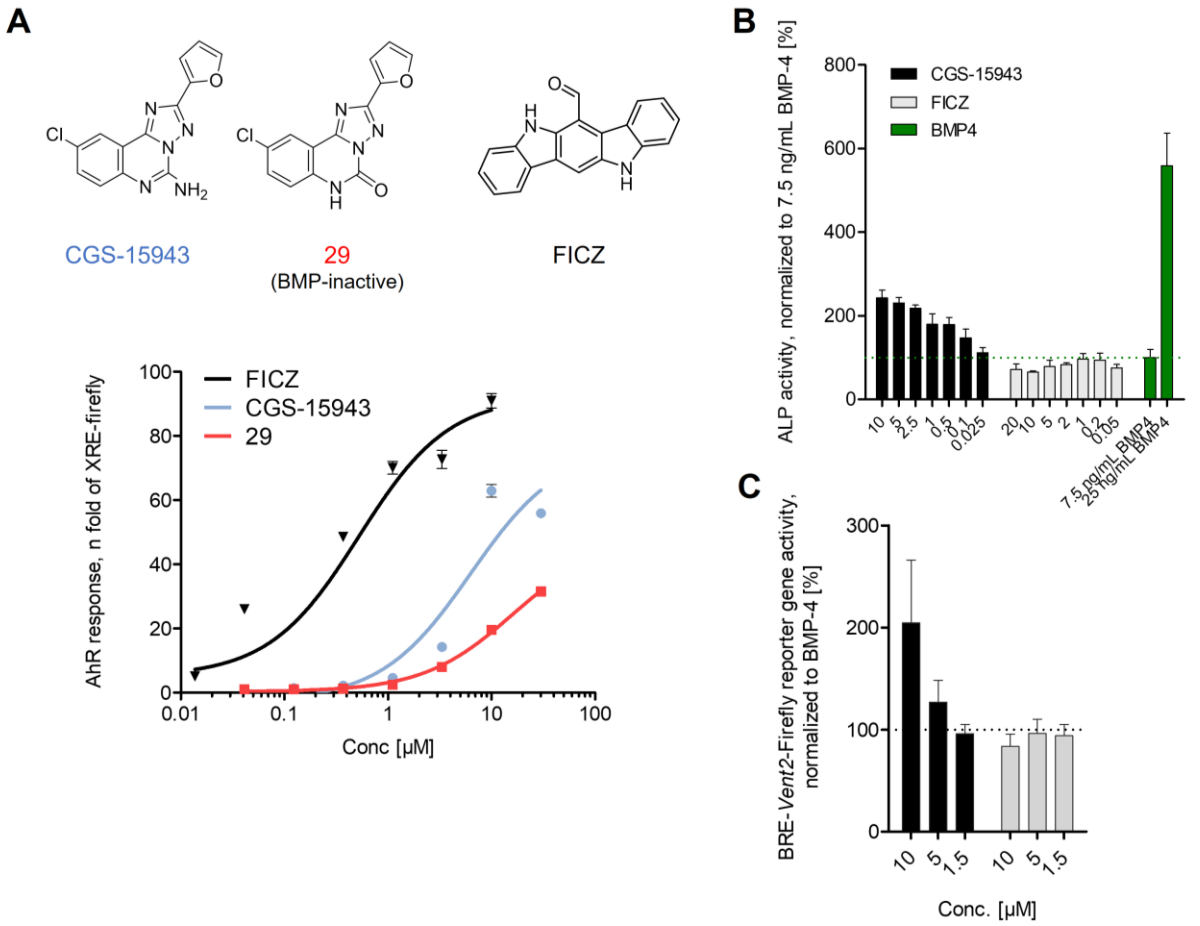

Figure 93: Assessment of CGS-15943 on AhR-dependent *XRE* expression and characterization of FICZ on ALP and *Vent2* induction suggests a AhR-independent BMP-enhanced response. (A) HepG2 cells were transfected with AhR responsive reporter plasmid transcribing *XRE*-luciferase and a *Renilla* control plasmid for 24 h, followed by compound treatment for 24 h. Luciferase activity was normalized to DMSO vehicle. Data is shown as mean ± SD of *n* = 3 experiments. (B) Dose-response relationship on ALP activity during BMP-induced osteogenesis in C2C12. Compounds were incubated along with 7.5 ng/mL BMP 4 in C2C12 and treated for 72 h. ALP activities were normalized to DMSO and bars are shown as mean ± SD for *n* = 3. (C) Dose-dependent profiles on BRE-*Vent2*-luc reporter in HEK293T cells. Cells were transiently transfected and treated with compounds and BMP-4 (10 ng/mL) for 22 h. Luciferase activity was normalized to DMSO and data is shown as mean ± SD of *n* = 2 experiments relative to DMSO (= 100%).

These findings were further supported when FICZ was assessed in the C2C12 osteogenic differentiation assay. No stimulation of BMP-dependent ALP activity was detected, as shown in Figure 93B in direct comparison with CGS-15943 and 29. In addition, FICZ was also inactive on the BRE-*Vent2*-luc reporter, providing compelling evidence of an AhR-independent

enhancement of BMP signaling by CGS-15943. Moreover, the published patent disclosed extensive SAR studies for CGS-15943 in which the amino group at the 5-position, essential for BMP/CK1 activity, was not required for AhR activation.[392] Efforts were made to increase the selectivity to AhR by replacing this critical function, thus reporting a very different SAR compared to the herein described SAR of BMP amplification. In addition, one of the most potent activators, TCDD, was shown to effectively inhibit osteogenic differentiation of human mesenchymal cells by interfering with BMP-2/TGF-β1/SMAD signaling, revealing an antagonistic response in BMP-dependent differentiation.[393]

Collectively, the inability of FICZ to enhance BMP-dependent differentiation and gene expression and the distinct structure-activity-relationships for AhR- and BMP-activity exclude AhR as a viable BMP-relevant target. The herein newly identified targets of CGS-15943 that explain its unparalleled BMP potentiating activity are CK1δ/ε and PI3K p110y. Yet, future studies should take AhR interference into account, and structural optimization to eliminate AhR activity might be considered, as AhR may affect cellular viability through apoptosis and potentially represents a counterproductive target as reported for the TCDD-mediated inhibition of osteogenesis.[393]

3.3.6 Summary and Outlook

In the initial screen of the mESC-based prototype BMP-mimetic differentiation assay developed by Jonas HALVER, the LOPAC/Prestwick libraries were tested for the identification of known bioactive compounds. Among 11 other hits, the adenosine receptor antagonist CGS-15943 was identified as the only hit that could be validated for its BMP-dependent reporter activity.[290,291] Moreover, the identified small molecule was the only one that showed selective activation of the BMP reporter compared within the TGFβ superfamily, showing a superior profile among all tested and profiled compounds and references. Furthermore, in direct comparison to the profiled BMP activators Ventromorphin, Isoliquiritigenin and PD407824, the BMP response of CGS-15943 exceeded the profile of a superior BMP activator in all BMP assays. However, CGS-15943 was not consistently able to induce BMP signaling in the absence of ligand, and thus CGS-15943 can be classified primarily as a BMP enhancer and a purely agonistic function could be excluded.

Furthermore, osteogenic effect was confirmed by upregulation of specific osteogenic drivers by CGS-15943 and functional validation was performed in a mineralization assay, highlighting its potential to enhance osteogenesis in a human-derived system. In addition to osteogenic validation, the ability of CGS-15943 to recapitulate BMP signaling in embryogenic development was demonstrated using *in vivo* zebrafish ventralization.

Next, to evaluate the structural dependence on BMP signaling, a structure-activity-relationship study was conducted with 39 newly synthesized derivatives by Stefan Lohmann, which revealed a narrow SAR with only one compound leading to significantly increased potency but providing important structural insights for upcoming optimization. Due to the very steep SAR, the incorporation of functional substituents for target identification approaches was not possible, and thus they were to date not considered for synthesis.

A combination of gene expression analyses and assessment of BMP/TGFβ-Smad regulation was used to decipher the quality, quantity, and dynamics of BMP signaling outputs. Here, studies on the dynamics of mediated activation during osteogenic differentiation using Smad quantification and gene expression analysis demonstrate nucleic Smad-dependent enhancement of signaling outputs by CGS-15943, leading to sustained and robust osteogenic differentiation. In addition, preincubation enhanced BMP signaling, strongly suggesting an attenuated negative regulatory mechanism.

These efforts were complemented by kinome and cell imaging profiling and several hypothesis-driven approaches to explain the BMP-potentiating mode of action of CGS-15943. To identify novel targets and since kinase-dependent regulatory crosstalks are common, CGS-15943 was profiled on the entire kinome. It was shown to be highly selective for targeting CK1α1/δ/ε, p110γ and DNA-PK and exhibited low nanomolar potency, the latter of which was de-validated by the highly selective and potent DNA-PK inhibitor AZD7648 that was published by AstraZeneca in 2019.[388] Given that CGS-15943 showed interesting selectivity among CK1 kinases, further biochemical validation against full-length kinases was performed by the group of Prof. KNIPPSCHILD, which revealed high selectivity against CK1δ/ε isoforms. Kinetic studies versus ATP revealed competitive inhibition of CK1ε and a mixed inhibition mode against the δ-isoform, revealing potential allosteric and competitive inhibition. In collaboration with Prof. BAUMANN, a crystal structure of CGS-15943 and CK1δ isoform was generated, confirming binding to the ATP-binding pocket with specific binding of the triazoloquinazoline to the hinge

region at the adenosine binding site and coordination into the hydrophobic pocket, without binding to the catalytic core. The binding mode and rigidity of the scaffold revealed its limited potential for further optimization, which strongly correlated with the observed BMP-dependent SAR of CGS-15943. Biological characterization of the closely related CK1δ/ε inhibitor SR-3029 revealed a correlation of CK1δ/ε-specific inhibition in the mESC assay and activity on the *Vent2* promoter and exhibited moderate potential for enhancing synergistic ALP activity. With this indication, overexpression of each CK1 isoform was performed and successful rescue of the observed reporter activation by CGS-15943 via CK1δ/ε was achieved, demonstrating a dependence of BMP-enhanced activity on specific CK1 modulation. To further substantiate this observation for C2C12, genetic validation via knockdown of specific CK1 isoforms should next be performed. This could be addressed by robust genomic knockdown via lentiviral transfection of RNA-interfering small hairpin RNAs specific for certain CK1 isoforms, which could ultimately be used to investigate the putative CK1-dependent regulatory mechanism for Smad signaling.

Furthermore, an unbiased morphological cell painting assay established and performed by the COMAS, revealed high biological similarity of CGS-15943 with selective and potent PI3Kα and γ inhibitors, the latter of which was a validated target for CGS-15943.[365] Biological characterization and combinatorial screening of characterized selective inhibitors of CK1 and PI3K isoforms to evaluate synergism of CK1- and PI3K-mediated amplification of BMP signaling outputs, showed an additive behavior on BMP-dependent ALP activity. These data provided insights into a dual mode-of-action of CGS-15943 in osteogenesis via its selective and unique kinase profile on CK1δ/ε and p110γ.

Further studies to assess selectivity and raise evidence for a p110γ-dependent BMP response, a set of chemical probes consist of kinase inhibitors with selectivity towards each p110 isoform, such as Alpelisib (PI3Kα), TGX-221 (p110β), AS-252424 (p110γ), Idelalisib (p110δ) should be tested and evaluated for BMP signaling outputs. Subsequent siRNA-mediated knockdown studies in combination with the selective compounds targeting distinct PI3K isoforms can be performed.[387]

Overall, although CGS-15943 has already been shown to target ADORA, AhR and PI3K, the additional targets CK1 and DNA-PK were identified by kinase activity in this thesis, revealing a polypharmacological chemical probe. However, CGS-15943 showed a clean kinome profile

and a unique cellular response and mechanism among all tested BMP activators tested based on its genuine dual CK1/PI3K-inhibition profile.

In addition to its demonstrated activity in osteogenic differentiation, CGS-15943 exhibited great potential to recapitulate BMP activation in embryogenic development in both mESC mesoderm specification and zebrafish ventralization. Thus, its capacity to enhance BMP activity in human embryogenic cell lines is of great interest, especially with respect to early mesoderm formation and hence in differentiation protocols in regenerative medicine.

The dual mechanism of action is of particular interest for the treatment of various cancer cells associated with Shh, Wnt and BMP signaling, since CGS-15943 could induce cancer apoptosis with a lower risk due to its unique and selective profile against specific isoforms of CK1 and PI3K and could open a great potential for various therapeutic applications among ossification or for cancer treatment.

4 CONCLUSION AND PERSPECTIVES

The BMP signaling pathway is among the major developmental pathways critical for embryogenesis and driving differentiation into multiple cell lineages. To name a few key functions, BMP regulates pluripotency exit, morphogenic mesoderm patterning during gastrulationas well as bone and cartilage development.[14,62,149] Dysregulations of BMP have been linked to a variety of diseases, including the development of cancer. Its numerous regulatory properties in lineage commitment demonstrate the tremendous potential of exogenous BMP modulation. In particular for BMP activators, there is an urgent need for high-quality chemical probes and therapeutics that mimic physiological BMP. However, the development of signaling activators or genuine small molecule growth factor or cytokine mimetics represents a challenging task in drug discovery. The highest specificity for a certain signaling pathway is achieved by highly conserved receptor-ligand binding. The complex ligand-receptor engagement, which is often accompanied by receptor (hetero)-oligomerization, is difficult to mimic by a small molecule modality and is more likely to be achieved by peptide- or protein-based agents. However, with SB-247464 as a granulocyte-colony stimulating factor mimetic or the thrombopoietin mimetic Eltrombopag, few small molecule examples exist.[394,395] Alternatively, perturbation of well-characterized signaling pathway components enables the rational development and design of activators. This process requires comprehensive basic research on the pathway of interest and profound knowledge on the biochemistry of the cellular target. Examples are the GSK3β-inhibitor CHIR-99021 as a Wnt/β-catenin activator or the Bayer-developed HIF-PH inhibitor Molidustat that induces erythropoietin (EPO) expression rather than being a receptor activator.[396–399]

A most critical requirement for the discovery of truly novel BMP activator modalities is the availability of a meaningful and unique screening assay. Most reported BMP activators were identified from screens in artificial reporter gene assays employing immortalized cell lines, which ultimately may miss attractive targets and mechanisms relevant in physiologically complex systems.

Therefore, building on previous results by Dr. Jonas HALVER (SCHADE group), this work established and optimized a physiological, morphogenic cellular screening assay using murine embryonic stem cells to recapitulate embryonic development in a 2D screening

approach.[290,291] Herein, the orchestration of BMP signaling cues during mesodermal differentiation has been successfully shown to be feasible in a phenotypic screening format by using high-quality chemical probes selective for distinct signaling pathways. This new assay setup was supposed to furnish novel BMP activator chemotypes that mimic the exogenous activity of BMP-4 and potentially expand the druggable space of BMP signaling effectors. Proof-of-concept could be demonstrated from screening a 7,000 compounds chemical diversity library and a 1,408 compounds library of known pharmacologically active agents. In addition, a stringent hit validation workflow was successfully established with a particular focus on the capacity of small molecule hit candidates to enhance osteogenesis. As a result of these efforts, two novel chemical modalities were identified that potently enhanced osteogenic BMP signaling, as illustrated in Figure 94.

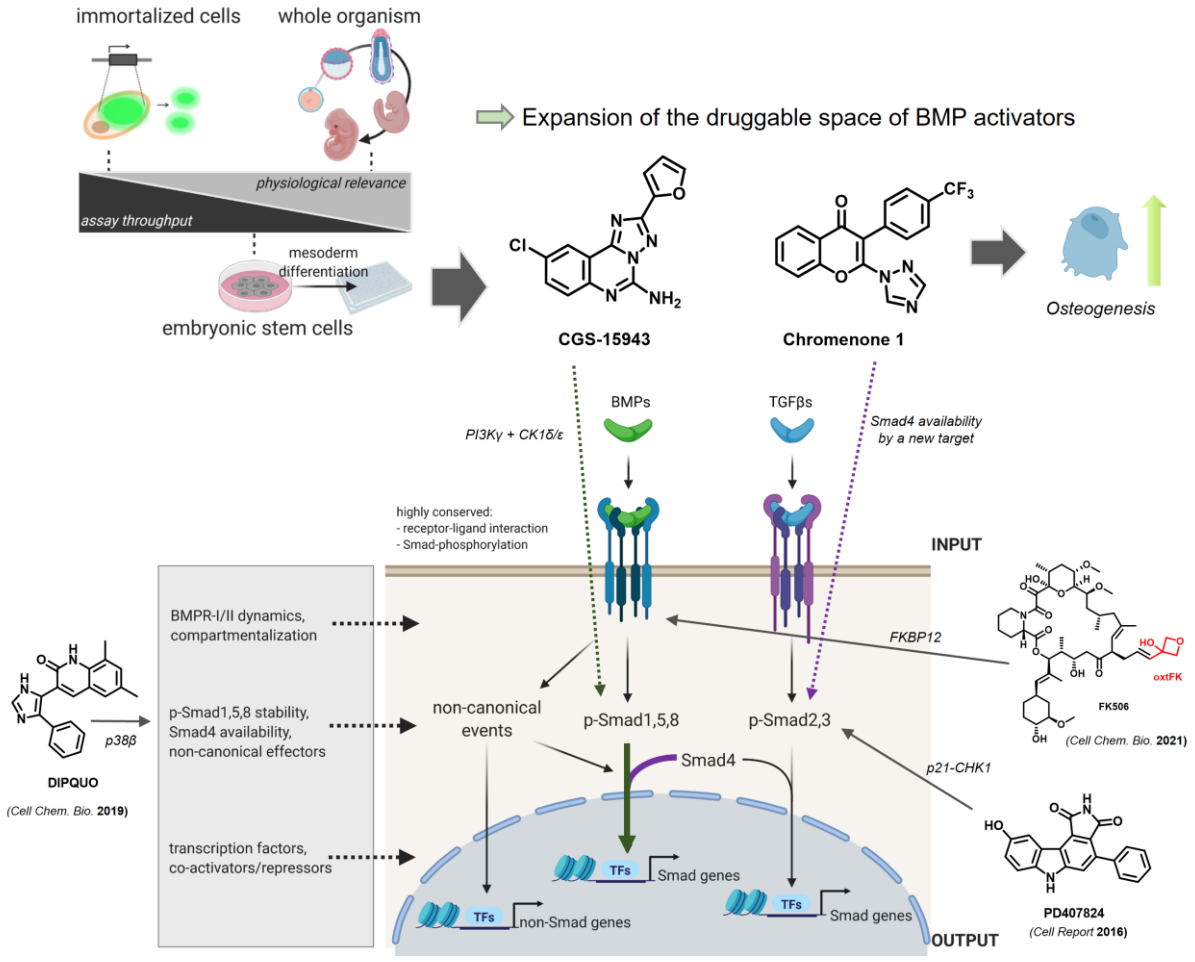

Figure 94: Schematic overview of the druggable space of BMP activators/sensitizers and its expansion by the identified BMP amplifiers Chromenone 1 and CGS-15943. Both chemotypes amplify BMP signaling via stabilization of BMP-Smad signaling outputs. Chromenone 1 enhances canonical nuclear BMP-Smad signaling outputs through an unparalleled, kinase-independent, non-toxic negative TGFβ-Smad feedback loop. In contrast, the identified selective CGS-15943 amplifies osteogenic BMP signaling outputs independent of a TGFβ-feedback via a proposed dual inhibition of CK1δ/ε and PI3Kγ (p110γ) isoforms.

With the identification of the 2-aminopyrimidine chemotype, including the autophagy inhibitor Autophinib, successful de-validation of false-positives could be demonstrated. Here, inhibition of VPS34 resulted in false-positive activity in the cardiogenic mESC assay, whereas GSK3β was the relevant off-target in the osteogenic C2C12 assay, which is known to crosstalk between canonical BMP and Wnt signaling. Considering that GSK3β functions as a central regulator for many signaling pathways, its targeting carries the risk of non-specific polypharmacology and should be avoided. De-validation provided further insight into how autophagy-related chemical probes impair cardiogenic differentiation, as shown by lipid kinase VPS34 and mitochondrial complex I inhibitors. Due to the perturbed cellular homeostasis during differentiation, autophagy-interfering modulators could generally appear as false-positives.

One of the identified and validated hits, the 2,3-disubstituted 4*H*-chromen-4-one Chromenone 1, proved to be a BMP signaling potentiator with high potency and efficacy representing a new BMP-activating chemotype. A combination of kinome and transcriptome profiling with biochemical evaluation of cytosolic and nuclear BMP/TGFβ-Smads revealed a unique mode-of-action. Chromenone 1 appeared to induce a pronounced, kinase-independent, negative TGFβ feedback that resulted in enhanced nuclear BMP-Smad signaling outputs. Future endeavors might decipher its direct cellular binding partner(s), which in turn, could furnish novel druggable regulators of the BMP pathway. The characterized set of Chromenones 1-3 serve as valuable chemical probes already at this stage and represent a valid starting point to generate a lead structure for early *in vivo* efficacy studies.

From screening of 1,408 known bioactive compounds, the triazolo[1,5-*c*]quinazoline CGS-15943 was identified and fully validated as another novel BMP activating chemotype and exhibited highest selectivity among all profiled hits as well as reported BMP modulators. It not only functionally rescued BMP blockade in the original stem cell-based phenotypic screening assay during mesodermal patterning, but also proved effective *in vivo* in zebrafish embryo development during gastrulation. Moreover, CGS-15943 amplified BMP signaling outputs to efficiently promote osteogenic differentiation and mineralization in murine C2C12 cells and human osteosarcoma cells *in vitro*, underscoring its versatile applicability as a BMP potentiator. The known adenosine receptor targets of CGS-15943 could not explain the underlying mechanism of action. However, CK1δ/ε and PI3Kγ were identified as novel targets

from kinome-wide profiling of CGS-15943. Thus, CGS-15943 turned out to amplify osteogenic BMP signaling outputs via a proposed dual inhibition of CK1δ/ε and PI3Kγ. This represents a unique mode-of-action that appeared to function as a critical regulator leading to enhanced nuclear BMP-Smad signaling independent of TGFβ-feedback mechanisms.

With the successful advent of identifying and characterizing these two small molecule modalities, a proof-of-concept could be presented that underscores the utility and impact of the underlying screening approach for the discovery of genuine and novel BMP activators or amplifiers, respectively. These efforts led to two high-quality, BMP-active chemical modalities with unique mode-of-actions on the BMP pathway and BMP-dependent developmental processes. Interestingly, both compound classes enhance BMP signaling outputs by stabilizing nuclear BMP-Smad levels in a distinct fashion. Chromenone 1 potentiates BMP signaling by downregulating TGFβ-Smad signaling in a kinase-independent manner, very much unlike the reported BMP sensitizer PD407824. Further, it exhibits a superior activity profile in the BMP assays and cellular toxicity profile compared to other BMP activator or sensitizer chemotypes tested. Strikingly, CGS-15943 selectively targets BMP signaling without affecting TGFβ-Smad signaling. Here, the regulatory functions of CK1δ/ε isoforms and PI3K class I γ-isoform may contribute to a novel role in Smad-biology. Interestingly, CGS-15943 was found to inhibit CK1δ in a rare mixed competitive and non-competitive manner, which might additionally explain its unique effect on BMP-Smad localization and stability. However, the molecular basis of this phenomenon remains to be investigated in greater detail and could reveal new critical regulatory functions.

As both BMP activators have shown an enhancing osteogenic activity profile *in vitro*, they offer great potential for therapeutic application to treat osteopenic diseases and skeletal trauma for which rhBMPs have been utilized to date. The herein identified BMP potentiators, Chromenone 1 and CGS-15943, mediate enhanced activity of basal BMP signaling. Their mode-of-actions differ from pure receptor agonists and pure BMP mimetics. However, amplification of basal BMP activity allows for local enhancement of BMP signaling in areas where BMP activity is physiologically insufficient. Such pharmacology would enable therapeutic applications without concomitant administration of rhBMPs and would demonstrate the potential of non-mimetic BMP amplifiers. Such sensitive balancing of basal BMP activity could potentially overcome the adverse effects of rhBMPs in the treatment of osteopenic diseases and skeletal trauma, such

as heterotopic ossification. Moreover, in applications and treatments requiring obligate rhBMP activity, simultaneous administration could lower the required doses of rhBMPs. Such a co-application would contribute to the stabilization and enhancement of the local osteogenic effect and would also be much more cost-effective. Clinical application for ossification with rhBMPs has already been successfully exploited, with great opportunities for BMP activators or potentiators for the treatment of bone degeneration, bone, and joint repair.[14,288] Since bone recovery is a slow process, combinatorial application would enhance this process for autograft formation and patient-derived bone tissue. A cost-effective treatment with a ligand-rhBMP-cocktail would be applicable for graft incorporation and bone-tissue regeneration. This is where the BMP-Smad enhancer may come into play, as signal transduction is amplified downstream of receptor-ligand complexation. Moreover, these BMP potentiators might be utilized for nano-scaffolds that have been developed to engineer bone tissue for graft formation. BMP-activating small molecules could be encapsulated or applied to nanofiber scaffolds, which have already successfully demonstrated synergistic osteogenesis by BMP-2 and dexamethasone, providing evidence for the potential incorporation of osteoblastogenic drugs to enhance differentiation and osteoblastic homeostasis.[400]

Furthermore, harnessing embryonic development as an enabling technology to identify BMP activators might translate to even more complex 3D systems in the future. Recent advances in the field of “synthetic embryology” have been made, for instance in the formation of embryonic organoids known as gastruloids. The first self-organizing human heart-like cardioids were reported in a multi-well format.[176] Interestingly, critical BMP cardiac mediators (i.e., BMP-2/-4, and BMPR2) that drive cardiac specification of the mesoderm were identified in this hESC-based model system. These findings highlight the relevance of the morphogenic effect of BMP-4 in cardiac mesoderm formation and the significance of recapitulating BMP signaling during mesoderm specification of the herein described mESC-based screening assay. This is further substantiated by a recently reported protocol for the generation of cardiac precursor gastruloids with distinct cardiac heart fields from differentiated mESCs, recapitulating early cardiogenesis in a murine system.[177] Importantly, BMP-4 has been shown to be important for intrinsic stem cell patterning and formation of human organizer.[174,175] Due to their complexity, these gastruloid model systems cannot be used for drug screening approaches. Therefore, the phenotypic BMP-dependent mESC assay represents a screening alternative to these sophisticated systems in order to capture the morphogenetic contributions of BMP signaling.

In conclusion, the methodology presented in this thesis enables the identification of novel BMP activators that expand the druggable space of currently available modalities. Future studies will have to unravel their modes-of-action in greater detail on the molecular level. It will be exciting to see the full potential of these new agents as BMP signaling amplifiers for various therapeutic applications and as tools for directed differentiation of pluripotent stem cells.

5 MATERIALS AND METHODS

5.1 Material

5.1.1 Chemicals, recombinant proteins, and reagents

Compounds listed below were purchased from different suppliers directly or from the Compound Management and Screening Center's (COMAS) small molecule library. All other compounds mentioned in this thesis have been synthesized either by M.Sc. Stefan LOHMANN from the department of Pharmaceutical and Medicinal Chemistry of the Pharmaceutical Institute in Kiel, or by chemists of the Chemical Biology department of the Max Planck Institute of Molecular Physiology in Dortmund.

Reagent	Supplier	Identifier
0.25% Trypsine/ 0.02% EDTA	Gibco	25200-056
2-Phospho-L-ascorbic acid	Sigma Aldrich	49752-10G
Acetone	Sigma Aldrich	32201
Autophinib	Selleckchem	S8596
AZD7648	Selleckchem	S8843
BIO	Selleckchem	S7198
Blasticidin	Sigma Aldrich	SBR00022
Bovine Serum Albumin (BSA)	Sigma Aldrich	A3059
Bradford assay reagent	Bio-Rad	5000204
BYL-719	MedChemExpress	HY-15244
Carbenicillin	Carl Roth	6344.2
CGS-15943	Sigma Aldrich	C199-25MG
CHIR99021	Sigma-Aldrich	SML1046
Cycloheximid	Sigma-Aldrich	C4859
DAPI	Carl Roth	6335.1
DMEM (with Glucose, L-Glutamine, Sodium	PAN-Biotech	P04-03590

pyruvate)		
DMEM, high glucose, pyruvate, no glutamine	Gibco	21969-035
DMEM, high glucose, no glutamine	Gibco	11960-044
DMEM, high glucose, pyruvate	Gibco	41966-029
DMH-1	Selleckchem	7146
DMSO, bio-grade	Carl Roth	A994.2
	Acros Organics	327182500
DMSO, BioScience Grade	Carl Roth	A994.2
Dorsomorphin (DM)	Tocris	3093
DPBS	Gibco	14190-094
EBSS	Sigma Aldrich	E3024
Ethanol, absolute	Fisher Chemical	10542382
Fetal bovine serum, Premium	PAN-Biotech	Batch# 151203
	Sigma-Aldrich	Batch# 9857
FICZ	Sigma Aldrich	SML1489
Formaldehyde solution (37%)	Carl Roth	P733.1
FuGENE® HD Transfection Reagent	Promega	E2693
G418, Geneticin	Sigma Aldrich	G8168
Gelatine in PBS, 0.1%	PAN Biotech	P06-20410
GelRed® Nucleic Acid Gel Stain	Biotium	41003
GlutaMAX™	Gibco	35050-038
Glycerol	Gerbu	2006.5000
Hoechst 33342	Sigma Aldrich	B2261
Hydrochloric acid (HCl)	J.T.Baker	15142675
Isoliquiritigenin	Selleckchem	S2404
Isopropanol	Honeywell	33539
LDN-193189	Sigma-Aldrich	SML0559
Leukemia inhibitory factor, LIF	Protein Chemistry Facility, MPI Dortmund	84-14_pOPIN-His-GST-LIF
L-Glutamine	Gibco	25030081
Lipofectamine® 2000	Invitrogen	11668-019

Lipofectamine® 3000	Invitrogen	L3000-001
LY294002	Selleckchem	S1105
ML-347	Sigma-Aldrich	SML1273
Non-essential amino acids (NEAA)	Gibco	11140-050
NP-40	Calbiochem	492016
Opti-MEM	Gibco	31985-062
PCR grade water	VWR	733-2573
PD407824	Sigma-Aldrich	PZ0111
Penicillin/Streptomycin	Gibco	15140-122
PF670462	Sigma Aldrich	SML0795
Phusion flash high-fidelity PCR master mix	Biolabs	M0530S
PIK-93	Selleckchem	S1489
Propidium iodide	Sigma Aldrich	P4864
Purmorphamine	Cayman Chemical	10009634
rhActivin A	Bio-Techne	338-AC
rhBMP-2	R&D Systems	355-BM-010
rhBMP-4	R&D Systems	314-BP-050
rhNoggin	StemCell Technologies	78060.1
rhTGFβ-2	Merck Millipore	GF113
RNase/DNase-free water (no DEPC)	Ambion	AM9938
Saponin	Carl Roth	9622.2
SAR405	Selleckchem	S7682
SB-431542	Selleckchem	S1067
SR-3029	Axon	2547
SYTOX™ Green Nucleic Acid Stain	Invitrogen	S7020
TripLE™ Cell Dissociation Buffer	Gibco	A12177-01
Tris	Carl Roth	4855.2
Triton-X100	Carl Roth	3051.3
TriTrack DNA Loading Dye (6X)	Thermo Fisher Scientific	R1161
Trypan Blue	Thermo Fisher Scientific	T10282

Trypsin-EDTA (0.25%), phenol red	Gibco	25200056
Ultra Low Range DNA Ladder	Thermo Fisher Scientific	SM1213
1 kb Plus DNA Ladder		SM1333
High Range DNA Ladder		SM1351
UltraPure™ Agarose	Invitrogen	16500-100
Ventromorphin/ Z19757816	Enamine	4254445/0003
ViaFect™ Transfection Reagent	Promega	E4983
Vismodegib	Selleckchem	S1082
VPS34-IN1	Selleckchem	S7980
β-Mercaptoethanol	Gibco	31350-010

5.1.2 Buffers and media

Buffer	Composition
293/Luc medium	DMEM (P04-03590) FBS 10% (v/v) 1% NEAA 10 µg/mL Blasticidin
C2C12 differentiation medium	DMEM (high Glucose, no Glutamine, no Pyruvate) 6% FBS (heat-inactivated) 1% GlutaMAX 1% Penicillin/Streptomycin
C2C12 maintenance medium	DMEM (high Glucose, no Glutamine, no Pyruvate) 10% FBS 1% GlutaMAX
C3H10T1/2 medium	DMEM (high Glucose, no Glutamine, no Pyruvate) 10% FBS (heat-inactivated) 3% L-Glutamin 1% N-Pyruvate 1% Penicillin/Streptomycin

Cytoplasmic extraction buffer	10 mM HEPES, 10 mM KCl, 0.1 mM EDTA, 1 mM Dithiothreitol, 0.5% Nonidet-P40, pH 7.5
FACS staining buffer SB	PBS 0.25% Saponin 2% FBS
Fixation buffer	4% formaldehyde in PBS
LB medium LB Agar	10 g/L Bacto Trypton 5 g/L Bacto Yeast Extract 10 g/L NaCl pH 7.4 + 1.5% Bacto Agar + 100 µg/mL antibiotic
Lysis buffer	100 mM Tris-HCl, pH 9.5 250 mM NaCl 25 mM $MgCl_2$ 1% Triton X-100 in ddH_2O
mESC differentiation medium	DMEM (high Glucose, Pyruvate, no Glutamine) 2-6% FBS 1% GlutaMAX 1% NEAA 1% Penicillin/Streptomycin 0.1 mM β-Mercaptoethanol
mESC freezing medium	DMEM (high Glucose, Pyruvate, no Glutamine) 20% FBS 10% DMSO 1% GlutaMAX 1% NEAA 1% Penicillin/Streptomycin 0.1 mM β-ME 15 ng/mL LIF
mESC maintenance medium for pluripotency	DMEM (high Glucose, Pyruvate, no Glutamine) 10% FBS 1% GlutaMAX

	1% NEAA 1% Penicillin/Streptomycin 0.1 mM β-Mercaptoethanol 15 ng/mL LIF
Mineralization medium	DMEM/F12 10% FCS 1% Penicillin/Streptomycin
Nuclear extraction buffer	10 mM HEPES, 400 mM NaCl, 1 mM EDTA, 1 mM Dithiothreitol, pH 7.5
Osteogenesis medium	DMEM/F12 10% FCS 1% Penicillin/Streptomycin 10 mM ß-glycerophosphate 0.2 mM Ascorbic acid 10 nM Dexamethasone
Permeabilization buffer	PBS 0.25% Triton-X 2% FBS
Standard cell culture medium	DMEM (P04-03590) FBS 10% (v/v)
TAE (50 ×)	2 M Tris-acetate 50 mM EDTA 5.71% (v/v) acetic acid

5.1.3 Cell lines

Cell line	Supplier	Identifier
293/Luc Cell Line	Cell Biolabs	AKR-230
C2C12 Mouse Myoblast Cell Line	ATCC	CRL-1772™
HEK293T	ATCC	CRL-3216™
Human Bone osteosarcoma cell line SaOS-2	Cell Lines Service	300331

Mouse CGR8-α*MHC*-GFP	Sanford-Burnham Medical Research Institute, Mercola Lab	Takahashi et al. 2003[292]

5.1.4 Bacterial strains

Bacterial strain	Supplier
Escherichia coli BL21-CodonPlus (DE3)	Agilent
Escherichia coli OmniMAX	ThermoFisher

5.1.5 Antibodies

Antibody	Supplier	Identifier
Anti-Histone H3	Abcam	ab1791
Anti-Smad2	Cell Signaling	5339
Donkey anti-Rabbit IgG (Alexa Fluor 750)	Invitrogen	ab175730
GAPDH Polyclonal Antibody	Invitrogen	PA5-85074
Goat anti-Mouse IgG (Alexa Fluor 488)	Invitrogen	A-11001
Goat Anti-Rabbit IgG (HRP)	Abcam	ab97051
Human/Mouse SSEA-1 Antibody	R&D Systems	MAB2155
pSmad1/5/9$^{Ser463/465}$	Cell Signaling	13820
Anti-Oct4	Abcam	ab19857

5.1.6 Oligonucleotides

Oligonucleotides were synthesized and desalted by IDT Technologies.

Gene		**Sequence**
mouse-Actb	Forward	5'-ACCCTAAGGCCAACCGTGA-3'
	Reverse	5'-ATGGCGTGAGGGAGAGCATA-3'
mouse-ALK3	Forward	5'-TGACCTGGGCCTAGCTGTTA-3'
	Reverse	5'TTCAGGCTTTCATCCAGCA-3'
mouse-Alp	Forward	5'-ATCTTTGGTCTGGCTCCCATG-3'
	Reverse	5'-TTTCCCGTTCACCGTCCAC-3'

mouse-BraT	Forward	5'-GACTTCGTGACGGCTGACAA-3'
	Reverse	5'-CGAGTCTGGGTGGATGTAG-3'
mouse-BMP2	Forward	5'-GGGACCCGCTGTCTTCTAGT-3'
	Reverse	5'-TCAACTCAAATTCGCTGAGGAC-3'
mouse-BMP4	Forward	5'-TGAGGAGTTTCCATCACGAAG-3'
	Reverse	5'-CTCACTGGTCCCTGGGATGT-3'
mouse-BMPR2	Forward	5'-TGGGAGGTGTTTATGAGGTGT-3'
	Reverse	5'-GAAAAGCCATCTGGTAATCTGG-3'
mouse-Cer1	Forward	5'-GTCAAGATGGTGATGCAAGTAGA-3'
	Reverse	5'-GGATGAAGGAACCCTGGGA-3'
mouse-Col1a1	Forward	5'-GGGGCAAGACAGTCATCGAA-3'
	Reverse	5'-GGTGGGAGGGAACCAGATTG-3'
mouse-Gapdh	Forward	5'-AGGTCGGTGTGAACGGATTTG-3'
	Reverse	5'-TGTAGACCATGTAGTTGAGGTCA-3'
mouse-Gsc	Forward	5'-CAACCAGCTGCACTGTC-3'
	Reverse	5'-TCTGGGTACTTCGTCTCCT-3'
mouse-Id1	Forward	5'-CCTAGCTGTTCGCTGAAGGC-3'
	Reverse	5'-CTCCGACAGACCAAGTACCAC-3'
mouse-Id2	Forward	5'-GAGGCACTCAGCTTAGCCAG-3'
	Reverse	5'-TCAGATGCCTGCAAGGACAG-3'
mouse-Id3	Forward	5'-GAGGCACTCAGCTTAGCCAG-3'
	Reverse	5'-TCAGCTGTCTGGATCGGGAG-3'
mouse-Kdr/Flk1	Forward	5'-AAGGAACTAGAATGCGGGCT-3'
	Reverse	5'-ACTCCCTGCTTTTACTGGGC-3'
mouse-Mef2c	Forward	5'-AGATCCCGATGCAGACGATT-3'
	Reverse	5'-AGACCGCCTGTGTTACCTG-3'
mouse-Mesp1	Forward	5'-CCATCGTTCCTGTACGCAGA-3'
	Reverse	5'-CTAGAAGAGCCAGCATGTCG-3'
mouse-Noggin	Forward	5'-CCTTCTGCCCGGTGCTGTAC-3'
	Reverse	5'-ACAGACTTGGATGGCTTACACACC-3'
mouse-Ocn	Forward	5'-ATGGCTTGAAGACCGCCTAC-3'
	Reverse	5'-AGGGCAGAGAGAGAGGACAG-3'

mouse-Oct4	Forward	5'-TAGGTGAGCCGTCTTTCCAC-3'
	Reverse	5'-GCTTAGCCAGGTTCGAGGAT-3'
mouse-Opn	Forward	5'-TTCTGGCAGCTCAGAGGAGA-3'
	Reverse	5'-TTCTGTGGCGCAAGGAGATT-3'
mouse-Osx	Forward	5'-CGCTTTGTGCCTTTGAAAT-3'
	Reverse	5'-CCGTCAACGACGTTATGC-3'
mouse-Runx2	Forward	5'-CCTGAACTCTGCACCAAGTCCT-3'
	Reverse	5'-TCATCTGGCTCAGATAGGAGGG-3'
mouse-Tnnt2	Forward	5'-CAGAGGAGGCCAACGTAGAAG-3'
	Reverse	5'-TCGATCAGAGTCTGTAGCTCATT-3'

5.1.7 Plasmids

Recombinant DNA	Supplier	Identifier
pBRE-*Id1*-luc (pGL3 BRE Luciferase)	Addgene	45126
pBRE-*xVent2*-luc (pGL2 BRE Luciferase)	Mercola Lab	Hata et al. 2000[88]
pCS2+Ck1α	Knippschild Lab	Dolde et al., 2018[401]
pCS2+Ck1δ	Knippschild Lab	Dolde et al., 2018[401]
pCS2+Ck1ε	Knippschild Lab	Dolde et al., 2018[401]
pRL-TK	Promega	E2231
pSBE4-luc (pBV-Luciferase)	Addgene	16495
pSTF (M50 Super 8x TOPFlash)	Addgene	12456
pWnt3a (Wnt3a cDNA in pUSEamp)	Upstate Biotechnology	21-124

5.1.8 Kits

Kit	Supplier	Identifier
CDP-Star reagent®	Roche	11759051001

CellTiter-Glo® Cell Viability Assay	Promega	G7570
Dual-Luciferase® Reporter Assay System	Promega	E1960
E.Z.N.A.® Plasmid DNA Mini Kit	Omega Bio-tek	D6943-01
Lysis buffer (5x)	Promega	E194A
MycoAlert™ mycoplasma detection kit	Lonza	LT07-118
NucleoSpin RNA, Mini Kit	Macherey-Nagel	740955
ONE-Glo™ Luciferase Assay System	Promega	E6120
Plasmid Midi Kit (100)	Qiagen	12145
qScript™ cDNA SuperMix	Quanta Biosciences	84033
RNAse-free DNAse Set	Qiagen	79256
RNeasy Mini Kit	Qiagen	74106
RT^2 First Strand Kit	Qiagen	330404
RT^2 Profiler™ PCR Array	Qiagen	PAMM-035ZG
RT^2 SYBR Green qPCR Mastermix	Qiagen	330503
Takyon™ No Rox SYBR MasterMix dTTP Blue	Eurogentec	UF-NSMT-B0701

5.1.9 Devices

Device	Identifier	Supplier
Agarose-gel chamber	Unit MIDI Plus	Carl-Roth
Autoclave	Laboklav 160MV	SHP
Biosafety Cabinet	NU-437-400E	Nuaire
Cell Counter	Countess™ I Countess™ II	Invitrogen
Cell freezing container	5100-0001	Nalgene
Centrifuge	5418 5804R 5427R 5810	Eppendorf
Echo Liquid Handler	ECHO® 520	Labcyte

	ECHO® 550	
Electrophoresis cell	Mini-PROTEAN Tetra Cell System	Bio-Rad
Flow Cytometer	BD LSRII analyzer	BD
Gilson Multichannel Finnpipettes	S97172 V90153 V74805 S89715	Thermo Fisher Scientific
High-Content Imaging Microscope System	ImageXpress Micro XL	Molecular Devices
Immunoblot Imager	Bioprint DS	Labexchange
Objective	CFI Plan Apochromat 60x	Nikon
Incubator	Galaxy 48S Galaxy 170S NU-4850E NU-5500E IN55	New Brunswick New Brunswick Nuaire Nuaire Memmert
Incubator shaker	Innova® 42 Multitron HT Pro	New Brunswick Infors-HT
Instant pot stove	Bleuet® 206 Plus	Campingaz
Liquid Dispenser	Multidrop® Combi	Thermo Fisher Scientific
Liquid nitrogen freezer tank	LS3000	Tec-lab
Matrix Electronic Pipette		Thermo Fisher Scientific
Microplate Mover	Orbitor RS	Thermo Fisher Scientific
Microscope	EVOS XL Core (2x, 4x, 10x, 20x) Primo Vert (4x, 10x, 20x, 40x) TCS SP5 (20x)	Life Technologies Zeiss Leica
Neubauer counting chamber		Brand
PCR Cycler	Biostep Prime Gradient	Techne
pH Meter	FiveEasy™	Mettler Toledo

Pipettes	Research Plus	Eppendorf
Pipetting aid	accu-jet® pro	Brand
Plate Reader	Tecan Infinite® M200	Tecan
	Spectramax Paradigm	Molecular Devices
	Envision	Perkin-Elmer
Plate Shaker	Teleshake	Thermo Fisher Scientific
Plate Washer	Elx405	BioTek
Power supply	Power PAC300	Bio-Rad
Realtime PCR Cycler	LightCycler® 480	Roche
Safe Aspiration System	Vacusafe comfort	Integra Biosciences
Scale	AX2202	Sartorius
	CS200	Ohaus
Small tube metal tip dispensing cassette	24073295	Thermo Fisher Scientific
Spectrophotometer	Nanodrop 2000c	Thermo Fisher Scientific
Stainless Steel Manifold	3-000-102	Drummond Scientific Company
Standard tube metal tip dispensing cassette	24072670	Thermo Fisher Scientific
Thermomixer comfort	5355	Eppendorf
Ultrasonic cleaner	EMMI30HC	EMAG AG
Vortex mixer	Vortex-Genie 2	Scientific Industries
Water bath		GFL

5.1.10 Software

Software	**Supplier**
BioRender Imaging Software	BioRender.com
ChemDraw Professional	PerkinElmer
Excel	Microsoft
Fiji-ImageJ	Fiji
FlowJo	FlowJo Software

GraphPad Prism	Graphpad Software
LC480 SW1.5.1	Roche
LAS X	Leica
MetaXpress Software 6	Molecular Devices
OriginLab	OriginLab Software
Quattro software	Quattro-research

5.1.11 Consumables

Name	Supplier	Identifier
12-well plate	Sarstedt	83.3921
24-well plate	Sarstedt	83.3922
2mL Screw Cap Micro Tube Conical	Sarstedt	72.694.006
384-well plate, black, µclear, flat	Greiner Bio-One	781091
384-well plate, white, flat	Greiner Bio-One	781080
384-well plate, white, low-volume	Corning	3826
384-well plate, white, PCR, conical	Sarstedt	72.1985.202
5 mL Round Bottom Polystyrene Test Tube, with Cell Strainer Snap Cap	Corning	352235
6-well plate	Sarstedt	83.3920
96-halfwell plate, white, flat	Corning	3693
96-deepwell plates, 2 mL	Eppendorf	0030502310
96-well plate, clear bottom, flat	Sarstedt	83.3924
96-well plate, clear, conical	Sarstedt	82.1583.001
Adhesive qPCR foil	Sarstedt	95.1999
Adhesive sealing film	Nerbe plus	04-095-0200
Cell culture dish, 10 cm	Sarstedt	83.3902
Cell culture flasks, 175 cm^2	Sarstedt	83.3912.002
Cell culture flasks, 25 cm^2	Sarstedt	83.3910.002
Cell culture flasks, 75 cm^2	Sarstedt	83.3911.002
Countess Cell Counting Chamber Slides	Invitrogen	C10283

	NanoEntek	CS-050
Cryovials	Greiner-Bio Greiner-Bio	121263 123263
Cuvettes	VWR	634-0676
Disposal bags	Brand	759705
DNA low-bind tube, 0.5 mL	Eppendorf	022431005
Echo Environmental Lid	Labcyte	LL-0310
Echo Qualified Microplates	Labcyte	LP-0200 PP-0200
Filter membrane	Brand	265.30
Glass Pasteur pipettes	Brand	747720
Luer-Lock solo Syringe, 10 mL Omnifix	Braun	4617100V
Luer-Lock solo Syringe, 20 mL Injekt	Braun	4606205V
Octagonal PET Storage Bottles	Corning	431732 431733
Parafilm M	neoLab®	PM996
PCR tubes, 0.2 mL	Biozym	BZYM711002
Pipette tips, 10 µL	Sarstedt TipOne®	70.1130.600 S1111-3700
Pipette tips, 1250 µL	Sarstedt	70.1186.100
Pipette tips, 200 µL	Sarstedt	70.760.502
Pipette tips, Matrix pipette, 125 µL	Thermo Fisher Scientific	7442
Pipette tips, Nuclease-free, 100 µL	Sarstedt	70.760.212
Pipette tips, Nuclease-free, 1000 µL	Sarstedt	70.3060.255
Pipette tips, Nuclease-free, 1250 µL	Sarstedt	70.1186.210
Pipette tips, Nuclease-free, 20 µL	Sarstedt	70.1114.210
Pipette tips, Nuclease-free, 200 µL	Sarstedt	70.1189.215
Precision Wipe Tissues	Kimtech	05511
Reagent Reservoir (25 mL), RNAse/DNAse-free	Vistalab	3054-1002
RNase decontamination solution	Sigma Aldrich	ZAP R2020

RT^2 Loading Reservoir	Qiagen	338162
SafeSeal Micro Tubes, 0.5 mL	Sarstedt	72.704
SafeSeal Micro Tubes, 1.5 mL	Sarstedt	72.706
SafeSeal Micro Tubes, 2 mL	Sarstedt	72.695.500
Screw cap tubes, 15 mL	Sarstedt	62.554.502
50 mL		62.547.354
Serological pipettes 1 mL	Sarstedt	86.1251.001
2 mL		86.1252.001
5 mL		86.1253.001
10 mL		86.1254.001
25 mL		86.1685.001
Standard Micro Tubes, 1.5 mL, brown	Sarstedt	72.690.004
Surface Disinfection Cleaner	Tana Professional	Apesin rapid
Syringe, 25g	BD Becton Dickinson	303175
Water bath sterilizer	Waro	Waroklar

5.2 Methods

5.2.1 Cell biology methods

5.2.1.1 Cell culture

All experiments were performed in a mammalian cell culture under a laminar floor cabinet using sterile equipment and medium. For sterilization, equipment was autoclaved at 121 °C for 20 min. Cells were incubated in a humidified incubator at 37 °C and 5% CO_2 and cell plates with small volumes were generally incubated in an additional humidity chamber. For FBS heat-inactivation, the FBS was incubated at 56 °C in a water bath for 45 min. All buffers used for cell culture were sterile filtered after preparation. Each cell culture was regularly tested for mycoplasma pneumoniae contamination using the MycoAlert™ Mycoplasma Detection Kit according to the manufacturer's protocol.

All compounds used in the experiments were dissolved in DMSO as 10 mM stock solutions and stored at -20 °C. For compounds treatments, DMSO levels did not exceed a final concentration of 0.5% (v/v) and DMSO was used as a standard vehicle for controls.

5.2.1.2 Thawing of cell lines

To thaw cells, a cryo-vial was collected from a liquid nitrogen tank and immediately thawed in a water bath at 37 °C for 2 min. In the meantime, 6 mL of pre-warmed culture medium was transferred to a 15 mL tube, and 1 mL was added carefully to the cryo-vial to ensure homogenous mixture and to thaw small ice clumps. The complete suspension was added to the prepared tube and the cells were centrifuged at 300 g for 3 min. Cells were resuspended in 1 mL culture medium and mixed by pipetting, followed by determination of the cell number, and transferring of the appropriate volume to a cell culture flask. Generally, cells were passaged for at least one more time before experimental usage.

5.2.1.3 Sub-cultivation of cell lines

Cell lines were cultivated in the respective medium until cells were confluent (70-90%), unless stated otherwise. Medium and trypsine/EDTA-solution were pre-warmed at 37 °C before usage. For passaging and seeding, medium was aspirated, and cells were washed once with PBS, followed by trypsination with 0.5 mL - 2 mL 0.25% trypsin/EDTA-solution for 5 min at 37 °C. Depending on the cell line, cells were detached by tapping against the culture flask and incubated for 2 min additionally. Cells were resuspended and collected with medium, followed by centrifugation at 300 g for 3 min. Medium was aspirated and the cell pellet was carefully resuspended in 1 mL – 2 mL culture medium by pipetting, to ensure a homogenous single cell suspension. Depending on the cell density, medium was added and 10 µL of the suspension were mixed with 10 µL trypan blue to determine the cell concentration with a Neubauer Counting chamber or an automated cell counter. For passaging, a suitable amount of cells were transferred into a new flask T25 (T75, T175) with 7 mL culture medium (12 mL, 20 mL) and/or further seeded into culture plates.

5.2.1.4 Cryo-conservation of cell lines

For long-term maintenance of cell lines, cells were harvested as described before and concentration was determined. Freezing medium was prepared with complete medium containing 10 – 20% FBS, depending on the cell line, and 10% (v/v) DMSO. The proper amount of cells were resuspended in freezing medium to achieve a final concentration of $0.5 – 2 \times 10^6$ cells/mL. Immediately, 1 mL of freshly mixed cells in freezing medium were transferred to each cryo-vial and stored in a freezing container at -80 °C for 24 h. To ensure the greatest possible reproducibility of the screens, a single batch was cryopreserved several times. After 24 h, the cryogenic vials were stored in the gas phase of liquid nitrogen for long-term storage.

5.2.1.5 Cultivation of pluripotent murine embryonic stem cells

The CGR8-mESC cell line carrying a *Myh6*-GFP reporter was cultivated in Leukemia inhibitory factor-containing (LIF) maintenance medium (high-glucose DMEM supplemented with 10% FBS, 1% GlutaMAX, 1% non-essential amino acids, 1% Penicillin-Streptomycin and 0.1 mM 2-mercaptoethanol, 15 ng/mL LIF). The cells were grown in periods of 2 – 3 days before passaging to maintain pluripotency and minimize spontaneous differentiation of the cell culture by seeding cells at low density, so individual pluripotent colonies can be formed, and confluency is kept below 70%. For passaging, 6-well plates were coated with 0.1% gelatine-solution (2 mL/well) for at least 10 min. Murine ESCs were washed with PBS and trypsinated for 5 min (300 µL/well) at 37 °C and 5% CO_2. After 5 min, the cells were dissolved by pipetting and incubated for another 2 min. The cells were collected with pre-warmed culture medium and centrifuged for 3 min at 300 g, followed by resuspension of the cell pellet with 1 mL LIF-containing maintenance medium and gentle pipetting to ensure a homogenous single cell suspension. Afterwards, the cell number was determined and 4×10^4 cells per well were seeded in 4 mL LIF-containing maintenance medium into pre-coated 6-well plates. To achieve optimal cell distribution, the plate was gently swung several times and incubated at 37 °C and 5% CO_2.

5.2.1.6 Phenotypic screening of murine embryonic stem cells

For assaying, mESCs were cultivated and harvested as described in 5.2.1.5. In principle, the cardiac differentiation assay was described before.[171,172,293] Here, the assay was modified and optimized for the screening of BMP-activating small molecules as described in the following. The centrifuged cell pellet was resuspended in LIF-free culture medium to allow spontaneous differentiation and cells were separated as described before. Cell number was determined and an appropriate volume of culture medium with a cell concentration of 0.02×10^6/mL was prepared. For coating, 384-well plates were incubated with 25 µL/well of 0.1% gelatine-solution (in PBS) for at least 30 min at room temperature. Gelatine-solution was aspirated with a steel manifold or automated plate washer Elx405, prior cell seeding of 25 µL per well (500 cells/well) using a Matrix pipette or dispensed with a Multidrop Combi Dispenser (Day 0) after extensive pre-washing of the standard cassette with pre-warmed medium. The plates were incubated at 37 °C, 5% CO_2, 95% humid atmosphere in additional humidity chambers. On Day 3, compounds and DMSO were added to the cells in quadruplicates for primary screening, in triplicates for IC_{50} determination using the Echo Liquid Handler (Labcyte) or in multiple wells for RNA isolation using a Matrix pipette. To induce cardiac differentiation, the BMP inhibitor DMH-1 was diluted in serum-reduced medium (4% FBS) and added to the wells with automated or manual dispensing. The final treatment concentration was set to 0.2% DMSO, 0.5 µM DMH-1 and 6% FBS. As a control, DMSO without DMH-1 and 10 ng/mL rhBMP-4 in DMH-1 control wells were used for calculation of the induction level of DMH-1. The plates were incubated for 24 h, unless otherwise stated, and medium was aspirated by automated plate washer. Complete serum-containing medium (10% FBS) was added to the wells (90 µL/well) on days 4, 7 and 9. After 11 days, medium was aspirated, and cells were fixed with 4% PFA in PBS and DAPI (1:1000 of 1 mg/mL stock-solution) or Hoechst33342 (1:1000 of 1 mg/mL stock-solution) for nuclear staining of the cells for 10 - 20 min at room temperature. Fixation was stopped by washing the plates three times with PBS on the plate washer Elx405 and 50 µL PBS was dispensed to each well. Washed plates were sealed with adhesive sealing films and centrifuged at 500 rpm for 1 min. The clear bottom of the plates was cleaned with isopropanol and the plates were imaged on an automated Image Xpress Micro XL System from Molecular Devices. For screening multiple plates, the automated microplate mover Orbitor RS was utilized. Fluorescent levels of GFP and DAPI were quantified using MetaXpress Software 5 – 6 by the “Multiwavelength Cell Scoring” algorithm. Intensity levels of the parameter “Mean Stain

Integrated Intensity" for GFP and "Total Cells" for DAPI were extracted and analyzed by Excel. DMH-1 levels were normalized to DMSO and all data are shown as the mean ± SEM of *Myh6*-GFP level of DMH-1 induction level or cell count, respectively. IC_{50}-values were calculated with GraphPad Prism 5 or Quattro Workflow 3.1., alternatively. Cell count levels below 70% of DMH-1 were considered false-positive due to cytotoxicity.

5.2.1.7 Osteoblastic differentiation assay

The osteoblastic differentiation assay is an orthogonal differentiation assay to primarily validate BMP-mimicking and BMP-synergistic compounds. Therefore, the BMP-sensitive murine pre-myoblast cell line C2C12 was cultivated and assayed. C2C12 needed to be passaged before the cellular monolayer became confluent (< 70% confluency) to prevent cellular contact and spontaneous myogenic differentiation. For the assay, C2C12 were seeded manually or by Multidrop Combi dispenser at 2×10^3 cells in 384-well plates (20 µL/well) in differentiation medium with heat-inactivated FBS-containing medium. After short centrifugation at 500 rpm for 30 sec, the plates were incubated for 16 h at 37 °C and 5% CO_2 at 95% humidity in humidity chambers to reduce plate edge effects caused by evaporation. Compounds were added manually and/or with the Echo Liquid Handler in DMSO (0.2%) and in triplicates. To induce osteogenic differentiation, BMP-4 was added to the wells (7.5 ng/mL) immediately after compound addition to reach a final volume of 50 µL/well and cells were incubated for 72 h. After treatment, medium was aspirated by automated plate washer BioTek Elx405 or manual steel manifold. To monitor cellular ALP-activity, substrate-containing CDP-Star was added to lysis buffer (1:100) and 15 µL CDP-lysis reagent were added per well. The plates were shaken for 5 min, followed by short centrifugation and incubation at room temperature in the dark. After 1 h incubation, the luminescence was measured on a Paradigm Reader (excitation 0.2 sec), and data was exported to Excel. In general, ALP-activity of 7.5 ng/mL BMP-4 in DMSO was set to 100% to calculate synergistic activity of tested compounds.

For BMP-dependent osteoblastic differentiation of murine mesenchymal stem cells, C3H10T1/2 cells were assayed. Therefore, 8×10^2 cells were seeded by Multidrop Combi dispenser with a standard cassette into 384-well plates for 24 h in 25 µL differentiation medium and incubated at 37 °C and 5% CO_2 at 95% humidity in humidity chambers. Recombinant human BMPs and/or compounds were added manually and/or with an Echo Liquid Handler

(10 µL/well) and incubated for 96 h in a humid atmosphere. Cellular lysis (25 µL/well) and Readout were performed similar to C2C12 assay.

5.2.1.8 Transfection of cell lines

Transfections were carried out for different cell lines and conditions, depending on the experiment and constructs. Detailed experimental conditions are listed in the table below and the general transfection is described in the sub-chapter 5.2.1.9.

Table 3: Overview of transfection conditions with constructs and usage. Each indicated volume is based on one experiment for one plate.L: Lipofectamine®2000; V: ViaFect™.

Experiment	Cell line	Recombinant DNA	Reagent [µL/µg DNA]	Nucleic acid	Cells	Incubation time
BMP-signaling modulation	HEK293T	pBRE-*Id1*-luc	L [3:1]	6 µg	3×10^6	16 h
BMP-signaling modulation	C2C12	pBRE-*Id1*-luc	V [6:1]	5 µg	1×10^6	16 h
BMP-signaling modulation	HEK293T	pBRE-*xVent2*-luc	L [3:1]	6 µg	3×10^6	16 h
TGFβ/AcA-signaling modulation	HEK293T	pSBE4-luc	L [3:1]	6 µg	3×10^6	16 h
Wnt-signaling modulation	HEK293T	pSTF	L [3:1]	3 µg	3×10^6	6 h
Wnt-signaling modulation	HEK293T	pWnt3a	L [3:1]	3 µg	3×10^6	6 h
Standardized control	HEK293T	pRL-TK	L [3:1]	0.3 µg	3×10^6	6-16 h
Standardized control	C2C12	pRL-TK	V [6:1]	0.5 µg	1×10^6	16 h
CK1 overexpression	HEK293T	pCS2+Ck1α	L [3:1]	2 µg	1×10^6	16 h
CK1 overexpression	HEK293T	pCS2+Ck1δ	L [3:1]	2 µg	1×10^6	16 h
CK1 overexpression	HEK293T	pCS2+Ck1ε	L [3:1]	2 µg	1×10^6	16 h

5.2.1.9 Luciferase reporter gene assays

To monitor the cellular effect of small molecules on different signaling pathways that are involved in the modulation of cardiogenic and embryogenic differentiation, luciferase-based reporter gene expression was performed. Therefore, HEK293T cells (or C2C12) cells were transiently transfected with a firefly luciferase reporter gene containing plasmid and a *Renilla* luciferase expressing plasmid pRL-TK as a standardized control, according to 5.2.1.8. Briefly, 6 µg of the respective plasmid with 0.3 µg of pRL-TK and Lipofectamine (3 µL/1 µg DNA) were added into 250 µL OptiMEM and incubated for 5 min at room temperature to transfer the plasmid-reagent into prepared Lipofectamine-solution. The mixture was incubated for 20 min and added to 3×10^6 HEK293T cells. Hence, HEK293T cells were collected, and cell number was determined to seed 3×10^6 cells per plate (96-well or 384-well plate) in 2% FBS-containing medium into a cell culture flask (4 mL total medium in a T25). The transfection reagent was added to the cells and incubated for 6 – 16 h, depending on the experiment, at 37 °C and 5% CO_2 at 95%. After transfection was completed, medium was aspirated and the cells were washed gently with PBS. The cells were trypsinated, centrifuged and the cell number was determined. The appropriate cell volume was diluted in 1% FBS-containing medium and 2.5×10^4 cells per well (2×10^3) were replated into a 96-well plate (384-well plate). For the assay, the plates were incubated for 2 h and compounds were added in triplicates with the respective growth factor to obtain a final DMSO concentration of 0.5% and 10 ng/mL GF. After 22 h, medium was aspirated and 50 µL (5 µL) lysis buffer was added into each well and incubated on a plate shaker at room temperature for 25 min. The luciferase activity was measured using the Dual Glo® Luciferase Assay Kit. For the 96-well plates, 10 µL firefly luciferase substrate was placed in a white half-well plate and 10 µL of the lysate was transferred to the substrate and mixed thoroughly by pipetting up and down. The luminescence was then measured on a Paradigm Reader or Envision, alternatively. When pRL-TK was transfected as a standardized control, 10 µL of *Renilla* Stop and Glo reagent was added to each well following the firefly measurement, and luminescence was read out. For 384-well plates, medium was aspirated using the BioTek plater washing device and 5 µL lysis buffer was added per well. The plates were centrifuged at 500 rpm for 30 sec and shaken on a plate shaker for 25 min, followed by the addition of 5 µL firefly luciferase to each well, short centrifugation, mixing and measurement of the luciferase on a Paradigm Reader or Envision. For *Renilla* luciferase measurement, 5 µL Stop and Glo buffer was added, and the plates were

shortly centrifuged and read out. Both luminescence values were extracted to Excel and the firefly luciferase signal was normalized to the *Renilla* luciferase signal. The induction control wells with the respective growth factor were set to 100% for the calculation of inhibition or activation levels of the compounds.

5.2.1.10 Luciferase inhibition assay

For the identification of small molecules that modulate the activity of the firefly luciferase and could lead to false-positive results in the reporter gene assays (see 5.2.1.9), compounds were tested using a 293/Luc cell line, containing a stably expressing firefly luciferase gene. To compare the results with the reporter gene assays, 293/Luc cells were seeded in a T25 culture flask in 2% FBS-containing medium for 16 h, followed by seeding into 96- or 384-well plates. After 2 h, compounds were added, incubated for 22 h and Readout was performed according to section 5.2.1.9 or with ONE-Glo Luciferase reagent according to the manufacturer's instructions.

To identify small molecules that modulate the standardized control *Renilla* luciferase of the reporter gene assays which leads to falsified normalization, *Renilla* luciferase lysates were generated and tested. For this purpose, pRL-TK transfected HEK293T were lysated and 9.5 µL of *Renilla* luciferase-containing lysate was incubated with compounds of interest (0.5 µL) for 1 h in a 96-halfwell plate. After incubation, 5 µL of *Renilla*-substrate of the Dual Glo Luciferase Assay Kit was added to the lysate and luminescence was measured in a Paradigm plate reader.

5.2.1.11 Cell viability assay

The cell toxicity for selected compounds was monitored in different assays and performed simultaneously as described for the respective assay. After compound treatment, the medium was aspirated and the cells were lysed using prepared CellTiter-Glo Luminescent Cell Viability Assay reagent (25 µL/well). The plates were incubated on a plate shaker for 10 min at room temperature and luminescence was measured on a Paradigm Reader to read out ATP-activity levels.

5.2.1.12 *In vitro* mineralization

These assays were performed by Dr. med. Eva MÜLLER (Magdeburg, Bertrand group). Human osteoblast-like cell line SaOS-2 were cultured in maintenance medium and seeded into 96-well plates (8×10^3 cells/well) in osteogenic differentiation medium (complete medium supplemented with 10 mM ß-glycerophosphate, 0.2 mM ascorbic acid and 10 nM dexamethasone, 2 ng/mL rhBMP-2 or rhBMP-4) to induce osteogenic mineralization over 11 days. Subsequently, differentiation medium was changed every three days and ascorbic acid was refreshed each day. To monitor the synergistic mineralization potential, the cells were treated with low concentrations of the indicated compounds in addition to BMP-treatment for 11 days. DMSO (0.01%) was used as a vehicle control.

Von Kossa staining: To stain the calcium level of mineralized osteoblasts, von Kossa staining was used in which silver ions replace calcium ions and form a visible metallic silver.[402,403] The cell cultures were washed twice with PBS and fixed with 4% PFA in PBS for 10 min. Fixation was stopped by washing the cells with water, an aqueous 5% silver nitrate ($AgNO_3$)-solution was added into the wells and the plates were exposed to sunlight for 1 h. Wells were rinsed with water and incubated with 1% 1,2,3-Trihydroxybenzol for 3 min, followed by washing and addition of 5% sodium thiosulfate ($Na_2S_2O_3$) for 3 min. The stained cells were washed twice with ethanol, dried and imaged using a 100 × magnification. For quantification, von Kossa-stained calcium deposits were analyzed using Image J. The area of black and white images was quantified after threshold substruction and the mean value for von Kossa stained area was calculated from at least four images for each test condition. Statistics were assessed by ANOVA-tests with GraphPad Prism 7.

5.2.1.13 Flow cytometry

To control the pluripotent potential of cultured mESC, regular batch control was carried out using staining of pluripotent marker proteins Oct4 and SSEA1 and further analysis by flow cytometry. Therefore, cultured pluripotent mESCs were washed with PBS and detached with TripLE-buffer for 5 min at 37 °C and 5% CO_2. Cells were harvested and dissociated with PBS and centrifuged at 300 g for 3 min, followed by fixation with 4% (v/v) PFA in PBS for 10 min at room temperature. After fixation cells were centrifuged and washed with PBS and permeabilized in FACS staining buffer (0.25% saponin/ 2% (v/v) FBS) for 30 min at room

temperature. Subsequently, permeabilized cells were centrifuged and stained with mouse anti-Oct4 (1:100) and/or mouse anti-SSEA1 (1:100) in staining buffer for 1 h at RT or overnight at 4 °C. Incubated cells were centrifuged and washed (2 x) and secondary antibodies (donkey anti-rabbit AlexaFluor 750 or goat anti-mouse Alexa Fluor 488) in staining buffer (1:1000) and/or DAPI (1:1000 of 1 mg/mL stock-solution) were added for 30 min at RT. Stained cells were washed twice, resuspended in 500 µL PBS and filtered through a FACS test tube with a cell strainer snap cap. The cell suspension was then analyzed on a BD LSRII Aria instrument by sorting at least 10,000 cells. The data from sorted cells was analyzed with FlowJo software by defining gates for living cells from forward and side scatter (FSC, SSC) and further gating for fluorescent cells.

5.1.2.14 Immunocytochemical staining and confocal imaging

For visualization and localization of pluripotent marker, mESC were seeded into 6-well plates (4×10^4 cells/well) and incubated with or without LIF. After 3 days, cells were washed with PBS and permeabilized with staining buffer (0.25% Triton-X, 2% FBS) at room temperature for 30 min, followed by addition of primary antibodies (1:100) in PBS for 1 h at RT or overnight at 4 °C, alternatively. The incubation was stopped, and the cells were washed with PBS (3 x), secondary antibodies (1:1000) and DAPI (1:1000) were added and the cells were stained for 1 h in the dark. Afterwards, cells were washed multiple times (3 x) with PBS and stored at 4 C in PBS. For fluorescence imaging, stained cells were imaged on a Leica SP5 confocal microscope using a 20 × objective and images were exported and analyzed using LAS X software and ImageJ.

5.2.2 Molecular biology methods

5.2.2.1 Agarose gel electrophoresis

To analyze DNA fragments, PCR products and DNA plasmids, DNA was separated using agarose gel electrophoresis. Therefore, 1 – 5% agarose, depending on product size, was suspended in 1 x TAE buffer and dissolved by heating in a microwave. For pre-staining, GelRed® was added (1:10,000) and the gel was filled into an agarose gel electrophoresis chamber. TAE buffer was added to the cooled down agarose gel and DNA samples that were

supplemented with 6 × DNA loading dye, and DNA marker were loaded onto the gel. The separation was started with an applied voltage of 80 V (50 V) for 1% (5%) agarose gel for 45 min (60 min) and the DNA was visualized by UV-light.

5.2.2.2 Heat-shock transformation of *E. coli*

Competent *Escherichia coli* strains OmniMAX or BL21-CodonPlus were transformed by heat shock with plasmid DNA. Bacteria was thawed on ice and 1 µL of plasmid DNA (450 ng/µL) was transferred to 100 µL E. coli, followed by incubation on ice for 30 min. The suspension was heat-shocked at 42 °C in a water bath for 90 sec, stopped on ice for 2 min and 1 mL of pre-warmed LB-medium was added and incubated on a thermo shaker at 37 °C, 500 rpm for 1 h. After incubation, the suspension was further diluted in LB-medium (1:1 and 1:2) and plated on LB agar plates containing the respective antibiotic (100 µg/mL) for selection of transformed bacteria and incubated at 37 °C overnight.

5.2.2.3 Plasmid amplification and isolation

To amplify transformed *E. coli*, an overnight culture was inoculated. Therefore, a bacterial colony of an agar plate or cells from a glycerol stock were picked up with a sterile pipette tip and transferred to a pre-warmed LB culture flask, supplemented with the respective antibiotic (100 µg/mL), and incubated overnight at 37 °C and 180 rpm. On the next day, the bacterial suspension was collected and centrifuged at 4 °C and 8000 rpm for 15 min in a cooled tabletop centrifuge. Obtained cell pellets were lysed and plasmid DNA was isolated and purified using the E.Z.N.A.® Plasmid DNA Mini Kit or Qiagen Plasmid Midi Kit according to the manufacturer's protocols. Isolated plasmids were dissolved in DNAse-free H_2O and plasmid concentrations were determined using a Nanodrop spectrophotometer. Plasmids were diluted (450 ng/mL), aliquoted and stored at -20 °C until further usage.

5.2.2.4 Glycerol stock preparation

For the storage of intact transformed *E. coli*, a glycerol stock was prepared for each amplified plasmid. Generally, 500 µL of an overnight culture were transferred to 500 µL of 50% glycerol-

water mixture in a cryo-vial and gently inverted multiple times. The cryo-vial was stored at -80 °C for long-term storage.

5.2.2.5 DNA sequencing

The transcription factor binding site and the multiple cloning site (MSC) of plasmids used for luciferase transcription reporter gene assays, were sequenced by single-tube sequencing at Microsynth AG.

5.2.2.6 RNA isolation

C2C12 cells were seeded into 12-well plates (24-well plate) at 2×10^5 cells/well (1×10^5 cells/well) and incubated for 16 h, followed by compound and/or growth factor addition for different durations depending on the experiment. For evaluation of embryonic differentiation, pluripotent mESC were seeded into 384-well plates and incubated for 3 days. Treatment was performed as indicated for each experiment at different time points and durations. RNA was isolated from assayed mESC from at least 12 wells for each condition. After treatment, C2C12 and mESC cells were washed with PBS, lysed, and homogenized by vortexing the viscous lysates for 1 min and flash-frozen in liquid nitrogen for further storage at -80 °C. Alternatively, the lysates were additionally disrupted using a sterile 25 g needle before flash freezing. The isolation was performed with the NucleoSpin® RNA Kit from Macherey Nagel or RNeasy Kit from Qiagen, according to the manufacturer's protocol. The concentration of isolated RNA was determined using a Nanodrop spectrophotometer and stored at -20 °C until further usage.

5.2.2.7 Reverse transcription

To generate complementary DNA (cDNA) from isolated RNA, equal amounts of RNA (250 ng – 500 ng) of one biological experiment was transcribed using the qScript cDNA Synthesis Kit on a PCR thermocycler following the manufacturer's instructions. Transcribed cDNA was further used for real-time RT-qPCR.

5.2.2.8 Quantitative real-time PCR

To quantify the mRNA level of a sample, quantitative reverse transcription polymerase chain reaction (RT-qPCR) was performed, by which transcribed cDNA is amplified and formed DNA is measured with a DNA intercalating dye. In real-time as the DNA is synthesized, the fluorescent signal intensifies per cycle and the crossing point (Cp or Ct) of the signal crossing the threshold can be determined.[404] Before quantification of samples of interest, all primer pairs were tested for their efficiency and for synthesized DNA artefacts by melting curve analysis. For that, a serial dilution of cDNA from a pool of samples was prepared (0.1 – 1,000 ng/well) and the efficiency was calculated by linear regression of Cp values. An efficiency of 90 – 110% was considered valid. Additional, optimal primer concentration was determined in a serial dilution of the primer sets between 50 – 500 nM.

In general, synthesized cDNA was pre-diluted in PCR-grade water to yield a concentration of 125 ng/µL and 4 µL were transferred into a 384-well PCR plate, followed by addition of 6 µL Master-Primer Mix per well. The Master Mix was prepared by mixing Takyon SYBR Master Mix with 5 µM primer stock solution (reverse/forward primer 1:1) in a ratio of 5:1. Plates were sealed with clear adhesive foils and centrifuged for 30 sec to dissolve any air bubbles in the wells. qRT-PCR was performed on a Lightcycler 480 with adjusted PCR cycling steps: heat-activation for 3 min (95 °C), followed by 45 cycles of a denaturation (95 °C for 3 sec), amplification (20 sec, 60 °C) and elongation step (20 sec, 72 °C), and a final melting curve determination (95 °C for 5 sec, 65 °C for 60 sec, followed by heating to 97 °C at continuous ramp rate). The Cp and Tm values were extracted from the Lightcycler software and relative gene expression was calculated by the ΔΔCp method.[405] As standardization control the Cp value from the housekeeping genes *Gapdh* and *Actb* were subtracted from the Cp value of the corresponding sample. Subsequently, the calculated ΔCp value from the control sample (DMSO or BMP control) was subtracted from each ΔCp value resulting in a ΔΔCp, which was used for gene expression value determination ($2^{-\Delta\Delta Cp}$). All data points are shown as mean of triplicates ± SD normalized to DMSO unless stated otherwise.

5.2.2.9 PCR array analysis

The PCR array analysis was performed with all reagents from Qiagen and according to Qiagen's instructions. C2C12 cells were seeded into 6-well plates (24-well plate) at 2×10^5

cells/well (8 × 10^4 cells/well) and incubated for 16 h, followed by compound and/or growth factor for 24 h. After treatment, C2C12 were washed, lysed and RNA was isolated with the RNeasy Kit. Reverse transcription was performed using the RT2 First Strand Kit on a PCR thermocycler and the samples were tested for their gene expression as described in 5.2.2.8 to validate the reproducibility and quality of the samples. The PCR Array was then performed by transferring generated cDNA onto a RT2 Profiler™ PCR Array plate (PAMM-035ZG) for Mouse TGFβ / BMP Signaling Pathway. The respective volume of RT2 SYBR Green qPCR Mastermix was added to the wells and the plate was sealed and shortly centrifuged. The array was run on a Lightcycler 480 following the cycling conditions of the manufacturer's instructions. Data extraction and expression analysis was done as described in 5.2.2.8. Additional internal profiler quality controls as reverse transcription controls, positive PCR controls and genomic DNA contamination controls were evaluated for each sample individually. All data points shown are the mean of triplicates normalized to DMSO and/or BMP-4 controls.

5.2.3 Biochemical methods

5.2.3.1 Immunoblotting and subcellular fractionation

These assays were performed by Daniel RIEGE (Kiel, Schade group). For quantification of Smad levels, C2C12 myoblasts were cultured in 10 cm dishes (2.5 × 10^6 cells/well) and treated with compounds and DMSO as indicated. To distinguish between cellular and nuclear protein levels, RIEGE established a protocol for subcellular fractionation. This was performed through a modified protocol based on Schreiber et al. 1989, by which cells were detached with trypsin, subsequently lysed with lysis buffer containing phosphatase inhibitor cocktail (Sigma) and cOmplete™ protease inhibitor cocktail (Roche), and subsequently washed with PBS (3 x) and cytoplasmic fraction was extracted with extraction buffer (10 mM HEPES, 10 mM KCl, 0.1 mM EDTA, 1 mM Dithiothreitol, 0.5% Nonidet-P40, pH 7.5).[406] Cells were centrifuged and pellets containing the nuclei were lysed in nuclear extraction buffer (10 mM HEPES, 400 mM NaCl, 1 mM EDTA, 1 mM Dithiothreitol, pH 7.5). For quantification of protein concentration, a Pierce™ BCA Protein Assay was performed. The required protein amount was loaded on self-cast polyacrylamide gels containing 0.5% trichlorethanol.[407] Afterwards, gels were illuminated with UV-light for 5 min and fluorescence and luminescence signals were imaged with an Intas

ChemoStar. Quantification was calculated with LabImage 1D software and antigen-specific luminescence intensities were normalized to total protein amount per lane.

5.2.3.2 Kinase activity and binding assays

To evaluate kinase modulation of small molecules, compounds were sent to Reaction Biology or to the SelectScreen™ Biochemical Kinase Profiling Service at Thermo Fisher Scientific and tested in a kinase panel using recombinant kinases in different assay technologies as described in the following.

I) Kinase HotSpot™ Profiling at Reaction Biology:

The Kinase HotSpot™ Profiling included 369 wildtype, 20 atypical and 17 lipid kinases that were tested in single dose duplicates. IC_{50}'s were determined by a 10 dose duplicate assay. In principle, the assays were based on quantification of radioactive labeled kinase substrate. Labelled ^{33}P-phosphate from added ATP is transferred to the kinase substrate. Therefore, ATP was added at a concentration at Km of each kinase and incubated for 2 h. Radiolabeled substrates are detected after filtering the reaction mixture on a P81 ion exchange filter membrane. In contrast, the activity of lipid kinases was screened by ADP-Glo substrate from Promega to quantify the amount of formed ADP.[408]

II) SelectScreen™ Adapta Assay at Thermo Fisher Scientific:

For kinase activity determination, the Adapta universal kinase assay utilizes fluorescent based detection of ADP via a fluorescence resonance energy transfer (FRET) signal. First, the kinase reaction with ATP concentration at Km of the kinases is incubated for 60 min and stopped with EDTA, followed by addition of a europium labeled anti-ADP antibody and an Alexa Fluor™ 647 labeled ADP tracer. The antibody and tracer form a complex which results in a high FRET signal which is decreased by formed ADP that displaces the tracer and inhibits complex formation. Kinase activity is calculated by the emission ratio from europium and Alexa Fluor™ 647. Compounds are tested at a final DMSO concentration of 1% DMSO.[409]

III) SelectScreen™ LanthaScreen Assay at Thermo Fisher Scientific:

The LanthaScreen kinase binding assay is based on FRET detection of europium-labeled anti-tag antibody and a kinase binding tracer conjugated with Alexa Fluor™ 647. Affinity-tagged kinases were used to which the antibody binds, and a FRET signal is induced by binding of the tracer. In presence of an inhibitor, the tracer is displaced, and the FRET signal decreases. For assaying, the kinases were incubated for 60 min with a test compound at 1% DMSO at room temperature and FRET signal was measured.[410]

IV) SelectScreen™ Z-Lyte Assay at Thermo Fisher Scientific:

The Z-Lyte biochemical assay employs a substrate peptide, labeled with one fluorophore on each end, that form a FRET signal and kinase activity is determined by monitoring cleaved peptide. Therefore, the peptide substrate is phosphorylated by a kinase at specific residues which then block the following proteolytic cleavage reaction of the peptide. Unphosphorylated peptide substrate is disrupted by added protease and the FRET signal is disturbed, which indicates the inhibition of the kinase reaction by a test compound. The reaction was induced by the addition of a test compound (1% DMSO) and ATP at concentration of the respective Km for 60 min at room temperature. After reaction, detection mixture was added and incubated for additional 60 min and fluorescence signals were read out and analyzed. The kinase activity is calculated by the emission ratio from coumarin at 445 nm and fluorescein at 520 nm.[411]

5.2.4 Computational methods/ Data analysis

5.2.4.1 Statistical analysis

Statistical analysis between two groups was performed with a paired or an unpaired t-test depending on the experimental setup with GraphPad Prism 5-7. The confidence level was set to 95% for three replicates and $n \geq 3$ independent biological experiments unless stated otherwise. Symbol meanings for the significance level are indicated as the following unless stated otherwise: ns: not significant; *: $p < 0.05$; **: $p < 0.01$; ***: $p < 0.001$. IC_{50} and EC_{50} values were calculated with GraphPad Prism 5-7 via nonlinear regression using a four-parameter fit unless stated otherwise. Replicates are defined as follows: N = technical replicates; n = biological replicates.

6 REFERENCES

1. Evans, M.J.; Kaufman, M.H. Establishment in culture of pluripotential cells from mouse embryos. *Nature* **1981**, 292(5819), 154–156.
2. Thomson, J.A.; Itskovitz-Eldor, J.; Shapiro, S.S.; Waknitz, M.A.; Swiergiel, J.J.; Marshall, V.S.; Jones, J.M. Embryonic stem cell lines derived from human blastocysts. *Science* **1998**, 282(5391), 1145–1147.
3. Bongso, A.; Richards, M. History and perspective of stem cell research. *Clinical Obstetrics & Gynaecology* **2004**, 18(6), 827–842.
4. Mason, C.; Dunnill, P. A brief definition of regenerative medicine. *Regenerative Medicine* **2008**, 3(1), 1–5.
5. Virani, S.S.; Alonso, A.; Benjamin, E.J.; Bittencourt, M.S.; Callaway, C.W.; Carson, A.P.; Chamberlain, A.M.; Chang, A.R.; Cheng, S.; Delling, F.N.*; et al.* Heart Disease and Stroke Statistics-2020 Update: A Report From the American Heart Association. *Circulation* **2020**, 141(9), e139-e596.
6. Elizabeth Wilkins; L Wilson; Kremlin Wickramasinghe; Prachi Bhatnagar; Jose Leal; Ramon Luengo-Fernandez; R Burns; Mike Rayner; Nick Townsend. European Cardiovascular Disease Statistics **2017**; European Heart Network: Belgium, 2017.
7. Wilkins, E, Wilson, L, Wickramasinghe, K, Bhatnagar, P, Leal, J, Luengo-Fernandez, R, Burns, R, Rayner, M & Townsend, N. European Cardiovascular Disease Statistics **2017**. Available online: https://ehnheart.org/images/CVD-statistics-report-August-2017.pdf.
8. Mudd, J.O.; Kass, D.A. Tackling heart failure in the twenty-first century. *Nature* **2008**, 451(7181), 919–928.
9. Wang, Y.-S.; Li, S.-H.; Guo, J.; Mihic, A.; Wu, J.; Sun, L.; Davis, K.; Weisel, R.D.; Li, R.-K. Role of miR-145 in cardiac myofibroblast differentiation. *Journal of Molecular and Cellular Cardiology* **2014**, 66, 94–105.
10. Parikh, V.N.; Liu, J.; Shang, C.; Woods, C.; Chang, A.C.; Zhao, M.; Charo, D.N.; Grunwald, Z.; Huang, Y.; Seo, K.*; et al.* Apelin and APJ orchestrate complex tissue-specific control of cardiomyocyte hypertrophy and contractility in the hypertrophy-heart failure transition. *American Journal of Physiology.* **2018**, 315(2), H348-H356.
11. Schade, D.; Plowright, A.T. Medicinal Chemistry Approaches to Heart Regeneration. *Journal of Medicinal Chemistry* **2015**, 58(24), 9451–9479.
12. Murphy, L.; Schwartz, T.A.; Helmick, C.G.; Renner, J.B.; Tudor, G.; Koch, G.; Dragomir, A.; Kalsbeek, W.D.; Luta, G.; Jordan, J.M. Lifetime risk of symptomatic knee osteoarthritis. *Arthritis and Rheumatism* **2008**, 59(9), 1207–1213.
13. Yelin, E.; Murphy, L.; Cisternas, M.G.; Foreman, A.J.; Pasta, D.J.; Helmick, C.G. Medical care expenditures and earnings losses among persons with arthritis and other rheumatic conditions in 2003, and comparisons with 1997. *Arthritis and Rheumatism* **2007**, 56(5), 1397–1407.
14. Salazar, V.S.; Gamer, L.W.; Rosen, V. BMP signalling in skeletal development, disease and repair. *Nature Reviews. Endocrinology* **2016**, 12(4), 203–221.
15. Arvidson, K.; Abdallah, B.M.; Applegate, L.A.; Baldini, N.; Cenni, E.; Gomez-Barrena, E.; Granchi, D.; Kassem, M.; Konttinen, Y.T.; Mustafa, K.*; et al.* Bone regeneration and stem cells. *Journal of Cellular and Molecular Medicine* **2011**, 15(4), 718–746.
16. Takahashi, K.; Yamanaka, S. Induction of pluripotent stem cells from mouse embryonic and adult fibroblast cultures by defined factors. *Cell* **2006**, 126(4), 663–676.

17. Takahashi, K.; Tanabe, K.; Ohnuki, M.; Narita, M.; Ichisaka, T.; Tomoda, K.; Yamanaka, S. Induction of pluripotent stem cells from adult human fibroblasts by defined factors. *Cell* **2007**, 131(5), 861–872.

18. Wernig, M.; Meissner, A.; Foreman, R.; Brambrink, T.; Ku, M.; Hochedlinger, K.; Bernstein, B.E.; Jaenisch, R. In vitro reprogramming of fibroblasts into a pluripotent ES-cell-like state. *Nature* **2007**, 448(7151), 318–324.

19. Yu, J.; Vodyanik, M.A.; Smuga-Otto, K.; Antosiewicz-Bourget, J.; Frane, J.L.; Tian, S.; Nie, J.; Jonsdottir, G.A.; Ruotti, V.; Stewart, R.*; et al.* Induced pluripotent stem cell lines derived from human somatic cells. *Science* **2007**, 318(5858), 1917–1920.

20. Velychko, S.; Adachi, K.; Kim, K.-P.; Hou, Y.; MacCarthy, C.M.; Wu, G.; Schöler, H.R. Excluding Oct4 from Yamanaka Cocktail Unleashes the Developmental Potential of iPSCs. *Cell Stem Cell* **2019**, 25(6), 737-753.e4.

21. Nobel Prizes 2012, **2012**. Available online: https://www.nobelprize.org/prizes/medicine/2012/advanced-information/.

22. Gurdon, J.B. The developmental capacity of nuclei taken from intestinal epithelium cells of feeding tadpoles. *Journal of Embryology and Experimental Morphology* **1962**, 10, 622–640.

23. Lebkowski, J. GRNOPC1: the world's first embryonic stem cell-derived therapy. *Regenerative Medicine* **2011**, 6(6 Suppl), 11–13.

24. Akabayashi, A.; Nakazawa, E.; Jecker, N.S. The world's first clinical trial for an aplastic anemia patient with thrombocytopenia administering platelets generated from autologous iPS cells. *International Journal of Hematology* **2019**, 109(2), 239–240.

25. Breckwoldt, K.; Letuffe-Brenière, D.; Mannhardt, I.; Schulze, T.; Ulmer, B.; Werner, T.; Benzin, A.; Klampe, B.; Reinsch, M.C.; Laufer, S.*; et al.* Differentiation of cardiomyocytes and generation of human engineered heart tissue. *Nature Protocols* **2017**, 12(6), 1177–1197.

26. National Library of Medicine (U.S.). A Study of iPS Cell-derived Cardiomyocyte Spheroids (HS-001) in Patients With Heart Failure (LAPiS Study) ClinicalTrials.gov, **2021**, (NCT04945018). Available online: https://clinicaltrials.gov/ct2/show/NCT04945018.

27. Längle, D.; Halver, J.; Rathmer, B.; Willems, E.; Schade, D. Small molecules targeting in vivo tissue regeneration. *ACS Chemical Biology* **2014**, 9(1), 57–71.

28. Li, T.; Luo, C.; Zhang, J.; Wei, L.; Sun, W.; Xie, Q.; Liu, Y.; Zhao, Y.; Xu, S.; Wang, L. Efficacy and safety of mesenchymal stem cells co-infusion in allogeneic hematopoietic stem cell transplantation: a systematic review and meta-analysis. *Stem Cell Research & Therapy* **2021**, 12(1), 246.

29. Ding, L.; Han, D.-M.; Zheng, X.-L.; Yan, H.-M.; Xue, M.; Liu, J.; Zhu, L.; Li, S.; Mao, N.; Guo, Z.-K.*; et al.* A study of human leukocyte antigen-haploidentical hematopoietic stem cells transplantation combined with allogenic mesenchymal stem cell infusion for treatment of severe aplastic anemia in pediatric and adolescent patients. *Stem Cells Translational Medicine* **2021**, 10(2), 291–302.

30. Mohamed, T.M.A.; Ang, Y.-S.; Radzinsky, E.; Zhou, P.; Huang, Y.; Elfenbein, A.; Foley, A.; Magnitsky, S.; Srivastava, D. Regulation of Cell Cycle to Stimulate Adult Cardiomyocyte Proliferation and Cardiac Regeneration. *Cell* **2018**, 173(1), 104-116.e12.

31. Diez-Cuñado, M.; Wei, K.; Bushway, P.J.; Maurya, M.R.; Perera, R.; Subramaniam, S.; Ruiz-Lozano, P.; Mercola, M. miRNAs that Induce Human Cardiomyocyte Proliferation Converge on the Hippo Pathway. *Cell Reports* **2018**, 23(7), 2168–2174.

32. Cao, N.; Huang, Y.; Zheng, J.; Spencer, C.I.; Zhang, Y.; Fu, J.-D.; Nie, B.; Xie, M.; Zhang, M.; Wang, H.*; et al.* Conversion of human fibroblasts into functional cardiomyocytes by small molecules. *Science* **2016**, 352(6290), 1216–1220.

33. Dimmeler, S.; Burchfield, J.; Zeiher, A.M. Cell-based therapy of myocardial infarction. *Arteriosclerosis, Thrombosis, and Vascular Biology* **2008**, 28(2), 208–216.

34. Rajala, K.; Pekkanen-Mattila, M.; Aalto-Setälä, K. Cardiac differentiation of pluripotent stem cells. *Stem Cells International* **2011**, 2011, 383709.

35. Neofytou, E.; O'Brien, C.G.; Couture, L.A.; Wu, J.C. Hurdles to clinical translation of human induced pluripotent stem cells. *The Journal of Clinical Investigation* **2015**, 125(7), 2551–2557.

36. Lund, R.J.; Närvä, E.; Lahesmaa, R. Genetic and epigenetic stability of human pluripotent stem cells. *Nature Reviews. Genetics* **2012**, 13(10), 732–744.

37. Lee, A.S.; Tang, C.; Rao, M.S.; Weissman, I.L.; Wu, J.C. Tumorigenicity as a clinical hurdle for pluripotent stem cell therapies. *Nature Medicine* **2013**, 19(8), 998–1004.

38. Itakura, G.; Kawabata, S.; Ando, M.; Nishiyama, Y.; Sugai, K.; Ozaki, M.; Iida, T.; Ookubo, T.; Kojima, K.; Kashiwagi, R.*; et al.* Fail-Safe System against Potential Tumorigenicity after Transplantation of iPSC Derivatives. *Stem Cell Reports* **2017**, 8(3), 673–684.

39. Zhao, T.; Zhang, Z.-N.; Rong, Z.; Xu, Y. Immunogenicity of induced pluripotent stem cells. *Nature* **2011**, 474(7350), 212–215.

40. Shi, Y.; Inoue, H.; Wu, J.C.; Yamanaka, S. Induced pluripotent stem cell technology: a decade of progress. *Nature Reviews. Drug Discovery* **2017**, 16(2), 115–130.

41. Sugita, S.; Mandai, M.; Kamao, H.; Takahashi, M. Immunological aspects of RPE cell transplantation. *Progress in Retinal and Eye Research* **2021**, 100950.

42. Zhu, W.; Godwin, C.R.; Cheng, L.; Scheetz, T.E.; Kuehn, M.H. Transplantation of iPSC-TM stimulates division of trabecular meshwork cells in human eyes. *Scientific Reports* **2020**, 10(1), 2905.

43. Ziegler, S.; Pries, V.; Hedberg, C.; Waldmann, H. Target identification for small bioactive molecules: finding the needle in the haystack. *Angewandte Chemie International Edition* **2013**, 52(10), 2744–2792.

44. Lee, J.A.; Berg, E.L. Neoclassic drug discovery: the case for lead generation using phenotypic and functional approaches. *Journal of Biomolecular Screening* **2013**, 18(10), 1143–1155.

45. Moffat, J.G.; Vincent, F.; Lee, J.A.; Eder, J.; Prunotto, M. Opportunities and challenges in phenotypic drug discovery: an industry perspective. *Nature Reviews. Drug Discovery* **2017**, 16(8), 531–543.

46. Ha, J.; Park, H.; Park, J.; Park, S.B. Recent advances in identifying protein targets in drug discovery. *Cell Chemical Biology* **2021**, 28(3), 394–423.

47. Ursu, A.; Schöler, H.R.; Waldmann, H. Small-molecule phenotypic screening with stem cells. *Nature Chemical Biology* **2017**, 13(6), 560–563.

48. Vandana, J.J.; Lacko, L.A.; Chen, S. Phenotypic technologies in stem cell biology. *Cell Chemical Biology* **2021**, 28(3), 257–270.

49. Esch, E.W.; Bahinski, A.; Huh, D. Organs-on-chips at the frontiers of drug discovery. *Nature Reviews. Drug Discovery* **2015**, 14(4), 248–260.

50. Sachs, N.; Ligt, J. de; Kopper, O.; Gogola, E.; Bounova, G.; Weeber, F.; Balgobind, A.V.; Wind, K.; Gracanin, A.; Begthel, H.*; et al.* A Living Biobank of Breast Cancer Organoids Captures Disease Heterogeneity. *Cell* **2018**, 172(1-2), 373-386.e10.

51. Muckom, R.; Bao, X.; Tran, E.; Chen, E.; Murugappan, A.; Dordick, J.S.; Clark, D.S.; Schaffer, D.V. High-throughput 3D screening for differentiation of hPSC-derived cell therapy candidates. *Science Advances* **2020**, 6(32), eaaz1457.

52. Skardal, A.; Shupe, T.; Atala, A. Organoid-on-a-chip and body-on-a-chip systems for drug screening and disease modeling. *Drug Discovery Today* **2016**, 21(9), 1399–1411.

53. Sung, J.H.; Wang, Y.I.; Narasimhan Sriram, N.; Jackson, M.; Long, C.; Hickman, J.J.; Shuler, M.L. Recent Advances in Body-on-a-Chip Systems. *Analytical Chemistry* **2019**, 91(1), 330–351.

54. Oleaga, C.; Riu, A.; Rothemund, S.; Lavado, A.; McAleer, C.W.; Long, C.J.; Persaud, K.; Narasimhan, N.S.; Tran, M.; Roles, J.*; et al.* Investigation of the effect of hepatic metabolism on off-target cardiotoxicity in a multi-organ human-on-a-chip system. *Biomaterials* **2018**, 182, 176–190.

55. Yang, L.; Han, Y.; Nilsson-Payant, B.E.; Gupta, V.; Wang, P.; Duan, X.; Tang, X.; Zhu, J.; Zhao, Z.; Jaffré, F.*; et al.* A Human Pluripotent Stem Cell-based Platform to Study SARS-CoV-2 Tropism and Model Virus Infection in Human Cells and Organoids. *Cell Stem Cell* **2020**, 27(1), 125-136.e7.

56. Baell, J.B.; Holloway, G.A. New substructure filters for removal of pan assay interference compounds (PAINS) from screening libraries and for their exclusion in bioassays. *Journal of Medicinal Chemistry* **2010**, 53(7), 2719–2740.

57. Dahlin, J.L.; Auld, D.S.; Rothenaigner, I.; Haney, S.; Sexton, J.Z.; Nissink, J.W.M.; Walsh, J.; Lee, J.A.; Strelow, J.M.; Willard, F.S.*; et al.* Nuisance compounds in cellular assays. *Cell Chemical Biology* **2021**, 28(3), 356–370.

58. Tummino, T.A.; Rezelj, V.V.; Fischer, B.; Fischer, A.; O'Meara, M.J.; Monel, B.; Vallet, T.; White, K.M.; Zhang, Z.; Alon, A.*; et al.* Drug-induced phospholipidosis confounds drug repurposing for SARS-CoV-2. *Science* **2021**, 373(6554), 541–547.

59. Kaelin, W.G. Common pitfalls in preclinical cancer target validation. *Nature Reviews. Cancer* **2017**, 17(7), 425–440.

60. Rose, F.; Basu, S.; Rexhepaj, E.; Chauchereau, A.; Del Nery, E.; Genovesio, A. Compound Functional Prediction Using Multiple Unrelated Morphological Profiling Assays. *SLAS technology* **2018**, 23(3), 243–251.

61. Ziegler, S.; Sievers, S.; Waldmann, H. Morphological profiling of small molecules. *Cell Chemical Biology* **2021**, 28(3), 300–319.

62. Sieber, C.; Kopf, J.; Hiepen, C.; Knaus, P. Recent advances in BMP receptor signaling. *Cytokine & Growth Factor Reviews* **2009**, 20(5-6), 343–355.

63. Di Chen; Zhao, M.; Mundy, G.R. Bone morphogenetic proteins. *Growth Factors* **2004**, 22(4), 233–241.

64. Urist, M.R. Bone: formation by autoinduction. *Science* **1965**, 150(3698), 893–899.

65. Urist, M.R.; Strates, B.S. Bone morphogenetic protein. *Journal of Dental Research* **1971**, 50(6), 1392–1406.

66. Chen, D.; Ji, X.; Harris, M.A.; Feng, J.Q.; Karsenty, G.; Celeste, A.J.; Rosen, V.; Mundy, G.R.; Harris, S.E. Differential roles for bone morphogenetic protein (BMP) receptor type IB and IA in differentiation and specification of mesenchymal precursor cells to osteoblast and adipocyte lineages. *The Journal of Cell Biology* **1998**, 142(1), 295–305.

67. Xu, R.-H.; Chen, X.; Li, D.S.; Li, R.; Addicks, G.C.; Glennon, C.; Zwaka, T.P.; Thomson, J.A. BMP4 initiates human embryonic stem cell differentiation to trophoblast. *Nature Biotechnology* **2002**, 20(12), 1261–1264.

68. Schultheiss, T.M.; Burch, J.B.; Lassar, A.B. A role for bone morphogenetic proteins in the induction of cardiac myogenesis. *Genes & Development* **1997**, 11(4), 451–462.

69. Bragdon, B.; Moseychuk, O.; Saldanha, S.; King, D.; Julian, J.; Nohe, A. Bone morphogenetic proteins: a critical review. *Cellular Signalling* **2011**, 23(4), 609–620.

70. Felin, J.E.; Mayo, J.L.; Loos, T.J.; Jensen, J.D.; Sperry, D.K.; Gaufin, S.L.; Meinhart, C.A.; Moss, J.B.; Bridgewater, L.C. Nuclear variants of bone morphogenetic proteins. *BMC Cell Biology* **2010**, 11, 20.

71. Rogers, A.C.; Nichols, B.A.; Loos, T.J.; Bridgewater, L.C. Nuclear Bmp4 interacts with the SCF E3 ubiquitin ligase complex and inhibits the cell cycle. *The FASEB Journal* **2012**, 26(S1).

72. Truksa, J.; Peng, H.; Lee, P.; Beutler, E. Bone morphogenetic proteins 2, 4, and 9 stimulate murine hepcidin 1 expression independently of Hfe, transferrin receptor 2 (Tfr2), and IL-6. *Proceedings of the National Academy of Sciences of the United States of America* **2006**, 103(27), 10289–10293.

73. Chen, C.; Ware, S.M.; Sato, A.; Houston-Hawkins, D.E.; Habas, R.; Matzuk, M.M.; Shen, M.M.; Brown, C.W. The Vg1-related protein Gdf3 acts in a Nodal signaling pathway in the pre-gastrulation mouse embryo. *Development* **2006**, 133(2), 319–329.

74. Miyazono, K.; Kamiya, Y.; Morikawa, M. Bone morphogenetic protein receptors and signal transduction. *Journal of Biochemistry* **2010**, 147(1), 35–51.

75. Dijke, P. ten; Yamashita, H.; Sampath, T.K.; Reddi, A.H.; Estevez, M.; Riddle, D.L.; Ichijo, H.; Heldin, C.H.; Miyazono, K. Identification of type I receptors for osteogenic protein-1 and bone morphogenetic protein-4. *The Journal of Biological Chemistry* **1994**, 269(25), 16985–16988.

76. Ebisawa, T.; Tada, K.; Kitajima, I.; Tojo, K.; Sampath, T.K.; Kawabata, M.; Miyazono, K.; Imamura, T. Characterization of bone morphogenetic protein-6 signaling pathways in osteoblast differentiation. *Journal of Cell Science* **1999**, 112(20), 3519–3527.

77. Hollnagel, A.; Oehlmann, V.; Heymer, J.; Rüther, U.; Nordheim, A. Id genes are direct targets of bone morphogenetic protein induction in embryonic stem cells. *The Journal of Biological Chemistry* **1999**, 274(28), 19838–19845.

78. Massagué, J.; Seoane, J.; Wotton, D. Smad transcription factors. *Genes & Development* **2005**, 19(23), 2783–2810.

79. Massagué, J. How cells read TGF-beta signals. *Nature Reviews. Molecular Cell Biology* **2000**, 1(3), 169–178.

80. Truksa, J.; Lee, P.; Beutler, E. Two BMP responsive elements, STAT, and bZIP/HNF4/COUP motifs of the hepcidin promoter are critical for BMP, SMAD1, and HJV responsiveness. *Blood* **2009**, 113(3), 688–695.

81. Karaulanov, E.; Knöchel, W.; Niehrs, C. Transcriptional regulation of BMP4 synexpression in transgenic Xenopus. *The EMBO Journal* **2004**, 23(4), 844–856.

82. Ishida, W.; Hamamoto, T.; Kusanagi, K.; Yagi, K.; Kawabata, M.; Takehara, K.; Sampath, T.K.; Kato, M.; Miyazono, K. Smad6 is a Smad1/5-induced smad inhibitor. Characterization of bone morphogenetic protein-responsive element in the mouse Smad6 promoter. *The Journal of Biological Chemistry* **2000**, 275(9), 6075–6079.

83. Korchynskyi, O.; Dijke, P. ten. Identification and functional characterization of distinct critically important bone morphogenetic protein-specific response elements in the Id1 promoter. *The Journal of Biological Chemistry* **2002**, 277(7), 4883–4891.

84. López-Rovira, T.; Chalaux, E.; Massagué, J.; Rosa, J.L.; Ventura, F. Direct binding of Smad1 and Smad4 to two distinct motifs mediates bone morphogenetic protein-specific transcriptional activation of Id1 gene. *The Journal of Biological Chemistry* **2002**, 277(5), 3176–3185.

85. Tsukamoto, S.; Mizuta, T.; Fujimoto, M.; Ohte, S.; Osawa, K.; Miyamoto, A.; Yoneyama, K.; Murata, E.; Machiya, A.; Jimi, E.*; et al.* Smad9 is a new type of transcriptional regulator in bone morphogenetic protein signaling. *Scientific Reports* **2014**, 4, 7596.

86. Wu, M.; Chen, G.; Li, Y.-P. TGF-β and BMP signaling in osteoblast, skeletal development, and bone formation, homeostasis and disease. *Bone Research* **2016**, 4, 16009.

87. Pyrowolakis, G.; Hartmann, B.; Müller, B.; Basler, K.; Affolter, M. A simple molecular complex mediates widespread BMP-induced repression during Drosophila development. *Developmental Cell* **2004**, 7(2), 229–240.

88. Hata, A.; Seoane, J.; Lagna, G.; Montalvo, E.; Hemmati-Brivanlou, A.; Massagué, J. OAZ Uses Distinct DNA- and Protein-Binding Zinc Fingers in Separate BMP-Smad and Olf Signaling Pathways. *Cell* **2000**, 100(2), 229–240.

89. Lee, H.-S.; Ja Park, M.; Lee, S.-Y.; Hwang, Y.-S.; Lee, H.; Roh, D.-H.; Kim, J.-I.; Park, J.-B.; Lee, J.-Y.; Kung, H.*; et al.* Transcriptional regulation of Xbr-1a/Xvent-2 homeobox gene: analysis of its promoter region. *Biochemical and Biophysical Research Communications* **2002**, 298(5), 815–823.

90. Zhong, Y.; Holland, P.W.H. The dynamics of vertebrate homeobox gene evolution: gain and loss of genes in mouse and human lineages. *BMC Evolutionary Biology* **2011**, 11, 169.

91. Derynck, R.; Zhang, Y.E. Smad-dependent and Smad-independent pathways in TGF-beta family signalling. *Nature* **2003**, 425(6958), 577–584.

92. Hoffmann, A.; Preobrazhenska, O.; Wodarczyk, C.; Medler, Y.; Winkel, A.; Shahab, S.; Huylebroeck, D.; Gross, G.; Verschueren, K. Transforming growth factor-beta-activated kinase-1 (TAK1), a MAP3K, interacts with Smad proteins and interferes with osteogenesis in murine mesenchymal progenitors. *The Journal of Biological Chemistry* **2005**, 280(29), 27271–27283.

93. Shibuya, H.; Iwata, H.; Masuyama, N.; Gotoh, Y.; Yamaguchi, K.; Irie, K.; Matsumoto, K.; Nishida, E.; Ueno, N. Role of TAK1 and TAB1 in BMP signaling in early Xenopus development. *The EMBO Journal* **1998**, 17(4), 1019–1028.

94. Yamaguchi, K.; Nagai, S.; Ninomiya-Tsuji, J.; Nishita, M.; Tamai, K.; Irie, K.; Ueno, N.; Nishida, E.; Shibuya, H.; Matsumoto, K. XIAP, a cellular member of the inhibitor of apoptosis protein family, links the receptors to TAB1-TAK1 in the BMP signaling pathway. *The EMBO Journal* **1999**, 18(1), 179–187.

95. Goswami, M.; Uzgare, A.R.; Sater, A.K. Regulation of MAP kinase by the BMP-4/TAK1 pathway in Xenopus ectoderm. *Developmental Biology* **2001**, 236(2), 259–270.

96. Kimura, N.; Matsuo, R.; Shibuya, H.; Nakashima, K.; Taga, T. BMP2-induced apoptosis is mediated by activation of the TAK1-p38 kinase pathway that is negatively regulated by Smad6. *The Journal of Biological Chemistry* **2000**, 275(23), 17647–17652.

97. Lai, C.-F.; Cheng, S.-L. Signal transductions induced by bone morphogenetic protein-2 and transforming growth factor-beta in normal human osteoblastic cells. *The Journal of Biological Chemistry* **2002**, 277(18), 15514–15522.

98. Nakamura, K.; Shirai, T.; Morishita, S.; Uchida, S.; Saeki-Miura, K.; Makishima, F. p38 mitogen-activated protein kinase functionally contributes to chondrogenesis induced by growth/differentiation factor-5 in ATDC5 cells. *Experimental Cell Research* **1999**, 250(2), 351–363.

99. Yang, G.; Yuan, G.; Li, X.; Liu, P.; Chen, Z.; Fan, M. BMP-2 induction of Dlx3 expression is mediated by p38/Smad5 signaling pathway in osteoblastic MC3T3-E1 cells. *Journal of Cellular Physiology* **2014**, 229(7), 943–954.

100. Mukherjee, A.; Rotwein, P. Akt promotes BMP2-mediated osteoblast differentiation and bone development. *Journal of Cell Science* **2009**, 122(Pt 5), 716–726.

101. Ghosh-Choudhury, N.; Abboud, S.L.; Nishimura, R.; Celeste, A.; Mahimainathan, L.; Choudhury, G.G. Requirement of BMP-2-induced phosphatidylinositol 3-kinase and Akt serine/threonine kinase in osteoblast differentiation and Smad-dependent BMP-2 gene transcription. *The Journal of Biological Chemistry* **2002**, 277(36), 33361–33368.

102. Viñals, F.; López-Rovira, T.; Rosa, J.L.; Ventura, F. Inhibition of PI3K/p70 S6K and p38 MAPK cascades increases osteoblastic differentiation induced by BMP-2. *FEBS Letters* **2002**, 510(1-2), 99–104.

103. Gazzerro, E.; Canalis, E. Bone morphogenetic proteins and their antagonists. *Reviews in Endocrine & Metabolic Disorders* **2006**, 7(1-2), 51–65.

104. Krause, C.; Guzman, A.; Knaus, P. Noggin. *The International Journal of Biochemistry & Cell Biology* **2011**, 43(4), 478–481.

105. Zimmerman, L.B.; Jesús-Escobar, J.M. de; Harland, R.M. The Spemann Organizer Signal noggin Binds and Inactivates Bone Morphogenetic Protein 4. *Cell* **1996**, 86(4), 599–606.

106. Bénazet, J.-D.; Bischofberger, M.; Tiecke, E.; Gonçalves, A.; Martin, J.F.; Zuniga, A.; Naef, F.; Zeller, R. A self-regulatory system of interlinked signaling feedback loops controls mouse limb patterning. *Science* **2009**, 323(5917), 1050–1053.

107. Piccolo, S.; Agius, E.; Leyns, L.; Bhattacharyya, S.; Grunz, H.; Bouwmeester, T.; Robertis, E.M. de. The head inducer Cerberus is a multifunctional antagonist of Nodal, BMP and Wnt signals. *Nature* **1999**, 397(6721), 707–710.

108. Foley, A.C.; Korol, O.; Timmer, A.M.; Mercola, M. Multiple functions of Cerberus cooperate to induce heart downstream of Nodal. *Developmental Biology* **2007**, 303(1), 57–65.

109. Takada, T.; Katagiri, T.; Ifuku, M.; Morimura, N.; Kobayashi, M.; Hasegawa, K.; Ogamo, A.; Kamijo, R. Sulfated polysaccharides enhance the biological activities of bone morphogenetic proteins. *The Journal of Biological Chemistry* **2003**, 278(44), 43229–43235.

110. Piccolo, S.; Agius, E.; Lu, B.; Goodman, S.; Dale, L.; Robertis, E.M. de. Cleavage of Chordin by Xolloid Metalloprotease Suggests a Role for Proteolytic Processing in the Regulation of Spemann Organizer Activity. *Cell* **1997**, 91(3), 407–416.

111. Kirkbride, K.C.; Townsend, T.A.; Bruinsma, M.W.; Barnett, J.V.; Blobe, G.C. Bone morphogenetic proteins signal through the transforming growth factor-beta type III receptor. *The Journal of Biological Chemistry* **2008**, 283(12), 7628–7637.

112. Samad, T.A.; Rebbapragada, A.; Bell, E.; Zhang, Y.; Sidis, Y.; Jeong, S.-J.; Campagna, J.A.; Perusini, S.; Fabrizio, D.A.; Schneyer, A.L.*; et al.* DRAGON, a bone morphogenetic protein co-receptor. *The Journal of Biological Chemistry* **2005**, 280(14), 14122–14129.

113. Brunner, P.; Hastar, N.; Kaehler, C.; Burdzinski, W.; Jatzlau, J.; Knaus, P. AMOT130 drives BMP-SMAD signaling at the apical membrane in polarized cells. *Molecular Biology of the Cell* **2020**, 31(2), 118–130.

114. Colucci, S.; Pagani, A.; Pettinato, M.; Artuso, I.; Nai, A.; Camaschella, C.; Silvestri, L. The immunophilin FKBP12 inhibits hepcidin expression by binding the BMP type I receptor ALK2 in hepatocytes. *Blood* **2017**, 130(19), 2111–2120.

115. Hartung, A.; Bitton-Worms, K.; Rechtman, M.M.; Wenzel, V.; Boergermann, J.H.; Hassel, S.; Henis, Y.I.; Knaus, P. Different routes of bone morphogenic protein (BMP) receptor endocytosis influence BMP signaling. *Molecular and Cellular Biology* **2006**, 26(20), 7791–7805.

116. Nohe, A.; Hassel, S.; Ehrlich, M.; Neubauer, F.; Sebald, W.; Henis, Y.I.; Knaus, P. The mode of bone morphogenetic protein (BMP) receptor oligomerization determines different BMP-2 signaling pathways. *The Journal of Biological Chemistry* **2002**, 277(7), 5330–5338.

117. Bragdon, B.; Thinakaran, S.; Bonor, J.; Underhill, T.M.; Petersen, N.O.; Nohe, A. FRET reveals novel protein-receptor interaction of bone morphogenetic proteins receptors and adaptor protein 2 at the cell surface. *Biophysical Journal* **2009**, 97(5), 1428–1435.

118. Chen, Y.-G. Endocytic regulation of TGF-beta signaling. *Cell research* **2009**, 19(1), 58–70.

119. Nohe, A.; Keating, E.; Underhill, T.M.; Knaus, P.; Petersen, N.O. Dynamics and interaction of caveolin-1 isoforms with BMP-receptors. *Journal of Cell Science* **2005**, 118(Pt 3), 643–650.

120. Guzman, A.; Zelman-Femiak, M.; Boergermann, J.H.; Paschkowsky, S.; Kreuzaler, P.A.; Fratzl, P.; Harms, G.S.; Knaus, P. SMAD versus non-SMAD signaling is determined by lateral mobility of bone morphogenetic protein (BMP) receptors. *The Journal of Biological Chemistry* **2012**, 287(47), 39492–39504.

121. Ehrlich, M.; Horbelt, D.; Marom, B.; Knaus, P.; Henis, Y.I. Homomeric and heteromeric complexes among TGF-β and BMP receptors and their roles in signaling. *Cellular Signalling* **2011**, 23(9), 1424–1432.

122. Goto, K.; Kamiya, Y.; Imamura, T.; Miyazono, K.; Miyazawa, K. Selective inhibitory effects of Smad6 on bone morphogenetic protein type I receptors. *The Journal of Biological Chemistry* **2007**, 282(28), 20603–20611.

123. Murakami, G.; Watabe, T.; Takaoka, K.; Miyazono, K.; Imamura, T. Cooperative inhibition of bone morphogenetic protein signaling by Smurf1 and inhibitory Smads. *Molecular Biology of the Cell* **2003**, 14(7), 2809–2817.

124. Zhang, Y.; Chang, C.; Gehling, D.J.; Hemmati-Brivanlou, A.; Derynck, R. Regulation of Smad degradation and activity by Smurf2, an E3 ubiquitin ligase. *Proceedings of the National Academy of Sciences of the United States of America* **2001**, 98(3), 974–979.

125. Inoue, Y.; Imamura, T. Regulation of TGF-beta family signaling by E3 ubiquitin ligases. *Cancer Science* **2008**, 99(11), 2107–2112.

126. Itóh, S.; Landström, M.; Hermansson, A.; Itoh, F.; Heldin, C.H.; Heldin, N.E.; Dijke, P. ten. Transforming growth factor beta1 induces nuclear export of inhibitory Smad7. *The Journal of Biological Chemistry* **1998**, 273(44), 29195–29201.

127. Yan, X.; Liu, Z.; Chen, Y. Regulation of TGF-beta signaling by Smad7. *Acta Biochimica et Biophysica Sinica* **2009**, 41(4), 263–272.

128. Fuentealba, L.C.; Eivers, E.; Ikeda, A.; Hurtado, C.; Kuroda, H.; Pera, E.M.; Robertis, E.M. de. Integrating patterning signals: Wnt/GSK3 regulates the duration of the BMP/Smad1 signal. *Cell* **2007**, 131(5), 980–993.

129. Alarcón, C.; Zaromytidou, A.-I.; Xi, Q.; Gao, S.; Yu, J.; Fujisawa, S.; Barlas, A.; Miller, A.N.; Manova-Todorova, K.; Macias, M.J.*; et al.* Nuclear CDKs drive Smad transcriptional activation and turnover in BMP and TGF-beta pathways. *Cell* **2009**, 139(4), 757–769.

130. Shi, W.; Chang, C.; Nie, S.; Xie, S.; Wan, M.; Cao, X. Endofin acts as a Smad anchor for receptor activation in BMP signaling. *Journal of Cell Science* **2007**, 120(Pt 7), 1216–1224.

131. Zhang, F.; Qiu, T.; Wu, X.; Wan, C.; Shi, W.; Wang, Y.; Chen, J.; Wan, M.; Clemens, T.L.; Cao, X. Sustained BMP signaling in osteoblasts stimulates bone formation by promoting angiogenesis and osteoblast differentiation. *Journal of Bone and Mineral Research* **2009**, 24(7), 1224–1233.

132. Schwappacher, R.; Weiske, J.; Heining, E.; Ezerski, V.; Marom, B.; Henis, Y.I.; Huber, O.; Knaus, P. Novel crosstalk to BMP signalling: cGMP-dependent kinase I modulates BMP receptor and Smad activity. *The EMBO Journal* **2009**, 28(11), 1537–1550.

133. Rodríguez-Carballo, E.; Ulsamer, A.; Susperregui, A.R.G.; Manzanares-Céspedes, C.; Sánchez-García, E.; Bartrons, R.; Rosa, J.L.; Ventura, F. Conserved regulatory motifs in osteogenic gene promoters integrate cooperative effects of canonical Wnt and BMP pathways. *Journal of Bone and Mineral Research* **2011**, 26(4), 718–729.

134. Liu, Z.; Tang, Y.; Qiu, T.; Cao, X.; Clemens, T.L. A dishevelled-1/Smad1 interaction couples WNT and bone morphogenetic protein signaling pathways in uncommitted bone marrow stromal cells. *The Journal of Biological Chemistry* **2006**, 281(25), 17156–17163.

135. Guo, X.; Wang, X.-F. Signaling cross-talk between TGF-beta/BMP and other pathways. *Cell Research* **2009**, 19(1), 71–88.

136. Rios, I.; Alvarez-Rodríguez, R.; Martí, E.; Pons, S. Bmp2 antagonizes sonic hedgehog-mediated proliferation of cerebellar granule neurones through Smad5 signalling. *Development* **2004**, 131(13), 3159–3168.

137. Li, J.; Feng, J.; Liu, Y.; Ho, T.-V.; Grimes, W.; Ho, H.A.; Park, S.; Wang, S.; Chai, Y. BMP-SHH signaling network controls epithelial stem cell fate via regulation of its niche in the developing tooth. *Developmental Cell* **2015**, 33(2), 125–135.

138. Dahlqvist, C.; Blokzijl, A.; Chapman, G.; Falk, A.; Dannaeus, K.; Ibâñez, C.F.; Lendahl, U. Functional Notch signaling is required for BMP4-induced inhibition of myogenic differentiation. *Development* **2003**, 130(24), 6089–6099.

139. Itoh, F.; Itoh, S.; Goumans, M.-J.; Valdimarsdottir, G.; Iso, T.; Dotto, G.P.; Hamamori, Y.; Kedes, L.; Kato, M.; Dijke Pt, P. ten. Synergy and antagonism between Notch and BMP receptor signaling pathways in endothelial cells. *The EMBO Journal* **2004**, 23(3), 541–551.

140. Sapkota, G.; Alarcón, C.; Spagnoli, F.M.; Brivanlou, A.H.; Massagué, J. Balancing BMP signaling through integrated inputs into the Smad1 linker. *Molecular Cell* **2007**, 25(3), 441–454.

141. Little, S.C.; Mullins, M.C. Extracellular modulation of BMP activity in patterning the dorsoventral axis. *Birth Defects Research. Part C, Embryo Today: Reviews* **2006**, 78(3), 224–242.

142. Spemann, H.; Mangold, H. Induction of embryonic primordia by implantation of organizers from a different species. 1923. *The International Journal of Developmental Biology* **2001**, 45(1), 13–38.

143. Robertis, E.M. de; Kuroda, H. Dorsal-ventral patterning and neural induction in Xenopus embryos. *Annual Review of Cell and Developmental Biology* **2004**, 20, 285–308.

144. Benezra, R.; Davis, R.L.; Lockshon, D.; Turner, D.L.; Weintraub, H. The protein Id: A negative regulator of helix-loop-helix DNA binding proteins. *Cell* **1990**, 61(1), 49–59.

145. Qi, X.; Li, T.-G.; Hao, J.; Hu, J.; Wang, J.; Simmons, H.; Miura, S.; Mishina, Y.; Zhao, G.-Q. BMP4 supports self-renewal of embryonic stem cells by inhibiting mitogen-activated protein kinase pathways. *Proceedings of the National Academy of Sciences of the United States of America* **2004**, 101(16), 6027–6032.

146. Ying, Q.-L.; Wray, J.; Nichols, J.; Batlle-Morera, L.; Doble, B.; Woodgett, J.; Cohen, P.; Smith, A. The ground state of embryonic stem cell self-renewal. *Nature* **2008**, 453(7194), 519–523.

147. Yuasa, S.; Itabashi, Y.; Koshimizu, U.; Tanaka, T.; Sugimura, K.; Kinoshita, M.; Hattori, F.; Fukami, S.; Shimazaki, T.; Ogawa, S.*; et al.* Transient inhibition of BMP signaling by Noggin induces cardiomyocyte differentiation of mouse embryonic stem cells. *Nature Biotechnology* **2005**, 23(5), 607–611.

148. Frank, S.; Zhang, M.; Schöler, H.R.; Greber, B. Small molecule-assisted, line-independent maintenance of human pluripotent stem cells in defined conditions. *PloS One* **2012**, 7(7), e41958.

149. Gunne-Braden, A.; Sullivan, A.; Gharibi, B.; Sheriff, R.S.M.; Maity, A.; Wang, Y.-F.; Edwards, A.; Jiang, M.; Howell, M.; Goldstone, R.*; et al.* GATA3 Mediates a Fast, Irreversible Commitment to BMP4-Driven Differentiation in Human Embryonic Stem Cells. *Cell Stem Cell* **2020**, 26(5), 693-706.e9.

150. Rao, J.; Pfeiffer, M.J.; Frank, S.; Adachi, K.; Piccini, I.; Quaranta, R.; Araúzo-Bravo, M.; Schwarz, J.; Schade, D.; Leidel, S.*; et al.* Stepwise Clearance of Repressive Roadblocks Drives Cardiac Induction in Human ESCs. *Cell Stem Cell* **2016**, 18(3), 341–353.

151. Kehat, I.; Kenyagin-Karsenti, D.; Snir, M.; Segev, H.; Amit, M.; Gepstein, A.; Livne, E.; Binah, O.; Itskovitz-Eldor, J.; Gepstein, L. Human embryonic stem cells can differentiate into myocytes with structural and functional properties of cardiomyocytes. *The Journal of Clinical Investigation* **2001**, 108(3), 407–414.

152. Guzzo, R.M.; Foley, A.C.; Ibarra, Y.M.; Mercola, M. Signaling Pathways in Embryonic Heart Induction. *Advances in Developmental Biology* **2007**, 18, 117–151.

153. Später, D.; Hansson, E.M.; Zangi, L.; Chien, K.R. How to make a cardiomyocyte. *Development* **2014**, 141(23), 4418–4431.

154. Vincent, S.D.; Buckingham, M.E. How to Make a Heart. Current topics in developmental biology **2010**, 90, 1–41.

155. Jiao, K.; Kulessa, H.; Tompkins, K.; Zhou, Y.; Batts, L.; Baldwin, H.S.; Hogan, B.L.M. An essential role of Bmp4 in the atrioventricular septation of the mouse heart. *Genes & Development* **2003**, 17(19), 2362–2367.

156. Burridge, P.W.; Keller, G.; Gold, J.D.; Wu, J.C. Production of de novo cardiomyocytes: human pluripotent stem cell differentiation and direct reprogramming. *Cell Stem Cell* **2012**, 10(1), 16–28.

157. Dierickx, P.; Doevendans, P.A.; Geijsen, N.; van Laake, L.W. Embryonic template-based generation and purification of pluripotent stem cell-derived cardiomyocytes for heart repair. *Journal of Cardiovascular Translational Research* **2012**, 5(5), 566–580.

158. Verma, V.; Purnamawati, K.; Manasi; Shim, W. Steering signal transduction pathway towards cardiac lineage from human pluripotent stem cells: a review. *Cellular Signalling* **2013**, 25(5), 1096–1107.

159. Pfeiffer, M.J.; Quaranta, R.; Piccini, I.; Fell, J.; Rao, J.; Röpke, A.; Seebohm, G.; Greber, B. Cardiogenic programming of human pluripotent stem cells by dose-controlled activation of EOMES. *Nature Communications* **2018**, 9(1), 440.

160. Cunningham, T.J.; Yu, M.S.; McKeithan, W.L.; Spiering, S.; Carrette, F.; Huang, C.-T.; Bushway, P.J.; Tierney, M.; Albini, S.; Giacca, M.*; et al.* Id genes are essential for early heart formation. *Genes & Development* **2017**, 31(13), 1325–1338.

161. Noseda, M.; Peterkin, T.; Simões, F.C.; Patient, R.; Schneider, M.D. Cardiopoietic factors: extracellular signals for cardiac lineage commitment. *Circulation Research* **2011**, 108(1), 129–152.

162. Cai, W.; Albini, S.; Wei, K.; Willems, E.; Guzzo, R.M.; Tsuda, M.; Giordani, L.; Spiering, S.; Kurian, L.; Yeo, G.W.*; et al.* Coordinate Nodal and BMP inhibition directs Baf60c-dependent cardiomyocyte commitment. *Genes & Development* **2013**, 27(21), 2332–2344.

163. Zhang, M.; Schulte, J.S.; Heinick, A.; Piccini, I.; Rao, J.; Quaranta, R.; Zeuschner, D.; Malan, D.; Kim, K.-P.; Röpke, A.*; et al.* Universal cardiac induction of human pluripotent stem cells in two and three-dimensional formats: implications for in vitro maturation. *Stem Cells* **2015**, 33(5), 1456–1469.

164. Lian, X.; Zhang, J.; Azarin, S.M.; Zhu, K.; Hazeltine, L.B.; Bao, X.; Hsiao, C.; Kamp, T.J.; Palecek, S.P. Directed cardiomyocyte differentiation from human pluripotent stem cells by modulating Wnt/β-catenin signaling under fully defined conditions. *Nature Protocols* **2013**, 8(1), 162–175.

165. Burridge, P.W.; Matsa, E.; Shukla, P.; Lin, Z.C.; Churko, J.M.; Ebert, A.D.; Lan, F.; Diecke, S.; Huber, B.; Mordwinkin, N.M.*; et al.* Chemically defined generation of human cardiomyocytes. *Nature Methods* **2014**, 11(8), 855–860.

166. Lanier, M.; Schade, D.; Willems, E.; Tsuda, M.; Spiering, S.; Kalisiak, J.; Mercola, M.; Cashman, J.R. Wnt inhibition correlates with human embryonic stem cell cardiomyogenesis: a structure-activity relationship study based on inhibitors for the Wnt response. *Journal of Medicinal Chemistry* **2012**, 55(2), 697–708.

167. Willems, E.; Lanier, M.; Forte, E.; Lo, F.; Cashman, J.; Mercola, M. A chemical biology approach to myocardial regeneration. *Journal of Cardiovascular Translational Research* **2011**, 4(3), 340–350.

168. Wang, H.; Hao, J.; Hong, C.C. Cardiac induction of embryonic stem cells by a small molecule inhibitor of Wnt/β-catenin signaling. *ACS Chemical Biology* **2011**, 6(2), 192–197.

169. Hao, J.; Daleo, M.A.; Murphy, C.K.; Yu, P.B.; Ho, J.N.; Hu, J.; Peterson, R.T.; Hatzopoulos, A.K.; Hong, C.C. Dorsomorphin, a selective small molecule inhibitor of BMP signaling, promotes cardiomyogenesis in embryonic stem cells. *PloS One* **2008**, 3(8), e2904.

170. Tojo, M.; Hamashima, Y.; Hanyu, A.; Kajimoto, T.; Saitoh, M.; Miyazono, K.; Node, M.; Imamura, T. The ALK-5 inhibitor A-83-01 inhibits Smad signaling and epithelial-to-mesenchymal transition by transforming growth factor-beta. *Cancer Science* **2005**, 96(11), 791–800.

171. Willems, E.; Cabral-Teixeira, J.; Schade, D.; Cai, W.; Reeves, P.; Bushway, P.J.; Lanier, M.; Walsh, C.; Kirchhausen, T.; Izpisua Belmonte, J.C.*; et al.* Small molecule-mediated TGF-β type II receptor degradation promotes cardiomyogenesis in embryonic stem cells. *Cell Stem Cell* **2012**, 11(2), 242–252.

172. Schade, D.; Lanier, M.; Willems, E.; Okolotowicz, K.; Bushway, P.; Wahlquist, C.; Gilley, C.; Mercola, M.; Cashman, J.R. Synthesis and SAR of b-annulated 1,4-dihydropyridines define cardiomyogenic compounds as novel inhibitors of TGFβ signaling. *Journal of Medicinal Chemistry* **2012**, 55(22), 9946–9957.

173. Metzger, J.J.; Simunovic, M.; Brivanlou, A.H. Synthetic embryology: controlling geometry to model early mammalian development. *Current Opinion in Genetics & Development* **2018**, 52, 86–91.

174. Warmflash, A.; Sorre, B.; Etoc, F.; Siggia, E.D.; Brivanlou, A.H. A method to recapitulate early embryonic spatial patterning in human embryonic stem cells. *Nature Methods* **2014**, 11(8), 847–854.

175. Martyn, I.; Kanno, T.Y.; Ruzo, A.; Siggia, E.D.; Brivanlou, A.H. Self-organization of a human organizer by combined Wnt and Nodal signalling. *Nature* **2018**, 558(7708), 132–135.

176. Hofbauer, P.; Jahnel, S.M.; Papai, N.; Giesshammer, M.; Deyett, A.; Schmidt, C.; Penc, M.; Tavernini, K.; Grdseloff, N.; Meledeth, C.*; et al.* Cardioids reveal self-organizing principles of human cardiogenesis. *Cell* **2021**, 184(12), 3299-3317.e22.

177. Rossi, G.; Broguiere, N.; Miyamoto, M.; Boni, A.; Guiet, R.; Girgin, M.; Kelly, R.G.; Kwon, C.; Lutolf, M.P. Capturing Cardiogenesis in Gastruloids. *Cell Stem Cell* **2021**, 28(2), 230-240.e6.

178. Majidinia, M.; Sadeghpour, A.; Yousefi, B. The roles of signaling pathways in bone repair and regeneration. *Journal of Cellular Physiology* **2018**, 233(4), 2937–2948.

179. Berendsen, A.D.; Olsen, B.R. Bone development. *Bone* **2015**, 80, 14–18.

180. Da Silva Madaleno, C.; Jatzlau, J.; Knaus, P. BMP signalling in a mechanical context - Implications for bone biology. *Bone* **2020**, 137, 115416.

181. Crane, J.L.; Xian, L.; Cao, X. Role of TGF-β Signaling in Coupling Bone Remodeling. *Methods in Molecular Biology* **2016**, 1344, 287–300.

182. Zou, M.-L.; Chen, Z.-H.; Teng, Y.-Y.; Liu, S.-Y.; Jia, Y.; Zhang, K.-W.; Sun, Z.-L.; Wu, J.-J.; Yuan, Z.-D.; Feng, Y.*; et al.* The Smad Dependent TGF-β and BMP Signaling Pathway in Bone Remodeling and Therapies. *Frontiers in Molecular Biosciences* **2021**, 8, 593310.

183. Rutkovskiy, A.; Stensløkken, K.-O.; Vaage, I.J. Osteoblast Differentiation at a Glance. *Medical Science Monitor Basic Research* **2016**, 22, 95–106.

184. Amarasekara, D.S.; Kim, S.; Rho, J. Regulation of Osteoblast Differentiation by Cytokine Networks. *International Journal of Molecular Sciences* **2021**, 22(6).

185. Kang, Q.; Song, W.-X.; Luo, Q.; Tang, N.; Luo, J.; Luo, X.; Chen, J.; Bi, Y.; He, B.-C.; Park, J.K.*; et al.* A comprehensive analysis of the dual roles of BMPs in regulating adipogenic and osteogenic differentiation of mesenchymal progenitor cells. *Stem Cells and Development* **2009**, 18(4), 545–559.

186. Cheng, H.; Jiang, W.; Phillips, F.; Haydon, R.; Peng, Y.; Zhou, L.; Luu, H.; An, N.; Breyer, B.; Vanichakarn, P.*; et al.* Osteogenic activity of the fourteen types of human bone morphogenetic proteins (BMPs). *Urologic Oncology: Seminars and Original Investigations* **2004**, 22(1), 79–80.

187. Tang, Q.-Q.; Otto, T.C.; Lane, M.D. Commitment of C3H10T1/2 pluripotent stem cells to the adipocyte lineage. *Proceedings of the National Academy of Sciences of the United States of America* **2004**, 101(26), 9607–9611.

188. Li, X.; Cao, X. BMP signaling and skeletogenesis. *Annals of the New York Academy of Sciences* **2006**, 1068, 26–40.

189. Katagiri, T.; Yamaguchi, A.; Komaki, M.; Abe, E.; Takahashi, N.; Ikeda, T.; Rosen, V.; Wozney, J.M.; Fujisawa-Sehara, A.; Suda, T. Bone morphogenetic protein-2 converts the differentiation pathway of C2C12 myoblasts into the osteoblast lineage. *The Journal of Cell Biology* **1994**, 127(6 Pt 1), 1755–1766.

190. Sinha, K.M.; Zhou, X. Genetic and molecular control of osterix in skeletal formation. *Journal of Cellular Biochemistry* **2013**, 114(5), 975–984.

191. Nishimura, R.; Hata, K.; Harris, S.; Ikeda, F.; Yoneda, T. Core-binding factor α1 (Cbfa1) induces osteoblastic differentiation of C2C12 cells without interactions with Smad1 and Smad5. *Bone* **2002**, 31(2), 303–312.

192. Gallea, S.; Lallemand, F.; Atfi, A.; Rawadi, G.; Ramez, V.; Spinella-Jaegle, S.; Kawai, S.; Faucheu, C.; Huet, L.; Baron, R.*; et al.* Activation of mitogen-activated protein kinase cascades is involved in regulation of bone morphogenetic protein-2-induced osteoblast differentiation in pluripotent C2C12 cells. *Bone* **2001**, 28(5), 491–498.

193. Rodríguez-Carballo, E.; Gámez, B.; Ventura, F. p38 MAPK Signaling in Osteoblast Differentiation. *Frontiers in Cell and Developmental Biology* **2016**, 4, 40.

194. Kim, H.J.; Kim, S.H. Tanshinone IIA enhances BMP-2-stimulated commitment of C2C12 cells into osteoblasts via p38 activation. *Amino Acids* **2010**, 39(5), 1217–1226.

195. Lin, S.; Svoboda, K.K.H.; Feng, J.Q.; Jiang, X. The biological function of type I receptors of bone morphogenetic protein in bone. *Bone Research* **2016**, 4, 16005.

196. Monroe, D.G.; McGee-Lawrence, M.E.; Oursler, M.J.; Westendorf, J.J. Update on Wnt signaling in bone cell biology and bone disease. *Gene* **2012**, 492(1), 1–18.

197. Styrkarsdottir, U.; Cazier, J.-B.; Kong, A.; Rolfsson, O.; Larsen, H.; Bjarnadottir, E.; Johannsdottir, V.D.; Sigurdardottir, M.S.; Bagger, Y.; Christiansen, C.*; et al.* Linkage of osteoporosis to chromosome 20p12 and association to BMP2. *PLoS Biology* **2003**, 1(3), E69.

198. Devlin, R.D.; Du, Z.; Pereira, R.C.; Kimble, R.B.; Economides, A.N.; Jorgetti, V.; Canalis, E. Skeletal overexpression of noggin results in osteopenia and reduced bone formation. *Endocrinology* **2003**, 144(5), 1972–1978.

199. Winkler, D.G.; Sutherland, M.K.; Geoghegan, J.C.; Yu, C.; Hayes, T.; Skonier, J.E.; Shpektor, D.; Jonas, M.; Kovacevich, B.R.; Staehling-Hampton, K.*; et al.* Osteocyte control of bone formation via sclerostin, a novel BMP antagonist. *The EMBO Journal* **2003**, 22(23), 6267–6276.

200. Sutherland, M.K.; Geoghegan, J.C.; Yu, C.; Winkler, D.G.; Latham, J.A. Unique regulation of SOST, the sclerosteosis gene, by BMPs and steroid hormones in human osteoblasts. *Bone* **2004**, 35(2), 448–454.

201. Albilia, J.B.; Tenenbaum, H.C.; Clokie, C.M.L.; Walt, D.R.; Baker, G.I.; Psutka, D.J.; Backstein, D.; Peel, S.A.F. Serum levels of BMP-2, 4, 7 and AHSG in patients with degenerative joint disease requiring total arthroplasty of the hip and temporomandibular joints. *Journal of Orthopaedic Research* **2013**, 31(1), 44–52.

202. Hunter, D.J.; Pike, M.C.; Jonas, B.L.; Kissin, E.; Krop, J.; McAlindon, T. Phase 1 safety and tolerability study of BMP-7 in symptomatic knee osteoarthritis. *BMC Musculoskeletal Disorders* **2010**, 11, 232.

203. Wang, R.N.; Green, J.; Wang, Z.; Deng, Y.; Qiao, M.; Peabody, M.; Zhang, Q.; Ye, J.; Yan, Z.; Denduluri, S.*; et al.* Bone Morphogenetic Protein (BMP) signaling in development and human diseases. *Genes & Diseases* **2014**, 1(1), 87–105.

204. Song, G.-A.; Kim, H.-J.; Woo, K.-M.; Baek, J.-H.; Kim, G.-S.; Choi, J.-Y.; Ryoo, H.-M. Molecular consequences of the ACVR1(R206H) mutation of fibrodysplasia ossificans progressiva. *The Journal of Biological Chemistry* **2010**, 285(29), 22542–22553.

205. Hildebrandt, S.; Kampfrath, B.; Fischer, K.; Hildebrand, L.; Haupt, J.; Stachelscheid, H.; Knaus, P. ActivinA Induced SMAD1/5 Signaling in an iPSC Derived EC Model of Fibrodysplasia Ossificans Progressiva (FOP) Can Be Rescued by the Drug Candidate Saracatinib. *Stem Cell Reviews and Reports* **2021**, 17(3), 1039–1052.

206. Lehmann, K.; Seemann, P.; Silan, F.; Goecke, T.O.; Irgang, S.; Kjaer, K.W.; Kjaergaard, S.; Mahoney, M.J.; Morlot, S.; Reissner, C.*; et al.* A new subtype of brachydactyly type B caused by point mutations in the bone morphogenetic protein antagonist NOGGIN. *American Journal of Human Genetics* **2007**, 81(2), 388–396.

207. Lehmann, K.; Seemann, P.; Stricker, S.; Sammar, M.; Meyer, B.; Süring, K.; Majewski, F.; Tinschert, S.; Grzeschik, K.-H.; Müller, D.*; et al.* Mutations in bone morphogenetic protein receptor 1B cause brachydactyly type A2. *Proceedings of the National Academy of Sciences of the United States of America* **2003**, 100(21), 12277–12282.

208. Dhiman, N.K.; Singh, A.K.; Sharma, N.K.; Jaiswara, C. Cleidocranial dysplasia. *National Journal of Maxillofacial Surgery* **2014**, 5(2), 206–208.

209. Kim, J.-M.; Yang, Y.-S.; Park, K.H.; Ge, X.; Xu, R.; Li, N.; Song, M.; Chun, H.; Bok, S.; Charles, J.F.*; et al.* A RUNX2 stabilization pathway mediates physiologic and pathologic bone formation. *Nature Communications* **2020**, 11(1), 2289.

210. Cai, J.; Pardali, E.; Sánchez-Duffhues, G.; Dijke, P. ten. BMP signaling in vascular diseases. *FEBS Letters* **2012**, 586(14), 1993–2002.

211. Jiang, Y.; Nohe, A.; Bragdon, B.; Tian, C.; Rudarakanchana, N.; Morrell, N.W.; Petersen, N.O. Trapping of BMP receptors in distinct membrane domains inhibits their function in pulmonary arterial hypertension. *American journal of physiology. Lung cellular and molecular physiology* **2011**, 301(2), L218-27.

212. Huang, H.; Song, T.-J.; Li, X.; Hu, L.; He, Q.; Liu, M.; Lane, M.D.; Tang, Q.-Q. BMP signaling pathway is required for commitment of C3H10T1/2 pluripotent stem cells to the adipocyte lineage. *Proceedings of the National Academy of Sciences of the United States of America* **2009**, 106(31), 12670–12675.

213. Elsen, M.; Raschke, S.; Tennagels, N.; Schwahn, U.; Jelenik, T.; Roden, M.; Romacho, T.; Eckel, J. BMP4 and BMP7 induce the white-to-brown transition of primary human adipose stem cells. *American journal of physiology. Cell Physiology* **2014**, 306(5), C431-40.

214. Perera, N.; Ritchie, R.H.; Tate, M. The Role of Bone Morphogenetic Proteins in Diabetic Complications. *ACS Pharmacology & Translational Science* **2020**, 3(1), 11–20.

215. Hussein, K.A.; Choksi, K.; Akeel, S.; Ahmad, S.; Megyerdi, S.; El-Sherbiny, M.; Nawaz, M.; Abu El-Asrar, A.; Al-Shabrawey, M. Bone morphogenetic protein 2: a potential new player in the pathogenesis of diabetic retinopathy. *Experimental Eye Research* **2014**, 125, 79–88.

216. Elmasry, K.; Habib, S.; Moustafa, M.; Al-Shabrawey, M. Bone Morphogenetic Proteins and Diabetic Retinopathy. *Biomolecules* **2021**, 11(4).

217. Katagiri, T.; Watabe, T. Bone Morphogenetic Proteins. *Cold Spring Harbor Perspectives in Biology* **2016**, 8(6).

218. Alarmo, E.-L.; Korhonen, T.; Kuukasjärvi, T.; Huhtala, H.; Holli, K.; Kallioniemi, A. Bone morphogenetic protein 7 expression associates with bone metastasis in breast carcinomas. *Annals of Oncology* **2008**, 19(2), 308–314.

219. Choi, S.; Yu, J.; Park, A.; Dubon, M.J.; Do, J.; Kim, Y.; Nam, D.; Noh, J.; Park, K.-S. BMP-4 enhances epithelial mesenchymal transition and cancer stem cell properties of breast cancer cells via Notch signaling. *Scientific Reports* **2019**, 9(1), 11724.

220. Helms, M.W.; Packeisen, J.; August, C.; Schittek, B.; Boecker, W.; Brandt, B.H.; Buerger, H. First evidence supporting a potential role for the BMP/SMAD pathway in the progression of oestrogen receptor-positive breast cancer. *The Journal of Pathology* **2005**, 206(3), 366–376.

221. Lai, T.-H.; Fong, Y.-C.; Fu, W.-M.; Yang, R.-S.; Tang, C.-H. Osteoblasts-derived BMP-2 enhances the motility of prostate cancer cells via activation of integrins. *The Prostate* **2008**, 68(12), 1341–1353.

222. Nguyen, A.; Scott, M.A.; Dry, S.M.; James, A.W. Roles of bone morphogenetic protein signaling in osteosarcoma. *International Orthopaedics* **2014**, 38(11), 2313–2322.

223. Clement, J.; Raida, M.; Sänger, J.; Bicknell, R.; Liu, J.; Naumann, A.; Geyer, A.; Waldau, A.; Hortschansky, P.; Schmidt, A.*; et al.* Bone morphogenetic protein 2 (BMP-2) induces in vitro invasion and in vivo hormone independent growth of breast carcinoma cells. *International Journal of Oncology* **2005**.

224. Owens, P.; Pickup, M.W.; Novitskiy, S.V.; Giltnane, J.M.; Gorska, A.E.; Hopkins, C.R.; Hong, C.C.; Moses, H.L. Inhibition of BMP signaling suppresses metastasis in mammary cancer. *Oncogene* **2015**, 34(19), 2437–2449.

225. Newman, J.H.; Augeri, D.J.; NeMoyer, R.; Malhotra, J.; Langenfeld, E.; Chesson, C.B.; Dobias, N.S.; Lee, M.J.; Tarabichi, S.; Jhawar, S.R.*; et al.* Novel bone morphogenetic protein receptor inhibitor JL5 suppresses tumor cell survival signaling and induces regression of human lung cancer. *Oncogene* **2018**, 37(27), 3672–3685.

226. Choi, Y.J.; Kim, S.T.; Park, K.H.; Oh, S.C.; Seo, J.H.; Shin, S.W.; Kim, J.S.; Kim, Y.H. The serum bone morphogenetic protein-2 level in non-small-cell lung cancer patients. *Medical Oncology* **2012**, 29(2), 582–588.

227. Voorneveld, P.W.; Stache, V.; Jacobs, R.J.; Smolders, E.; Sitters, A.I.; Liesker, A.; Korkmaz, K.S.; Lam, S.M.; Miranda, N.F.C.C. de; Morreau, H.*; et al.* Reduced expression of bone morphogenetic protein receptor IA in pancreatic cancer is associated with a poor prognosis. *British Journal of Vancer* **2013**, 109(7), 1805–1812.

228. Kowalczewski, C.J.; Saul, J.M. Biomaterials for the Delivery of Growth Factors and Other Therapeutic Agents in Tissue Engineering Approaches to Bone Regeneration. *Frontiers in Pharmacology* **2018**, 9, 513.

229. Carreira, A.C.; Lojudice, F.H.; Halcsik, E.; Navarro, R.D.; Sogayar, M.C.; Granjeiro, J.M. Bone morphogenetic proteins: facts, challenges, and future perspectives. *Journal of Dental Research* **2014**, 93(4), 335–345.

230. Werle, S.; AbuNahleh, K.; Boehm, H. Bone morphogenetic protein 7 and autologous bone graft in revision surgery for non-union after lumbar interbody fusion. *Archives of Orthopaedic and Trauma Surgery* **2016**, 136(8), 1041–1049.

231. DeVine, J.G.; Dettori, J.R.; France, J.C.; Brodt, E.; McGuire, R.A. The use of rhBMP in spine surgery: is there a cancer risk? *Evidence-Based Spine-Care Journal* **2012**, 3(2), 35–41.

232. Gottfried, O.N.; Dailey, A.T. Mesenchymal stem cell and gene therapies for spinal fusion. *Neurosurgery* **2008**, 63(3), 380-91; discussion 391-2.

233. Lowery, J.W.; Brookshire, B.; Rosen, V. A Survey of Strategies to Modulate the Bone Morphogenetic Protein Signaling Pathway: Current and Future Perspectives. *Stem Cells International* **2016**, 2016, 7290686.

234. Seol, Y.-J.; Park, Y.-J.; Lee, S.-C.; Kim, K.-H.; Lee, J.-Y.; Kim, T.-I.; Lee, Y.-M.; Ku, Y.; Rhyu, I.-C.; Han, S.-B.*; et al.* Enhanced osteogenic promotion around dental implants with synthetic binding motif mimicking bone morphogenetic protein (BMP)-2. *Journal of Biomedical Materials Research. Part A* **2006**, 77(3), 599–607.

235. Akkiraju, H.; Bonor, J.; Olli, K.; Bowen, C.; Bragdon, B.; Coombs, H.; Donahue, L.R.; Duncan, R.; Nohe, A. Systemic injection of CK2.3, a novel peptide acting downstream of bone morphogenetic protein receptor BMPRIa, leads to increased trabecular bone mass. *Journal of Orthopaedic Research* **2015**, 33(2), 208–215.

236. Neugebauer, J.M.; Kwon, S.; Kim, H.-S.; Donley, N.; Tilak, A.; Sopory, S.; Christian, J.L. The prodomain of BMP4 is necessary and sufficient to generate stable BMP4/7 heterodimers with enhanced bioactivity in vivo. *Proceedings of the National Academy of Sciences of the United States of America* **2015**, 112(18), E2307-16.

237. Kuroda, R.; Usas, A.; Kubo, S.; Corsi, K.; Peng, H.; Rose, T.; Cummins, J.; Fu, F.H.; Huard, J. Cartilage repair using bone morphogenetic protein 4 and muscle-derived stem cells. *Arthritis and Rheumatism* **2006**, 54(2), 433–442.

238. Bramlage, C.P.; Häupl, T.; Kaps, C.; Ungethüm, U.; Krenn, V.; Pruss, A.; Müller, G.A.; Strutz, F.; Burmester, G.-R. Decrease in expression of bone morphogenetic proteins 4 and 5 in synovial tissue of patients with osteoarthritis and rheumatoid arthritis. *Arthritis Research & Therapy* **2006**, 8(3), R58.

239. Wang, L.; Park, P.; Zhang, H.; La Marca, F.; Claeson, A.; Valdivia, J.; Lin, C.-Y. BMP-2 inhibits the tumorigenicity of cancer stem cells in human osteosarcoma OS99-1 cell line. *Cancer Biology & Therapy* **2011**, 11(5), 457–463.

240. Thompson, M.C.; Fuller, C.; Hogg, T.L.; Dalton, J.; Finkelstein, D.; Lau, C.C.; Chintagumpala, M.; Adesina, A.; Ashley, D.M.; Kellie, S.J.*; et al.* Genomics identifies medulloblastoma subgroups that are enriched for specific genetic alterations. *Journal of Clinical Oncology* **2006**, 24(12), 1924–1931.

241. Grimmer, M.R.; Weiss, W.A. BMPs oppose Math1 in cerebellar development and in medulloblastoma. *Genes & Development* **2008**, 22(6), 693–699.

242. Hardwick, J.C.; Kodach, L.L.; Offerhaus, G.J.; van den Brink, G.R. Bone morphogenetic protein signalling in colorectal cancer. *Nature Reviews. Cancer* **2008**, 8(10), 806–812.

243. Yu, P.B.; Hong, C.C.; Sachidanandan, C.; Babitt, J.L.; Deng, D.Y.; Hoyng, S.A.; Lin, H.Y.; Bloch, K.D.; Peterson, R.T. Dorsomorphin inhibits BMP signals required for embryogenesis and iron metabolism. *Nature Chemical Biology* **2008**, 4(1), 33–41.

244. Hao, J.; Ho, J.N.; Lewis, J.A.; Karim, K.A.; Daniels, R.N.; Gentry, P.R.; Hopkins, C.R.; Lindsley, C.W.; Hong, C.C. In vivo structure-activity relationship study of dorsomorphin analogues identifies selective VEGF and BMP inhibitors. *ACS Chemical Biology* **2010**, 5(2), 245–253.

245. Dasgupta, B.; Seibel, W. Compound C/Dorsomorphin: Its Use and Misuse as an AMPK Inhibitor. *Methods in Molecular Biology* **2018**, 1732, 195–202.

246. Ao, A.; Hao, J.; Hopkins, C.R.; Hong, C.C. DMH1, a novel BMP small molecule inhibitor, increases cardiomyocyte progenitors and promotes cardiac differentiation in mouse embryonic stem cells. *PloS One* **2012**, 7(7), e41627.

247. Cuny, G.D.; Yu, P.B.; Laha, J.K.; Xing, X.; Liu, J.-F.; Lai, C.S.; Deng, D.Y.; Sachidanandan, C.; Bloch, K.D.; Peterson, R.T. Structure-activity relationship study of bone morphogenetic protein (BMP) signaling inhibitors. *Bioorganic & Medicinal Chemistry Letters* **2008**, 18(15), 4388–4392.

248. Engers, D.W.; Frist, A.Y.; Lindsley, C.W.; Hong, C.C.; Hopkins, C.R. Synthesis and structure-activity relationships of a novel and selective bone morphogenetic protein receptor (BMP) inhibitor derived from the pyrazolo1.5-apyrimidine scaffold of dorsomorphin: the discovery of ML347 as an ALK2 versus ALK3 selective MLPCN probe. *Bioorganic & Medicinal Chemistry Letters* **2013**, 23(11), 3248–3252.

249. Boergermann, J.H.; Kopf, J.; Yu, P.B.; Knaus, P. Dorsomorphin and LDN-193189 inhibit BMP-mediated Smad, p38 and Akt signalling in C2C12 cells. *The International Journal of Biochemistry & Cell Biology* **2010**, 42(11), 1802–1807.

250. Yu, P.B.; Deng, D.Y.; Lai, C.S.; Hong, C.C.; Cuny, G.D.; Bouxsein, M.L.; Hong, D.W.; McManus, P.M.; Katagiri, T.; Sachidanandan, C.*; et al.* BMP type I receptor inhibition reduces heterotopic corrected ossification. *Nature Medicine* **2008**, 14(12), 1363–1369.

251. Kajimoto, H.; Kai, H.; Aoki, H.; Uchiwa, H.; Aoki, Y.; Yasuoka, S.; Anegawa, T.; Mishina, Y.; Suzuki, A.; Fukumoto, Y.*; et al.* BMP type I receptor inhibition attenuates endothelial dysfunction in mice with chronic kidney disease. *Kidney International* **2015**, 87(1), 128–136.

252. Lee, Y.-C.; Cheng, C.-J.; Bilen, M.A.; Lu, J.-F.; Satcher, R.L.; Yu-Lee, L.-Y.; Gallick, G.E.; Maity, S.N.; Lin, S.-H. BMP4 promotes prostate tumor growth in bone through osteogenesis. *Cancer Research* **2011**, 71(15), 5194–5203.

253. Derwall, M.; Malhotra, R.; Lai, C.S.; Beppu, Y.; Aikawa, E.; Seehra, J.S.; Zapol, W.M.; Bloch, K.D.; Yu, P.B. Inhibition of bone morphogenetic protein signaling reduces vascular calcification and atherosclerosis. *Arteriosclerosis, Thrombosis, and Vascular Biology* **2012**, 32(3), 613–622.

254. Vogt, J.; Traynor, R.; Sapkota, G.P. The specificities of small molecule inhibitors of the TGFß and BMP pathways. *Cellular Signalling* **2011**, 23(11), 1831–1842.

255. Mohedas, A.H.; Xing, X.; Armstrong, K.A.; Bullock, A.N.; Cuny, G.D.; Yu, P.B. Development of an ALK2-biased BMP type I receptor kinase inhibitor. *ACS Chemical Biology* **2013**, 8(6), 1291–1302.

256. Agarwal, S.; Loder, S.J.; Breuler, C.; Li, J.; Cholok, D.; Brownley, C.; Peterson, J.; Hsieh, H.H.; Drake, J.; Ranganathan, K.*; et al.* Strategic Targeting of Multiple BMP Receptors Prevents Trauma-Induced Heterotopic Ossification. *Molecular Therapy* **2017**, 25(8), 1974–1987.

257. Sanchez-Duffhues, G.; Williams, E.; Goumans, M.-J.; Heldin, C.-H.; Dijke, P. ten. Bone morphogenetic protein receptors: Structure, function and targeting by selective small molecule kinase inhibitors. *Bone* **2020**, 138, 115472.

258. Sanvitale, C.E.; Kerr, G.; Chaikuad, A.; Ramel, M.-C.; Mohedas, A.H.; Reichert, S.; Wang, Y.; Triffitt, J.T.; Cuny, G.D.; Yu, P.B.*; et al.* A new class of small molecule inhibitor of BMP signaling. *PloS One* **2013**, 8(4), e62721.

259. Mohedas, A.H.; Wang, Y.; Sanvitale, C.E.; Canning, P.; Choi, S.; Xing, X.; Bullock, A.N.; Cuny, G.D.; Yu, P.B. Structure-activity relationship of 3,5-diaryl-2-aminopyridine ALK2 inhibitors reveals unaltered binding affinity for fibrodysplasia ossificans progressiva causing mutants. *Journal of Medicinal Chemistry* **2014**, 57(19), 7900–7915.

260. Kausar, T.; Nayeem, S.M. Identification of small molecule inhibitors of ALK2: a virtual screening, density functional theory, and molecular dynamics simulations study. *Journal of Molecular Modeling* **2018**, 24(9), 262.

261. Sánchez-Duffhues, G.; Williams, E.; Benderitter, P.; Orlova, V.; van Wijhe, M.; Garcia de Vinuesa, A.; Kerr, G.; Caradec, J.; Lodder, K.; Boer, H.C. de*; et al.* Development of Macrocycle Kinase Inhibitors for ALK2 Using Fibrodysplasia Ossificans Progressiva-Derived Endothelial Cells. *JBMR Plus* **2019**, 3(11), e10230.

262. Goto, M.; Chow, J.; Muramoto, K.; Chiba, K.; Yamamoto, S.; Fujita, M.; Obaishi, H.; Tai, K.; Mizui, Y.; Tanaka, I.*; et al.* E6201 (3S,4R,5Z,8S,9S,11E)-14-(ethylamino)-8, 9,16-trihydroxy-3,4-dimethyl-3,4,9,19-tetrahydro-1H-2-benzoxacyclotetradecine-1,7(8H)-dione, a novel kinase inhibitor of mitogen-activated protein kinase/extracellular signal-regulated kinase kinase (MEK)-1 and MEK kinase-1: in vitro characterization of its anti-inflammatory and antihyperproliferative activities. *The Journal of Pharmacology and Experimental Therapeutics* **2009**, 331(2), 485–495.

263. Fortin, J.; Tian, R.; Zarrabi, I.; Hill, G.; Williams, E.; Sanchez-Duffhues, G.; Thorikay, M.; Ramachandran, P.; Siddaway, R.; Wong, J.F.*; et al.* Mutant ACVR1 Arrests Glial Cell Differentiation to Drive Tumorigenesis in Pediatric Gliomas. *Cancer Cell* **2020**, 37(3), 308-323.e12.

264. Valer, J.A.; Sánchez-de-Diego, C.; Gámez, B.; Mishina, Y.; Rosa, J.L.; Ventura, F. Inhibition of phosphatidylinositol 3-kinase α (PI3Kα) prevents heterotopic ossification. *EMBO Molecular Medicine* **2019**, 11(9), e10567.

265. Taşdemir, U.; Kirtay, M.; Keleş, A.; Çil, N.; Abban, G.; Dodurga, Y. Autogenous Tooth Bone Graft and Simvastatin Combination Effect on Bone Healing. *The Journal of Craniofacial Surgery* **2020**, 31(8), 2350–2354.

266. Feng, C.; Xiao, L.; Yu, J. C.; Li, D. Y.; Tang, T. Y.; Liao, W.; Wang, Z.-R.; & Lu, A. Q.. Simvastatin promotes osteogenic differentiation of mesenchymal stem cells in rat model of osteoporosis through BMP-2/Smads signaling pathway. *European Review for Medical and Pharmacological Sciences* **2020**, 24(1), 434-443.

267. Yang, J.; Li, X.; Al-Lamki, R.S.; Wu, C.; Weiss, A.; Berk, J.; Schermuly, R.T.; Morrell, N.W. Sildenafil potentiates bone morphogenetic protein signaling in pulmonary arterial smooth muscle cells and in experimental pulmonary hypertension. *Arteriosclerosis, Thrombosis, and Vascular Biology* **2013**, 33(1), 34–42.

268. Li, H.; Nie, B.; Du, Z.; Zhang, S.; Long, T.; Yue, B. Bacitracin promotes osteogenic differentiation of human bone marrow mesenchymal stem cells by stimulating the bone morphogenetic protein-2/Smad axis. *Biomedicine & Pharmacotherapy* **2018**, 103, 588–597.

269. Kim, H.-Y.; Park, S.-Y.; Choung, S.-Y. Enhancing effects of myricetin on the osteogenic differentiation of human periodontal ligament stem cells via BMP-2/Smad and ERK/JNK/p38 mitogen-activated protein kinase signaling pathway. *European Journal of Pharmacology* **2018**, 834, 84–91.

270. Vrijens, K.; Lin, W.; Cui, J.; Farmer, D.; Low, J.; Pronier, E.; Zeng, F.-Y.; Shelat, A.A.; Guy, K.; Taylor, M.R.*; et al.* Identification of small molecule activators of BMP signaling. *PloS One* **2013**, 8(3), e59045.

271. Genthe, J.R.; Min, J.; Farmer, D.M.; Shelat, A.A.; Grenet, J.A.; Lin, W.; Finkelstein, D.; Vrijens, K.; Chen, T.; Guy, R.K.*; et al.* Ventromorphins: A New Class of Small Molecule Activators of the Canonical BMP Signaling Pathway. *ACS Chemical Biology* **2017**, 12(9), 2436–2447.

272. Bradford, S.T.J.; Ranghini, E.J.; Grimley, E.; Lee, P.H.; Dressler, G.R. High-throughput screens for agonists of bone morphogenetic protein (BMP) signaling identify potent benzoxazole compounds. *The Journal of Biological Chemistry* **2019**, 294(9), 3125–3136.

273. Spiekerkoetter, E.; Tian, X.; Cai, J.; Hopper, R.K.; Sudheendra, D.; Li, C.G.; El-Bizri, N.; Sawada, H.; Haghighat, R.; Chan, R.*; et al.* FK506 activates BMPR2, rescues endothelial dysfunction, and reverses pulmonary hypertension. *The Journal of Clinical Investigation* **2013**, 123(8), 3600–3613.

274. Long, L.; Ormiston, M.L.; Yang, X.; Southwood, M.; Gräf, S.; Machado, R.D.; Mueller, M.; Kinzel, B.; Yung, L.M.; Wilkinson, J.M.*; et al.* Selective enhancement of endothelial BMPR-II with BMP9 reverses pulmonary arterial hypertension. *Nature Medicine* **2015**, 21(7), 777–785.

275. Spiekerkoetter, E.; Sung, Y.K.; Sudheendra, D.; Scott, V.; Del Rosario, P.; Bill, M.; Haddad, F.; Long-Boyle, J.; Hedlin, H.; Zamanian, R.T. Randomised placebo-controlled safety and tolerability trial of FK506 (tacrolimus) for pulmonary arterial hypertension. *The European Respiratory Journal* **2017**, 50(3).

276. Peiffer, B.J.; Le Qi; Ahmadi, A.R.; Wang, Y.; Guo, Z.; Peng, H.; Sun, Z.; Liu, J.O. Activation of BMP Signaling by FKBP12 Ligands Synergizes with Inhibition of CXCR4 to Accelerate Wound Healing. *Cell Chemical Biology* **2019**, 26(5), 652-661.e4.

277. Plikus, M.V.; Guerrero-Juarez, C.F.; Ito, M.; Li, Y.R.; Dedhia, P.H.; Zheng, Y.; Shao, M.; Gay, D.L.; Ramos, R.; Hsi, T.-C.*; et al.* Regeneration of fat cells from myofibroblasts during wound healing. *Science* **2017**, 355(6326), 748–752.

278. Lee, K.-W.; Yook, J.-Y.; Son, M.-Y.; Kim, M.-J.; Koo, D.-B.; Han, Y.-M.; Cho, Y.S. Rapamycin promotes the osteoblastic differentiation of human embryonic stem cells by blocking the mTOR pathway and stimulating the BMP/Smad pathway. *Stem Cells and Development* **2010**, 19(4), 557–568.

279. Larraufie, M.-H.; Gao, X.; Xia, X.; Devine, P.J.; Kallen, J.; Liu, D.; Michaud, G.; Harsch, A.; Savage, N.; Ding, J.*; et al.* Phenotypic screen identifies calcineurin-sparing FK506 analogs as BMP potentiators for treatment of acute kidney injury. *Cell Chemical Biology* **2021**.

280. Gonsalez, S.R.; Cortês, A.L.; Da Silva, R.C.; Lowe, J.; Prieto, M.C.; Da Silva Lara, L. Acute kidney injury overview: From basic findings to new prevention and therapy strategies. *Pharmacology & Therapeutics* **2019**, 200, 1–12.

281. Himmelfarb, J.; Chertow, G.M.; McCullough, P.A.; Mesana, T.; Shaw, A.D.; Sundt, T.M.; Brown, C.; Cortville, D.; Dagenais, F.; Varennes, B. de*; et al.* Perioperative THR-184 and AKI after Cardiac Surgery. *Journal of the American Society of Nephrology* **2018**, 29(2), 670–679.

282. Cao, Y.; Wang, C.; Zhang, X.; Xing, G.; Lu, K.; Gu, Y.; He, F.; Zhang, L. Selective small molecule compounds increase BMP-2 responsiveness by inhibiting Smurf1-mediated Smad1/5 degradation. *Scientific Reports* **2014**, 4, 4965.

283. Kato, S.; Sangadala, S.; Tomita, K.; Titus, L.; Boden, S.D. A synthetic compound that potentiates bone morphogenetic protein-2-induced transdifferentiation of myoblasts into the osteoblastic phenotype. *Molecular and Cellular Biochemistry* **2011**, 349(1-2), 97–106.

284. Okada, M.; Sangadala, S.; Liu, Y.; Yoshida, M.; Reddy, B.V.B.; Titus, L.; Boden, S.D. Development and optimization of a cell-based assay for the selection of synthetic compounds that potentiate bone morphogenetic protein-2 activity. *Cell Biochemistry and Function* **2009**, 27(8), 526–534.

285. Feng, L.; Cook, B.; Tsai, S.-Y.; Zhou, T.; LaFlamme, B.; Evans, T.; Chen, S. Discovery of a Small-Molecule BMP Sensitizer for Human Embryonic Stem Cell Differentiation. *Cell Reports* **2016**, 15(9), 2063–2075.

286. Baek, S.; Choi, S.-W.; Park, S.-J.; Lee, S.-H.; Chun, H.-S.; Kim, S.H. Quinoline compound KM11073 enhances BMP-2-dependent osteogenic differentiation of C2C12 cells via activation of p38 signaling and exhibits in vivo bone forming activity. *PloS One* **2015**, 10(3), e0120150.

287. Cook, B.; Rafiq, R.; Lee, H.; Banks, K.M.; El-Debs, M.; Chiaravalli, J.; Glickman, J.F.; Das, B.C.; Chen, S.; Evans, T. Discovery of a Small Molecule Promoting Mouse and Human Osteoblast Differentiation via Activation of p38 MAPK-β. *Cell Chemical Biology* **2019**, 26(7), 926-935.e6.

288. Lowery, J.W.; Rosen, V. Bone Morphogenetic Protein-Based Therapeutic Approaches. *Cold Spring Harbor Perspectives in Biology* **2018**, 10(4).

289. Yadin, D.; Knaus, P.; Mueller, T.D. Structural insights into BMP receptors: Specificity, activation and inhibition. *Cytokine & Growth Factor Reviews* **2016**, 27, 13–34.

290. Jonas Halver. Identifizierung und Charakterisierung neuer Stimulatoren der kardialen Differenzierung pluripotenter Stammzellen. Ph.D. Dissertation, TU Dortmund 2017.

291. Schade, D.; Halver, J. BMP-Mimetics. EP20170189054, **2018**, (WO2019042889 (A1)).

292. Takahashi, T.; Lord, B.; Schulze, P.C.; Fryer, R.M.; Sarang, S.S.; Gullans, S.R.; Lee, R.T. Ascorbic acid enhances differentiation of embryonic stem cells into cardiac myocytes. *Circulation* **2003**, 107(14), 1912–1916.

293. Halver, J.; Wenzel, K.; Sendker, J.; Carrillo García, C.; Erdelmeier, C.A.J.; Willems, E.; Mercola, M.; Symma, N.; Könemann, S.; Koch, E.*; et al.* Crataegus Extract WS®1442 Stimulates Cardiomyogenesis and Angiogenesis From Stem Cells: A Possible New Pharmacology for Hawthorn? *Frontiers in Pharmacology* **2019**, 10, 1357.

294. Colas, A.R.; McKeithan, W.L.; Cunningham, T.J.; Bushway, P.J.; Garmire, L.X.; Duester, G.; Subramaniam, S.; Mercola, M. Whole-genome microRNA screening identifies let-7 and mir-18 as regulators of germ layer formation during early embryogenesis. *Genes & Development* **2012**, 26(23), 2567–2579.

295. Niwa, H.; Miyazaki, J.; Smith, A.G. Quantitative expression of Oct-3/4 defines differentiation, dedifferentiation or self-renewal of ES cells. *Nature Genetics* **2000**, 24(4), 372–376.

296. Ladd, A.N.; Yatskievych, T.A.; Antin, P.B. Regulation of avian cardiac myogenesis by activin/TGFbeta and bone morphogenetic proteins. *Developmental Biology* **1998**, 204(2), 407–419.

297. Olsen, O.E.; Hella, H.; Elsaadi, S.; Jacobi, C.; Martinez-Hackert, E.; Holien, T. Activins as Dual Specificity TGF-β Family Molecules: SMAD-Activation via Activin- and BMP-Type 1 Receptors. *Biomolecules* **2020**, 10(4).

298. Xie, C.; Jiang, W.; Lacroix, J.J.; Luo, Y.; Hao, J. Insight into Molecular Mechanism for Activin A-Induced Bone Morphogenetic Protein Signaling. *International Journal of Molecular Sciences* **2020**, 21(18).

299. Hackland, J.O.S.; Frith, T.J.R.; Thompson, O.; Marin Navarro, A.; Garcia-Castro, M.I.; Unger, C.; Andrews, P.W. Top-Down Inhibition of BMP Signaling Enables Robust Induction of hPSCs Into Neural Crest in Fully Defined, Xeno-free Conditions. *Stem Cell Reports* **2017**, 9(4), 1043–1052.

300. Niwa, H.; Burdon, T.; Chambers, I.; Smith, A. Self-renewal of pluripotent embryonic stem cells is mediated via activation of STAT3. *Genes & Development* **1998**, 12(13), 2048–2060.

301. Brambrink, T.; Foreman, R.; Welstead, G.G.; Lengner, C.J.; Wernig, M.; Suh, H.; Jaenisch, R. Sequential expression of pluripotency markers during direct reprogramming of mouse somatic cells. *Cell Stem Cell* **2008**, 2(2), 151–159.

302. Berrill, A.; Tan, H.L.; Wuang, S.C.; Fong, W.J.; Choo, A.B.H.; Oh, S.K.W. Assessment of stem cell markers during long-term culture of mouse embryonic stem cells. *Cytotechnology* **2004**, 44(1-2), 77–91.

303. Furue, M.; Okamoto, T.; Hayashi, Y.; Okochi, H.; Fujimoto, M.; Myoishi, Y.; Abe, T.; Ohnuma, K.; Sato, G.H.; Asashima, M.*; et al.* Leukemia inhibitory factor as an anti-apoptotic mitogen for pluripotent mouse embryonic stem cells in a serum-free medium without feeder cells. *In vitro cellular & developmental biology. Animal* **2005**, 41(1-2), 19–28.

304. Ventura, C.; Maioli, M. Opioid peptide gene expression primes cardiogenesis in embryonal pluripotent stem cells. *Circulation Research* **2000**, 87(3), 189–194.

305. Palmer, B.D.; Thompson, A.M.; Booth, R.J.; Dobrusin, E.M.; Kraker, A.J.; Lee, H.H.; Lunney, E.A.; Mitchell, L.H.; Ortwine, D.F.; Smaill, J.B.*; et al.* 4-Phenylpyrrolo3,4-ccarbazole-1,3(2H,6H)-dione inhibitors of the checkpoint kinase Wee1. Structure-activity relationships for chromophore modification and phenyl ring substitution. *Journal of Medicinal Chemistry* **2006**, 49(16), 4896–4911.

306. Jester, B.W.; Gaj, A.; Shomin, C.D.; Cox, K.J.; Ghosh, I. Testing the promiscuity of commercial kinase inhibitors against the AGC kinase group using a split-luciferase screen. *Journal of Medicinal Chemistry* **2012**, 55(4), 1526–1537.

307. Fung, S.L.; Wu, X.; Maceren, J.P.; Mao, Y.; Kohn, J. In Vitro Evaluation of Recombinant Bone Morphogenetic Protein-2 Bioactivity for Regenerative Medicine. *Tissue Engineering. Part C, Methods* **2019**, 25(9), 553–559.

308. Wu, X.; Ding, S.; Ding, Q.; Gray, N.S.; Schultz, P.G. A small molecule with osteogenesis-inducing activity in multipotent mesenchymal progenitor cells. *Journal of the American Chemical Society* **2002**, 124(49), 14520–14521.

309. Conejo, R.; Valverde, A.M.; Benito, M.; Lorenzo, M. Insulin produces myogenesis in C2C12 myoblasts by induction of NF-κB and downregulation of AP-1 activities. *Journal of Cellular Physiology* **2001**, 186(1), 82–94.

310. Millán, J.L. Alkaline Phosphatases: Structure, substrate specificity and functional relatedness to other members of a large superfamily of enzymes. *Purinergic Signalling* **2006**, 2(2), 335–341.

311. Namiki, M.; Akiyama, S.; Katagiri, T.; Suzuki, A.; Ueno, N.; Yamaji, N.; Rosen, V.; Wozney, J.M.; Suda, T. A kinase domain-truncated type I receptor blocks bone morphogenetic protein-2-induced signal transduction in C2C12 myoblasts. *The Journal of Biological Chemistry* **1997**, 272(35), 22046–22052.

312. Fukuda, T.; Kokabu, S.; Ohte, S.; Sasanuma, H.; Kanomata, K.; Yoneyama, K.; Kato, H.; Akita, M.; Oda, H.; Katagiri, T. Canonical Wnts and BMPs cooperatively induce osteoblastic differentiation through a GSK3beta-dependent and beta-catenin-independent mechanism. *Differentiation; Research in Biological Diversity* **2010**, 80(1), 46–52.

313. Hassel, S.; Yakymovych, M.; Hellman, U.; Rönnstrand, L.; Knaus, P.; Souchelnytskyi, S. Interaction and functional cooperation between the serine/threonine kinase bone morphogenetic protein type II receptor with the tyrosine kinase stem cell factor receptor. *Journal of Cellular Physiology* **2006**, 206(2), 457–467.

314. Zhang, J.; Zhang, W.; Dai, J.; Wang, X.; Shen, S.G. Overexpression of Dlx2 enhances osteogenic differentiation of BMSCs and MC3T3-E1 cells via direct upregulation of Osteocalcin and Alp. *International Journal of Oral Science* **2019**, 11(2), 12.

315. Miyazono, K.; Maeda, S.; Imamura, T. BMP receptor signaling: transcriptional targets, regulation of signals, and signaling cross-talk. *Cytokine & Growth Factor Reviews* **2005**, 16(3), 251–263.

316. Shu, D.Y.; Ng, K.; Wishart, T.F.L.; Chui, J.; Lundmark, M.; Flokis, M.; Lovicu, F.J. Contrasting roles for BMP-4 and ventromorphins (BMP agonists) in TGFβ-induced lens EMT. *Experimental Eye Research* **2021**, 206, 108546.

317. Robke, L.; Laraia, L.; Carnero Corrales, M.A.; Konstantinidis, G.; Muroi, M.; Richters, A.; Winzker, M.; Engbring, T.; Tomassi, S.; Watanabe, N.*; et al.* Phenotypic Identification of a Novel Autophagy Inhibitor Chemotype Targeting Lipid Kinase VPS34. *Angewandte Chemie International Edition* **2017**, 56(28), 8153–8157.

318. Ceballos, J.; Schwalfenberg, M.; Karageorgis, G.; Reckzeh, E.S.; Sievers, S.; Ostermann, C.; Pahl, A.; Sellstedt, M.; Nowacki, J.; Carnero Corrales, M.A.*; et al.* Synthesis of Indomorphan Pseudo-Natural Product Inhibitors of Glucose Transporters GLUT-1 and -3. *Angewandte Chemie International Edition* **2019**, 58(47), 17016–17025.

319. Reckzeh, E.S.; Karageorgis, G.; Schwalfenberg, M.; Ceballos, J.; Nowacki, J.; Stroet, M.C.M.; Binici, A.; Knauer, L.; Brand, S.; Choidas, A.*; et al.* Inhibition of Glucose Transporters and Glutaminase Synergistically Impairs Tumor Cell Growth. *Cell Chemical Biology* **2019**, 26(9), 1214-1228.e25.

320. Karageorgis, G.; Reckzeh, E.S.; Ceballos, J.; Schwalfenberg, M.; Sievers, S.; Ostermann, C.; Pahl, A.; Ziegler, S.; Waldmann, H. Chromopynones are pseudo natural product glucose uptake inhibitors targeting glucose transporters GLUT-1 and -3. *Nature Chemistry* **2018**, 10(11), 1103–1111.

321. Shyh-Chang, N.; Daley, G.Q.; Cantley, L.C. Stem cell metabolism in tissue development and aging. *Development* **2013**, 140(12), 2535–2547.

322. Ellen Kreipke, R.; Wang, Y.; Miklas, J.W.; Mathieu, J.; Ruohola-Baker, H. Metabolic remodeling in early development and cardiomyocyte maturation. *Seminars in Cell & Developmental Biology* **2016**, 52, 84–92.

323. Richters, A.; Basu, D.; Engel, J.; Ercanoglu, M.S.; Balke-Want, H.; Tesch, R.; Thomas, R.K.; Rauh, D. Identification and further development of potent TBK1 inhibitors. *ACS Chemical Biology* **2015**, 10(1), 289–298.

324. Robke, L.; Futamura, Y.; Konstantinidis, G.; Wilke, J.; Aono, H.; Mahmoud, Z.; Watanabe, N.; Wu, Y.-W.; Osada, H.; Laraia, L.*; et al.* Discovery of the novel autophagy inhibitor aumitin that targets mitochondrial complex I. *Chemical Science* **2018**, 9(11), 3014–3022.

325. Kaiser, N.; Corkery, D.; Wu, Y.; Laraia, L.; Waldmann, H. Modulation of autophagy by the novel mitochondrial complex I inhibitor Authipyrin. *Bioorganic & Medicinal Chemistry* **2019**, 27(12), 2444–2448.

326. Bago, R.; Malik, N.; Munson, M.J.; Prescott, A.R.; Davies, P.; Sommer, E.; Shpiro, N.; Ward, R.; Cross, D.; Ganley, I.G.*; et al.* Characterization of VPS34-IN1, a selective inhibitor of Vps34, reveals that the phosphatidylinositol 3-phosphate-binding SGK3 protein kinase is a downstream target of class III phosphoinositide 3-kinase. *The Biochemical Journal* **2014**, 463(3), 413–427.

327. Ronan, B.; Flamand, O.; Vescovi, L.; Dureuil, C.; Durand, L.; Fassy, F.; Bachelot, M.-F.; Lamberton, A.; Mathieu, M.; Bertrand, T.*; et al.* A highly potent and selective Vps34 inhibitor alters vesicle trafficking and autophagy. *Nature Chemical Biology* **2014**, 10(12), 1013–1019.

328. Meijer, L.; Skaltsounis, A.-L.; Magiatis, P.; Polychronopoulos, P.; Knockaert, M.; Leost, M.; Ryan, X.P.; Vonica, C.A.; Brivanlou, A.; Dajani, R.*; et al.* GSK-3-selective inhibitors derived from Tyrian purple indirubins. *Chemistry & Biology* **2003**, 10(12), 1255–1266.

329. Ring, D.B.; Johnson, K.W.; Henriksen, E.J.; Nuss, J.M.; Goff, D.; Kinnick, T.R.; Ma, S.T.; Reeder, J.W.; Samuels, I.; Slabiak, T.*; et al.* Selective glycogen synthase kinase 3 inhibitors potentiate insulin activation of glucose transport and utilization in vitro and in vivo. *Diabetes* **2003**, 52(3), 588–595.

330. Schuh, T. Hit-Validierung BMP-aktivierender niedermolekularer Substanzen. Bachelor Thesis, TU Dortmund **2019**.

331. Pobbati, A.V.; Mejuch, T.; Chakraborty, S.; Karatas, H.; Bharath, S.R.; Guéret, S.M.; Goy, P.-A.; Hahne, G.; Pahl, A.; Sievers, S.*; et al.* Identification of Quinolinols as Activators of TEAD-Dependent Transcription. *ACS Chemical Biology* **2019**, 14(12), 2909–2921.

332. Schneidewind, T.; Brause, A.; Pahl, A.; Burhop, A.; Mejuch, T.; Sievers, S.; Waldmann, H.; Ziegler, S. Morphological Profiling Identifies a Common Mode of Action for Small Molecules with Different Targets. *Chembiochem* **2020**, 21(22), 3197–3207.

333. Samanta, R.; Narayan, R.; Bauer, J.O.; Strohmann, C.; Sievers, S.; Antonchick, A.P. Oxidative regioselective amination of chromones exposes potent inhibitors of the hedgehog signaling pathway. *Chemical Communications* **2015**, 51(5), 925–928.

334. Keski-Oja, J.; Blasi, F.; Leof, E.B.; Moses, H.L. Regulation of the synthesis and activity of urokinase plasminogen activator in A549 human lung carcinoma cells by transforming growth factor-beta. *The Journal of Cell Biology* **1988**, 106(2), 451–459.

335. Samarakoon, R.; Higgins, C.E.; Higgins, S.P.; Higgins, P.J. TGF-beta1-Induced Expression of the Poor Prognosis SERPINE1/PAI-1 Gene Requires EGFR Signaling: A New Target for Anti-EGFR Therapy. *Journal of Oncology* **2009**, 2009, 342391.

336. Taylor, L.M.; Khachigian, L.M. Induction of platelet-derived growth factor B-chain expression by transforming growth factor-beta involves transactivation by Smads. *The Journal of Biological Chemistry* **2000**, 275(22), 16709–16716.

337. Lian, N.; Lin, T.; Liu, W.; Wang, W.; Li, L.; Sun, S.; Nyman, J.S.; Yang, X. Transforming growth factor β suppresses osteoblast differentiation via the vimentin activating transcription factor 4 (ATF4) axis. *The Journal of Biological Chemistry* **2012**, 287(43), 35975–35984.

338. Datta, R.; Bansal, T.; Rana, S.; Datta, K.; Chattopadhyay, S.; Chawla-Sarkar, M.; Sarkar, S. Hsp90/Cdc37 assembly modulates TGFβ receptor-II to act as a profibrotic regulator of TGFβ signaling during cardiac hypertrophy. *Cellular Signalling* **2015**, 27(12), 2410–2424.

339. Shang, Y.; Xu, X.; Duan, X.; Guo, J.; Wang, Y.; Ren, F.; He, D.; Chang, Z. Hsp70 and Hsp90 oppositely regulate TGF-β signaling through CHIP/Stub1. *Biochemical and Biophysical Research Communications* **2014**, 446(1), 387–392.

340. Arrowsmith, C.H.; Audia, J.E.; Austin, C.; Baell, J.; Bennett, J.; Blagg, J.; Bountra, C.; Brennan, P.E.; Brown, P.J.; Bunnage, M.E.*; et al.* The promise and peril of chemical probes. *Nature Chemical Biology* **2015**, 11(8), 536–541.

341. Williams, M.; Francis, J.; Ghai, G.; Braunwalder, A.; Psychoyos, S.; Stone, G.A.; Cash, W.D. Biochemical characterization of the triazoloquinazoline, CGS 15943, a novel, non-xanthine adenosine antagonist. *The Journal of Pharmacology and Experimental Therapeutics* **1987**, 241(2), 415–420.

342. Ghai, G.; Francis, J.E.; Williams, M.; Dotson, R.A.; Hopkins, M.F.; Cote, D.T.; Goodman, F.R.; Zimmerman, M.B. Pharmacological characterization of CGS 15943A: a novel nonxanthine adenosine antagonist. *The Journal of Pharmacology and Experimental Therapeutics* **1987**, 242(3), 784–790.

343. Holtzman, S.G. Discriminative effects of CGS 15943, a competitive adenosine receptor antagonist, in monkeys: comparison to methylxanthines. *The Journal of Pharmacology and Experimental Therapeutics* **1996**, 277(2), 739–746.

344. Howell, L.L.; Byrd, L.D. Effects of CGS 15943, a nonxanthine adenosine antagonist, on behavior in the squirrel monkey. *The Journal of Pharmacology and Experimental Therapeutics* **1993**, 267(1), 432–439.

345. Ongini, E.; Dionisotti, S.; Gessi, S.; Irenius, E.; Fredholm, B.B. Comparison of CGS 15943, ZM 241385 and SCH 58261 as antagonists at human adenosine receptors. *Naunyn-Schmiedeberg's Archives of Pharmacology* **1999**, 359(1), 7–10.

346. He, W.; Cronstein, B.N. Adenosine A1 receptor regulates osteoclast formation by altering TRAF6/TAK1 signaling. *Purinergic Signalling* **2012**, 8(2), 327–337.

347. Mediero, A.; Cronstein, B.N. Adenosine and bone metabolism. *Trends in Endocrinology and Metabolism* **2013**, 24(6), 290–300.

348. Katagiri, T.; Imada, M.; Yanai, T.; Suda, T.; Takahashi, N.; Kamijo, R. Identification of a BMP-responsive element in Id1, the gene for inhibition of myogenesis. *Genes to Cells* **2002**, 7(9), 949–960.

349. Morikawa, M.; Koinuma, D.; Miyazono, K.; Heldin, C.-H. Genome-wide mechanisms of Smad binding. *Oncogene* **2013**, 32(13), 1609–1615.

350. Schulte-Merker, S.; Hammerschmidt, M.; Beuchle, D.; Cho, K.W.; Robertis, E.M. de; Nusslein-Volhard, C. Expression of zebrafish goosecoid and no tail gene products in wild-type and mutant no tail embryos. *Development* **1994**, 120(4), 843–852.

351. Langdon, Y.G.; Mullins, M.C. Maternal and zygotic control of zebrafish dorsoventral axial patterning. *Annual Review of Genetics* **2011**, 45, 357–377.

352. Imai, Y.; Gates, M.A.; Melby, A.E.; Kimelman, D.; Schier, A.F.; Talbot, W.S. The homeobox genes vox and vent are redundant repressors of dorsal fates in zebrafish. *Development* **2001**, 128(12), 2407–2420.

353. Heining, E.; Bhushan, R.; Paarmann, P.; Henis, Y.I.; Knaus, P. Spatial segregation of BMP/Smad signaling affects osteoblast differentiation in C2C12 cells. *PloS One* **2011**, 6(10), e25163.

354. Yamato, K.; Hashimoto, S.; Imamura, T.; Uchida, H.; Okahashi, N.; Koseki, T.; Ishisaki, A.; Kizaki, M.; Miyazono, K.; Ikeda, Y.*; et al.* Activation of the p21(CIP1/WAF1) promoter by bone morphogenetic protein-2 in mouse B lineage cells. *Oncogene* **2001**, 20(32), 4383–4392.

355. Drissi, H.; Hushka, D.; Aslam, F.; Nguyen, Q.; Buffone, E.; Koff, A.; van Wijnen, A.; Lian, J.B.; Stein, J.L.; Stein, G.S. The cell cycle regulator p27kip1 contributes to growth and differentiation of osteoblasts. *Cancer Research* **1999**, 59(15), 3705–3711.

356. Chang, S.-F.; Chang, T.-K.; Peng, H.-H.; Yeh, Y.-T.; Lee, D.-Y.; Yeh, C.-R.; Zhou, J.; Cheng, C.-K.; Chang, C.A.; Chiu, J.-J. BMP-4 induction of arrest and differentiation of osteoblast-like cells via p21 CIP1 and p27 KIP1 regulation. *Molecular Endocrinology* **2009**, 23(11), 1827–1838.

357. Abbas, T.; Dutta, A. p21 in cancer: intricate networks and multiple activities. *Nature Reviews. Cancer* **2009**, 9(6), 400–414.

358. Micheli, L.; Leonardi, L.; Conti, F.; Maresca, G.; Colazingari, S.; Mattei, E.; Lira, S.A.; Farioli-Vecchioli, S.; Caruso, M.; Tirone, F. PC4/Tis7/IFRD1 stimulates skeletal muscle regeneration and is involved in myoblast differentiation as a regulator of MyoD and NF-kappaB. *The Journal of Biological Chemistry* **2011**, 286(7), 5691–5707.

359. Onishi, Y.; Park, G.; Iezaki, T.; Horie, T.; Kanayama, T.; Fukasawa, K.; Ozaki, K.; Hinoi, E. The transcriptional modulator Ifrd1 is a negative regulator of BMP-2-dependent osteoblastogenesis. *Biochemical and Biophysical Research Communications* **2017**, 482(2), 329–334.

360. Sartori, R.; Gregorevic, P.; Sandri, M. TGFβ and BMP signaling in skeletal muscle: potential significance for muscle-related disease. *Trends in Endocrinology and Metabolism* **2014**, 25(9), 464–471.

361. Pierce, G.F.; Vande Berg, J.; Rudolph, R.; Tarpley, J.; Mustoe, T.A. Platelet-derived growth factor-BB and transforming growth factor beta 1 selectively modulate glycosaminoglycans, collagen, and myofibroblasts in excisional wounds. *The American Journal of Pathology* **1991**, 138(3), 629–646.

362. Chowdhury, S.; Schulz, L.; Palmisano, B.; Singh, P.; Berger, J.M.; Yadav, V.K.; Mera, P.; Ellingsgaard, H.; Hidalgo, J.; Brüning, J.*; et al.* Muscle-derived interleukin 6 increases exercise capacity by signaling in osteoblasts. *The Journal of Clinical Investigation* **2020**, 130(6), 2888–2902.

363. Conley, B.A.; Smith, J.D.; Guerrero-Esteo, M.; Bernabeu, C.; Vary, C.P. Endoglin, a TGF-beta receptor-associated protein, is expressed by smooth muscle cells in human atherosclerotic plaques. *Atherosclerosis* **2000**, 153(2), 323–335.

364. Knippschild, U.; Krüger, M.; Richter, J.; Xu, P.; García-Reyes, B.; Peifer, C.; Halekotte, J.; Bakulev, V.; Bischof, J. The CK1 Family: Contribution to Cellular Stress Response and Its Role in Carcinogenesis. *Frontiers in Oncology* **2014**, 4, 96.

365. Edling, C.E.; Selvaggi, F.; Ghonaim, R.; Maffucci, T.; Falasca, M. Caffeine and the analog CGS 15943 inhibit cancer cell growth by targeting the phosphoinositide 3-kinase/Akt pathway. *Cancer Biology & Therapy* **2014**, 15(5), 524–532.

366. Bibian, M.; Rahaim, R.J.; Choi, J.Y.; Noguchi, Y.; Schürer, S.; Chen, W.; Nakanishi, S.; Licht, K.; Rosenberg, L.H.; Li, L.*; et al.* Development of highly selective casein kinase 1δ/1ε (CK1δ/ε) inhibitors with potent antiproliferative properties. *Bioorganic & Medicinal Chemistry Letters* **2013**, 23(15), 4374–4380.

367. Lineweaver, H.; Burk, D. The Determination of Enzyme Dissociation Constants. *Journal of the American Chemical Society* **1934**, 56(3), 658–666.

368. Garuti, L.; Roberti, M.; Bottegoni, G. Non-ATP competitive protein kinase inhibitors. *Current Medicinal Chemistry* **2010**, 17(25), 2804–2821.

369. Palmer, T.; Bonner, P.L. Enzyme Inhibition. In Enzymes; Elsevier, **2011**; 126–152.

370. García-Reyes, B.; Witt, L.; Jansen, B.; Karasu, E.; Gehring, T.; Leban, J.; Henne-Bruns, D.; Pichlo, C.; Brunstein, E.; Baumann, U.*; et al.* Discovery of Inhibitor of Wnt Production 2 (IWP-2) and Related Compounds As Selective ATP-Competitive Inhibitors of Casein Kinase 1 (CK1) δ/ε. *Journal of Medicinal Chemistry* **2018**, 61(9), 4087–4102.

371. Halekotte, J.; Witt, L.; Ianes, C.; Krüger, M.; Bührmann, M.; Rauh, D.; Pichlo, C.; Brunstein, E.; Luxenburger, A.; Baumann, U.*; et al.* Optimized 4,5-Diarylimidazoles as Potent/Selective Inhibitors of Protein Kinase CK1δ and Their Structural Relation to p38α MAPK. *Molecules* **2017**, 22(4).

372. Long, A.; Zhao, H.; Huang, X. Structural basis for the interaction between casein kinase 1 delta and a potent and selective inhibitor. *Journal of Medicinal Chemistry* **2012**, 55(2), 956–960.

373. Rosenberg, L.H.; Lafitte, M.; Quereda, V.; Grant, W.; Chen, W.; Bibian, M.; Noguchi, Y.; Fallahi, M.; Yang, C.; Chang, J.C.*; et al.* Therapeutic targeting of casein kinase 1δ in breast cancer. *Science Translational Medicine* **2015**, 7(318), 318ra202.

374. Badura, L.; Swanson, T.; Adamowicz, W.; Adams, J.; Cianfrogna, J.; Fisher, K.; Holland, J.; Kleiman, R.; Nelson, F.; Reynolds, L.*; et al.* An inhibitor of casein kinase I epsilon induces phase delays in circadian rhythms under free-running and entrained conditions. *The Journal of Pharmacology and Experimental Therapeutics* **2007**, 322(2), 730–738.

375. Monastyrskyi, A.; Nilchan, N.; Quereda, V.; Noguchi, Y.; Ruiz, C.; Grant, W.; Cameron, M.; Duckett, D.; Roush, W. Development of dual casein kinase 1δ/1ε (CK1δ/ε) inhibitors for treatment of breast cancer. *Bioorganic & Medicinal Chemistry* **2018**, 26(3), 590–602.

376. Thorne, N.; Shen, M.; Lea, W.A.; Simeonov, A.; Lovell, S.; Auld, D.S.; Inglese, J. Firefly luciferase in chemical biology: a compendium of inhibitors, mechanistic evaluation of chemotypes, and suggested use as a reporter. *Chemistry & Biology* **2012**, 19(8), 1060–1072.

377. Knight, Z.A.; Gonzalez, B.; Feldman, M.E.; Zunder, E.R.; Goldenberg, D.D.; Williams, O.; Loewith, R.; Stokoe, D.; Balla, A.; Toth, B.*; et al.* A pharmacological map of the PI3-K family defines a role for p110alpha in insulin signaling. *Cell* **2006**, 125(4), 733–747.

378. Furet, P.; Guagnano, V.; Fairhurst, R.A.; Imbach-Weese, P.; Bruce, I.; Knapp, M.; Fritsch, C.; Blasco, F.; Blanz, J.; Aichholz, R.*; et al.* Discovery of NVP-BYL719 a potent and selective phosphatidylinositol-3 kinase alpha inhibitor selected for clinical evaluation. *Bioorganic & Medicinal Chemistry Letters* **2013**, 23(13), 3741–3748.

379. Arris, C.E.; Boyle, F.T.; Calvert, A.H.; Curtin, N.J.; Endicott, J.A.; Garman, E.F.; Gibson, A.E.; Golding, B.T.; Grant, S.; Griffin, R.J.*; et al.* Identification of novel purine and pyrimidine cyclin-dependent kinase inhibitors with distinct molecular interactions and tumor cell growth inhibition profiles. *Journal of Medicinal Chemistry* **2000**, 43(15), 2797–2804.

380. Chaussade, C.; Rewcastle, G.W.; Kendall, J.D.; Denny, W.A.; Cho, K.; Grønning, L.M.; Chong, M.L.; Anagnostou, S.H.; Jackson, S.P.; Daniele, N.*; et al.* Evidence for functional redundancy of class IA PI3K isoforms in insulin signalling. *The Biochemical Journal* **2007**, 404(3), 449–458.

381. Fritsch, C.; Huang, A.; Chatenay-Rivauday, C.; Schnell, C.; Reddy, A.; Liu, M.; Kauffmann, A.; Guthy, D.; Erdmann, D.; Pover, A. de*; et al.* Characterization of the novel and specific PI3Kα inhibitor NVP-BYL719 and development of the patient stratification strategy for clinical trials. *Molecular Cancer Therapeutics* **2014**, 13(5), 1117–1129.

382. Gámez, B.; Rodríguez-Carballo, E.; Graupera, M.; Rosa, J.L.; Ventura, F. Class I PI-3-Kinase Signaling Is Critical for Bone Formation Through Regulation of SMAD1 Activity in Osteoblasts. *Journal of Bone and Mineral Research* **2016**, 31(8), 1617–1630.

383. Nojima, J.; Kanomata, K.; Takada, Y.; Fukuda, T.; Kokabu, S.; Ohte, S.; Takada, T.; Tsukui, T.; Yamamoto, T.S.; Sasanuma, H.*; et al.* Dual roles of smad proteins in the conversion from myoblasts to osteoblastic cells by bone morphogenetic proteins. *The Journal of Biological Chemistry* **2010**, 285(20), 15577–15586.

384. Waddell, D.S.; Liberati, N.T.; Guo, X.; Frederick, J.P.; Wang, X.-F. Casein kinase Iepsilon plays a functional role in the transforming growth factor-beta signaling pathway. *The Journal of Biological Chemistry* **2004**, 279(28), 29236–29246.

385. Gruber, W.; Frischauf, A.-M.; Aberger, F. An old friend with new skills: Imiquimod as novel inhibitor of Hedgehog signaling in basal cell carcinoma. *Oncoscience* **2014**, 1(9), 567–573.

386. Goodwin, J.F.; Knudsen, K.E. Beyond DNA repair: DNA-PK function in cancer. *Cancer Discovery* **2014**, 4(10), 1126–1139.

387. Garces, A.E.; Stocks, M.J. Class 1 PI3K Clinical Candidates and Recent Inhibitor Design Strategies: A Medicinal Chemistry Perspective. *Journal of Medicinal Chemistry* **2019**, 62(10), 4815–4850.

388. Fok, J.H.L.; Ramos-Montoya, A.; Vazquez-Chantada, M.; Wijnhoven, P.W.G.; Follia, V.; James, N.; Farrington, P.M.; Karmokar, A.; Willis, S.E.; Cairns, J.*; et al.* AZD7648 is a potent and selective DNA-PK inhibitor that enhances radiation, chemotherapy and olaparib activity. *Nature Communications* **2019**, 10(1), 5065.

389. Goldberg, F.W.; Finlay, M.R.V.; Ting, A.K.T.; Beattie, D.; Lamont, G.M.; Fallan, C.; Wrigley, G.L.; Schimpl, M.; Howard, M.R.; Williamson, B.*; et al.* The Discovery of 7-Methyl-2-(7-methyl1,2,4triazolo1,5-apyridin-6-yl)amino-9-(tetrahydro-2H-pyran-4-yl)-7,9-dihydro-8H-purin-8-one (AZD7648), a Potent and Selective DNA-Dependent Protein Kinase (DNA-PK) Inhibitor. *Journal of Medicinal Chemistry* **2020**, 63(7), 3461–3471.

390. Kolluri, S.K.; Jin, U.-H.; Safe, S. Role of the aryl hydrocarbon receptor in carcinogenesis and potential as an anti-cancer drug target. *Archives of Toxicology* **2017**, 91(7), 2497–2513.

391. O'Donnell, E.F.; Jang, H.S.; Liefwalker, D.F.; Kerkvliet, N.I.; Kolluri, S.K. Discovery and Mechanistic Characterization of a Select Modulator of AhR-regulated Transcription (SMAhRT) with Anti-cancer Effects. *Apoptosis* **2021**, 26(5-6), 307–322.

392. Corsello, S.; Spangler, R.; Nagari, R.; Golub, T.; Madec, A. Aryl hydrocarbon receptor (ahr) activator compounds as cancer therapeutics. US201862767474P, **2019**, (WO2020102506 (A1)).

393. Liu, X.; Li, X.; Tao, Y.; Li, N.; Ji, M.; Zhang, X.; Chen, Y.; He, Z.; Yu, K.; Yu, Z. TCDD inhibited the osteogenic differentiation of human fetal palatal mesenchymal cells through AhR and BMP-2/TGF-β/Smad signaling. *Toxicology* **2020**, 431, 152353.

394. Erickson-Miller, C.L.; Delorme, E.; Tian, S.-S.; Hopson, C.B.; Landis, A.J.; Valoret, E.I.; Sellers, T.S.; Rosen, J.; Miller, S.G.; Luengo, J.I.*; et al.* Preclinical activity of eltrombopag (SB-497115), an oral, nonpeptide thrombopoietin receptor agonist. *Stem Cells* **2009**, 27(2), 424–430.

395. Tian, S.S.; Lamb, P.; King, A.G.; Miller, S.G.; Kessler, L.; Luengo, J.I.; Averill, L.; Johnson, R.K.; Gleason, J.G.; Pelus, L.M.*; et al.* A small, nonpeptidyl mimic of granulocyte-colony-stimulating factor. *Science* **1998**, 281(5374), 257–259.

396. Sato, N.; Meijer, L.; Skaltsounis, L.; Greengard, P.; Brivanlou, A.H. Maintenance of pluripotency in human and mouse embryonic stem cells through activation of Wnt signaling by a pharmacological GSK-3-specific inhibitor. *Nature Medicine* **2004**, 10(1), 55–63.

397. Livnah, O.; Stura, E.A.; Johnson, D.L.; Middleton, S.A.; Mulcahy, L.S.; Wrighton, N.C.; Dower, W.J.; Jolliffe, L.K.; Wilson, I.A. Functional mimicry of a protein hormone by a peptide agonist: the EPO receptor complex at 2.8 A. *Science* **1996**, 273(5274), 464–471.

398. Qureshi, S.A.; Kim, R.M.; Konteatis, Z.; Biazzo, D.E.; Motamedi, H.; Rodrigues, R.; Boice, J.A.; Calaycay, J.R.; Bednarek, M.A.; Griffin, P.*; et al.* Mimicry of erythropoietin by a nonpeptide molecule. *Proceedings of the National Academy of Sciences of the United States of America* **1999**, 96(21), 12156–12161.

399. Beck, H.; Jeske, M.; Thede, K.; Stoll, F.; Flamme, I.; Akbaba, M.; Ergüden, J.-K.; Karig, G.; Keldenich, J.; Oehme, F.*; et al.* Discovery of Molidustat (BAY 85-3934): A Small-Molecule Oral HIF-Prolyl Hydroxylase (HIF-PH) Inhibitor for the Treatment of Renal Anemia. *ChemMedChem* **2018**, 13(10), 988–1003.

400. Gong, T.; Xie, J.; Liao, J.; Zhang, T.; Lin, S.; Lin, Y. Nanomaterials and bone regeneration. *Bone Research* **2015**, 3, 15029.

401. Dolde, C.; Bischof, J.; Grüter, S.; Montada, A.; Halekotte, J.; Peifer, C.; Kalbacher, H.; Baumann, U.; Knippschild, U.; Suter, B. A CK1 FRET biosensor reveals that DDX3X is an essential activator of CK1ε. *Journal of Cell Science* **2018**, 131(1).

402. Kóssa, G. Über die im Organismus künstlich erzeugbaren Verkalkungen, **1901**.

403. Meloan, S.N.; Puchtler, H. Chemical Mechanisms of Staining Methods: Von Kossa's Technique: What von Kossa Really Wrote and a Modified Reaction for Selective Demonstration of Inorganic Phosphates. *Journal of Histotechnology* **1985**, 8(1), 11–13.

404. Kubista, M.; Andrade, J.M.; Bengtsson, M.; Forootan, A.; Jonák, J.; Lind, K.; Sindelka, R.; Sjöback, R.; Sjögreen, B.; Strömbom, L.*; et al.* The real-time polymerase chain reaction. *Molecular Aspects of Medicine* **2006**, 27(2-3), 95–125.

405. Livak, K.J.; Schmittgen, T.D. Analysis of relative gene expression data using real-time quantitative PCR and the 2(-Delta Delta C(T)) Method. *Methods* **2001**, 25(4), 402–408.

406. Schreiber, E.; Matthias, P.; Müller, M.M.; Schaffner, W. Rapid detection of octamer binding proteins with 'mini-extracts', prepared from a small number of cells. *Nucleic Acids Research* **1989**, 17(15), 6419.

407. Ladner, C.L.; Edwards, R.A.; Schriemer, D.C.; Turner, R.J. Identification of trichloroethanol visualized proteins from two-dimensional polyacrylamide gels by mass spectrometry. *Analytical Chemistry* **2006**, 78(7), 2388–2396.

408. Anastassiadis, T.; Deacon, S.W.; Devarajan, K.; Ma, H.; Peterson, J.R. Comprehensive assay of kinase catalytic activity reveals features of kinase inhibitor selectivity. *Nature Biotechnology* **2011**, 29(11), 1039–1045.

409. Adapta® Universal Kinase Assay and Substrates. Thermo Fisher Scientific Homepage. https://www.thermofisher.com/de/de/home/industrial/pharma-biopharma/drug-discovery-development/target-and-lead-identification-and-validation/kinasebiology/kinase-activity-assays/adapta-universal-kinase-assay.html (accessed on 24 September, 2021).

410. LanthaScreen TR-FRET Kinase Assays. Thermo Fisher Scientific Homepage: https://www.thermofisher.com/de/de/home/industrial/pharma-biopharma/drug-discovery-development/target-and-lead-identification-and-validation/kinasebiology/kinase-activity-assays/lanthascreen-tr-fret-toolbox.html (accessed on 24 September, 2021).

411. Z'-LYTE™ Kinase Assay Kits. Thermo Fisher Scientific Homepage. https://www.thermofisher.com/de/de/home/industrial/pharma-biopharma/drug-discovery-development/target-and-lead-identification-and-validation/kinasebiology/kinase-activity-assays/z-lyte.html (accessed on 24 September, 2021).

7 ABBREVIATIONS

Abbreviation	Definition
AcA	Activin A
ADORA	Adenosine A Receptor
ADP	Adenosine diphosphate
AhR	Aryl hydrocarbon receptor
AKI	Acute kidney injury
ALK	Anaplastic lymphoma kinase/ ALK tyrosine kinase receptor
ALP	Alkaline phosphatase
ATP	Adenosine triphosphate
BIO	6-BIO, (2'Z,3'E)-6-Bromoindirubin-3'-oxime
BISC	BMP-induced signaling complex
BMP	Bone Morphogenetic Protein
BMPR	BMP receptor
BraT	Brachyury T
BRE	BMP-responsive element
CAD	Cationic amphiphilic agent
CCD	Cleidocranial dysplasia
CCP	Clathrin coated pits
CDK	Cyclin-dependent kinase
cDNA	complementary DNA
Cer	Cerberus
CHD	Coronary heart disease
CHIP	Hsc70 interacting protein
CHK	Checkpoint kinase
CK	Casein kinase
CM	Cardiomyocyte
Col1a1	Collagen, type I, α1
COMAS	Compound Management and Screening Center
Conc.	Concentration
Cp	Crossing point

CPA	Cell painting assay
CRC	Colorectal cancer
CVD	Cardiovascular disease
d	Day
DAPI	4′,6-diamidino-2-phenylindole
DHP	1,4-Dihydropyridine
DM	Dorsomorphin
DMEM	Dulbecco's modified Eagle's medium
DMH-1	Dorsomorphin homologue 1
DMSO	Dimethyl sulfoxide
DNA	Deoxyribonucleic acid
DNA-PK	DNA-dependent protein kinase
DNase	Deoxyribonuclease
DR	Diabetic retinopathy
EC50	Half maximal effective concentration
ECM	Extracellular matrix
EDTA	Ethylenediaminetetraacetic acid
EGFR	Epidermal Growth Factor Receptor
EMT	Epithelial mesenchymal transition
ERK	Extracellular signal-regulated kinase
ES/ ESC	Embryonic stem cell
FACS	Fluorescence-activated cell sorter
FBS	Fetal bovine serum
FGF	Fibroblast growth factors
FKBP	FK506 binding protein
Fluc	Firefly-Luciferase
FOP	Fibrodysplasia ossificans progressiva
FRET	Fluorescence resonance energy transfer
GDF	Growth Differentiation Factor
GF	Growth factor
GFP	Green fluorescent protein
GLUT	Glucose transporters

GNP	Granule cell precursor
GPCR	G protein-coupled receptors
Gsc	Goosecoid
GSK3	glycogen synthase kinase 3
h	Hour
HEPES	4-(2-hydroxyethyl)-1-piperazineethanesulfonic acid
HHT	Hereditary hemorrhagic telangiectasia
hi	Heat-inactivated
IC50	Half maximal inhibitory concentration
Id	Inhibitor of DNA binding
Il	Interleukin
iPSC	Induced pluripotent stem cell
ITD-1	Inducer of TGFBR II degradation
LB	lysogeny broth medium
LIF	leukemia inhibitory factor
LOPAC	Library of Pharmacologically Active Compounds
Luc	Luciferase
MAPK	Mitogen-activated protein kinase
Mef2c	Myocyte-specific enhancer factor 2C
mESC	Murine embryonic stem cell
Mesp1	Mesoderm posterior 1 homolog
mRNA	messenger-RNA
MSC	Mesenchymal stem cell
Myh6	Myosin Heavy Chain 6
MyoD	Myoblast determination protein
NLS	Nuclear localization signal
Nog	Noggin
NSCLC	non-small cell lung cancer
OA	Osteoarthritis
OAZ	OE/EBF-associated zinc-finger protein
Ocn	Osteocalcin
Osx	Osterix

PAH	Pulmonary arterial hypertension
PAIN	Pan Assay Interference Compound
PBS	Phosphate-buffered saline
PCR	Polymerase chain reaction
PDD	Phenotypic Drug Discovery
PFC	Preformed receptor complexes
PI3K	Phosphoinositol-3 kinase
PPAR	Peroxisome proliferator-activated receptor
PS/ PSC	Pluripotent stem cell
qPCR	Quantitative polymerase chain reaction
RA	Rheumatoid arthritis
rh	Recombinant human
RLU	Relative Light Units
Rluc	*Renilla*-Luciferase
RNA	Ribonucleic acid
RNase	Ribonuclease
Rpm	Rounds per minute
RT	Room temperature
RT-qPCR	Reverse Transcription qPCR
Runx2	Runt-related transcription factor 2 (CBF-α-1)
SAR	Structure-activity relationship
SBE	SMAD-binding element
SD	Standard deviation
SEM	Standard error of mean
Shh	Sonic hedgehog
TDD	Targeted Drug Discovery
TGFβ	Transforming Growth Factor β
Tnnt2	Troponin T2
VEGFR	Vascular endothelial growth factor
XRE	Xenobiotic-responsive element

8 APPENDIX

8.1 Supplementary Figures

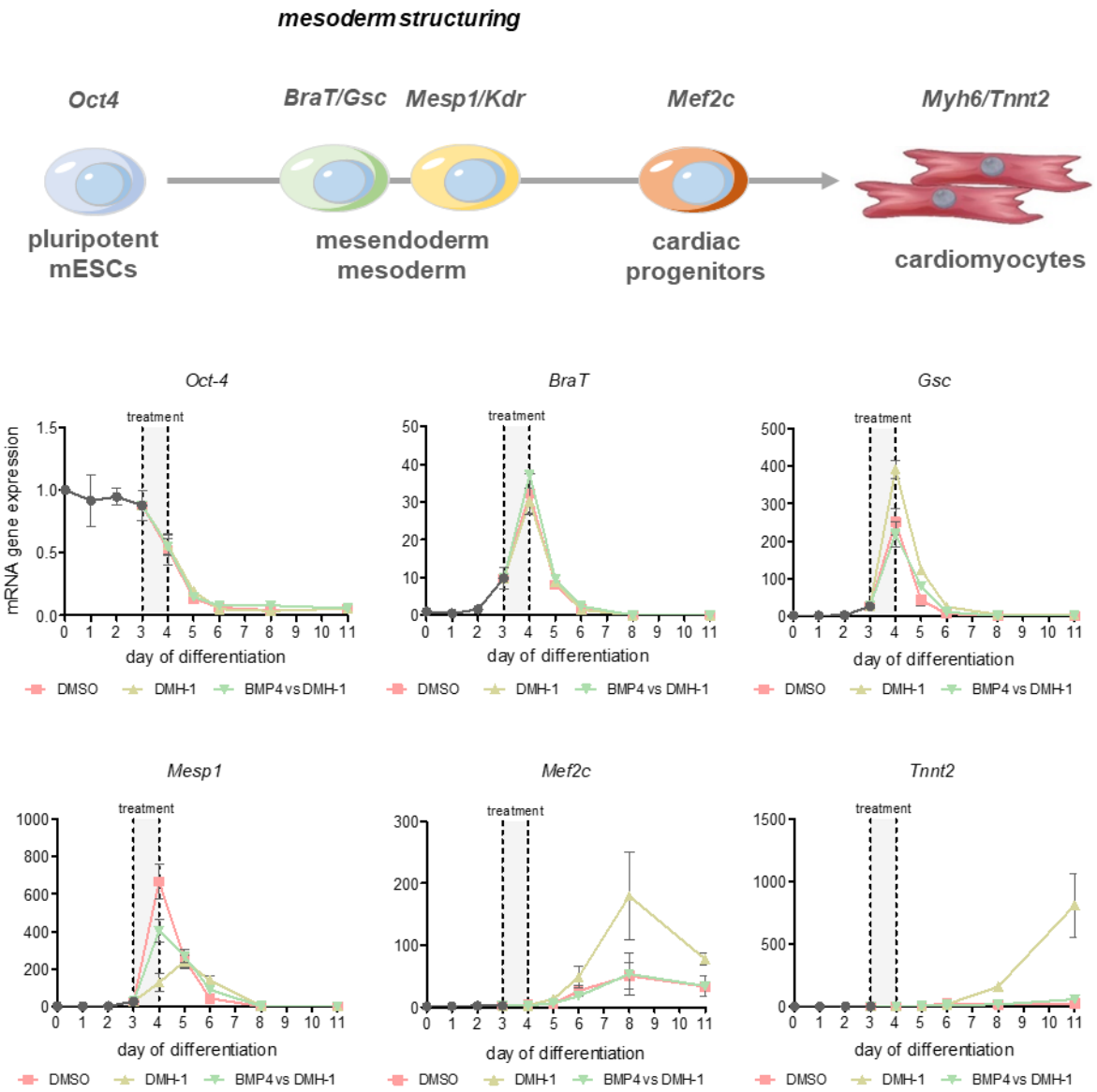

Figure 95: DMH-1 stimulates mesodermal structuring towards cardiovascular progenitors and its phenotype is fully rescued by BMP-4. Cardiac differentiation of mESCs is illustrated based on marker genes specific for different cell lineages. Quantification of temporal mRNA gene expression levels of cell-specific markers during spontaneous mESC differentiation (DMSO) compared to DMH-1 (0.5 µM) treatment in presence or absence of 10 ng/mL BMP-4 in the BMP-sensitive time frame (d3-4). MESC-*Myh6*-GFP were treated with DMSO, DMH-1 or BMP-4 and DMH-1 24 h and RNA was isolated for each time point. Data points represent the mean and respective SD of three independent experiments (n = 3) and is normalized to day 0.

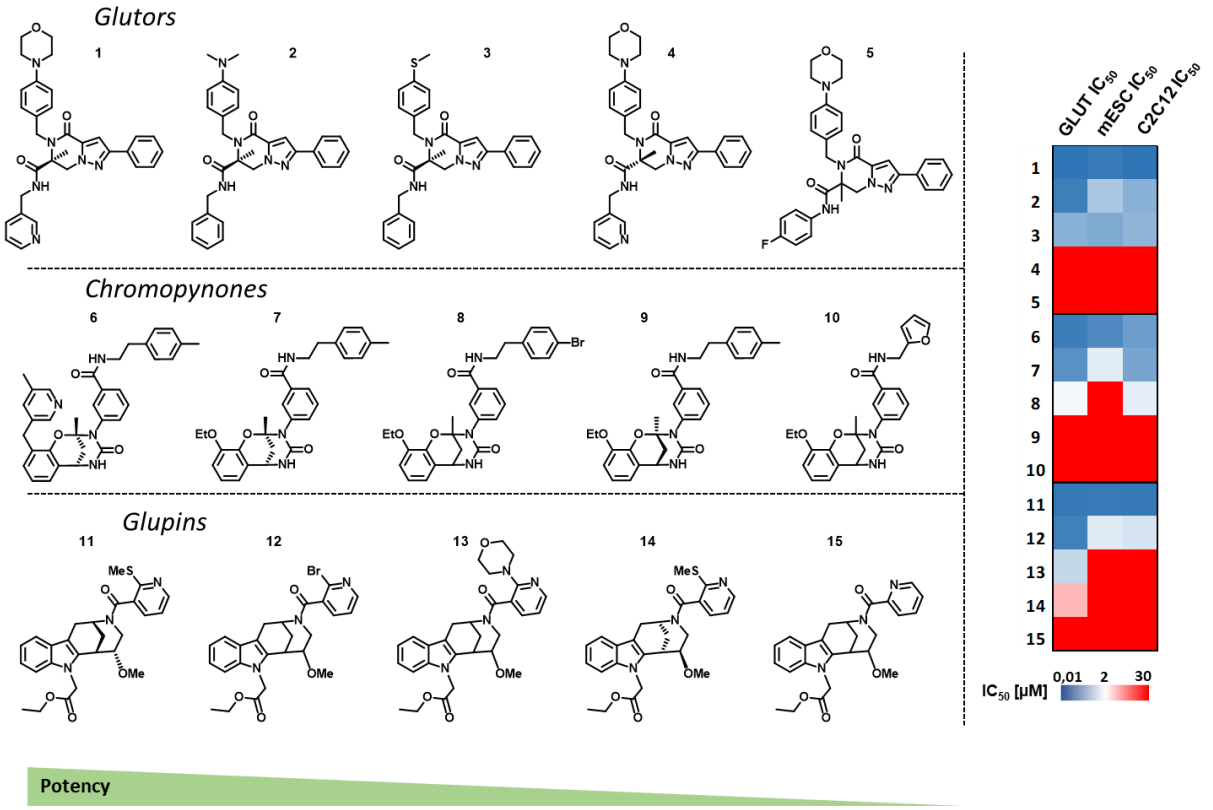

Figure 96: Distinct chemotypes of GLUT inhibitors potently inhibited both morphogenetic assays, indicating a strong correlation between glucose transporter inhibition and calculated antagonistic potency in BMP-dependent osteogenic and cardiac differentiation. The heatmap illustrates the calculated IC_{50}'s ($n \geq 2$) of dose-response in differentiation assays and literature-reported IC_{50}.[318–320]

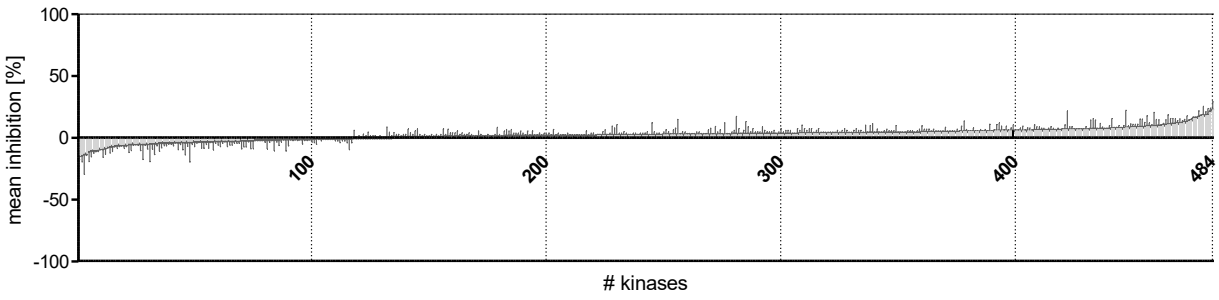

Figure 97: Kinase profiling of Chromenone 1. Activity profile of the full kinase screening set (484 kinases) against 1 µM Chromenone 1. No kinase was modulated beyond >25%. Activities were monitored by biochemical inhibition of selected kinases at Life Technologies in three biochemical assay formats (Adapta, Z-Lyte, Lantha). Data is shown as the mean ± SD of two replicates ($n = 2$) for each kinase.

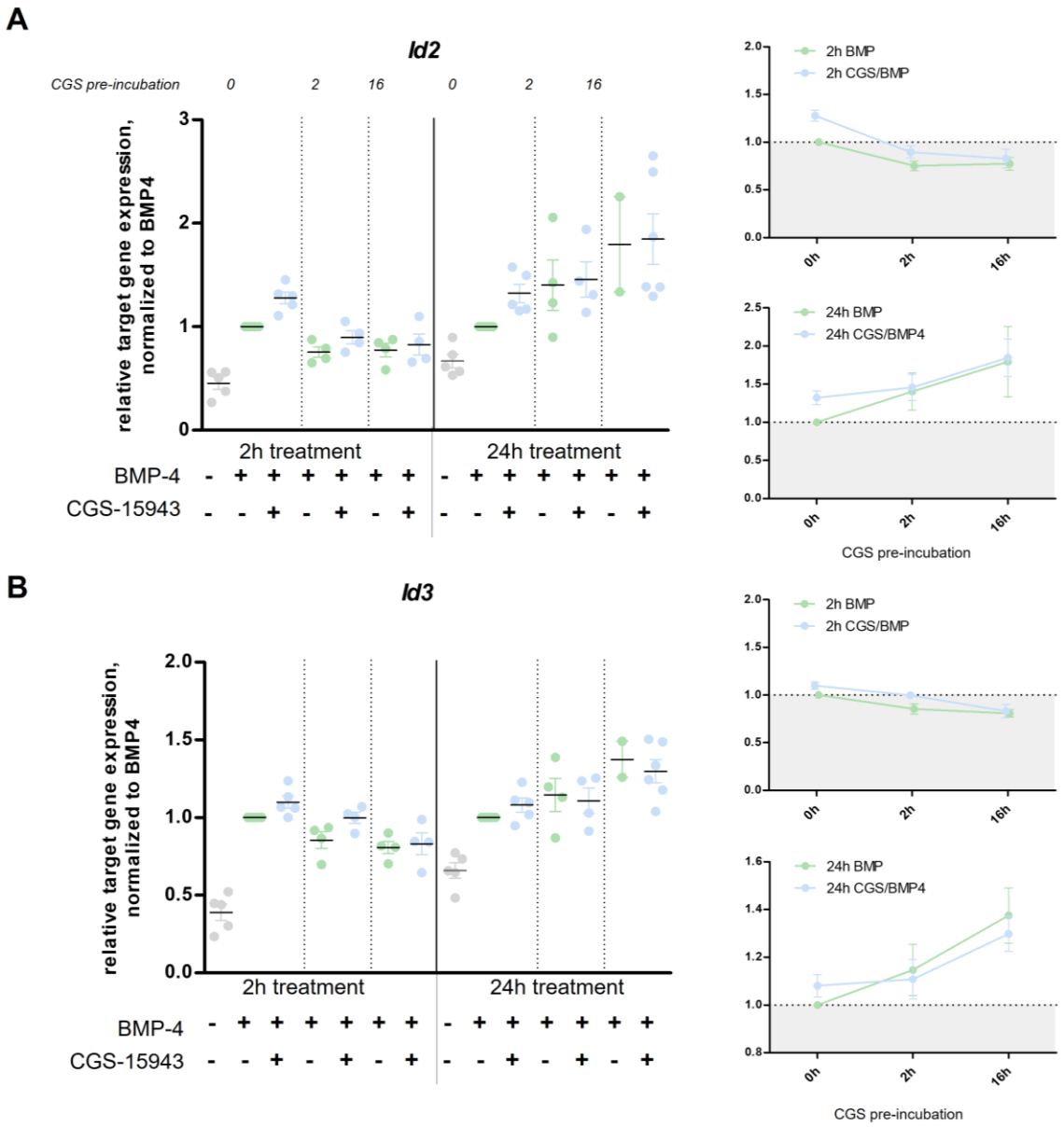

Figure 98: BMP-dependent *Id2/Id3* expression dynamics upon CGS-15943 exposure reveal a long-term upregulation after 24 h. Relative quantification of gene expression for BMP target genes was determined by qRT-PCR. Treatment with DMSO vehicle (grey dot), 7.5 ng/mL BMP-4 (green) and/or 5 µM CGS-15943 (blue) was performed for 24 h with different pre-incubation times of CGS-15943 for 2 h and 16 h. Cell lysates were taken after 2 h and 24 h. Data points represent mean ± SD (n = 4), normalized to 7.5 ng/mL BMP-4.

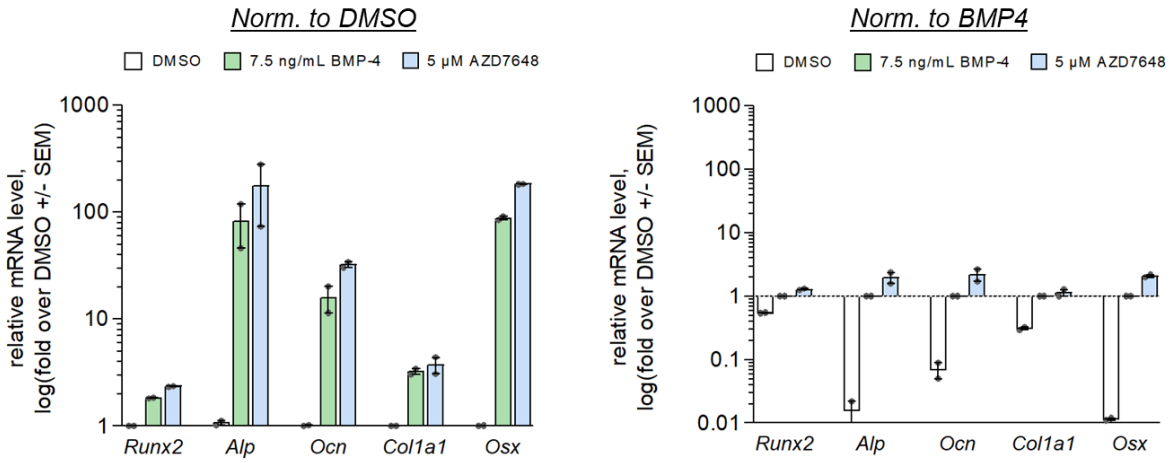

Figure 99: Relative quantification of BMP-dependent osteogenic gene expression transcripts did not confirm efficient osteogenic induction by DNA-PK inhibitor AZD7648 at 5 µM. C2C12 cells were treated with DMSO and/or BMP-4 (7.5 ng/mL) in the presence or absence of compound for 72 h. Data is shown as mean ± SEM (*n* = 2) and normalized to DMSO or 7.5 ng/mL BMP-4 (base line = 1).

8.2 Supplementary Tables

Table 4: Results of kinase profiling of Chromenone 1 at SelectScreen versus 484 kinases. Activities were monitored by biochemical inhibition of selected kinases with 1 µM Chromenone 1 at Life Technologies in three biochemical assay formats (Adapta, Z-Lyte, Lantha). Data is shown as the mean of residual kinase activity ± SD of two replicates (n = 2) for each kinase.

Kinase	mean r.a. [%]	Kinase	mean r.a. [%]	Kinase	mean r.a. [%]
AAK1	98,5	ERBB4 (HER4)	96	NTRK1 (TRKA)	109
ABL1	91,5	ERN1	99	NTRK2 (TRKB)	97,5
ABL1 E255K	96	ERN2	99,5	NTRK3 (TRKC)	94,5
ABL1 F317I	98	FER	97,5	NUAK1 (ARK5)	104,5
ABL1 F317L	97,5	FES (FPS)	93	NUAK2	95
ABL1 G250E	97,5	FGFR1	98,5	PAK1	95,5
ABL1 H396P	99	FGFR1 V561M	99	PAK2 (PAK65)	103,5
ABL1 M351T	93	FGFR2	99	PAK3	95,5
ABL1 Q252H	97	FGFR2 N549H	98	PAK4	99,5
ABL1 T315I	96,5	FGFR3	98,5	PAK6	94
ABL1 Y253F	97,5	FGFR3 G697C	86,5	PAK7 (KIAA1264)	98,5
ABL2 (Arg)	98	FGFR3 K650E	98,5	PASK	101,5
ACVR1 (ALK2)	96,5	FGFR3 K650M	96,5	PDGFRA (PDGFR alpha)	95
ACVR1 (ALK2) R206H	102,5	FGFR3 V555M	99	PDGFRA D842V	99
ACVR1B (ALK4)	102,5	FGFR4	95,5	PDGFRA T674I	99
ACVR2A	93	FGR	97,5	PDGFRA V561D	96
ACVR2B	96,5	FLT1 (VEGFR1)	98	PDGFRB (PDGFR beta)	97,5
ACVRL1 (ALK1)	114	FLT3	96,5	PDK1	87,5
ADCK3	94	FLT3 D835Y	94,5	PDK1 Direct	100
ADRBK1 (GRK2)	97	FLT3 ITD	89,5	PEAK1	92
ADRBK2 (GRK3)	101	FLT4 (VEGFR3)	93,5	PHKG1	97,5
AKT1 (PKB alpha)	97	FRAP1 (mTOR)	98,5	PHKG2	91,5
AKT2 (PKB beta)	95	FRK (PTK5)	96,5	PI4K2A (PI4K2 alpha)	105
AKT3 (PKB gamma)	89	FYN	98	PI4K2B (PI4K2 beta)	97,5
ALK	93	FYN A	100	PI4KA (PI4K alpha)	104
ALK C1156Y	99,5	GAK	100	PI4KB (PI4K beta)	110,5
ALK F1174L	96,5	GRK1	101,5	PIK3C2A (PI3K-C2 alpha)	99
ALK L1196M	97	GRK4	100	PIK3C2B (PI3K-C2 beta)	103
ALK R1275Q	94	GRK5	101	PIK3C2G (PI3K-C2 gamma)	100,5
ALK T1151_L1152insT	103	GRK6	99,5	PIK3C3 (hVPS34)	105
AMPK (A1/B1/G2)	107	GRK7	99	PIK3CA E542K/PIK3R1 (p110 alpha E542K/p85 alpha)	96,5
AMPK (A1/B1/G3)	105	GSG2 (Haspin)	99	PIK3CA E545K/PIK3R1 (p110 alpha E545K/p85 alpha)	97
AMPK (A1/B2/G1)	101	GSK3A (GSK3 alpha)	98	PIK3CA/PIK3R1 (p110 alpha/p85 alpha)	95
AMPK (A1/B2/G2)	98,5	GSK3B (GSK3 beta)	98	PIK3CA/PIK3R3 (p110 alpha/p55 gamma)	106
AMPK (A1/B2/G3)	95	HCK	94	PIK3CB/PIK3R1 (p110 beta/p85 alpha)	100,5
AMPK (A2/B1/G2)	82	HIPK1 (Myak)	97	PIK3CB/PIK3R2 (p110 beta/p85 beta)	114,5
AMPK (A2/B1/G3)	97	HIPK2	101	PIK3CD/PIK3R1 (p110 delta/p85 alpha)	110
AMPK (A2/B2/G1)	99	HIPK3 (YAK1)	99,5	PIK3CG (p110 gamma)	102
AMPK (A2/B2/G2)	104	HIPK4	97,5	PIM1	100
AMPK (A2/B2/G3)	99,5	HUNK	104,5	PIM2	100,5
AMPK A1/B1/G1	100	ICK	101,5	PIM3	94,5
AMPK A2/B1/G1	98	IGF1R	95,5	PIP4K2A	104
ANKK1	92,5	IKBKB (IKK beta)	94	PIP5K1A	99,5
AURKA (Aurora A)	96	IKBKE (IKK epsilon)	96	PIP5K1B	99
AURKB (Aurora B)	95	INSR	94,5	PIP5K1C	106
AURKC (Aurora C)	97	INSRR (IRR)	95,5	PKMYT1	100,5
AXL	98,5	IRAK1	92,5	PKN1 (PRK1)	96,5
AXL R499C	102	IRAK3	100,5	PKN2 (PRK2)	99,5
BLK	84	IRAK4	96	PLK1	93
BMPR1A (ALK3)	97	ITK	96,5	PLK2	96
BMPR1B (ALK6)	98,5	JAK1	100,5	PLK3	97,5
BMPR2	81,5	JAK2	97	PLK4	104
BMX	90,5	JAK2 JH1 JH2	100,5	PRKACA (PKA)	97,5

BRAF	99,5	JAK2 JH1 JH2 V617F	99	PRKACB (PRKAC beta)	101,5
BRAF	96,5	JAK3	106	PRKACG (PRKAC gamma)	101
BRAF V599E	98	KDR (VEGFR2)	101	PRKCA (PKC alpha)	96,5
BRAF V599E	99,5	KIT	102,5	PRKCB1 (PKC beta I)	113
BRSK1 (SAD1)	96,5	KIT A829P	98,5	PRKCB2 (PKC beta II)	97,5
BRSK2	96,5	KIT D816H	98,5	PRKCD (PKC delta)	97
BTK	95,5	KIT D816V	99	PRKCE (PKC epsilon)	98,5
CAMK1 (CaMK1)	109	KIT D820E	100,5	PRKCG (PKC gamma)	96
CAMK1D (CaMKI delta)	93	KIT N822K	99	PRKCH (PKC eta)	103
CAMK1G (CAMKI gamma)	95,5	KIT T670E	103	PRKCI (PKC iota)	95,5
CAMK2A (CaMKII alpha)	97	KIT T670I	98,5	PRKCN (PKD3)	98
CAMK2B (CaMKII beta)	110,5	KIT V559D	98,5	PRKCQ (PKC theta)	91
CAMK2D (CaMKII delta)	96,5	KIT V559D T670I	102,5	PRKCZ (PKC zeta)	99
CAMK2G (CaMKII gamma)	94,5	KIT V559D V654A	101	PRKD1 (PKC mu)	87,5
CAMK4 (CaMKIV)	103	KIT V560G	98,5	PRKD2 (PKD2)	98
CAMKK1 (CAMKKA)	94,5	KIT V654A	96	PRKG1	106,5
CAMKK2 (CaMKK beta)	102,5	KIT Y823D	102	PRKG2 (PKG2)	98,5
CASK	99,5	KSR2	95,5	PRKX	97
CDC42 BPA (MRCKA)	102,5	LATS2	101	PTK2 (FAK)	94
CDC42 BPB (MRCKB)	101	LCK	91	PTK2B (FAK2)	95
CDC42 BPG (MRCKG)	99,5	LIMK1	91	PTK6 (Brk)	99
CDC7/DBF4	97	LIMK2	96,5	RAF1 (cRAF) Y340D Y341D	100,5
CDK1/cyclin B	100,5	LRRK2	111	RAF1 (cRAF) Y340D Y341D	84
CDK11 (Inactive)	103,5	LRRK2 FL	105	RET	98,5
CDK11/cyclin C	97,5	LRRK2 G2019S	102	RET A883F	98,5
CDK13/cyclin K	97	LRRK2 G2019S FL	113	RET G691S	103,5
CDK14 (PFTK1)/cyclin Y	95	LRRK2 I2020T	100,5	RET M918T	95,5
CDK16 (PCTK1)/cyclin Y	103	LRRK2 R1441C	93	RET S891A	98,5
CDK17/cyclin Y	98,5	LTK (TYK1)	100	RET V804E	96
CDK18/cyclin Y	96	LYN A	96	RET V804L	95,5
CDK2/cyclin A	94,5	LYN B	97	RET V804M	98
CDK2/cyclin A1	93,5	MAP2K1 (MEK1)	100,5	RET Y791F	97
CDK2/cyclin E1	99	MAP2K1 (MEK1)	79	RIPK2	100
CDK2/cyclin O	97,5	MAP2K1 (MEK1) S218D S222D	97,5	RIPK3	93,5
CDK3/cyclin E1	108,5	MAP2K2 (MEK2)	98,5	ROCK1	98
CDK4/cyclin D1	92,5	MAP2K2 (MEK2)	82	ROCK2	102,5
CDK4/cyclin D3	104,5	MAP2K4 (MEK4)	99,5	ROS1	90,5
CDK5 (Inactive)	103	MAP2K5 (MEK5)	97,5	RPS6KA1 (RSK1)	95,5
CDK5/p25	97	MAP2K6 (MKK6)	101,5	RPS6KA2 (RSK3)	98,5
CDK5/p35	95	MAP2K6 (MKK6)	82,5	RPS6KA3 (RSK2)	98
CDK6/cyclin D1	107,5	MAP2K6 (MKK6) S207E T211E	101,5	RPS6KA4 (MSK2)	96
CDK7/cyclin H/MNAT1	103	MAP3K10 (MLK2)	99	RPS6KA5 (MSK1)	98,5
CDK8/cyclin C	98	MAP3K11 (MLK3)	103,5	RPS6KA6 (RSK4)	98,5
CDK9 (Inactive)	94	MAP3K14 (NIK)	105	RPS6KB1 (p70S6K)	91
CDK9/cyclin K	102,5	MAP3K19 (YSK4)	105	SBK1	96
CDK9/cyclin T1	98	MAP3K2 (MEKK2)	100	SGK (SGK1)	101
CDKL5	97,5	MAP3K3 (MEKK3)	94	SGK2	97,5
CHEK1 (CHK1)	91	MAP3K5 (ASK1)	99,5	SGKL (SGK3)	98
CHEK2 (CHK2)	96,5	MAP3K7/MAP3K7IP1 (TAK1-TAB1)	94,5	SIK1	103,5
CHUK (IKK alpha)	104	MAP3K8 (COT)	86	SIK3	100
CLK1	96,5	MAP3K9 (MLK1)	88,5	SLK	101
CLK2	94,5	MAP4K1 (HPK1)	97,5	SNF1LK2	96,5
CLK3	100,5	MAP4K2 (GCK)	95,5	SPHK1	101
CLK4	93,5	MAP4K3 (GLK)	103,5	SPHK2	99
CSF1R (FMS)	105	MAP4K4 (HGK)	94	SRC	94
CSK	95	MAP4K5 (KHS1)	95	SRC N1	93,5
CSNK1A1 (CK1 alpha 1)	98	MAPK1 (ERK2)	96	SRMS (Srm)	93,5
CSNK1A1L	96	MAPK10 (JNK3)	99	SRPK1	95,5
CSNK1D (CK1 delta)	96,5	MAPK10 (JNK3)	93,5	SRPK2	101,5
CSNK1E (CK1 epsilon)	94	MAPK11 (p38 beta)	93,5	STK16 (PKL12)	103
CSNK1E (CK1 epsilon) R178C	96,5	MAPK12 (p38 gamma)	94,5	STK17A (DRAK1)	98
CSNK1G1 (CK1 gamma 1)	96	MAPK13 (p38 delta)	96,5	STK17B (DRAK2)	104
CSNK1G2 (CK1 gamma 2)	97,5	MAPK14 (p38 alpha)	89	STK22B (TSSK2)	94,5
CSNK1G3 (CK1 gamma 3)	98,5	MAPK14 (p38 alpha) Direct	98,5	STK22D (TSSK1)	91,5
CSNK2A1 (CK2 alpha 1)	91,5	MAPK15 (ERK7)	100	STK23 (MSSK1)	99,5
CSNK2A2 (CK2 alpha 2)	96,5	MAPK3 (ERK1)	97	STK24 (MST3)	102
DAPK1	100,5	MAPK7 (ERK5)	97	STK25 (YSK1)	106
DAPK2	93,5	MAPK8 (JNK1)	92	STK3 (MST2)	105

DAPK3 (ZIPK)	100	MAPK8 (JNK1)	92,5	STK32B (YANK2)	98
DCAMKL1 (DCLK1)	96	MAPK9 (JNK2)	94,5	STK32C (YANK3)	99,5
DCAMKL2 (DCK2)	98,5	MAPK9 (JNK2)	90	STK33	98,5
DDR1	99,5	MAPKAPK2	98,5	STK38 (NDR)	98
DDR2	99,5	MAPKAPK3	94	STK38L (NDR2)	98
DDR2 N456S	97	MAPKAPK5 (PRAK)	95,5	STK39 (STLK3)	96
DDR2 T654M	94,5	MARK1 (MARK)	88,5	STK4 (MST1)	98,5
DMPK	98,5	MARK2	95	SYK	98
DNA-PK	96	MARK3	98	TAOK1	102,5
DYRK1A	88,5	MARK4	95,5	TAOK2 (TAO1)	100,5
DYRK1B	101,5	MASTL	99	TAOK3 (JIK)	97
DYRK2	99	MATK (HYL)	95,5	TBK1	94,5
DYRK3	98,5	MELK	92,5	TEC	100,5
DYRK4	97	MERTK (cMER)	97,5	TEK (Tie2)	91,5
EEF2K	93,5	MERTK (cMER) A708S	99	TEK (TIE2) R849W	102,5
EGFR (ErbB1)	100	MET (cMet)	98,5	TEK (TIE2) Y1108F	98,5
EGFR (ErbB1) C797S	98	MET (cMet) Y1235D	100	TEK (TIE2) Y897S	107
EGFR (ErbB1) d746-750	99,5	MET D1228H	106	TESK1	104,5
EGFR (ErbB1) d747-749 A750P	94,5	MET M1250T	101,5	TESK2	93,5
EGFR (ErbB1) G719C	105	MINK1	93,5	TGFBR1 (ALK5)	100
EGFR (ErbB1) G719S	98,5	MKNK1 (MNK1)	77,5	TGFBR2	97,5
EGFR (ErbB1) L858R	95	MKNK2 (MNK2)	98,5	TLK1	110,5
EGFR (ErbB1) L861Q	102	MLCK (MLCK2)	100	TLK2	103,5
EGFR (ErbB1) T790M	97	MLK4	104	TNIK	98,5
EGFR (ErbB1) T790M C797S L858R	97,5	MST1R (RON)	100,5	TNK1	96
EGFR (ErbB1) T790M L858R	95	MST4	100	TNK2 (ACK)	99
EIF2AK2 (PKR)	103,5	MUSK	90	TTK	94,5
EPHA1	97,5	MYLK (MLCK)	98	TXK	96,5
EPHA2	93	MYLK2 (skMLCK)	97,5	TYK2	97
EPHA3	92,5	MYLK4	97,5	TYRO3 (RSE)	97,5
EPHA4	83,5	MYO3A (MYO3 alpha)	96	ULK1	101
EPHA5	92	MYO3B (MYO3 beta)	101,5	ULK2	101
EPHA6	99,5	NEK1	98	ULK3	97
EPHA7	97	NEK2	101,5	VRK2	98,5
EPHA8	97	NEK4	94,5	WEE1	96,5
EPHB1	97,5	NEK6	96,5	WNK1	96,5
EPHB2	93	NEK8	91,5	WNK2	98
EPHB3	99,5	NEK9	97,5	WNK3	96,5
EPHB4	89,5	NIM1K	96,5	YES1	96
ERBB2 (HER2)	102,5	NLK	98,5	ZAK	99
				ZAP70	99,5

Table 5: Results of kinase profiling of CGS-15943 at Reaction Biology versus 408 kinases. Activities were monitored by biochemical inhibition of selected kinases with 1 µM CGS-15943 and IC_{50}'s were calculated for potently inhibited kinases. Data is shown as the mean of residual kinase activity ± SD of two replicates (n = 2) for each kinase. N.c. = not confirmed.

Kinase	**Mean r.a. [%]**	**IC_{50}**	**Kinase**	**Mean r.a. [%]**	**IC_{50}**	**Kinase**	**Mean r.a. [%]**	**IC_{50}**
ABL1	98,9		FYN	102,7		PKCepsilon		
ABL2/ARG	95,1		GCK/MAP4K2	86,0		PKCeta	93,5	
ACK1	101,1		GLK/MAP4K3	112,1		PKCg	96,2	
AKT1	86,4		GRK1	90,2		PKCiota	87,8	
AKT2	82,5		GRK2	92,6		PKCmu/PRKD1	95,7	
AKT3	99,7		GRK3	100,1		PKCnu/PRKD3	84,8	
ALK	99,9		GRK4	95,3		PKCtheta	101,5	
ALK1/ACVRL1	101,4		GRK5	100,0		PKCzeta	127,0	58,7
ALK2/ACVR1	135,9	n.c.	GRK6	104,0		PKD2/PRKD2	112,6	
ALK3/BMPR1A	108,3		GRK7	94,5		PKG1a	98,2	
ALK4/ACVR1B	94,6		GSK3a	91,8		PKG1b	98,1	
ALK5/TGFBR1	105,3		GSK3b	111,0		PKG2/PRKG2	99,1	
ALK6/BMPR1B	102,3		Haspin	91,9		PKN1/PRK1	110,4	
ARAF	87,6		HCK	103,9		PKN2/PRK2	109,4	
ARK5/NUAK1	88,5		HGK/MAP4K4	75,2		PKN3/PRK3	90,0	
ASK1/MAP3K5	96,7		HIPK1	88,3		PLK1	94,7	

Aurora A		91,5		HIPK2		98,7		PLK2		105,4	
Aurora B		103,4		HIPK3		105,7		PLK3		91,5	
Aurora C		100,7		HIPK4		116,1		PLK4/SAK		89,0	
AXL		86,5		HPK1/MAP4K1		111,1		PRKX		84,7	
BLK		110,9		IGF1R		102,6		PYK2		101,2	
BMPR2		69,8	37,3	IKKa/CHUK		111,5		RAF1		103,3	
BMX/ETK		92,6		IKKb/IKBKB		103,4		RET		111,1	
BRAF		73,0		IKKe/IKBKE		91,2		RIPK2		105,3	
BRK		107,8		IR		97,5		RIPK3		80,7	
BRSK1		96,8		IRAK1		104,0		RIPK4		107,9	
BRSK2		101,0		IRAK4		121,6		RIPK5		113,4	
BTK		103,1		IRR/INSRR		99,8		ROCK1		101,8	
c-Kit		104,4		ITK		100,8		ROCK2		100,0	
c-MER		75,6		JAK1		105,1		RON/MST1R		99,2	
c-MET		88,8		JAK2		91,1		ROS/ROS1		117,0	
c-Src		118,1		JAK3		104,6		RSK1		105,1	
CAMK1a		98,8		JNK1		106,5		RSK2		95,7	
CAMK1b		92,1		JNK2		106,2		RSK3		105,3	
CAMK1d		90,9		JNK3		94,1		RSK4		97,2	
CAMK1g		103,3		KDR/VEGFR2		109,7		SBK1		93,0	
CAMK2a		97,1		KHS/MAP4K5		91,5		SGK1		100,3	
CAMK2b		99,7		KSR1		98,2		SGK2		89,4	
CAMK2d		94,9		KSR2		100,9		SGK3/SGKL		100,7	
CAMK2g		94,2		LATS1		100,3		SIK1		97,0	
CAMK4		85,3		LATS2		81,4		SIK2		101,9	
CAMKK1		89,9		LCK		89,0		SIK3		105,9	
CAMKK2		105,3		LCK2/ICK		103,3		SLK/STK2		91,0	
CDC7/DBF4		116,7		LIMK1		104,5		SNARK/NUAK2		96,8	
CDK1/cyclin A		99,7		LIMK2		97,7		SNRK		91,8	
CDK1/cyclin B		98,2		LKB1		98,0		SRMS		106,8	
CDK1/cyclin E		113,2		LOK/STK10		91,7		SRPK1		100,5	
CDK14/cyclin (PFTK1)	Y	101,0		LRRK2		77,4		SRPK2		105,7	
CDK16/cyclin (PCTAIRE)	Y	180,0	n.c.	LYN		103,9		SSTK/TSSK6		93,3	
CDK17/cyclin (PCTK2)	Y	94,6		LYN B		101,5		STK16		105,6	
CDK18/cyclin (PCTK3)	Y	92,4		MAK		88,9		STK21/CIT		79,4	
CDK19/cyclin C		96,9		MAPKAPK2		97,3		STK22D/TSSK1		93,4	
CDK2/cyclin A		91,6		MAPKAPK3		102,4		STK25/YSK1		95,4	
CDK2/Cyclin A1		102,3		MAPKAPK5/PRAK		128,4	34,9	STK32B/YANK2		99,2	
CDK2/cyclin E		92,7		MARK1		102,2		STK32C/YANK3		106,5	
CDK2/cyclin E2		108,5		MARK2/PAR-1Ba		112,9		STK33		94,0	
CDK2/cyclin O		97,2		MARK3		110,2		STK38/NDR1		76,2	
CDK3/cyclin E		91,5		MARK4		99,9		STK38L/NDR2		107,5	
CDK3/cyclin E2		100,5		MEK1		103,2		STK39/STLK3		98,3	
CDK4/cyclin D1		112,0		MEK2		117,4		SYK		71,0	
CDK4/cyclin D3		100,7		MEK3		131,2	n.c.	TAK1		95,1	
CDK5/p25		108,7		MEK5		105,3		TAOK1		98,1	
CDK5/p35		102,2		MEKK1		120,8		TAOK2/TAO1		110,1	
CDK6/cyclin D1		112,1		MEKK2		106,3		TAOK3/JIK		104,5	
CDK6/cyclin D3		98,4		MEKK3		130,8	n.c.	TBK1		94,7	
CDK7/cyclin H		90,9		MEKK6		102,6		TEC		93,5	
CDK9/cyclin K		102,0		MELK		76,7		TESK1		110,1	
CDK9/cyclin T1		99,4		MINK/MINK1		68,6		TESK2		116,6	
CDK9/cyclin T2		92,7		MKK4		110,9		TGFBR2		111,0	
CHK1		116,4		MKK6		100,3		TIE2/TEK		109,6	
CHK2		99,8		MKK7		101,7		TLK1		90,9	
CK1a1		42,0	0,853	MLCK/MYLK		96,5		TLK2		110,4	
CK1a1L		74,7		MLCK2/MYLK2		91,5		TNIK		86,3	
CK1d		18,3	0,244	MLK1/MAP3K9		85,4		TNK1		61,5	
CK1epsilon		40,9	0,584	MLK2/MAP3K10		74,3		TRKA		94,9	
CK1g1		68,6		MLK3/MAP3K11		76,9		TRKB		101,0	
CK1g2		71,8		MLK4		117,9		TRKC		96,9	
CK1g3		91,6		MNK1		76,2		TSSK2		93,4	
CK2a		81,8		MNK2		113,8		TSSK3/STK22C		116,4	
CK2a2		63,2		MRCKa/CDC42BPA		105,8		TTBK1		95,8	
CLK1		91,4		MRCKb/CDC42BPB		99,2		TTBK2		97,2	
CLK2		95,4		MSK1/RPS6KA5		87,9		TXK		85,3	
CLK3		94,7		MSK2/RPS6KA4		102,4		TYK1/LTK		104,0	
CLK4		55,8		MSSK1/STK23		92,6		TYK2		90,2	
COT1/MAP3K8		95,0		MST1/STK4		103,4		TYRO3/SKY		126,3	n.c.
CSK		96,2		MST2/STK3		96,7		ULK1		100,8	
CTK/MATK		99,9		MST3/STK24		91,4		ULK2		91,9	
DAPK1		88,8		MST4		92,0		ULK3		91,7	
DAPK2		97,0		MUSK		91,3		VRK1		95,0	

DCAMKL1	95,6	MYLK3	91,3	VRK2	85,2	
DCAMKL2	96,6	MYLK4	84,4	WEE1	102,1	
DDR1	90,3	MYO3A	83,6	WNK1	79,8	
DDR2	106,7	MYO3b	120,8	WNK2	97,3	
DLK/MAP3K12	100,5	NEK1	94,6	WNK3	111,7	
DMPK	101,6	NEK11	103,5	YES/YES1	99,1	
DMPK2	95,7	NEK2	99,3	YSK4/MAP3K19	103,3	
DRAK1/STK17A	101,0	NEK3	112,7	ZAK/MLTK	85,4	
DYRK1/DYRK1A	84,4	NEK4	106,3	ZAP70	95,0	
DYRK1B	72,8	NEK5	92,2	ZIPK/DAPK3	101,6	
DYRK2	89,9	NEK6	103,1	AMPK(A1/B1/G1)	96,7	
DYRK3	103,3	NEK7	103,4	AMPK(A1/B1/G2)	107,1	
DYRK4	109,5	NEK8	89,4	AMPK(A1/B1/G3)	94,3	
EGFR	98,7	NEK9	87,5	AMPK(A1/B2/G1)	102,7	
EPHA1	102,4	NIM1	93,3	AMPK(A2/B1/G1)	99,2	
EPHA2	97,4	NLK	99,4	AMPK(A2/B2/G1)	93,9	
EPHA3	90,9	OSR1/OXSR1	88,5	AMPK(A2/B2/G2)	98,8	
EPHA4	102,4	P38a/MAPK14	98,9	AMPK(A2/B2/G3)	104,1	
EPHA5	97,2	P38b/MAPK11	107,6	DNA-PK	97,9	
EPHA6	102,3	P38d/MAPK13	114,2	EEF2K	30,1	0,209
EPHA7	98,6	P38g	104,2	EIF2AK1	90,6	
EPHA8	96,1	p70S6K/RPS6KB1	103,9	EIF2AK2	75,0	
EPHB1	95,2	p70S6Kb/RPS6KB2	105,0	EIF2AK3	88,3	
EPHB2	99,3	PAK1	101,4	EIF2AK4	110,4	
EPHB3	100,7	PAK2	105,9	mTOR/FRAP1	96,4	
EPHB4	95,6	PAK3	65,1	PDK1/PDHK1	87,4	
ERBB2/HER2	106,3	PAK4	115,8	PDK2/PDHK2	97,7	
ERBB4/HER4	92,0	PAK5	100,3	PDK3/PDHK3	125,7	
ERK1	104,9	PAK6	99,0	PDK4/PDKH4	67,8	
ERK2/MAPK1	102,1	PASK	99,1	TRPM7/CHAK1	90,0	
ERK5/MAPK7	109,9	PBK/TOPK	113,4	PI3KC2A	93,4	
ERK7/MAPK15	100,2	PDGFRa	93,2	PI3KC3	97,1	
ERN1/IRE1	90,9	PDGFRb	96,6	PI4Ka	71,5	
ERN2/IRE2	112,8	PDK1/PDPK1	112,9	PI4Kb	78,4	
FAK/PTK2	98,6	PEAK1	107,1	PI4K2A	58,1	
FER	107,6	PHKg1	107,6	PIP5K1A	93,7	
FES/FPS	101,7	PHKg2	94,5	PIP5K1C	97,8	
FGFR1	99,2	PIM1	107,3	SPHK1	98,1	
FGFR2	97,6	PIM2	111,7	SPHK2	105,4	
FGFR3	114,6	PIM3	94,4	PI3Ka (p110a/p85a)	108,0	
FGFR4	106,9	PKA	91,4	PI3Kb (p110b/p85a)	53,4	
FGR	102,6	PKAcb	98,3	PI3Kg (p110g)	92,8	
FLT1/VEGFR1	91,3	PKAcg	99,7	PI3Kd (p110d/p85a)	26,4	
FLT3	68,1	PKCa	98,8	PI3K (p110a/p65a)	70,8	
FLT4/VEGFR3	92,9	PKCb1	90,6	PI3K (p110a(E542K)/p85a)	34,8	
FMS	108,3	PKCb2	93,0	PI3K (p110a(E545K)/p85a)	58,5	
FRK/PTK5	96,1	PKCd	103,7	PI3K (p110a(H1047R)/p85a)	42,0	

8.3 Structural formula directory

BMP Inhibitors

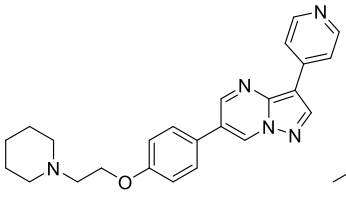

Dorsomorphin (DM)

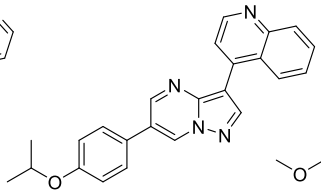

DMH-1

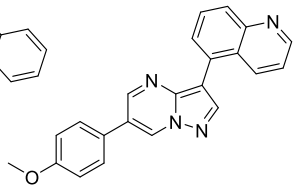

ML-347

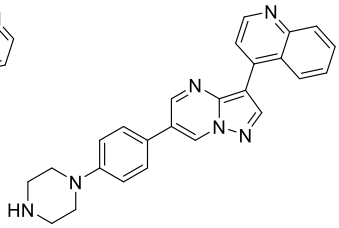

LDN-193189

TGFβ Inhibitors

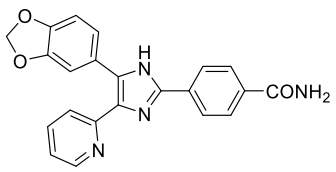

SB-431542

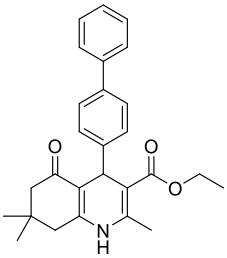

ITD-1/ DHP-1

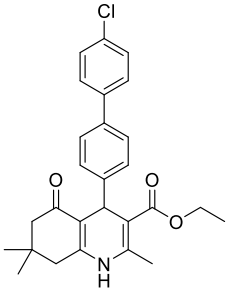

DHP-2

BMP Sensitizer and Activators

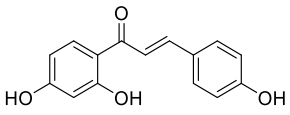

Isoliquiritigenin

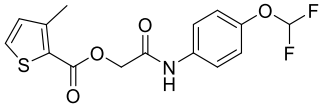

Ventromorphin

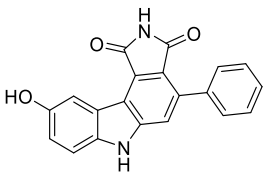

PD-407824

GSK3/ VPS34 Inhibitor

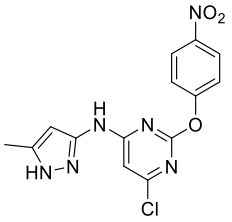

Autophinib

VPS34 Inhibitors

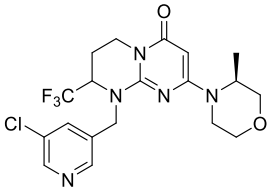

SAR405

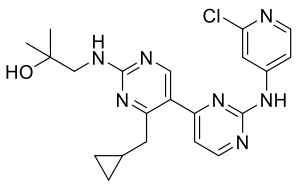

VPS34-IN1

GSK3 Inhibitors

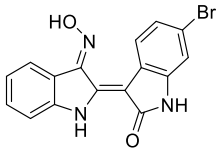

6-BIO

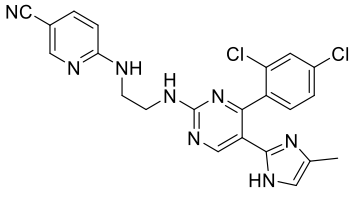

CHIR99021

Autophagy/ Mitochondrial complex I inhibitors

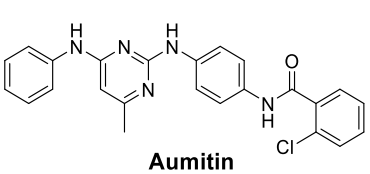

Aumitin

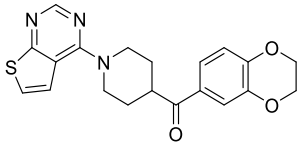

Authipyrin

Chromenones, 4*H*-chromen-4-ones

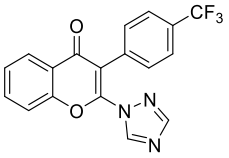

Chromenone 1

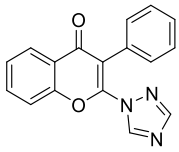

Chromenone 2

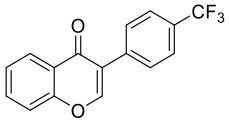

Chromenone 3

CGS-15943, triazolo[1,5-*c*]quinazolines

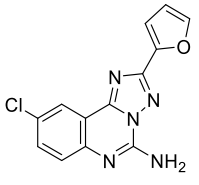

1 (CGS-15943)

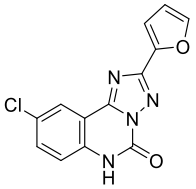

2

CK1 inhibitors

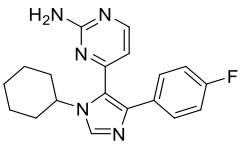

PF-670462

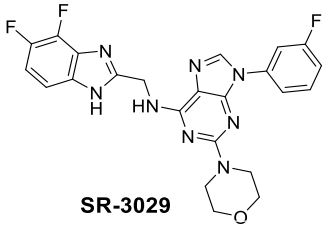

SR-3029

Class I PI3K inhibitors

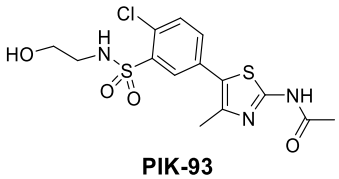

PIK-93

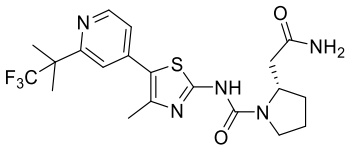

BYL-719

LY294002

AhR activator

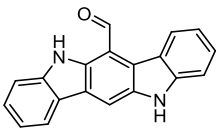

FICZ

DNA-PK inhibitor

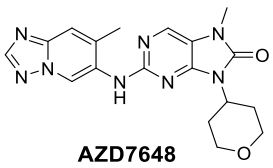

AZD7648

8.4 List of Figures

EIDESSTATTLICHE VERSICHERUNG (AFFIDAVIT)

Weßeler, Fabian **149990**

Name, Vorname
(Surname, first name)

Matrikel-Nr.
(Enrolment number)

Belehrung:

Wer vorsätzlich gegen eine die Täuschung über Prüfungsleistungen betreffende Regelung einer Hochschulprüfungsordnung verstößt, handelt ordnungswidrig. Die Ordnungswidrigkeit kann mit einer Geldbuße von bis zu 50.000,00 € geahndet werden. Zuständige Verwaltungsbehörde für die Verfolgung und Ahndung von Ordnungswidrigkeiten ist der Kanzler/die Kanzlerin der Technischen Universität Dortmund. Im Falle eines mehrfachen oder sonstigen schwerwiegenden Täuschungsversuches kann der Prüfling zudem exmatrikuliert werden, § 63 Abs. 5 Hochschulgesetz NRW.

Die Abgabe einer falschen Versicherung an Eides statt ist strafbar.

Wer vorsätzlich eine falsche Versicherung an Eides statt abgibt, kann mit einer Freiheitsstrafe bis zu drei Jahren oder mit Geldstrafe bestraft werden, § 156 StGB. Die fahrlässige Abgabe einer falschen Versicherung an Eides statt kann mit einer Freiheitsstrafe bis zu einem Jahr oder Geldstrafe bestraft werden, § 161 StGB.

Die oben stehende Belehrung habe ich zur Kenntnis genommen:

Official notification:

Any person who intentionally breaches any regulation of university examination regulations relating to deception in examination performance is acting improperly. This offence can be punished with a fine of up to EUR 50,000.00. The competent administrative authority for the pursuit and prosecution of offences of this type is the chancellor of the TU Dortmund University. In the case of multiple or other serious attempts at deception, the candidate can also be unenrolled, Section 63, paragraph 5 of the Universities Act of North Rhine-Westphalia.

The submission of a false affidavit is punishable.

Any person who intentionally submits a false affidavit can be punished with a prison sentence of up to three years or a fine, Section 156 of the Criminal Code. The negligent submission of a false affidavit can be punished with a prison sentence of up to one year or a fine, Section 161 of the Criminal Code.

I have taken note of the above official notification.

Ort, Datum
(Place, date)

Unterschrift
(Signature)

Titel der Dissertation:
(Title of the thesis):
Stem Cell-Based Phenotypic Screening and Characterization of Novel BMP Mimetics

Ich versichere hiermit an Eides statt, dass ich die vorliegende Dissertation mit dem Titel selbstständig und ohne unzulässige fremde Hilfe angefertigt habe. Ich habe keine anderen als die angegebenen Quellen und Hilfs- mittel benutzt sowie wörtliche und sinngemäße Zitate kenntlich gemacht.

Die Arbeit hat in gegenwärtiger oder in einer anderen Fassung weder der TU Dortmund noch einer anderen Hochschule im Zusammenhang mit einer staatlichen oder akademischen Prüfung vorgelegen.

I hereby swear that I have completed the present dissertation independently and without inadmissible external support. I have not used any sources or tools other than those indicated and have identified literal and analogous quotations.

The thesis in its current version or another version has not been presented to the TU Dortmund University or another university in connection with a state or academic examination.*

*Please be aware that solely the German version of the affidavit ("Eidesstattliche Versicherung") for the PhD thesis is the official and legally binding version.

Ort, Datum
(Place, date)

Unterschrift
(Signature)